UNIVERSITY OF MONTENEGRO
INSTITUTE FOR INTERDISCIPLINARY AND MULTIDISCIPLINARY STUDIES
PhD PROGRAMME "SUSTAINABLE DEVELOPMENT"

MSc David Kočović

SYNTHESIS, PHYSICOCHEMICAL CHARACTERIZATION AND POTENTIAL BIOLOGICAL ACTIVITY OF NEW PYRAZOLE AND AMOXICILLIN COMPLEX COMPOUNDS

Doctoral dissertation

Podgorica, 2025.

UNIVERZITET CRNE GORE
INSTITUT ZA INTERDISCIPLINARNE I
MULTIDISCIPLINARNE STUDIJE
PhD PROGRAMME "SUSTAINABLE DEVELOPMENT"

Mr David Kočović

SINTEZA, FIZIČKO-HEMIJSKA KARAKTERIZACIJA I PROCJENA POTENCIJALNE BIOLOŠKE AKTIVNOSTI NOVOSINTETIZOVANIH KOMPLEKSNIH JEDINJENJA NA BAZI PIRAZOLA I AMOKSICILINA

Doktorska disertacija

Podgorica, 2025.

INFORMATION ON THE AUTHOR

Name and surname: *David Kočović*
Date of birth: *17.06.1996.*
Study programme and the year of finalization: *Sustainable development, 2025.*

INFORMATION ON THE DOCTORAL DISSERTATION

Thesis: *Synthesis, physicochemical characterization and potential biological activity of new pyrazole and amoxicillin complex compounds*
Mentor: *Prof. dr Željko Jaćimović, Full professor of the Faculty of Metallurgy and Technology, University of Montenegro*

Thesis and Candidate Assessment Committee:

- *Dr Miljan Bigović, Associate Professor of the Faculty of Science and Mathematics, University of Montenegro, member of the commission*
- *Dr Milica Kosović-Perutović, Docent of the Faculty of Metallurgy and Technology, University of Montenegro, member of the commission*
- *Dr Radovan Stojanović, Full Professor of the Faculty of Electrical Engineering, University of Montenegro, member of the commission*
- *Dr Željko Jaćimović, Full Professor of the Faculty of Metallurgy and Technology, University of Montenegro (mentor);*

Date of the Thesis and Candidate Assessment: *23rd of December 2022.*

Doctoral Dissertation Evaluation Committee:

- *Dr Miljan Bigović, Associate Professor of the Faculty of Science and Mathematics, University of Montenegro, member of the commission*
- *Dr Aida Šapčanin, Full Professor of the Faculty of Pharmacy, University of Sarajevo, member of the commission*
- *Dr Željko Jaćimović, Full Professor of the Faculty of Metallurgy and Technology, University of Montenegro (mentor);*

Doctoral Dissertation Defense Committee:

- *Dr Miljan Bigović, Associate Professor of the Faculty of Science and Mathematics, University of Montenegro, member of the commission*
- *Dr Aida Šapčanin, Full Professor of the Faculty of Pharmacy, University of Sarajevo, member of the commission*
- *Dr Željko Jaćimović, Full Professor of the Faculty of Metallurgy and Technology, University of Montenegro (mentor);*

Defense date: *26th of December 2025.*

Promotion date:

Acknowledgements

First and foremost, I would like to express my deepest gratitude to my mentor, Prof. Dr Željko Jaćimović, for his unwavering guidance, patience, and support throughout this journey. Through his insights, extensive knowledge and encouragements I have been able to come to this point, and his guidance has been invaluable at every stage of my doctoral research.

Special thanks are extended to Professors Aida Šapčanin, Miljan Bigović, Gerald Giester, Sergiu Shova and Zoran Tomić, whose expertise, collaboration, and generous support played a crucial role in the realization of this thesis.

I would also like to extend heartfelt appreciation to my colleague and friend, Ana Radović. Our friendship came as a gift, and as the first result of our PhD theses, a one that I am sure will last a lifetime.

I am immensely thankful to my family, especially to my parents and my sister, for their love, understanding, support and continuous motivation, as in this, so in every journey I undevoured on. I am here because of you.

For her unwavering love, kindness, gentle spirit and for the way she clears the dark clouds from my mind, I owe gratitude and much more to my Vladana.

Finally, I thank my colleagues at the Institute for Medicines and Medical Devices for their encouragement and support throughout this process.

To all of you — thank you.

University of Montenegro
Institute for interdisciplinary and multidisciplinary studies
PhD programme "Sustainable development"

Synthesis, physicochemical characterization and potential biological activity of new pyrazole and amoxicillin complex compounds

Abstract

Pyrazole and its derivatives, among various other proven applications, present an important medical potential with numerous pharmacological activities. The limited number of safe and effective pharmacologically active substances indicates the need for the formation of new, safer, more efficient and effective solutions, i.e. active substances. Pyrazole derivatives are utilized as versatile ligands for synthesizing mono, bi, or polynuclear metal complexes. The role of pyrazolyl ligand depends on its oxidation state. Various possibilities for substitution at the pyrazole ring significantly enhance the diversity of coordination modes of pyrazole derivatives. Additionally, as one of the most commonly used antibiotics, amoxicillin, was presented a part of this research. During the research, numerous attempts of creating amoxicillin complexes have been conducted, with interesting results. With the current absence of overall data or already-existent pharmacological activity, ligands that have been the focus of this thesis are: 5-(4-bromophenyl)-3-methyl-1H-pyrazole, 4-methylpyrazole and 3-amino-4,5-dihydro-1-phenyl-1H-pyrazole and amoxicillin trihydrate. Other than the four previously mentioned ligands, the results of the attempts of syntheses with 2-(3-Aminophenyl)-5-methyl-2,4-dihydro-pyrazol-3-one hydrochloride are presented.

The crystal and molecular structure of the synthesized complexes were determined by different combinations of techniques such are X-ray powder diffraction, C H N analyses, FTIR spectroscopy and single-crystal X-ray structure analysis. Since for further application of the selected compounds, more assays were conducted for the initial estimation of their potential, with emphasis on biological activity.

Keywords: Pyrazole derivatives, complexes, amoxicillin, crystal structures, antioxidative capacity, in vitro assays.

Scientific field: Chemistry.

The branch of scientific field: Inorganic chemistry.

UDK number: 542

Preface

Synthesis, physicochemical characterization and potential biological activity of new pyrazole and amoxicillin complex compounds is a doctoral thesis through which we saw to continue the ongoing journey and previous work done in the field of complex compounds of pyrazole derivatives and other moieties with transition metals, and explore properties and potentials of novel complexes created throughout the course of this research. With focus on medical aspects of such products, we have embarked on a mission to create new complexes from the selection of pyrazole derivatives and well known compound of amoxicillin, describe them and test some for their properties.

As the field of pharmacology has long been driven by the research in the domain of novel compounds and structural modifications of compounds, pyrazole derivatives were a class that was well researched, and amoxicillin as a product of such a process, was used in further experiments. The rise of antibiotic resistance and the humanities strugle with cancerous diseases, seeks solutions, and one of more classical approaches to treating these problems can be found in discoveries of new active pharmaceutical ingredients (API). With this said, a selection of representative examples from the novel complex compounds, designed and described as part of this thesis, have been tested for their antioxidative, antimicrobial and anticancer properties.

The research can be divided into two main sections: first one, starting with the theoretical background with overview of pyrazole and its derivatives and amoxicilin, their metal complexes and ways of coordination, uses in the medicinal field; and the second one, representing the experimental section that dives into succesful syntheses, physico-chemical characterizations, as well as in-vitro experiments with chosen representatives.

The outcomes of this research are intended to contribute to existing knowledge, further advancing the field of creation or serving as a foundation for the development of novel APIs.

Summary

Nitrogen-containing heterocyclic compounds and their derivatives are important sources of therapeutic agents. Pyrazole, the main representative of the eponymous class of organic compounds, has the characteristic two nitrogen atoms and provides numerous functionalities and stereochemical complexity in a five-membered ring structure. Pyrazoles are used in numerous spheres, and this thesis focuses on their high potential and applications in the field of pharmacy.

Complexes of metals with pyrazole and its derivatives have attracted the attention of many authors, as evidenced by a large number of published scientific works, as well as works of a review nature. Additionally, these compounds are interesting not only from a theoretical, but also a practical point of view. Namely, pyrazoles are part of many medicines (especially antipyretics and antirheumatics), herbicides and fungicides, and some pyrazole derivatives can also be used as extractants of various metal ions. In recent times, knowledge about the biocoordination chemistry of pyrazole and its derivatives has been expanded.

Amoxicillin as a member of penicillin-derived substances, is an extremely valuable class of β-lactamic antibiotics. The resistance of bacteria to these antibiotics, comes from ß-lactamase enzymes that break down the structure of these antibiotics, more precisely their ß-lactam ring. One of the potential ways to renew the effectiveness of this well-known class of antibiotics is to create complex compounds in such a manner that its structure serves the purpose to protect the main structure without negatively acting on its effectiveness. Amoxicillin, from a perspective of coordination chemistry, shows high potential for syntheses of complex compounds.

An example of the application of one of the pyrazole representatives in the field of medicine is fomepizole and its use in cases of ethylene glycol or methanol poisoning. Fomepizole (*4-methylpyrazole, L2*) is a ligand used for the purposes of this study. In addition to fomepizole, to obtain complex compounds with a series of transition metals, during the preparation of the doctoral dissertation, the following ligands were used for

obtaining complexes with selected metals: *5-(4-bromophenyl)-3-methyl-1H-pyrazole (L1), 3-amino-4,5-dihydro-1-phenyl-1H-pyrazol (L3), 2-(3-Aminophenyl)-5-methyl-2,4-dihydro-pyrazol-3-one hydrochloride (L4)* and *amoxicillin trihydrate (L5)*.

For ***5-(4-bromophenyl)-3-methyl-1H-pyrazole (L1)*** the syntheses that have been tried were with following metal salts: $Cu(NO_3)_2 \cdot H_2O$, $Zn(OAC)_2 \cdot 2H_2O$, $Ni(OAC)_2 \cdot 2H_2O$, $PdCl_2$, K_2PtCl_4, $CoCl_2$, $Co(OAC)_2$, $Pd(OAC)_2$, RuI_3. There were attempts of syntheses with *L1* with $Cu(NO_3)_2 \cdot H_2O$ in DMF, *L1* and RuI_3 in ethanol, *L1* and $Pd(OAC)_2$ in ethanol, *L1* and $PdCl_2$ in ethanol/water, *L1* and K_2PtCl_4 in ethanol/water, *L1* and $Co(OAC)_2$ in methanol, *L1* and $Pd(OAC)_2$ in ethanol. With *L1* a monocrystal of the ligand was obtained as well as three complexes: $[ZnL_2(OAc)_2]$, $[Co_4L_8Cl_8]$ and $[CoL_3Cl \cdot H_2O]$. Two obtained monocrystal complexes with L1 that have been obtained simultaneously from the reaction with $CoCl_2$ in ethanol, as well as the monocrystal of the ligand, have been characterized with SC-XRD technique and described in the experimental part of this thesis. The complex obtained from the reaction of L1 and $Zn(OAC)_2 \cdot 2H_2O$ in ethanol, has been characterized by XRPD, CHN and IR spectroscopy and described in the experimental part of this thesis.

From the attempts of synthetic reactions of ***fomepizole* (*L2*)** with metal salts: $Cu(NO_3)_2 \cdot H_2O$, $Zn(OAC)_2 \cdot 2H_2O$, $Ni(OAC)_2 \cdot 2H_2O$, $PdCl_2$, K_2PtCl_4, $CoCl_2$, $Co(OAC)_2$, $Pd(OAC)_2$, $RuCl_3$, six complexes were obtained: $[CuL_2(NO_3)_2]$, $[CoL_4Cl_2]$, $[Ni(OAc)_2L_4]$, $[Zn(OAc)_2L_2]$, $[PtL_3Cl_2]$ *and* $[Pd(L\text{-}H)_3]$. The attempts of syntheses with no obtained products were *L2* and $Cu(NO_3)_2 \cdot H_2O$ in DMSO, *L2* and $PdCl_2$ in DMSO, *L2* and $Co(OAC)_2$ in ethanol, *L2* and $RuCl_3 \cdot H_2O$ in methanol, and *L2* and $Pd(OAC)_2$ in ethanol. For the complex obtained with $Cu(NO_3)_2 \cdot H_2O$ the characterization has been done via XRPD, SC-XRD and IR spectroscopy, additionally the tests of bactericidal properties have been conducted for this complex. Complex obtained with $CoCl_2$ the characterization was conducted through XRPD and SC-XRD analyses. Complexes of L2 and $Zn(OAC)_2 \cdot 2H_2O$ and $Ni(OAC)_2 \cdot 2H_2O$ were characterized through SC-XRD, CHN and IR spectroscopy, additionally the thermogravimetric tests and tests of antioxidative potential have been conducted for these complexes. Complexes with K_2PtCl_4 and $Pd(OAC)_2$ have been characterized by CHN, IR and XRPD techniques, in addition the tests of bactericidal and cytotoxic properties have been conducted for these complexes.

Ligand ***3-Amino-4,5-dihydro-1-phenyl-1H-pyrazole* (*L3*)** was used in synthetic reactions with metal salts: $Cu(NO_3)_2 \cdot H_2O$, $Zn(OAC)_2 \cdot 2H_2O$, $Ni(OAC)_2 \cdot 2H_2O$, $PdCl_2$, K_2PtCl_4, $CoCl_2$, $Co(OAC)_2$, $Pd(OAC)_2$, RuI_3, $Mn(OAC)_2 \cdot 4H_2O$ and from these reactions two complexes were obtained: $[PtL_2Cl_2]$ and $[PdL_2(OAc)_2]$. The attempts of syntheses with no obtained products were *L3* and $Cu(NO_3)_2 \cdot H_2O$ in methanol, *L3* and $PdCl_2$ in ethanol and water mixture, *L3* and RuI_3 in methanol, *L3* and $Zn(OAC)_2 \cdot 2H_2O$ in methanol. The obtained complexes with K_2PtCl_4 and $Pd(OAC)_2$ were characterized by XRPD, CHN and IR spectroscopy. To screen for its potential properties, ligand *3-Amino-4,5-dihydro-1-phenyl-1H-pyrazole* was tested for bactericidal and cytotoxic properties.

From the attempts of synthetic reactions of ***2-(3-Aminophenyl)-5-methyl-2,4-dihydro-pyrazol-3-one hydrochloride* (*L4*)** with metal salts: $Cu(NO_3)_2 \cdot H_2O$ (in ethanol), $Zn(OAC)_2 \cdot 2H_2O$ (in DMSO), $Ni(OAC)_2 \cdot 2H_2O$ (in DMSO), K_2PtCl_4 (in water), $CoCl_2$ (in water), $Pd(OAC)_2$ (in water), RuI_3 (in water), no complexes were obtained.

***Amoxicillin trihydrate* (*L5*)** was used in the attempts of synthetic reactions with metal salts: $Cu(NO_3)_2 \cdot H_2O$ (in ethanol), $Zn(OAC)_2 \cdot 2H_2O$ (in DMSO), K_2PtCl_4 (in water), $Pd(OAC)_2$ (in water), RuI_3 (in water), $RuCl_3$ (in water), $Cu(OAC)_2$ (mechanochemical synthesis, methanol/water), $Co(OAC)_2$ (mechanochemical synthesis, methanol/water), $Pd(OAC)_2$ (mechanochemical synthesis, methanol/water), $Cu(NO_3)_2 \cdot H_2O$ (in methanol/water), $CoCl_2$ (in methanol/water). From these reactions a new complex of formulae $[ZnL(H_2O)_2]$, a degradation product *Methyl 5-(4-hydroxyphenyl)-6-oxo-1,6-dihydropyrazine-2-carboxylate,* as well as three more products have been obtained. The obtained complex $[ZnL(H_2O)_2]$ was characterized by XRPD, CHN and IR spectroscopy, while a degradation product *Methyl 5-(4-hydroxyphenyl)-6-oxo-1,6-dihydropyrazine-2-carboxylate* was characterized by XRPD, IR and SC-XRD. Finally, additional three amorphous products have been achieved, yet were not characterized, due to insufficient purity and observed instability.

To screen for their potential application as pharmacologically active ingredients, a selection of the products was made, that have been examined for their thermal, antioxidative, antibacterial and cytotoxic properties.

Contents

1. Introduction

From its discovery, even thou many analogues were produced, after many decades, in the year 1954, *levo-β*-(1-pyrazolyl) the first pyrazole derivative was separated from a natural origin – seeds of watermelons. Pyrazole and its derivatives are known for their diverse biological activities [1–3], ranging from antinociceptive [4–7] and antidepressant [8,9] activities to potentially exhibiting antiallergic [10] properties, with some pyrazole derivatives even demonstrating the ability to inhibit the mutagenic effects of certain carcinogens. Due to the two different nitrogen atoms in the pyrazole ring and the usually simple structure of the pyrazoles, they are significant as ligands in coordination chemistry, linkers for porous coordination polymers and metal-organic frameworks [11,12], as well as precursors for energetic materials [13] or in chemical vapor deposition processes. Due to the ease of coordination, pyrazoles are good candidates for metal ion sensing [14]. Because of their aromatic character, pyrazole-based compounds are also good candidates for the preparation of luminescent metal complexes. Besides the practical aspects, the pyrazole derivatives and their metal complexes can be used for modeling biochemical and enzymatic processes [15]. Numerous pyrazoles also show remarkable catalytic activity [16-18]. Thus, the biologically and potentially pharmacologically active pyrazole-based compounds are the focus of the research activity of our group [19–22]. Besides, some d-metal ions, play vital roles in biological systems. Therefore, investigating the structural characteristics of transition metal complexes with bioactive ligands [19] may yield valuable insights and hold the potential for novel pharmacologically active substances. On the other hand, the detailed structural characterization of the new complexes in correlation with their spectroscopic, thermal, and other physicochemical properties is crucial for the design of new complex compounds with desired pharmacological activities.

In this thesis a thorough review of syntheses of eleven new complexes of *5-(4-Bromophenyl)-3-methyl-1H-pyrazole* (L1), *4-methylpyrazole* (L2) and *3-Amino-4,5-dihydro-1-phenyl-1H-pyrazole* (L3) and *amoxicillin trihydrate* (L5) with a series of transition metals, solved structure for monocrystal of L1, and of the results of additional assays done in order to estimate the different biological potentials of selected obtained products, is given. In addition to the aforementioned results, the thesis also describes the

alternate ways of syntheses that resulted in already described structures - a degradation product of L5 and a complex of L2, with new data conducted from further characterizations and assays conducted, as well as results of syntheses with L5 that could not be taken to further characterization. In order to determine the crystal and molecular structures of the compounds the techniques X-ray powder diffraction, IR spectroscopy, CHN analyses and Single crystal X-ray diffraction were used. Besides the aforementioned, their thermal properties were analyzed, as well as a first screening tests of biological activities, the antioxidative capacity, antibiotic sensitivity testing, cytotoxicity and anticancerogenic properties of selected complexes were determined.

All the used reagents and solvents were of analytical grade and utilized without further purification. During the experimental phase, numerous solvents and metal salts have been used in attempts of different syntheses, yet the focus was set mainly on organic and safe solvents and transition metals with known bioactivity. Most of the obtained complexes were synthesized by dissolving metal salts and ligands in warm solvents separately, and combining them together in 2:1 ligand-to-metal molar ratio, at ambiental temperature. Many further attempts have been carried out with different ligands, metal salts, solvents and methods of synthesis (reflux, mechanochemical synthesis, utilization of catalyzers, variation of solvents used, etc).

2. Theoretical part

2.1. Pyrazole properties

Pyrazoles are five-membered heterocycles containing two nitrogen atoms (positions 1 and 2) that constitute a class of compounds particularly useful in organic synthesis, as well as one of the most studied groups of compounds among the azole family [23]. The name "pyrazole" was given by Ludwig Knorr in 1883. The main representative of this class of compounds is Pyrazole (1,2 diazole). By reduction pyrazoline and pyrazolidine are produced. Pyrazole nucleus integrated in various chemical structures provides potential applications in numerous domains. Nitrogen atoms in pyrazole structure can change their states between "pyridine-like" and "pyrole-like" nitrogen, which is characterized as a tautomeric nature. The prototrophic annular tautomerism (Figure 1) in pyrazoles is a phenomenon where the occurrence of deprotonation of one nitrogen atom occurs and another adjacent nitrogen gets protonated, by a hydrogen atom moving from one nitrogen to another. This is accompanied by a change in structure and changes in the properties of these compounds.

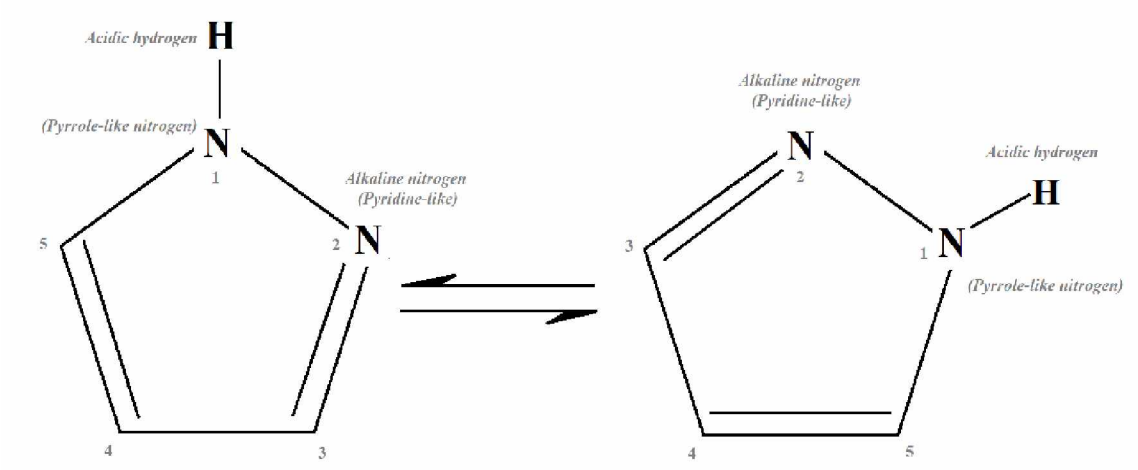

Figure 1. Prototrophic annular tautomerism of pyrazoles

Pyrazoles are rare in nature, with the main reason of the presence of a single (-N-N-) bond in their structure, which is difficult for formation by organisms [24]. With their synthetic origin, pyrazoles are quite reactive and have a grand potential as biologically active compounds. As shown in Figure 1 pyrazoles with their nitrogen atoms unoccupied (N-unsubstituted pyrazoles) have amphoteric properties, whence pyrrole-like nitrogen

donates its proton and pyridine-like nitrogen accepts protons. Another characteristic is that the nitrogen atoms in its structure allow simultaneous donating and acceptance of hydrogen bonds, which favors the establishment of intermolecular interactions [24]. With these properties there is a strong influence from the medium of syntheses conducted with other compounds. As an example, polar and protic solvents favor the reaction with the pyrazole, which means that pyrazole reacts with the solvent much more easily in linear and cyclic oligomers, without formation of pyrazole-pyrazole clusters [25]. These electron-rich heterocyclic systems have three positions with nucleophilic nature (N1, N2, C4) and two electrophilic positions (C3, C5), which serves as an additional argument for their aforementioned reactivity. When the nucleophilic reactions happen, experimentally they dominate on position 4, and other two positions are quite difficult to be reactive. The reason behind is mostly for the nitrogens acting as meta-directors.

There are 3 partially reduced forms of pyrazole: 1-pyrazoline, 2-pyrazoline and 3-pyrazoline, as presented in the Figure 2.

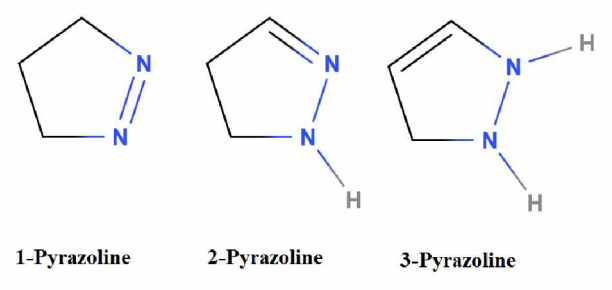

Figure 2. Partially reduced forms of pyrazole

Many pyrazole derivatives have gained application on the clinical level, for their diverse biological activities, antimicrobial, anticancer, cytotoxic, analgesic, anti-inflammatory, antihypertensive, CNS activity like antiepileptic, antidepressant, and others [26].

As previously described, azoles are able to accept or donate H^+ ions, as well as act as hydrogen-bond acceptors or hydrogen-bond donors. The main reason for their importance in supramolecular chemistry is their characteristic to act as hydrogen-bond donor via the N-H group. The melting point of pyrazoles is highly affected by these interactions, hence the 4-methylpyrazole, described in this thesis, is liquid on room temperature, as pyridine. [27]

2.2. Potential of pyrazole derivatives in pharmacology

There is a wide presence of heterocyclic systems in highly used drugs, which gives focus on their critical role in pharmaceuticals. Some pyrazole derivatives have also exhibited various biological activities and high synthetic potential. Out of the top 10 selling medicines in 2010, 8 of these medicines had active pharmaceutical ingredients (API) with heterocyclic systems [28]. As previously stated, pyrazoles are π-excess aromatic heterocyclic systems which makes them favorable precursors for synthetic reactions in pharmacological studies. Many of the APIs are characterized by the presence of a pyrazole core [28 - 30]. Historically, one of the earliest examples is *Phenazone* – or *Antipyrine* (Figure 3), used as an analgesic, antipyretic and anti-inflammatory API. Often classified as nonsteroidal anti-inflammatory drug (NSAID), this compound has been patented in 1883. and presents one of the earliest synthetic APIs. While being popular in use in the time of its origin, today it has been mostly replaced by new APIs as is ibuprofen and similar substances. The active groups within phenazone include the pyrazolone ring – a group believed to be responsible for its pharmacological activity, as well as the methyl and phenyl substituents that seem to enhance its efficacy [29].

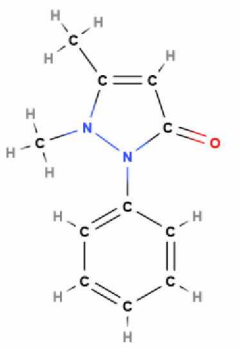

Figure 3. Structure of phenazone

Another well-documented API is *Phenylbutazone* (Figure 4), a NSAID medicine that was used widely, yet was withdrawn from human use due to severe adverse effects and available substitute APIs, with the exception as treatment of ankylosing spondylitis.

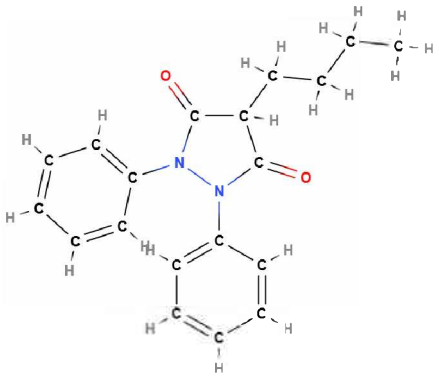

Figure 4. Structure of phenylbutazone

Similarly, *Lonazolac* (Figure 5) is a NSAID substance indicated for the treatment of inflammatory rheumatic diseases of spine and joints. It is a monocarboxylic acid – arylacetic acid derivative, a member of monochlorobenzenes and pyrazoles.

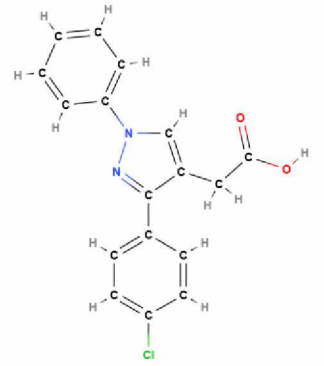

Figure 5. Structure of lonazolac

Another representative is *Rimonabant* (Figure 6). This API was an anorectic anti-obeisty drug, approved in Europe in 2006 but was pulled from the global market in 2008 because of serious psychiatric side effects.

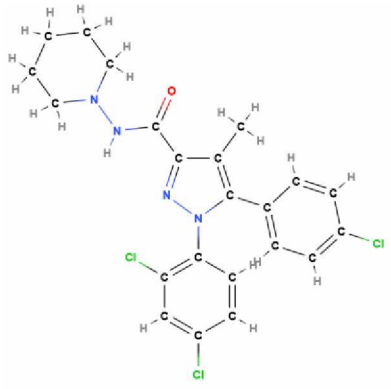

Figure 6. Structure of rimonabant

The pyrazole scaffold is also contained in *Celecoxib* (Figure 7), a NSAID medicine, a COX-2 inhibitor, used to relieve mild to moderate pain and treat the symptoms of inflammation, stiffness and joint pain in arthritis. With its interesting structure, two substituted aromatic rings must keep their adjacent positions for the proper COX-2 inhibition activity, declared by Penning T. D. et al, a team that has been researching structure-activity relationship between many of its derivatives, with results indicating high variations on its derivatives inhibition activity [30].

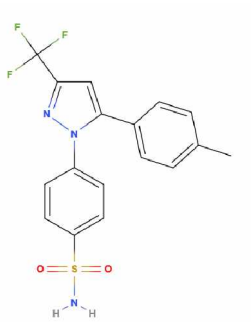

Figure 7. Structure of celecoxib

A great example of an API with a pyrazole core is *Crizotinib* (Figure 8). Crizotinib is an API used to treat non-small cell lung carcinoma. This substance is a *tyrosine kinase inhibitor (TKI)* which was firstly approved for use on humans in 2011, and is a token of advancement in precision medicine for specific patients suffering from lung cancer.

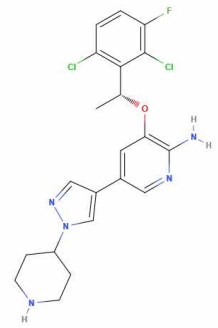

Figure 8. Structure of crizotinib

Another example of a NSAID API with pyrazole core is *Tepoxalin* (Figure 9). Tepoxalin is mostly used in veterinary medicine. It is a unique NSAID for its inhibitory properties of both *cyclooxygenase (COX-1 and COX-2)* and *lipoxygenase (LOX)* enzymes. Tepoxalins' active groups include its ability to inhibit COX-1, COX-2, and LOX enzymes, while its mode of action involves the additional reduction of prostaglandin and leukotriene synthesis, alongside the inhibition of NF-κB activation, which leads to enhanced effects of anti-inflammatory effects [31].

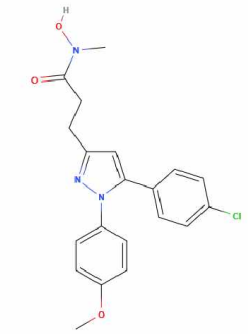

Figure 9. Structure of tepoxalin

Novalgin, *Metamizole* or *Dipyrone* (Figure 10) is used as an analgesic, antipyretic and spasmolytic. This NSAID is unique for its high effectiveness, and use in treating severe pain and high fever, when other NSAIDs prove insufficient. However, it is banned or strictly regulated in many countries, due to its possibility of causing serious side effects.

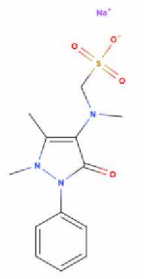

Figure 10. Structure of novalgin

Ramifenazone (Figure 11) also demonstrates analgesic, antipyretic, anti-inflammatory and antimicrobial activities properties. Unfortunately, there is a lack of data concerning this NSAID and its clinical use compared to other substances from this group, so its use is limited. It has limited approval and is more common in research settings than in clinical use.

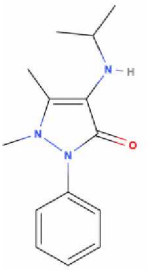

Figure 11. Structure of ramifenazone

As was the case with Tepoxalin, *Deracoxib* (Figure 12) is a NSAID medicine of coxib class used in veterinary medicine. A selective *COX-2* inhibitor, that treats the pain with a lower risk of gastrointestinal side effects compared to most other NSAIDs.

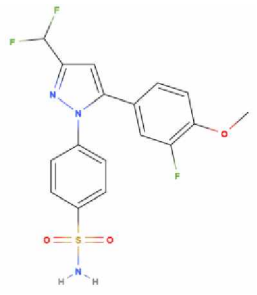

Figure 12. Structure of deracoxib

Pyrazofurin (Figure 13) is a substance with antibiotic, antiviral and anti-cancer properties, yet has not passed its human clinical trials for its detected severe side effects. This powerful *OMP decarboxylase* inhibitor reduces the availability of pyrimidines, and blocks the growth and replication of cancer cells and viruses. Although its serious side effects stop it from being used clinically, research is continued in order to find a way to use its potential.

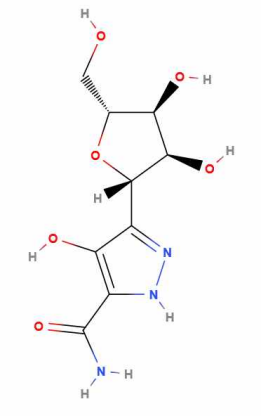

Figure 13. Structure of pyrazofurin

Another example of a representative with a pyrazole ring with great pharmacological potential is *Difenamizole* (Figure 14). With a potential to be used as a NSAID and analgesic medicine, Difenamizole unlike traditional NSAIDs, may modulate some immune responses. Due to limited data, it is not available for clinical use.

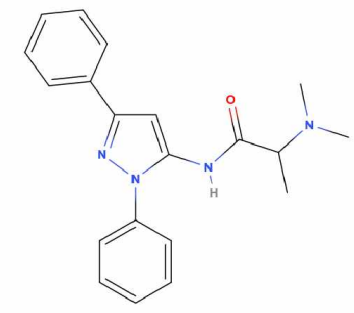

Figure 14. Structure of difenamizole

Furthermore, *Mepirizole* (Figure 15) is a pyrimidine-pyrazole derivative used as a NSAID medicine. The structure of mepirizole features a pyrimidine ring substituted with methoxy

and pyrazole groups, which contribute to its pharmacological activity. Its structure allows meprizole to form complexes with metal ions and influences meprizole to form mostly bidentate structures [32].

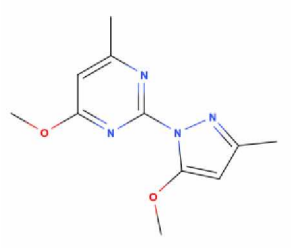

Figure 15. Structure of mepirizole

With many of the previously mentioned examples being NSAID or anticancer agents, *AS-19* (Figure 16) is a representative that is used in the treatment of amnesia caused by medicine. This substance is known to improve long-term memory acquisition, yet hinders short-term memory formation.

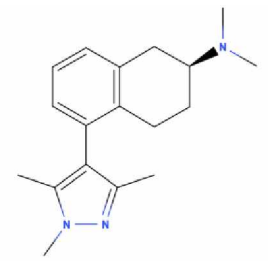

Figure 16. Structure of AS-19

Furthermore, another example of the diverse spectrum of activity is *Mepiprazole* (Figure 17), an anxilytic medicine of the phenylpiperazine group, with antidepressant properties. Recognized for its structure as a pyrimidine-pyrazole derivative, the pyrazole ring affects this compounds ability to bond and act as a bidentate ligand, coordinating through two nitrogen atoms, one from each ring. [33].

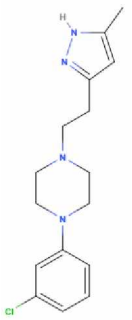

Figure 17. Structure of mepiprazole

In addition to monocyclic pyrazole rings, there are APIs with pyrazole ring fused to a six-membered aromatic ring, usually in positions C4 and C5 of pyrazole ring, such is the example of indazole. Notable example is *Axitinib* (Figure 18), a tyrosine kinase inhibitor API used to treat renal cell carcinoma (kidney cancer). Axitinibs' mode of action is the blockage of proteins that promote cancer cell growth, slowing or halting the progression of cancer.

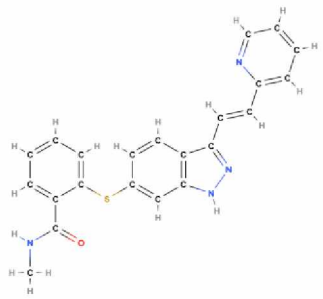

Figure 18. Structure of axitinib

Another fused pyrazole system used as an API is *Zaleplon* (Figure 19). This API belongs to nonbenzodiazepine group and used in medicines to treat insomnia.

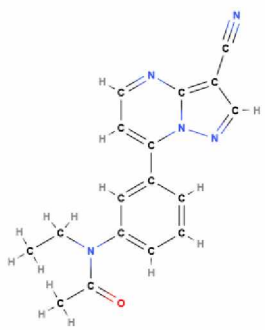

Figure 19. Structure of zaleplon

A widely used API, which is a representative of fused pyrazole systems is *Sildenafil* (Figure 20). This API is used to treat erectile dysfunction and pulmonary arterial hypertension.

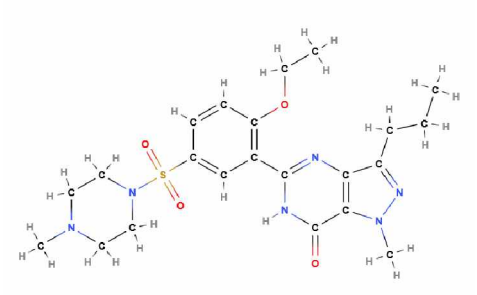

Figure 20. Structure of sildenafil

Furthermore, *Indiplon* (Figure 21) belongs to a group of nonbenzodiazepines, and is used as a hypnotic sedative.

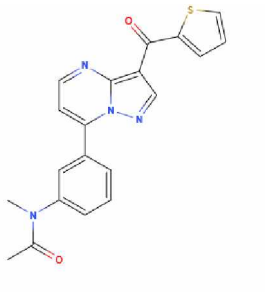

Figure 21. Structure of indiplon

As a last example of APIs with fused pyrazole systems, *Apixaban* (Figure 22) is an anticoagulant used for treating blood clots (thrombosis and pulmonary embolism).

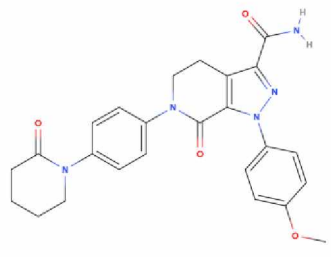

Figure 22. Structure of apixaban

As can be noticed from the list of pyrazole core-containing APIs, the biggest part of pyrazole derivatives presented in the aforementioned list are used as NSAID medicines. Many different compounds are also present, ranging from anxiolytics to antibiotics and oncology APIs. While in the list of APIs containing pyrazole fused to a six-membered ring, in their structure, it can be seen that these examples are quite heterogeneous.

One group of pyrazole derivatives that has shown promising potential in the production of APIs is **aminopyrazoles** (Figure 23) [34]. Aminopyrazoles can have substituted amino groups, free amino groups, or the amino function can be integrated in other heterocycles. The position of the amino group in pyrazole derivatives can affect the biological activity of the complex. For instance, previously mentioned Novalgin and a compound with analgesic properties – Aminophenazone, have their amino group at the position 4. Other than these two aminopyrazoles, there are numerous clinical trials for this chemotype (position 4 amino group pyrazoles) for CDK inhibitors – medicines used as tumor suppressors [34].

Aminopyrazoles with their amino group in position 3, tend to be characterized by their anticancer, anti-inflammatory and anti-infective properties [34,35]. In literature some compounds that are characterized by an aminopyrazole structure, have expressed sub-micromolar activity against Methicillin-sensitive *Staphylococcus aureus* (MSSA) and Methicillin-resistant *S. aureus* (MRSA) [35]. Additionally, there is data on pyrido[2,3-b]indole derivatives that are efficient and able to block Gram-negative strains of bacteria [36]. This position of amino group has also shown HIV-1 reverse transcriptase inhibitory [37], antitumor [38] and anti-inflammatory [39] properties. 3-Aminopyrazoles that show higher values in the term of their antitumour and anti-inflammatory properties, are mostly characterized by unsubstituted scaffolds on N1 position and have bulky aromatic rings on their C4 position [34].

Aminopyrazoles that have their amino group attached at the position 4, show anticonvulsant and antioxidant properties and have the potential to be used as coloring agents [34].

Most diverse, in relation to their biological properties, of all aminopyrazoles are the ones that have their amino group in position 5. These aminopyrazoles have been used as kinase inhibitors, anticancer, antibacterial, antimalarial, and anti-inflammatory agents [34].

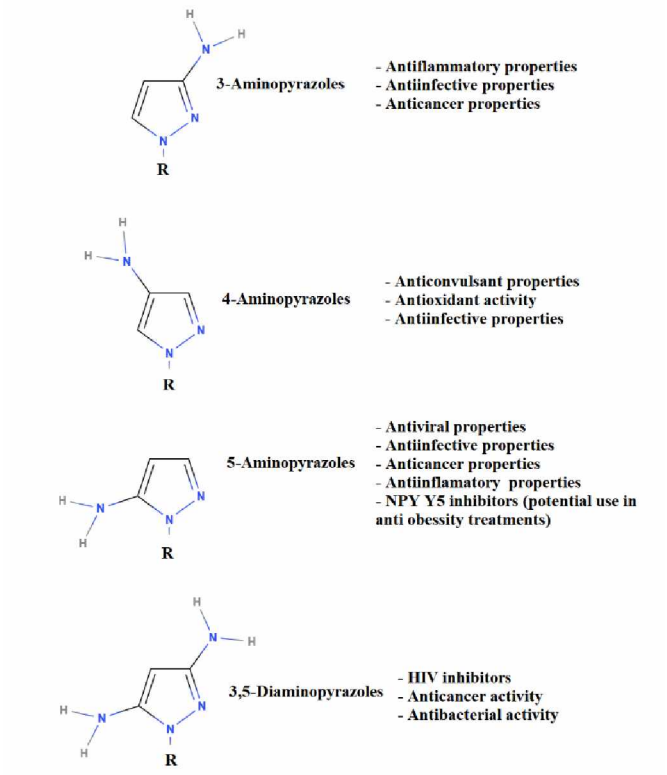

Figure 23. Biological properties of different Aminopyrazoles

Another group of pyrazole derivatives with potential in the production of APIs in the field of anti-inflammatory, antibiotic and analgesic medicines, are pyrazole derivatives with **sulfonamide** moieties. Maybe the most potent representative of this group is sulfaphenazole (Figure 24) – a sulfonamide antibacterial compound used in the treatment of leprosy [40]. Another examples of this potential are aforementioned deracoxib (NSAID) and celecoxib (NSAID).

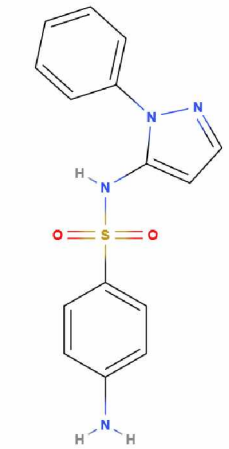

Figure 24. Structure of sulfaphenazole

As these are wide groups of compounds, pyrazole derivatives with alkyl and aryl groups, as are the ligands used in this study, show potential in various fields of application. H. Kumar has indicated that with the addition of aryl or alkyl groups, and the position that they bind to, the obtained compounds can have different effects [41]. One, simple yet effective, example is 4-methylpyrazole used as a ligand in this study. There are many pyrazoles with alkyl and aryl groups, that are used as potential focus points of further substitutions and bindings of different ions or groups.

The addition of halogen elements to the pyrazole structure can have numerous different effects on the derivative. In the comparison of pyrazole derivatives presented by the H. Kumar, addition of halogen elements in some cases enhanced pharmacological properties of the compounds, as are COX 2 inhibitory, anti-inflammatory and antibiotic properties, in some cases characterized as remarkable [41].

2.3. Pyrazole ligands of interest

The ligands investigated in this study include 5-(4-Bromophenyl)-3-methyl-1H-pyrazole (L1), 4-methylpyrazole (L2), 3-Amino-4,5-dihydro-1-phenyl-1H-pyrazole (L3) and amoxicillin trihydrate (L5). A thorough review of the scientific literature revealed that only 4-methylpyrazole and amoxicillin trihydrate have been previously described in published research. For the other two compounds, 5-(4-Bromophenyl)-3-methyl-1H-

pyrazole and 3-Amino-4,5-dihydro-1-phenyl-1H-pyrazole, no scientific papers were found, indicating that these compounds have not yet been explored in detail within the scientific community.

Furthermore, there is no existing data in the literature indicating that 5-(4-Bromophenyl)-3-methyl-1H-pyrazole and 3-Amino-4,5-dihydro-1-phenyl-1H-pyrazole have been utilized as ligands in metal-organic synthesis. Therefore, the present study aims to investigate the potential of these ligands in coordination chemistry and their application in metal-organic frameworks or complexes, contributing novel insights to the field.

Additionally, one more ligand has been initially examined. During the course of the research for this thesis, ligand 2-(3-aminophenyl)-5-methyl-2,4-dihydro-pyrazol-3-one hydrochloride (L4) was subject of experimental evaluation. This compound has shown lower reactivity as well as a high instability of the obtained complex compounds, which resulted in the introduction of a new ligand 3-amino-4,5-dihydro-1-phenyl-1H-pyrazole (L3). During the syntheses of complex compounds, which include L4 and a series of transition metals, compounds that are very unstable or their degradation products that are already known and characterized were obtained, so it was experimentally impossible to characterize them physico-chemically because characterization techniques require stable compounds. Although L4 is, theoretically speaking, structurally suitable ligand for synthesis, repeated experiments in an attempt to obtain stable products with L4 in combination with metals such as Ru, Zn, Ni, Pt, Pd, Co and Cu have not been successful, despite attempts to change the types of syntheses, molar ratios of ligands and metal salts, types and amounts of solvents, etc. Syntheses of L5 with other pyrazole derivatives have also been tested, yet were unsuccessful. Still, even with the difficulties that presented themselves in the process, some of the obtained products of syntheses with L5, are presented as part of this thesis.

2.3.1. 5-(4-bromophenyl)-3-methyl-1H-pyrazole

The molecule presented in the Figure 25. is 5-(4-Bromophenyl)-3-methyl-1H-pyrazole. It consists of a pyrazole ring core, at position 3 of the pyrazole ring there is a methyl

group attached, at position 5 of the pyrazole ring a phenyl ring is connected, which is further substituted with a bromine atom at the para-position on the phenyl ring.

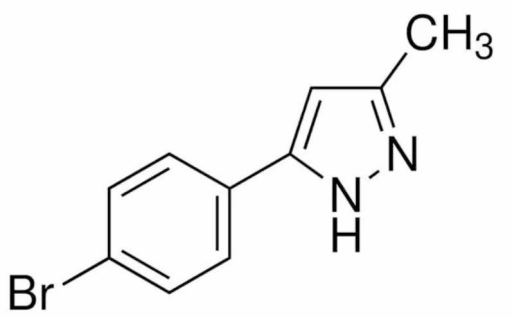

Figure 25. 5-(4-bromophenyl)-3-methyl-1H-pyrazole

2.3.2. 4-methylpyrazole

4-methylpyrazole, also known as fomepizole (Figure 26), is a heterocyclic organic compound, a substituted pyrazole, a pyrazole ring with a methyl group attached to the carbon at position 4 of the ring. The presence of the methyl group at this position of the pyrazole ring changes the distribution of electrons and steric effects of the molecule. This change in steric effects influences the reactivity and interaction with metal centers in coordination chemistry, and makes fomepizole more suitable for synthesis of complex compounds.

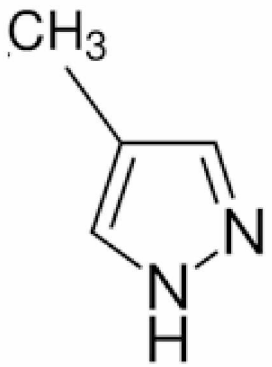

Figure 26. 4-methylpyrazole

4-methylpyrazole is best known for its use in methanol or ethylene glycol poisonings, where it's used as an antidote with its properties to inhibit the enzyme alcohol dehydrogenase, thus preventing the metabolism of methanol and ethylene glycol into their harmful metabolites. There is still a lack of data available for fomepizole complexes, yet this compound has shown great results in its use as ligand in metal-organic syntheses.

2.3.3. 3-amino-4,5-dihydro-1-phenyl-1H-pyrazole

3-amino-4,5-dihydro-1-phenyl-1H-pyrazole (Figure 27) features a 2-pyrazoline ring, with a phenyl ring at position 1 and an amine group at position 3. Amino group attached to the pyrazoline ring contributes to the molecules nucleophilicity and basicity, which makes it more susceptible for complex formations.

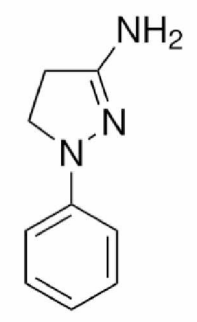

Figure 27. 3-amino-4,5-dihydro-1-phenyl-1H-pyrazole

2.3.4. 2-(3-Aminophenyl)-5-methyl-2,4-dihydro-pyrazol-3-one hydrochloride

2-(3-Aminophenyl)-5-methyl-2,4-dihydro-pyrazol-3-one hydrochloride (Figure 28) consists of a 2-pyrazoline ring, with a phenyl ring at position 2, a carbonyl group at position 3 and a methyl group at position 5. There is an amino group attached to the phenyl ring at position 3, that creates nucleophilic spot of this compound, and with that showing potential as an additional place for bonding and complex formations.

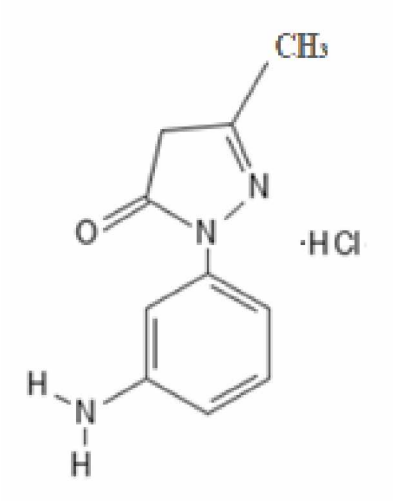

Figure 28. 2-(3-Aminophenyl)-5-methyl-2,4-dihydro-pyrazol-3-one hydrochloride

2.4. Complexes of pyrazoles and its derivatives

In addition to their quite vast biological and synthetic applications, numerous pyrazole derivatives have been used in further syntheses in order to form metal complexes. The pyridine-like nitrogen being the focus point of interactions. This electrophilic position in pyrazole enables easier reactions with transition metals, yet as aforementioned pyrole-like nitrogen can be reactive as well, in circumstances as are heightened pH value of the medium, the reactions can result in egzobidentant nitrogen coordination, with two metal ions connected to both of the nitrogens. From the more complex formations the interesting compounds utilized as ligands are Tris(1-pyrazolyl)borates, also known as scorpionates.

The syntheses of pyrazole complexes are dominantly conducted through substitution reactions of N-H group of the pyrazole ligand. Depending on the properties of ligands used, as well as metal ions and the conditions (solvents, temperature, procedure, etc) of the process the number or possible outcomes of syntheses varies significantly. Even by using the same ligands and metal ions, multiple products - complexes can be obtained. Such a case is presented in this thesis.

The ligand-metal reactions of pyrazoles, and their coordination have multiple effects:

- increase of the acidity of the pyrazole N-H group due to pyridine-like nitrogens' electron donation to the Lewis acidic metal center; With this more acidic nature of the N-H group, the probability of pyrazolate complex is increased through deprotonation by even the slight increase in pH value of the medium in which the synthesis is conducted. Even if the deprotonation does not take place, the N-H group will most likely act as a hydrogen bond donor [42].
- pyrazole placement in proximity of other ligands with possible intramolecular hydrogen bonding. The establishment of intramolecular hydrogen bonding affects the coordination of the complex obtained as well as its properties.

As for pyrazole coordinations, they can be found in both catamer and cyclic oligomer forms (Figure 29). These formations affect the aggregation state of pyrazoles. If the substituents are less bulky (lower in molar mass), they form catemers or trimers (the case of 4-methylpyrazole). These formations usually result in lower melting points. It is interesting that the melting point of 4-methylpyrazole is at 25°C, which is drastically lower than the pyrazoles' at 66°C. The reason behind this phenomenon is the inability of the trimeric structure to form extended hydrogen bond formations, on the contrary of catemer structures formed by pyrazole. Bulkier substituents are more probable to form dimers, tetramers or even hexamers. Other than the previously-stated, solvents have effect on the aggregation of pyrazoles. Solvents with higher ability to act as hydrogen-bond acceptors, are more prone to interact with the pyrazole molecules themselves, while on the contrary, more inert solvents allow for more intensive intermolecular hydrogen bonding between pyrazole molecules [43].

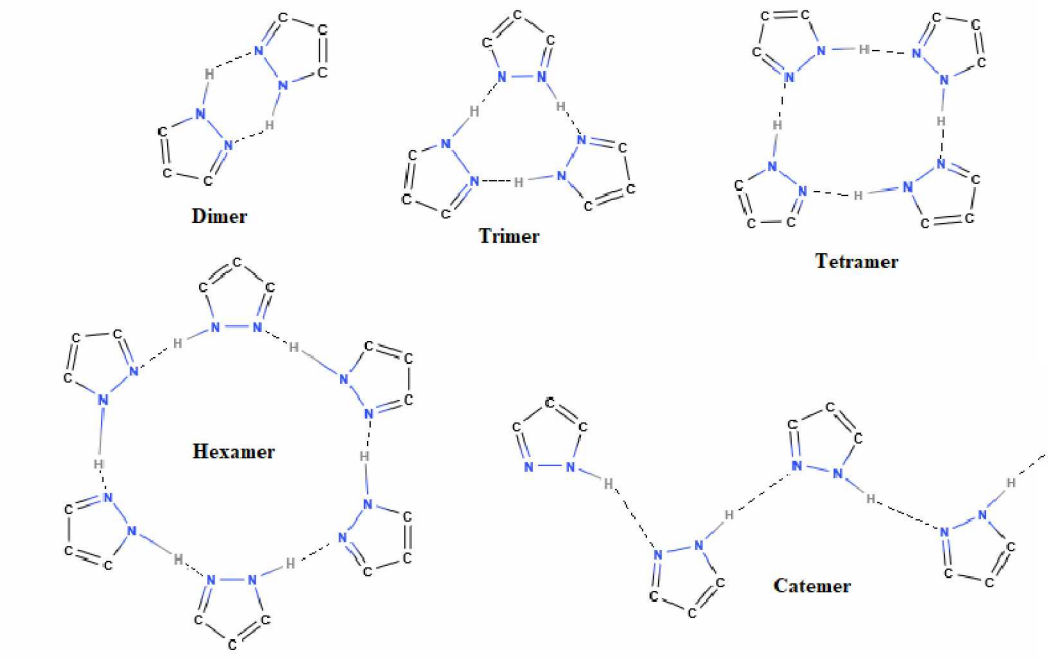

Figure 29. Pyrazole coordinations (oligomers)

In their reactions with metal precursors, the properties of a pyrazole derivatives are heavily influenced by the properties of the substituents. This effect and the possible outcomes of a synthesis are well represented in reactions of $TiCl_4$ and pyrazole derivatives (Figure 30) [44].

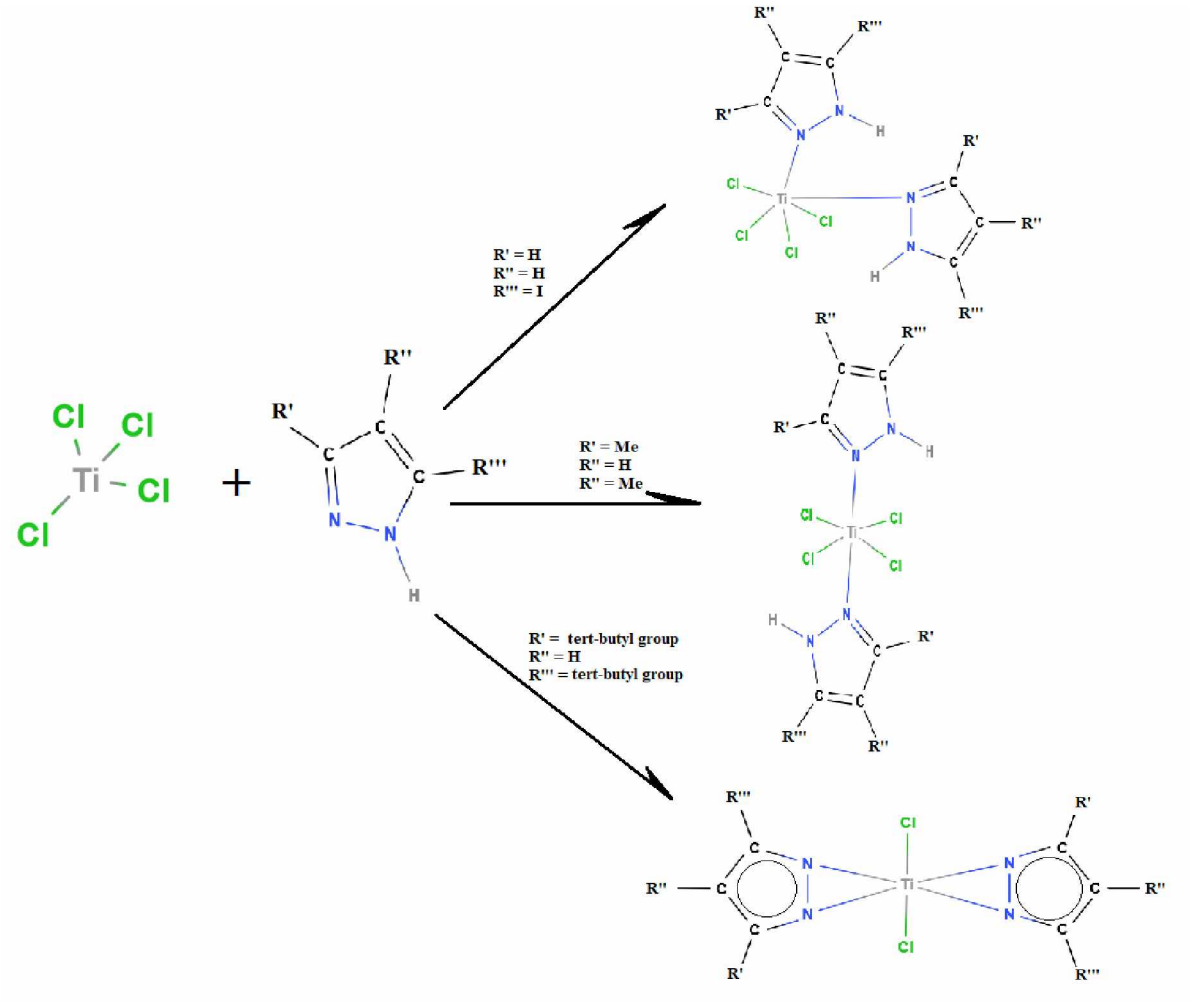

Figure 30. Influence of substituents on outcomes of syntheses in reaction of $TiCl_4$ and pyrazole derivatives

In addition to prototropic tautomerism, which is characteristic in pyrazoles, the phenomenon of metallotropy is also present, yet kinetically more difficult [43]. This equilibrium occurs in complexes of pyrazoles with metals, as presented in Figure 31.

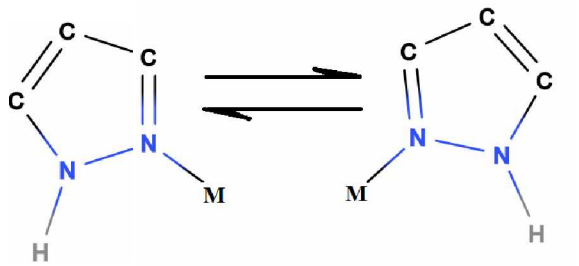

Figure 31. Metallotropy in pyrazoles

The number of derivatives that can be obtained with the same metal ion can be different (most often between 1 and 6 derivatives), which depends on numerous factors: nature of the metal ion, coordination abilities of the ligand-partner, the position and number of substituents on the pyrazole ring, etc.

The pyrazolato anion mostly bonds exobidentately (bridged) to two same or different metals or metalloids, which results in a di- or polymeric structures. As an interesting example of polynuclear complexes, the structure of the tetranuclear complex Cu(II) with 1H-pyrazole, this metallocage complex is presented in the Figure 32 [45]. The association of four Cu(II) ions and two azamacrocyclic receptors in which two ligand units are connected by 1,5-Diaminopentane can be seen from the figure. Parallel dimeric cage formations of complexes show almost square planar geometry, resulting in the red color of the crystals obtained.

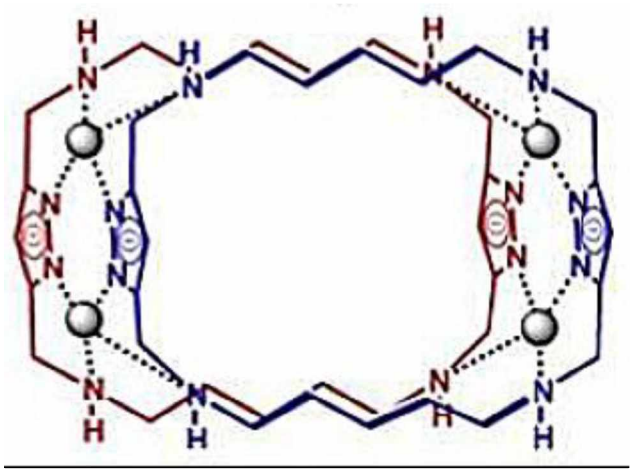

Figure 32. Tetranuclear complex Cu(II) with 1H-pyrazole (example of an exobidentately bound complex)

With exobidentate coordination of the pyrazolato ion mentioned to dominate the obtained structures of complex compounds, there are rare examples of endobidentate coordinations. An example of endobidentate coordination is presented in the Figure 33 as the Ti(IV) and 3,5-disubstituted complex [46].

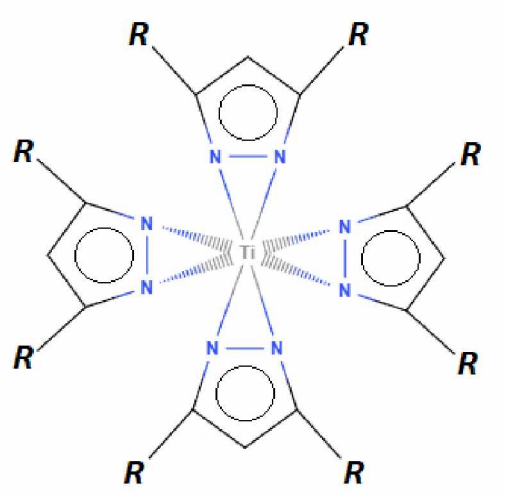

Figure 33. Ti complex [$Ti(\eta^2\text{- }R_2pz)_4$] (R= Me,Ph)

In cases when the substituent in pyrazole derivatives contain donor atoms (such are O, N, S, P), the bond to the metal ion can also be realized through the heteroatom of the substituent. In this way, ligands can achieve higher denticity, between 2 and 6, or more [47].

As an example of potential of higher denticity of pyrazole derivatives in complex compounds a bispidine pyrazole-based hexadentate ligand is presented in the Figure 34 [48]. Synthesis of the aforementioned ligand was realized through multiple steps that include double amino alkylation between 1,3-diphenyl-2-propanone, bis(pyrazolyl)ethanamine and paraformaldehyde by method of reflux in ethanol with acetic acid as reagent (described as a double Mannich reaction).

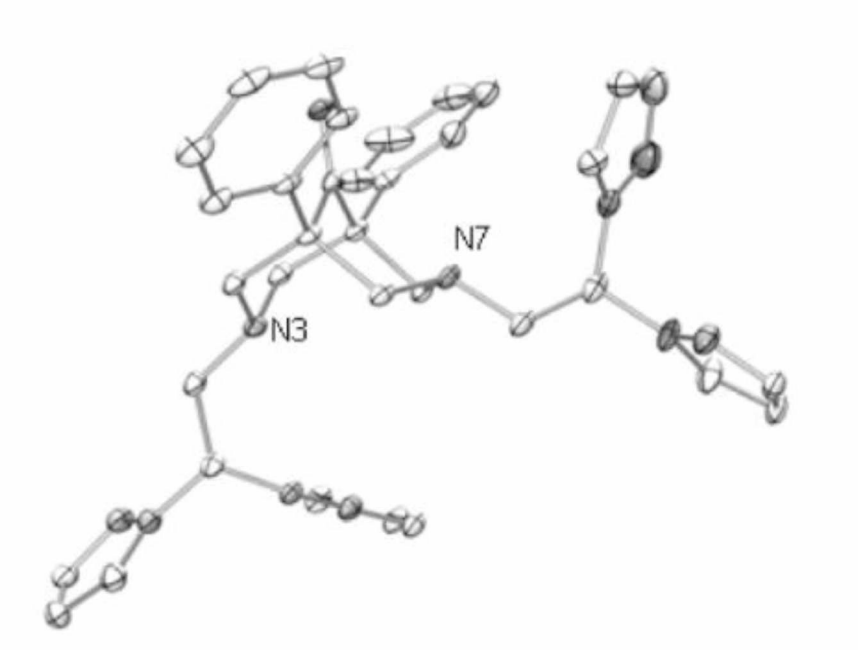

Figure 34. Bispidine pyrazole-based hexadentate metal-free ligand

A crystal structure of the ligand in question shows high potential and stability in its boat–chair conformer form. The reason being the electron pair repulsion and the large formation of the amine substituents (N3 and N7 bispidine atoms). With the addition of metal ion, the structure adopts the chair–chair formation (Figure 35).

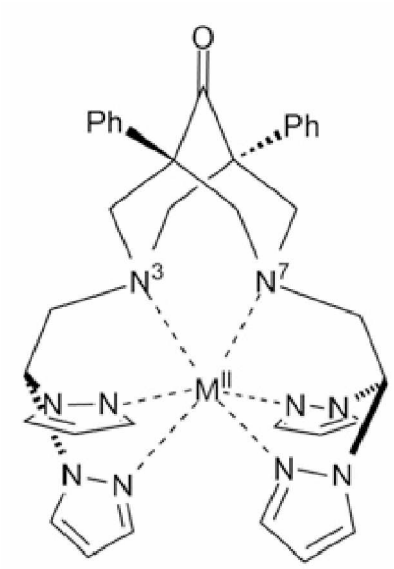

Figure 35. Structure plot of M-ligand complexes

As can be seen from the Figure 36 both trigonal planes are made up of one of the tertiary amines from the bispidine backbone (N3 or N7) and the two appended pyrazolyl donors.

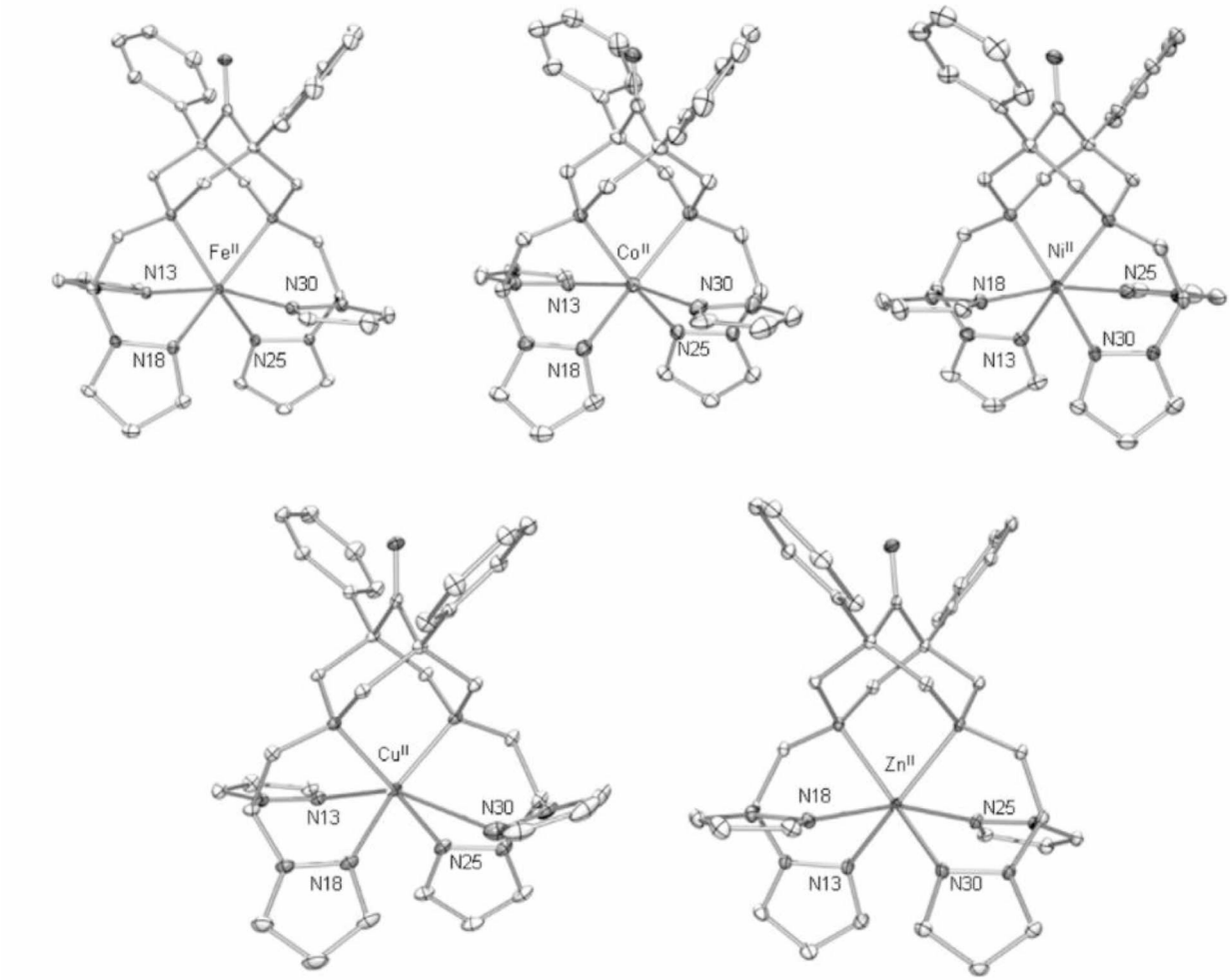

Figure 36. Experimental structures of the M -complexes with the pyrazole-based ligand

The complexes obtained with the same bispidine pyrazole-based hexadentate ligand and a series of transition metals (Figure 36), display somewhat flexible fragments of the octahedral complex. The result of this is a less strained complex, especially as pyrazole groups have free rotations and the nitrogen donors are fixated in a stable structure with the metals acting as its anchor [48].

In 1966 a novel and versatile class of ligands was introduced, combining characteristics of both cyclopentadienide and beta-diketonate ligands. Since their discovery, nearly two

thousand scientific papers have been published exploring the chemistry of these ligands and the complexes with 70 different elements from the periodic table have been reported. This structurally quite interesting class of pyrazole derivatives are poly(1-pyrazolyl) borates, known as scorpionates due to the way of twisting and the possible binding of the pseudoaxial group R to the metal ion. With a general formula of $[R_nB(Pz)_{4-n}]^-$, where n= 0, 1 or 2, Pz= pyrazol-1-yl group, and R= H, alkyl or aryl group (Figure 37 and 38) [49].

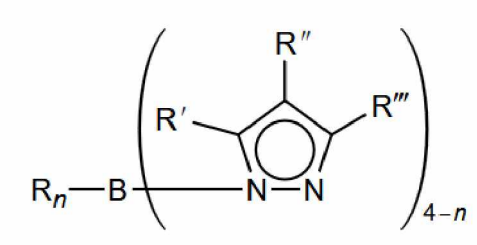

Figure 37. General structure of polypyrazolylborate anions

The name „scorpionates“ describes the formation of the bonding of the ligand, as two pyrazolyl groups resemble pincers, and the R' the tail of the scorpion.

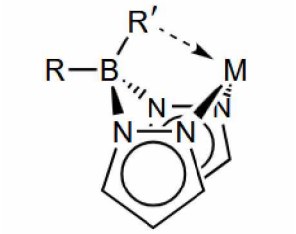

Figure 38. Bonding in polypyrazolylborate-metal complexes

Tl scorpionate complexes with ligands where n=1 and R=H (as presented by the structure in Figure 39) $[HB(pz)_3]$ are almost always monomeric in the crystal [49]. An exemption of this, and an example of the interesting structures scorpionates can create, is the tetrameric complex of Tl, with cyclopropyl in its structure. This structure is a tetrahedron of Tl presented in a Figure 39.

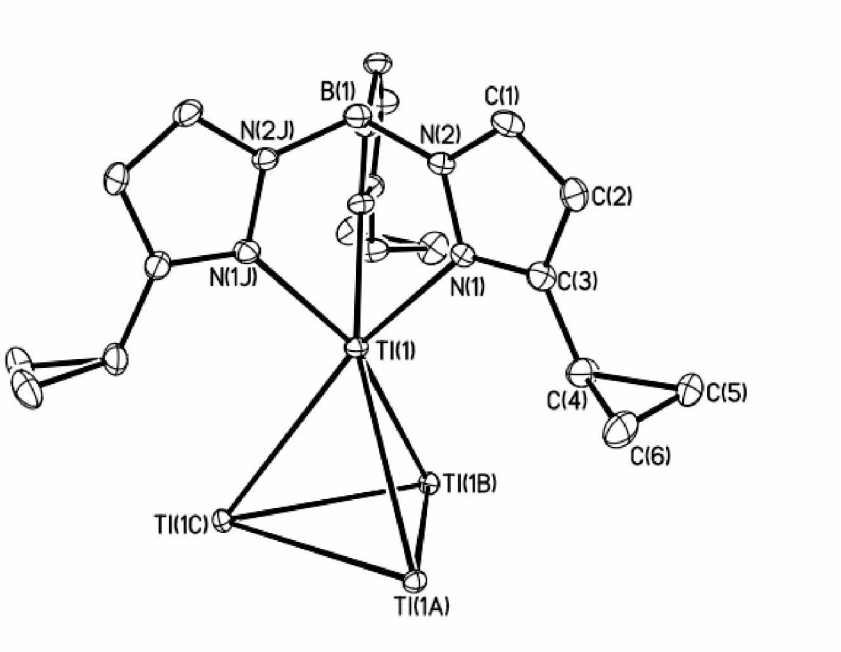

Figure 39. The structure of tetrameric complex of Tl (with three apical ligands omitted for clarity)

Another interesting complex of scorpionate structure (Figure 40) is presented in the same paper as the previous with further structural modeling of the same parent tridentate ligand $[HB(pz)_3]$. This complicated La complex described by authors with formulae $[La[Tp^{CONHtBu}]_2]^+$ (Tp= $HB(pz)_3$; *t*B*u*= *3-t-butyl group*) shows La as the nucleus of the complex holding the structure firmly, due to properties of Lanthanum.

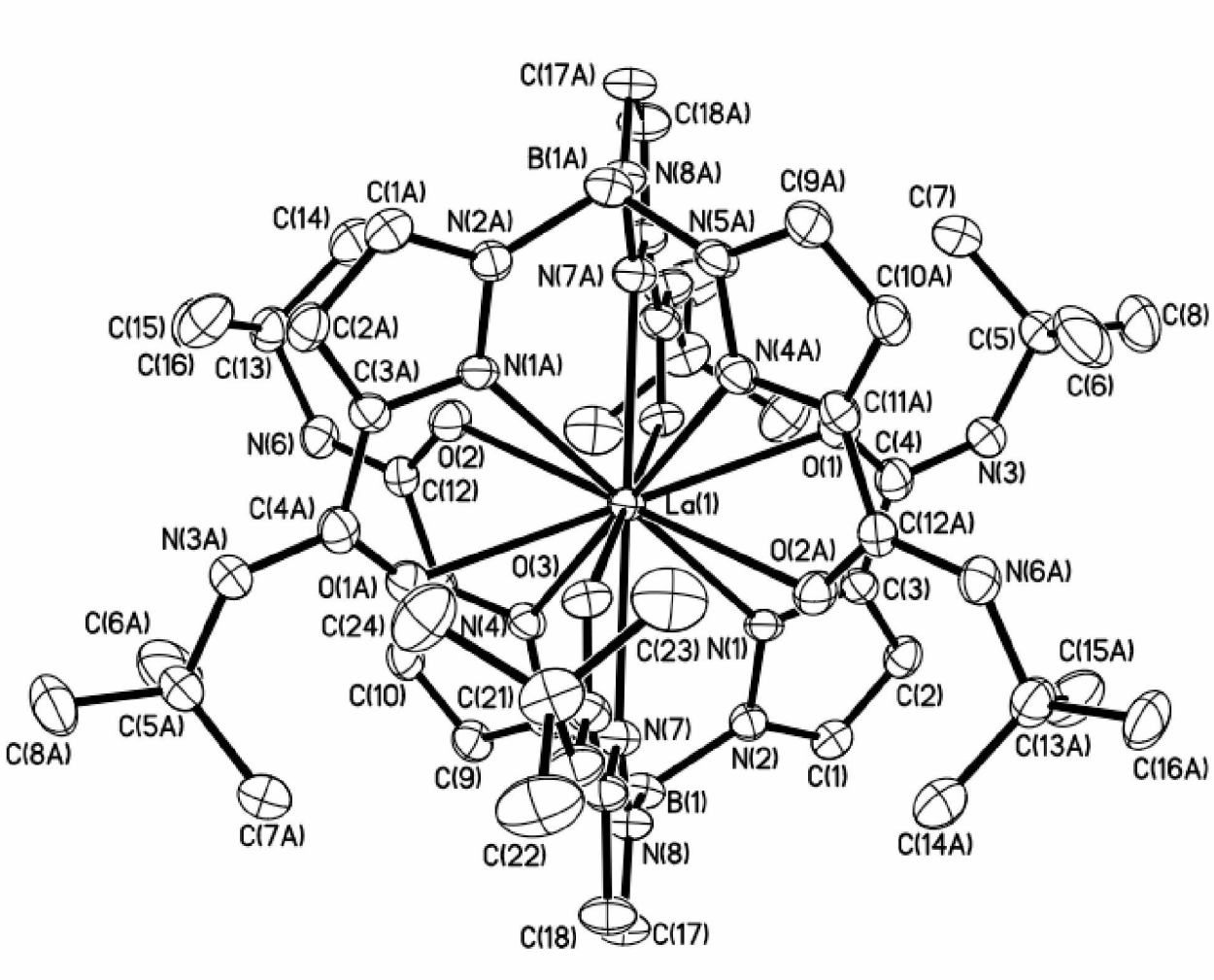

Figure 40. Structure of the complex $[La[Tp^{CONHtBu}]_2]^+$

2.4.1. Cancer treatment potential of pyrazole complexes with transition metals

Pyrazole and its derivatives bond to metal atoms as monodentate or bridging bidentate ligands and this strong affinity towards metals may lead to the formation of metal-organic frameworks [50]. N–H/N hydrogen bonding is prevalent interaction in the assembly of pyrazolyl molecules [51]. Their hydrogen bonding capacity may lead to the formation of extended molecular networks [52].

Over the past several decades, pyrazole complexes with transition metals have attracted growing interest in numerous researches. One of the pioneers of pyrazole complexes used in this field of research was *cis-dichlorobis(pyrazole)platinum(II)* [53]. This complex has

shown anticancer properties [54]. Many more pyrazole and its derivative complexes have since been synthesized and have gone through experiments in search for possible therapeutic effects for treating cancer [47-55], antimicrobial properties [55- 63], anti-viral agents [63- 65], etc. Given that the pyrazole motif makes up the core structure of numerous biologically active compounds, pharmacological interest in pyrazole-derived compounds is growing [53].

For anticancer activity and pyrazole complexes the research began at the start of this century with the discovery of platinum complexes that have exhibited anticancer activity against several human colorectal cell lines, human gastric cell line AGS and murine leukemia cells L1210 [53]. The activity of one pyrazole-Pt complex has stood out, with its activity being similar to that of cisplatin, with IC_{50} values ranging from 2.1μM to 6.5 μM for all tested human cell lines, and IC_{50} of 4.6μM for murine cell lines. Dichloro-bis(pyrazole)platinum(II), the compound discussed (Figures 41 and 42) has shown promising activity, close to that of cisplatin, yet its therapeutic use is somewhat limited due to its toxic side effects [74].

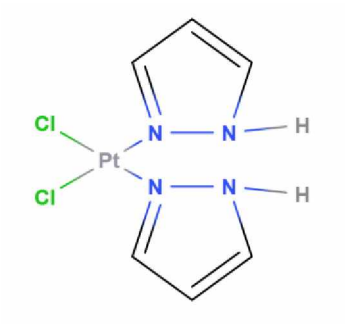

Figure 41. Dichloro-bis(pyrazole)platinum(II)

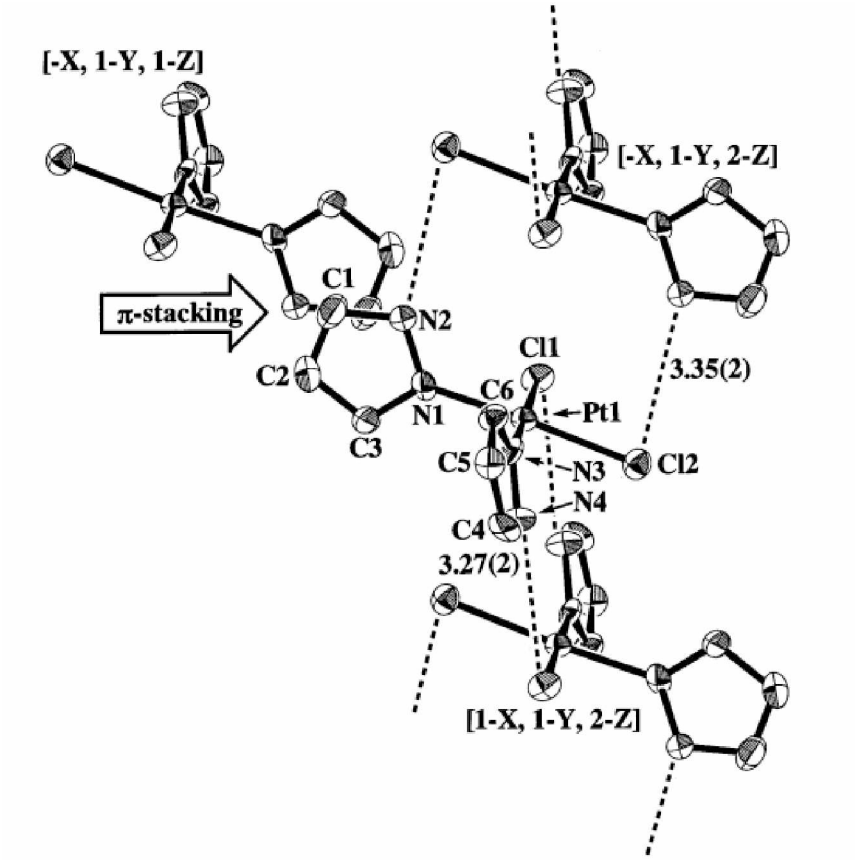

Figure 42. Structure of dichloro-bis(pyrazole)platinum(II)

Numerous other pyrazole complexes have been tested for anticancer activity, and some of them have shown promising results. A selection of these complexes are presented in the Table 1.

Table 1. Pyrazole derived complexes with high cytotoxic activity

Compound	IC_{50} value and cell line	Reference
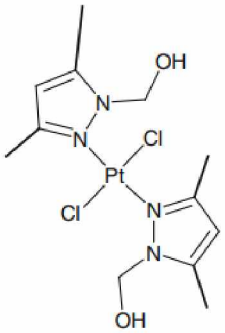	3.5 μM L1210 murine leukemia cells (cisplatin reference 1.2 μM)	[53]

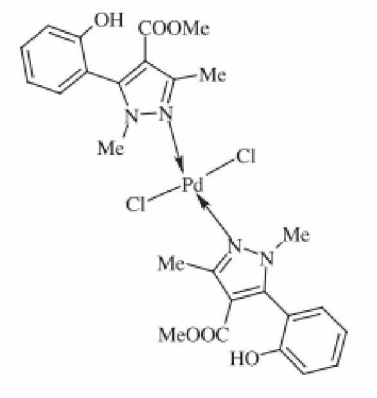	8.9 µM for NALM-6 25.7 µM for HL-60 NALM-6 human leukemia cells (cisplatin reference 0.7 µM) HL-60 human leukemia cells (cisplatin reference 0.7 µM)	[75]
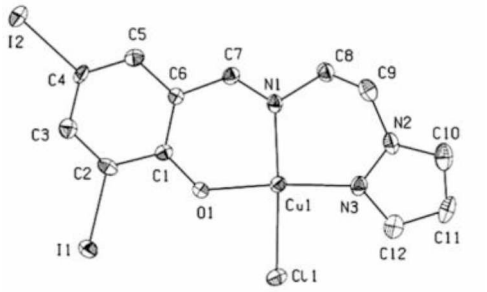	39 µM for PC-3 26 µM for MCF-7 PC-3 human prostate cancer cells (cisplatin reference 51 µM) MCF-7 human breast cancer cells (cisplatin reference 28 µM)	[76]
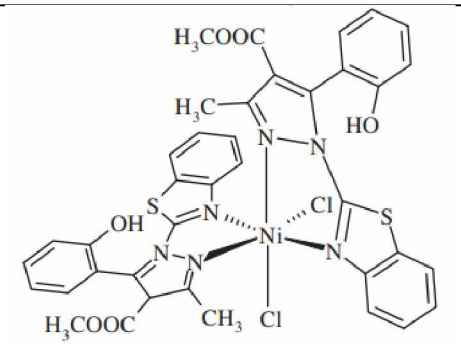	8.0 µM NALM-6 human leukemia cells (cisplatin reference 0.7 µM)	[77]

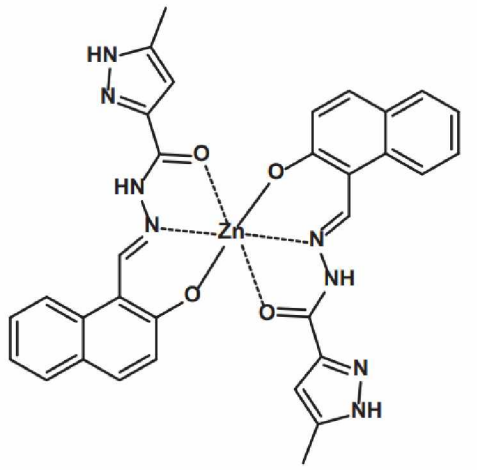	35 µM for PC-3 0.5 µM for MCF-7 PC-3 human prostate cancer cells (cisplatin reference 57 µM) MCF-7 human breast cancer cells (cisplatin reference 21 µM)	[78]
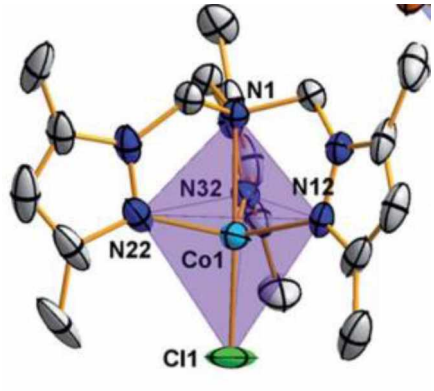	21.3 µM for A549 1.3 µM for CaCo-2 A549 human prostate cancer cells (cisplatin reference 17 µM) CaCo-2 human breast cancer cells (cisplatin reference 5.6 µM)	[79]

For organometallic complexes, there is an interest in synthesizing novel complexes with gold(III), especially with their potential as anticancer agents. However, these complexes have been studied less than expected, as for their instability and proneness to rapid reduction. To improve their potential to be used as anticancer APIs, it is suggested that ligands with strong binding affinity, especially ones containing atoms that act as hard base donors, might be the answer for potential stabilization of gold(III) complexes [79,80].

2.5. Amoxicillin properties

Amoxicillin (Figure 43) is a semisynthetic penicillin that has been in use since the 1970s. It remains one of the most widely prescribed penicillins globally, both on its own and in combination with the β-lactamase inhibitor (BLI) clavulanic acid. Recognized by the World Health Organization (WHO) as a "core access antibiotic," amoxicillin is an aminopenicillin derived by adding an amino group to the penicillin structure to enhance its effectiveness against antibiotic resistance. This medication is used to treat infections caused by beta-lactamase–negative bacteria, including those affecting the ear, nose, and throat, lower respiratory and urinary tracts, acute bacterial sinusitis, skin and soft tissues, and for the eradication of *Helicobacter pylori* [82].

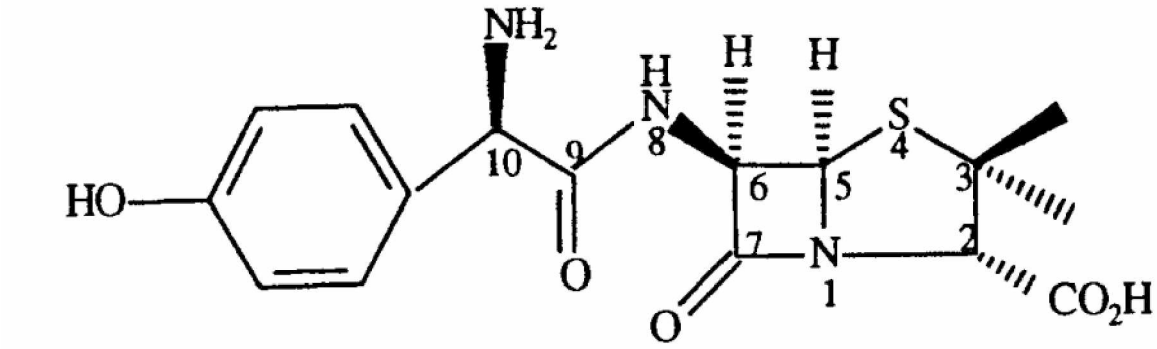

Figure 43. Structure of amoxicillin

The limited spectrum of penicillin prompted the search for derivatives with bactericidal activity against both Gram-positive and Gram-negative bacteria. The first significant breakthrough was ampicillin, developed by scientists at Beecham Laboratories in the United Kingdom and introduced in 1961. Amoxicillin was subsequently derived from ampicillin and launched in 1972 by Beecham as a novel semisynthetic penicillin. Structurally, amoxicillin differs from ampicillin by the addition of a hydroxyl group to the benzene ring (Figure 44) [82].

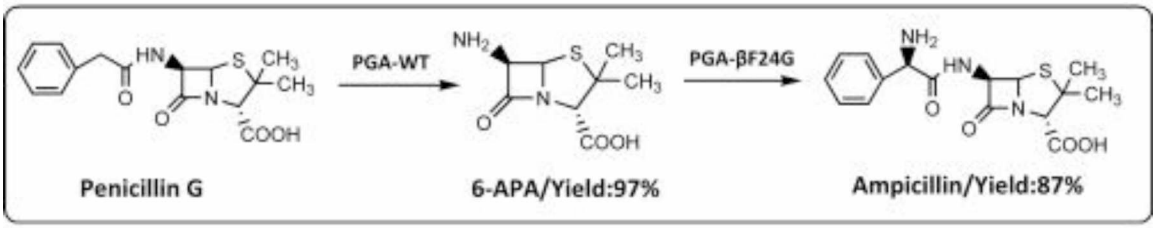

Figure 44. Synthesis of Ampicillin from Penicillin

Clavulanic acid, a substance commonly used with amoxicillin, while containing a β-lactam ring, has minimal antibiotic activity on its own. Instead, it functions as a "suicide inhibitor," irreversibly binding to bacterial β-lactamase enzymes, thereby protecting amoxicillin and other penicillins from hydrolysis [82].

The bactericidal effect of amoxicillin is exerted by targeting penicillin-binding protein (PBP) 1A, an enzyme crucial for bacterial cell wall synthesis. The β-lactam ring of amoxicillin opens and acylates the transpeptidase domain of PBP 1A, leading to irreversible inactivation. Without functional PBP 1A, bacteria are unable to synthesize peptidoglycan, a critical component of the cell wall. This disruption halts cell wall elongation, increases permeability, and ultimately causes cell lysis and death [82].

What is interesting in its structure, is that the amoxicillin may be found in an aqueous medium as a cation while pH < 3, zwitterion in the range of pH 3−7.5, or anion with pH 7.5-10 (Figure 45) [85]. Amoxicillin contains three sites that may reversibly dissociate a proton to form a negative charged anion. Amoxicillin may donate a proton from the carboxylic group, a proton from the amine group, as well as from its phenol group.

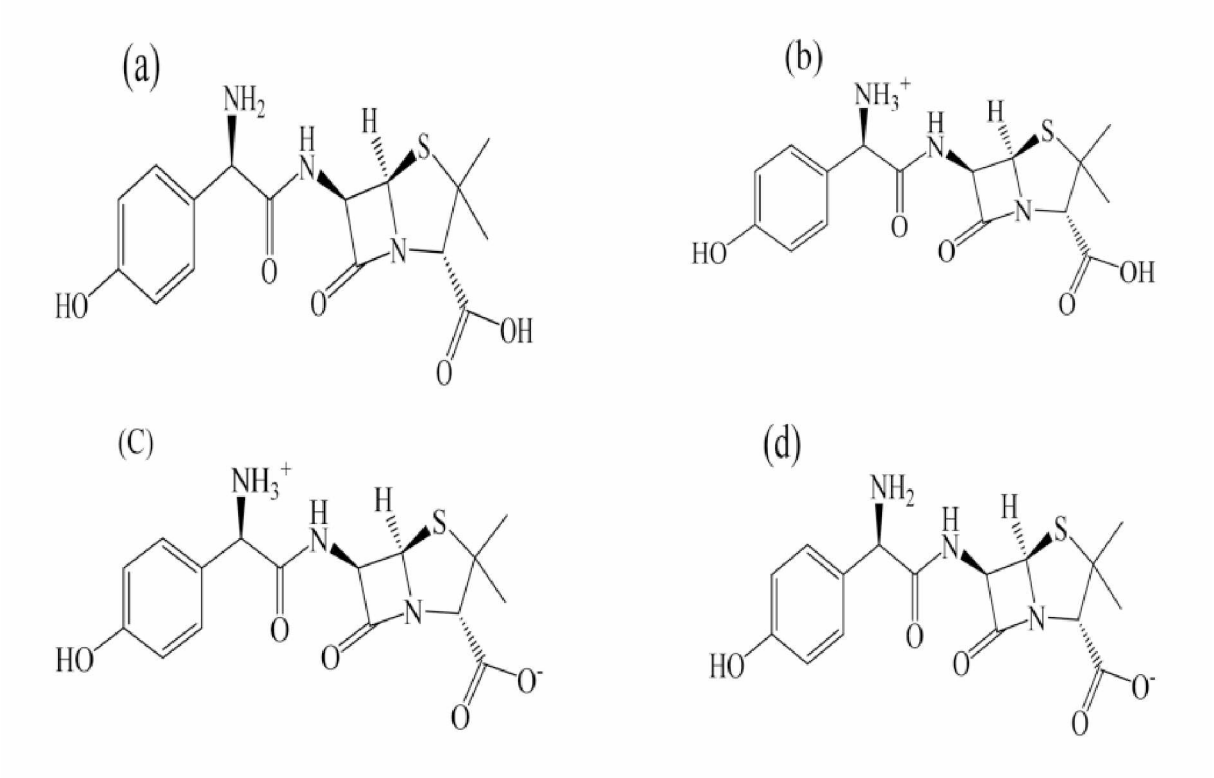

Figure 45. Structure of amoxicillin at different pH (a) Amoxicillin - solid state, (b) Amoxicillin - pH< 3, (c) Amoxicillin - pH 3-7.5, (d) Amoxicillin - pH 7.5-10

2.5.1. Complexes of amoxicillin

One approach to tackling antibiotic resistance involves enhancing the effectiveness of existing antibiotics by chelating them to develop new, more potent APIs. Transition metals, even in trace amounts, exhibit unique coordination properties and chemical reactivity. These properties allow them to form complexes with APIs, using the antibiotics as ligands. By coordinating with the metals, antibiotics gain the ability to inhibit microbial growth through novel mechanisms, significantly improving their antimicrobial activity. As a result, metal-antibiotic complexes are often more effective than antibiotics in their free form. This is attributed to their ability to act as complexing agents for metal ions, enabled by the presence of multiple electron donor atoms in their molecular structure [86,87].

Amoxicillin shows high potential for creating complex compounds with transition metals. And as described in some journals that have dealt in this matter, complexation of amoxicillin was achieved with numerous elements (such as: Zn(II), Co(II), Ni(II), Cu(II),

Fe(III), even La(III), Ce(III), Sm(III) and Y(III)). The proposed structure for these metal complexes is in most part presented as is in Figure 46.

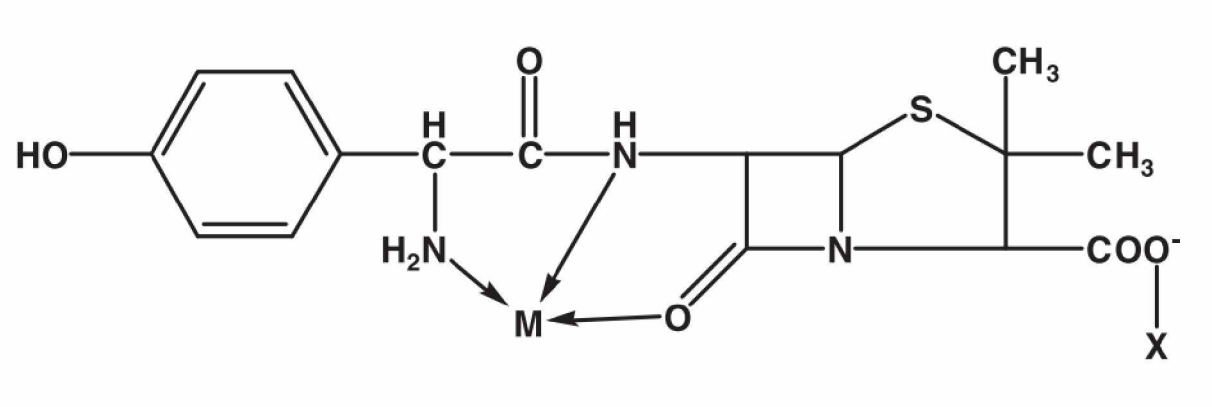

Figure 46. Structure mostly proposed for amoxicillin metal complexes

It was demonstrated that amoxicillin forms complexes with Fe(II), Co(II) and Mn(II), resulting in the formation of $M(Amx)_2Cl_2$ complexes (Figure 47) [88]. As stated, the characterization of these complexes through IR spectroscopy indicated that amoxicillin acts as a bidentate ligand, coordinating to the metal ions via its carboxyl and carbonyl groups [88]. Additionally, the role of copper(II) ions has been highlighted in the electrochemical detection of amoxicillin, suggesting that the formation of metal-amoxicillin complexes can influence the antibiotic's redox behavior [86].

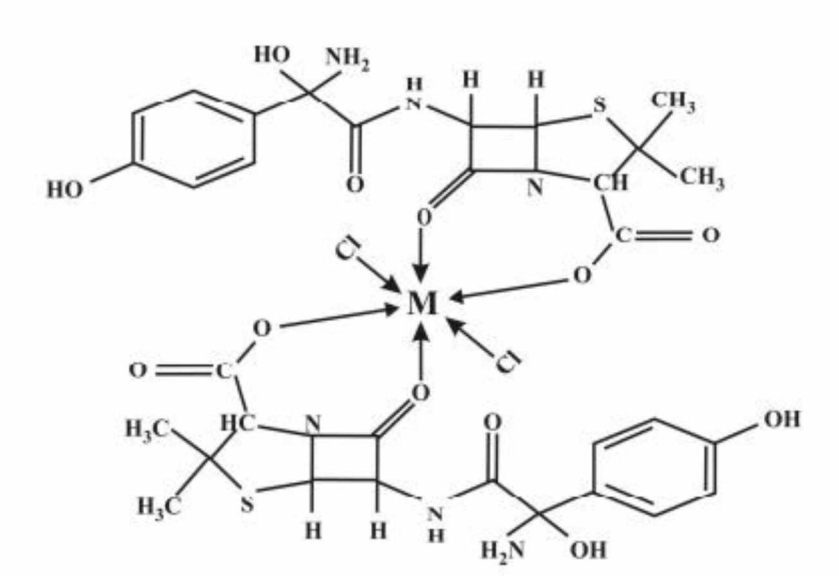

Figure 47. Proposed structure of amoxicillin complexes

Additionally, in some examples throughout literature it was stated that the obtained transition metal complexes with an amoxicillin-derived Schiff base, make an octahedral geometry. For the complexes in question, the characterization has been conducted through utilization of UV-Vis and EPR spectroscopy [89].

What can be noticed through literature review, is that most of the results for amoxicillin-metal based complexes is that there have not yet been single crystal structures of complexes reported so far, as was reported, and very low occurrence of crystalline products [89]. Additionally, big part of available literature shows that the stated obtained complexes were characterized and confirmed through means of:

- Potentiometric pH data (indication of complex formation in this paper was the release of proton H^+) – Stated complexes with Co(II), Cu(II), Ni(II), Zn(II), Eu(III), Tb(III), and a series of amino acids [85],
- UV-Vis and IR measurements – Stated complexes with Cu(II), Fe(II) and Zn(II) [86],
- Potentiometric pH data, UV-Vis, IR measurements and thermal analyses – Stated complexes with Cu(II), Fe(II) Co(II), Ni(II) and Zn(II) [87].

As most of the complexes obtained are amorphous, the structures of complexes have mostly been proposed without definite structural analysis, and as the behavior of the amoxicillin changes in different pH values of the environment, amoxicillin will prove to be a challenge for the syntheses of stable complexes with transition metals.

2.6. Potential uses of transition metals in pharmacology

Metal ions have been used in syntheses of various APIs, metalloenzymes and imaging agents. Syntheses of transition metal complexes with radioactive isotopes resulted in widely used radiopharmaceuticals and MRI contrast agents [90]. Many APIs today contain metal ions such as Pt, Pa, Cu, Ni, Zn, Au, Fe, Tc, Gd, Mn, Co, Sm, etc [91].

2.6.1. Copper

Copper (Cu) is a Group 11 chemical element, a red ductile metal. In its ionic form, copper has high affinity for ligands, which makes it one of the most used metals for metal-ligand syntheses. With its affinity to bind, in biological systems, all measurable copper is found in complexes or chelation form. In biological systems, many enzymes are copper-dependent [92], such as:

- Cytochrome c Oxidase or Complex IV is an enzyme found in mitochondria of eukaryotes, bacteria and archaea. As the last enzyme in the respiratory electron transport chain of cells, role of this protein is the reduction of oxygen. From four cytochrome c molecules, Complex IV gains four electrons and transfers them to oxygen molecule and four protons, converting them to water [93].
- Superoxide dismutase is an enzyme found in all cells, with a function of disproportionation of superoxide in prevention of its accumulation preventing damage to tissues, and speeds up certain chemical reactions in the body [94].
- Tyrosinase is found in animal and plant tissues and catalyzes the production of melanin, by hydroxylation of tyrosine [95].
- Dopamine beta-hydroxylase is an enzyme that converts dopamine to norepinephrine by hydroxylation [92].

- Lysyl oxidase is an enzyme that catalyzes oxidation of terminal amino group of lysyl amino acids in collagen and elastin [92].
- Amine oxidases – involved in oxidation of primary amines to aldehydes and ammonia [96].
- Ceruloplasmin is a major copper and iron mobilization protein in the blood.
- Factor V is an enzyme involved in coagulation of blood [92].
- Peptidylglycine alpha-amidating monooxygenase – syntheses of neuroendocrine peptides [97].

As described, for humans copper has high significance in biochemical processes, as both constituent of various compounds or as an essential trace element. In its elemental state it is bound to ceruloplasmin, albumin and other proteins, yet as a compound it is in a form of ligand-metal complex and interacts mainly with proteins and nucleic acids [98]. Numerous complexes with Cu(II) show anti-inflammatory, antiulcerogenic, chemotherapeutic, antiviral and/or antibacterial activities [98]. With that said, excessive levels of copper may result in liver and kidney damage, anemia, immunotoxicity, and developmental toxicity [99].

2.6.2. Nickel

Nickel (Ni) is a Group 10 chemical element, a silver color, hard and ductile metal. Nickel is an essential micronutrient for humans, and affects hormonal activity and lipid metabolism, as well as part of enzymes such is urease, and has important role in biological systems. Nickel complexes have been reported to show anticonvulant, antiepileptic, antibacterial, antifungal, antimicrobial, antioxidant and anticancer activities [100]. Depending on the ligand in question, Ni(II) complexes have interactions with biomolecules such are serum albumins or DNA [100].

2.6.3. Cobalt

Cobalt (Co) is a Group 9 chemical element, gray, hard and somewhat lustrous metal. Cobalt is an essential transition metal that is valued in synthesis of metal-ligand

complexes and pharmaceutical chemistry due to its tolerability by humans and the existent reviews of cobalt-based therapeutic research [101,102]. Yet the biological properties of its complexes vary significantly on the chelation coordination.

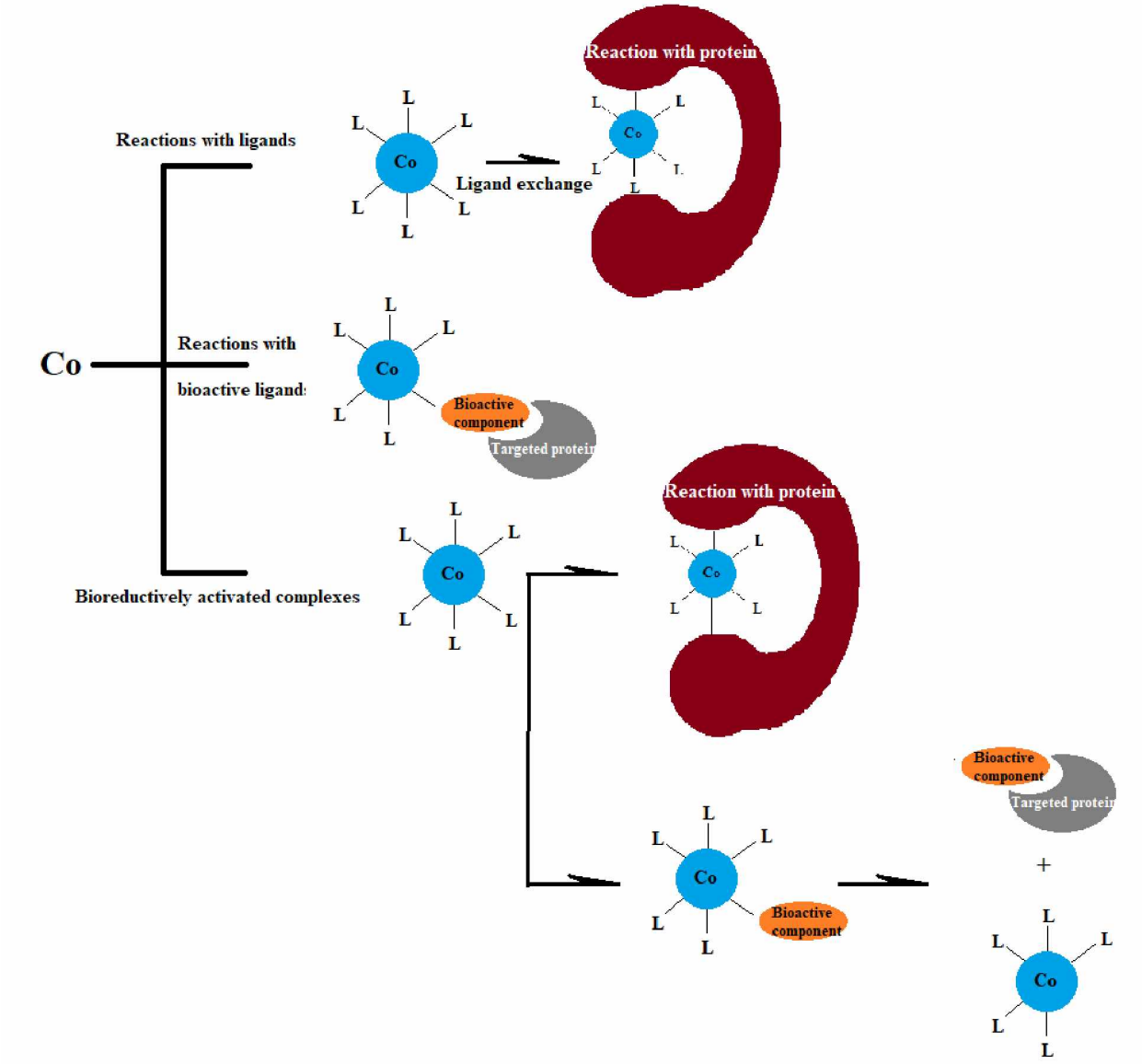

Figure 48. Different modes of action of bioactive cobalt complexes

In the Figure 48, 3 different modes of interactions of bioactive cobalt complexes are presented. With the diversity of its interactions, cobalt can act as both carrier, binder or a reactive focus of the obtained complex – API. Cobalt complexes are investigated for selective protein inhibition, bioactivity enhancement, bioreductive prodrug activation, as

well as for cobalt-based metallacarborane HIV protease inhibition and cobalt nanoparticles for magnetic hyperthermia applications [103].

2.6.4. Zinc

Zinc (Zn) is a Group 12 chemical element, bluish-white and a slightly brittle metal. Zinc is an essential transition metal with the lowest melting point of all transition metals. Zinc deficiency in humans is connected with anemia, hypogonadism, short stature, impaired wound healing and geophagia [104]. It is a part of many enzymes and plays a role in protein synthesis and in cell division. The demonstration of zincs role in the pathophysiology and treatment of affective disorders has been presented in review articles [105]. Zincs potential role in diabetes has been described with the role of zinc transporter *SLC30A8/ZnT8* and its polymorphism which increases susceptibility of type 2 diabetes [106].

A significant field of exploration of "zinc fingers" – small protein structures that are characterized by the coordination of one or more Zn ions, that act as stabilizers of its structure. Zinc finger compounds can be designed to target a particular DNA sequence and bind to it. With attached enzyme that breaks both DNA strands at a targeted site, zinc fingers show high potential in gene therapy [104].

2.6.5. Platinum

Platinum (Pt) is a Group 10 chemical element, dense, ductile, silverish transition metal. Platinum is one of the least reactive metals and has great resistance to corrosion. Platinum is under research for treatment of many types of carcinoma conditions. This non-essential metal is a part of many APIs such are cisplatin, carboplatin and oxaliplatin (all used in treatment of cancerous conditions) [90]. The use of platinum in anticancer medicines arises from its cytotoxicity when in its 2+ charge. At first platinum is introduced into an organism as a non-toxic 4+ charge, when it gets in contact with the tumor or desired tissue it can be converted to its 2+ charge via laser, and with that it can selectively destroy malignant cells. The biokinetics of platinum medicines depend on agents-ligands used.

2.6.6. Palladium

Palladium (Pd) is a Group 10 chemical element, a rare silvery metal transition metal. Some palladium complexes have shown great antitumor activity often surpassing platinum complexes [107]. Clinical trials with palladium complexes are challenging due to their high lability and low solubility of obtained complexes. More than 800 anticancer palladium complexes have been discovered since 1980s [108]. The first palladium complex that was approved for clinical use was padeliporfin, an API used in therapy of prostate cancer, and was approved on 10th of November 2017 [109]. This API triggers the production of high levels of oxygen radicals that cause the destruction of the vessels supplying blood to the affected tissue and destroy cancer cells, this is one of the four main modes of action for palladium complexes (Figure 49).

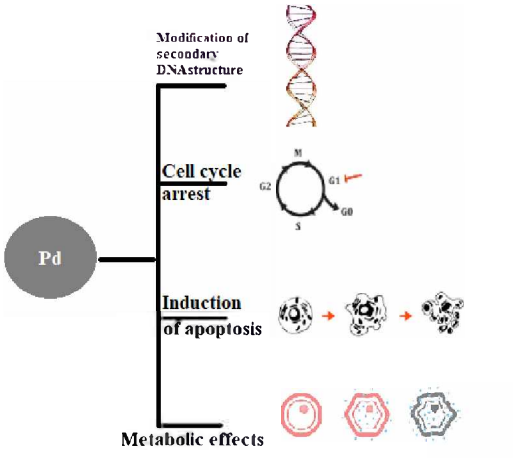

Figure 49. Different modes of action of bioactive palladium complexes in combating cancer cells

3. Materials and methods

3.1. Mechanochemical synthesis

Mechanochemical syntheses were performed using a benchtop ball mill Laboratory Mini Mill Pulverisette 23 (Fritsch GmbH).

3.2. Elemental CHN analyses

Elemental CHN analyses have been conducted by a classical CHN analysis.

3.3. Infrared spectroscopy

IR analyses have been analyzed by Thermo Nicolet iS20 FTIR spectrophotometer with Smart iTR™ ATR Sampling accessories and Thermo Nicolet Nexus 670 FTIR instrument (for all other complexes), in the range of 4000–400 cm^{-1}.

3.4. X-ray powder diffraction analyses

XRPD analyses have been conducted on Malvern Panalytical Empyrean 3 X-ray powder diffractometer.

The samples have been ground in an agate mortars, than deposited in an indentation of a Silicon zero background plate and pressed gently. Hexagon formation was formed using metal plate-knife with removal of the outer layers. To improve particle statistics and minimize the influence of preferred orientation, the samples have been rotated at 60 rpm about the scattering vector. The mode of scanning was continuous scan in Bragg-Brentano geometry, with Cu radiation (generator settings 40mA, 45kV; K-Alpha1:1.54060 Å). X-ray powder diffractometer was equipped with 0.04° Soller slits, 1/8° divergence slit, 1/2° antiscatter slit, 10mm mask, ASS receiving 7.5 mm. Scan was performed from [°2θ]=5.0020° to [°2θ]=69.9940°, with step size [°2θ] =0.0030° and time per step t=6.12s. The software used for data collection was *Datacollector*, and for data interpretation *Highscore+*. Silicon zero background plate was used because of limited sampe quantity available, which compared to backloading technique provides higher intensities and sharper, better defined peaks, yet results in higher occurrences of preffered orientation phenomenon depending on the crystal systems that prove more prone to this occurrence,

such are monoclinic systems for example. Bragg-Brentano reflection geometry was used to analyze the samples, instead of transmission mode, due to previously described situation (as in the choice of the holder used).

3.5. Single crystal X-ray diffraction analyses

X-ray structural analyses (SC-XRD) have been conducted on Xcalibur, Eos instrument and Stoe 4-circle diffractometer with MoKα radiation (λ = 0.71073 Å) and graphite monochromator. The conditions are described in each of the respective headings for obtained complexes, as part of the results (heading 4).

3.6. Thermogravimetric analyses

The TG–DSC data were collected using a TA Instruments SDT Q600 thermal analyzer. Additionally, the TG–MS measurements were taken with the same thermal analyzer coupled online with the Hiden Analytical HPR-20/QIC mass spectrometer. The mass spectra were recorded in multiple ion detection (MID) mode by SEM detector.

3.7. Determination of antioxidative potential

Antioxidative potential was tested via the scavenging effect on the DPPH radical (DPPH), according to a slightly modified method using Trolox solutions [110]. The solutions have been tested using 96-well microplates. The method is based on spectrophotometric monitoring of transforming the violet-colored, stable, nitrogen-centered DPPH radical (2,2-diphenyl-12-picrylhydrazyl) into the reduced, yellow-colored form of DPPH-H.

3.8. Determination of bactericidal activity

To test the antibacterial effect on pure cultures of *Escherichia coli* and bacteria from the genus *Salmonella spp*, 4 preparations prepared in three concentrations were used, for concentration levels of 10^{-2}mol/dm^3, 10^{-4}mol/dm^3 and 10^{-5}mol/dm^3. The agar diffusion (Kirby-Bauer) method was used for this investigation, in which the Mueller-Hinton medium prepared according to the standard procedure was used, sterilized in an autoclave, cooled and poured into sterile Petri dishes, left to cool, and then used for inoculation of test bacteria. , using the swab method [111, 112].

3.9. Determination of cytotoxicity

The samples were tested on Cervix adenocarcinoma cell line (HeLa), human colon carcinoma (LS174), non-small cell lung carcinoma (A549) and a normal cell line, human fetal lung fibroblast cell line (MRC-5) were grown in RPMI-1640 medium (Sigma) at 37°C. Media were supplemented with 10% fetal bovine serum, L-glutamine, and penicillin-streptomycin (Sigma). The effect of the investigated extracts on survival of the specified cell lines was determined by the microculture tetrazolium test (MTT) according to Mosmann [113] with modification by Ohno and Abe [114] 72 h after addition of the extracts.

4. Results and discussion

4.1. Synthesis and characterization of Zn(II) and Co(II) complexes with **5-(4-Bromophenyl)-3-methyl-1H-pyrazole (L1)**

During this research the complexes formed with 5-(4-Bromophenyl)-3-methyl-1H-pyrazole (L1) were with Co(II) and Zn(II) of formulae $[ZnL_2(OAc)_2]$, $[Co_4L_8Cl_8]$ and $[CoL_3Cl \cdot H_2O]$ presented in the Table 2. Additionally, as part of the experiment, a monocrystal of the ligand L1 was successfully obtained and characterized through SC-XRD.

Table 2. Formulae and color of complexes of Co(II) and Zn(II) with 5-(4-Bromophenyl)-3-methyl-1H-pyrazole

Complex	**Color**
$ZnL_2(OAc)_2$	Transparent white
$Co_4L_8Cl_8$	Azure blue
$CoL_3Cl \cdot H_2O$	Clear light pink

4.1.1. Crystal and molecular structure of 5-(4-Bromophenyl)-3-methyl-1H-pyrazole (L1)

Monocrystal of the ligand L1 (5-(4-bromophenyl)-3-methyl-1H-pyrazole), that has been purchased from Sigma–Aldrich, was obtained using the following procedure: 0.05 g of L1 was dissolved in 5 ml of ethanol, slowly heated and left to crystallize. After 24 h clear light pink single crystals of the title compound were filtered and washed with ethanol. The obtained single crystals have been analyzed with SC-XRD to obtain the molecular and crystal structure that is shown in the Figure 50. Basic crystallographic data are presented in the Table 3.

Table 3. Data collection and handling of SC-XRD data of 5-(4-Bromophenyl)-3-methyl-1H-pyrazole

	L1
Empirical formula	$C_{10}H_9BrN_2$
Formula weight	237.1
Temperature	293 K
Wavelength(Å)	0.71073
Crystal size (mm)	0.30 0.20 0.15
Crystal habitus	Prism
Crystal color	Pink
Crystal system	Orthorhombic
Space group	P -19
Unit cell dimensions(Å)	a= 5.9070(3); b= 9.2731(7); c= 17.5641(14)
Unit cell angles (°)	α= 90 ; β= 90; γ= 90
Volume	962.09(12)
Z	4
Density (calc.) (g cm^{-3})	1.637
Absorption coefficient (mm^{-1})	4.224
*R*int	0.039
F (000)	472
Data/Parameters	2196 /119
Goodness-of-fit on F^2	1.001
R/w*R* [I > 2σ (I)]	0.0504 / 0.0947

The H atoms bonded to pyrazole and phenyl ring were placed at calculated positions and refined as riding atoms with U_{iso}(H) set to 1.2Ueq of the parent atom. The H atoms of the methyl group were positioned geometrically and allowed to rotate around the C–C bond to best fit the experimental electron density (HFIX 137 in the SHELX program suite [115]), with U_{iso}(H) set to 1.5U_{eq}(C).

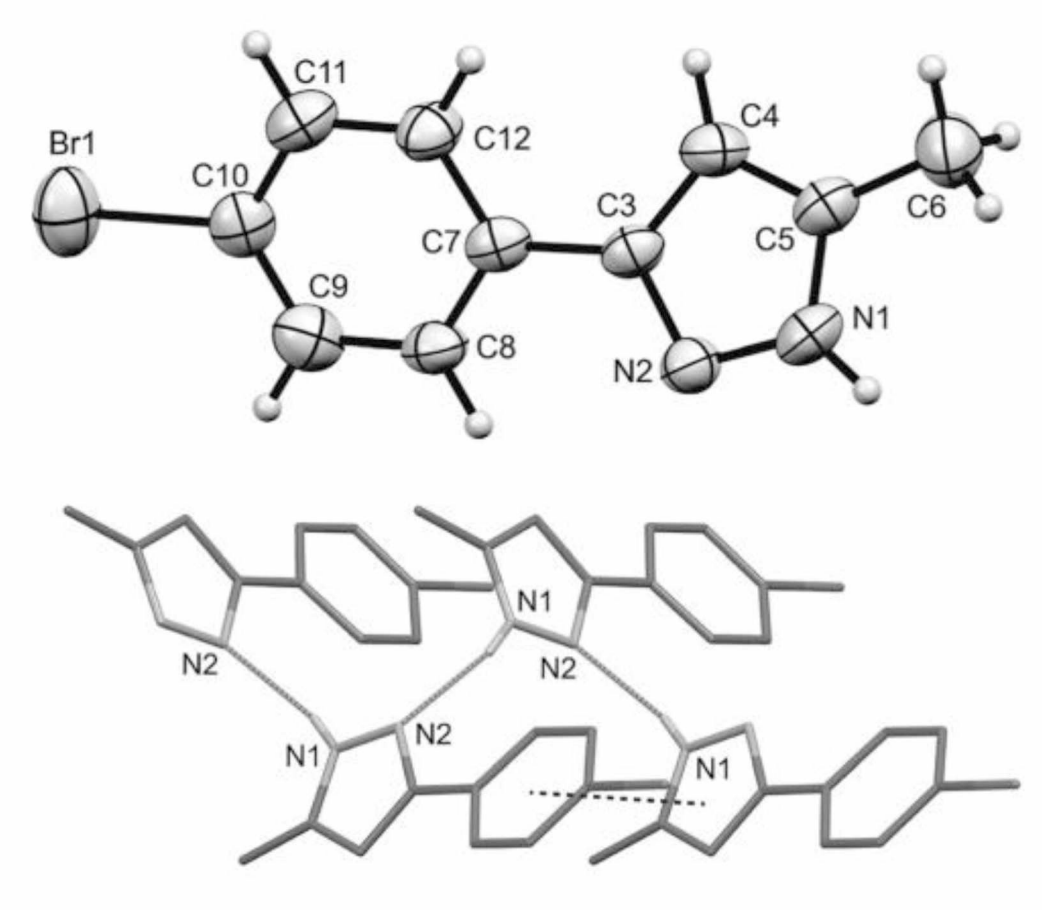

Figure 50. Molecular and crystal structure of 5-(4-Bromophenyl)-3-methyl-1H-pyrazole (L1)

Substituents at the pyrazole ring give more possibilities for supramolecular arrangements. Between phenyl-pyrazole molecules stacking interactions are possible [116]. The addition of bromine to phenyl ring may lead to the halogen bonding [117]. Their variability in coordination modes extends their coordinative properties [118]. Phenol-pyrazole ligands influence the structural and magnetic properties of transition metal complexes [119, 120]. Brominated phenyl pyrazoles serve as ligands in the synthesis of molecular magnets [121, 122]. Steric effects of the phenol-pyrazoles, are important for the structural variability of the coordination compounds [123]. Bond lengths in the title molecule follow the pattern like in related bromophenyl-1H-pyrazole derivatives [124–126]. As in the crystal structure of [124], in the title molecule there are no Br/Br interactions. But, in the crystal structures of [125, 126] the Br/Br interaction of type I [127] is present, $\theta1 = \theta2 = 163°$ in Ref. [125] and $\theta1 = \theta2 = 156°$ in Ref. [126]. Molecules

of the title compound are connected through the N1–H1/N2i (the H/N distance is 2.24 Å, the N–H/N bond angle is 160°), (i = −1/2 + x, 1/2 − y, 1 − z). View along the c axis (lower part of the Figure 50) shows assembly of molecules into a zigzag chain. The dotted black line depicts the closest phenole-pyrazole intermolecular distance. Centroids of the phenol and pyrazole rings from neighboring molecules are at a distance of 4.158(4) Å. Angle between the mean planes of the neighboring rings is 18.0(3)°. Such an arrangement of two cycles creates an opportunity for stacking interaction between their π-systems. Molecular chains are directed along the axis a. There are no significant inter-chain contacts. Br atom is not involved in significant intermolecular interactions.

4.1.2. Synthesis and characterization of $[ZnL_2(OAc)_2]$

Synthesis of a complex $[ZnL_2(OAc)_2]$: The warm ethanolic solution (3 cm^3) $[Zn(OAc)_2 \cdot 2H_2O]$ (0.055 g, 0.25 mmol) was mixed with warm ethanolic solution (3 cm^3) of the ligand L1 (0.118 g, 0.5 mmol) with mild heating. The transparent reaction mixture was left to crystallize. After 48 hours, white, transparent microcrystalline precipitate was filtered, washed with ethanol and dried in air. Yield: 0.063 g (36.3 %).

From the reaction mixture, new complex compound of formulae: $[ZnL_2(OAc)_2]$ was crystallized. The complex was analyzed via XRPD, IR and CHN analyses. The complex was prepared by reacting zinc acetate with 5-(4-Bromophenyl)-3-methyl-1H-pyrazole in hot ethanolic solution (Figure 51). Results of CHN analysis are presented in the Table 4.

Table 4. Results of the CHN analysis for the complex $[ZnL_2(OAc)_2]$

	Theoretical $[ZnL_2(OAc)_2]$	Found
C%	*43.80 %*	*44.44 %*
H%	*3.65 %*	*3.53 %*
N%	*8.52 %*	*9.20 %*

On the basis of CHN analysis and FTIR results, a structure of the complex was determined (Figure 51).

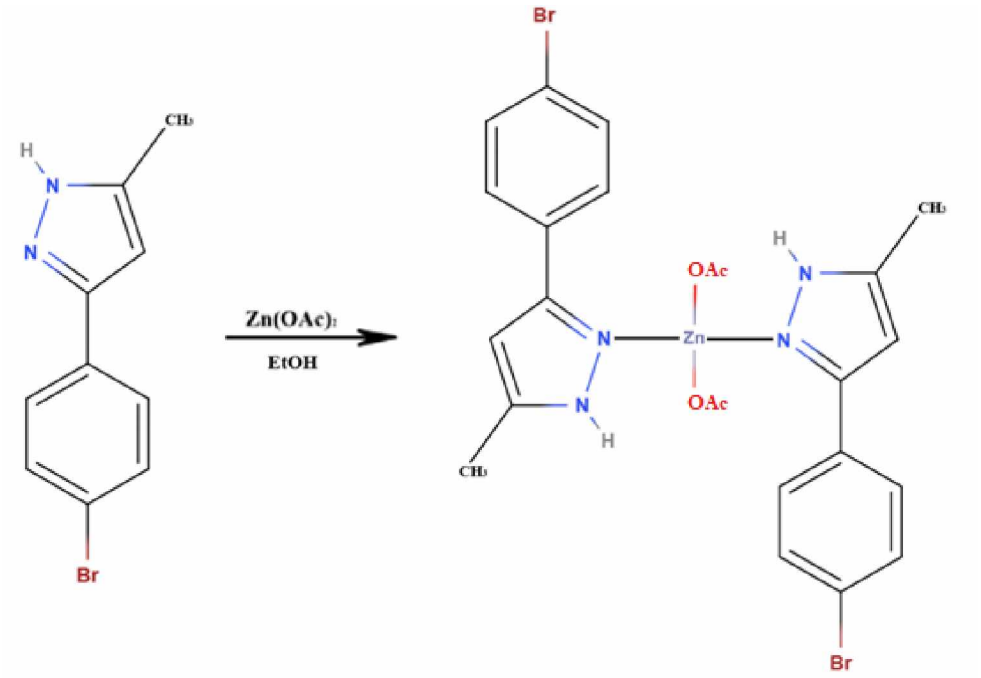

Figure 51. Synthesis of the Zn(II) complex of 5-(4-Bromophenyl)-3-methyl-1H-pyrazole

4.1.2.1. X-ray powder diffraction data of [ZnL2(OAc)$_2$]

The powder diffractogram of *ZnL$_2$(OAc)$_2$* is presented in Figure 52. Most dominant 8 peaks of the diffractogram are listed in the Table 5, with their d spacings and relative intensities.

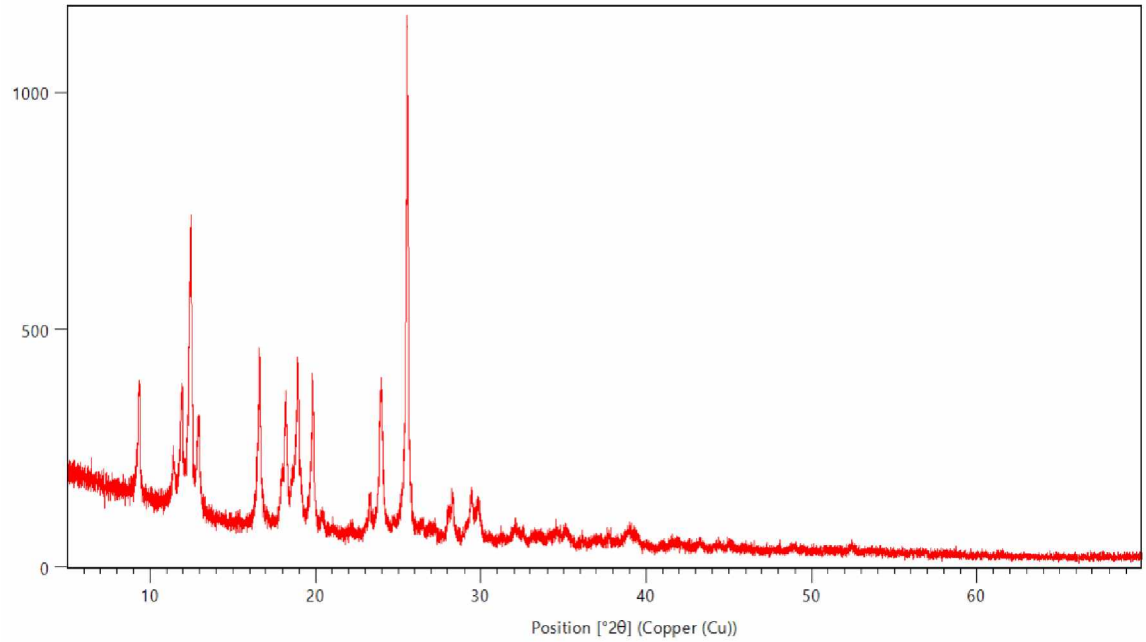

Figure 52. The powder diffractogram of $ZnL_2(OAc)_2$

Table 5. Eight most dominant diffraction lines in powder diffractogram of $ZnL_2(OAc)_2$

Pos. [°2θ]	d-spacing [Å]	Rel. Int. [%]
11.8898	7.43731	21.10
12.4272	7.11690	51.74
16.5820	5.34185	32.71
18.1912	4.87279	21.52
18.9045	4.69048	30.03
19.8060	4.47899	28.19
23.9466	3.71307	31.68
25.5266	3.48671	100.00

Presented in the Figure 53 are the diffractograms of $Zn(OAc)_2$, L1 and the product $ZnL_2(OAc)_2$. Similar volumes of all 3 samples were used during the analyses and all of the samples were analyzed with the same measuring conditions. From the Figure 53, it is visible that the synthesis resulted in a new crystalline product, and not a mixture of metal salt and ligand.

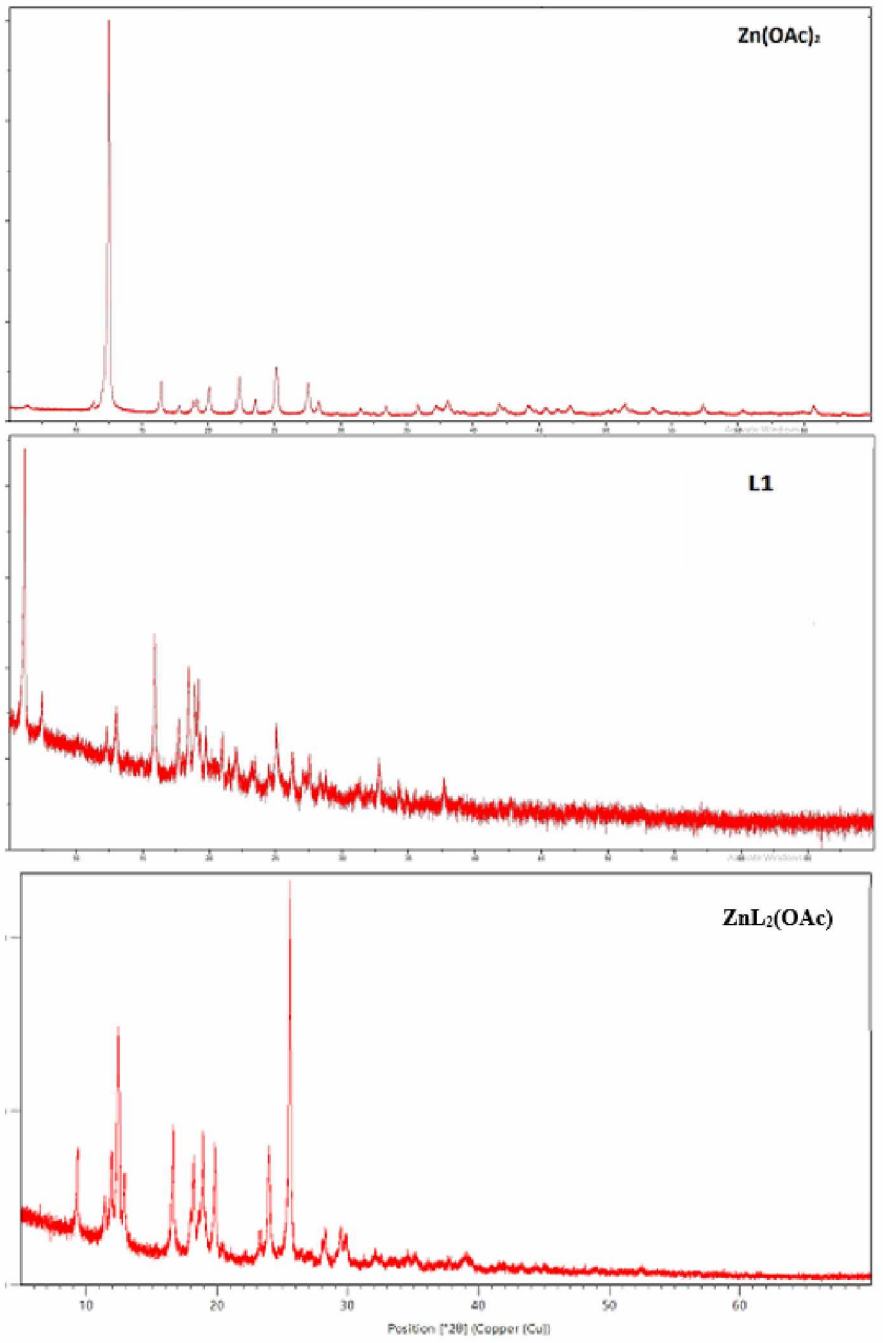

Figure 53. The powder diffractograms of $Zn(OAc)_2$, L1 and $ZnL_2(OAc)_2$

4.1.2.2. FTIR data of [ZnL2(OAc)$_2$]

IR spectra of the complex *ZnL$_2$(OAc)$_2$* contains the following dominant bands: 3169.0 cm^{-1}, 3127.0 cm^{-1}, 1633.3 cm^{-1}, 1566.7 cm^{-1}, 1392.3 cm^{-1}, 1146.50 cm^{-1}, 1034.3 cm^{-1}, 1002.9 cm^{-1}, 866.78 cm^{-1}, 616.1 cm^{-1}. Through interpretation [128], the IR spectra of the complex is in accordance with the proposed structure.

From the obtained results, a deduction can be made that the previously described synthesis of Zn(OAc)$_2$ and L1, has resulted in a new crystalline metal complex of formula: [ZnL$_2$(OAc)$_2$]. The most probable coordination, in relation to the preference of pyrazolones to bind with their pyridine like nitrogen, is presented in the Figure 51. In this case, and to achieve higher stability, it is expected that Zn is coordinated by two pyridine like nitrogen from L1 and two oxygen atoms from acetate ligands, in a tetrahedral environment.

4.1.3. Synthesis and characterization of [Co$_4$L$_8$Cl$_8$]

Synthesis of a complex [Co$_4$L$_8$Cl$_8$]: The warm ethanolic solution (3 cm^3) [CoCl$_2$·6H$_2$O] (0.033 g, 0.25 mmol) was mixed with warm ethanolic solution (3 cm^3) of the ligand L1 (0.118 g, 0.5 mmol) with mild heating. The dark blue reaction mixture was left to crystallize. After 3 days, 4 different crystalline products were obtained: azure blue plate single crystal (complex [Co$_4$L$_8$Cl$_8$]), clear light pink crystals (complex [CoL$_3$Cl·H$_2$O]), net-like fibrous greyish crystals (ligand) and white monocrystals (ligand). Single crystals of both products were carefully isolated, filtered, washed with ethanol and dried in air. Total yield: 0.092 g (60.9 %). Both complexes originate from the same solution, with two more crystalline products (both identified as ligand). The [Co$_4$L$_8$Cl$_8$] complex is obtained as azure blue plate single crystal, while the [CoL$_3$Cl]·H$_2$O complex crystallizes in clear light pink crystals. The compounds are characterized by SC-XRD.

From the reaction mixtures, new complex compound of formulae: [Co$_4$L$_8$Cl$_8$] was crystallized (Figure 54). The crystal and molecular structure of the synthesized complex

was determined by single-crystal X-ray structure analysis. The complex was prepared by reacting cobalt chloride with 5-(4-Bromophenyl)-3-methyl-1H-pyrazole in hot ethanolic solutions.

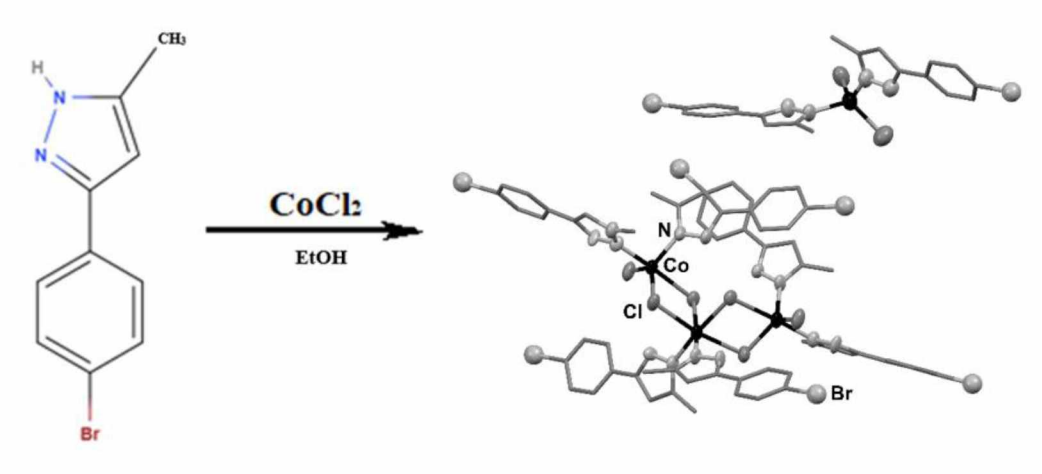

Figure 54. Synthesis of the [$Co_4L_8Cl_8$] complex of 5-(4-Bromophenyl)-3-methyl-1H-pyrazole (representation of a mononuclear structure)

4.1.3.1. Crystal and molecular structure of [$Co_4L_8Cl_8$]

The crystal and molecular structure of the obtained complex was solved via SC-XRD analysis. Table 6 contains crystallographic data of the complex *$Co_4L_8Cl_8$*.

Table 6. Data collection and handling of SC-XRD data of $Co_4L_8Cl_8$

	$Co_4L_8Cl_8$
Empirical formula	$C_{80}H_{73}Br_8Cl_8Co_4N_{16}$
Formula weight	2417.14
Temperature	293 K
Wavelength(Å)	0.71073
Crystal habitus	Plate
Crystal color	Azure blue
Crystal system	Triclinic
Space group	P -1
Unit cell dimensions(Å)	a= 12.381(2); b= 13.603(2); c= 29.809(3)
Unit cell angles (°)	α= 88.315(12) ; β= 85.221(12); γ= 67.960(18)
Volume	4637.2(14)
Z	2
Density (calc.) (g cm^{-3})	1.731

Absorption coefficient (mm^{-1})	4.431
*R*int	0.184
F (000)	2378
Data/Parameters	16150 /1048
Goodness-of-fit on F^2	0.898
R/w*R* [I > 2σ (I)]	0.0840 / 0.2051

The molecular structure is shown in the Figures 55, 56. and 57. Figure shows content of the asymmetric unit. Atom labelling depicts color codes of atoms. As can be seen in the Figure 55, in the mononuclear unit of the complex, the central atom of Co is coordinated with pyridine-like N atoms of two ligands, and with two Cl atoms, in tetrahedral geometry. Stereochemistry of Co(II) complexes, due to the lack of ligand field stabilization energy, depends mostly on the size of the cation and the structural properties of the ligand. With that said, Co (II) complexes will favor tetrahedral or higher structural formations.

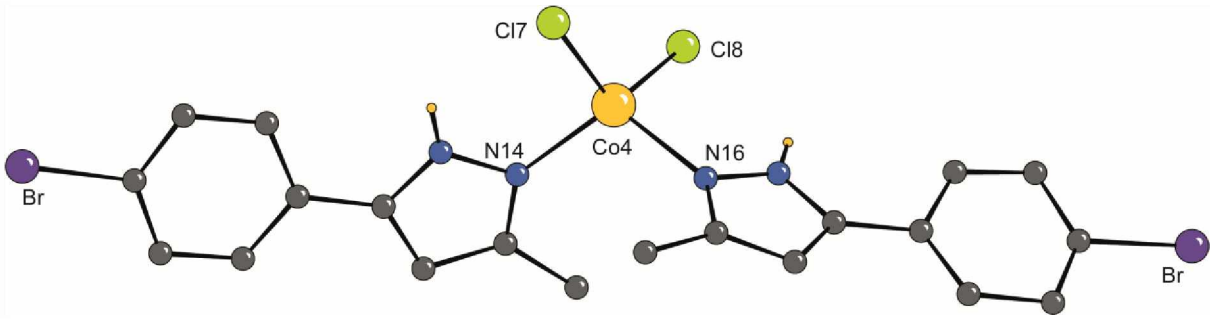

Figure 55. Molecular and crystal structure of mononuclear unit of a complex $Co_4L_8Cl_8$

In the Figure 56, the structure that consists of isolated units of mononuclear and trinuclear complexes are presented.

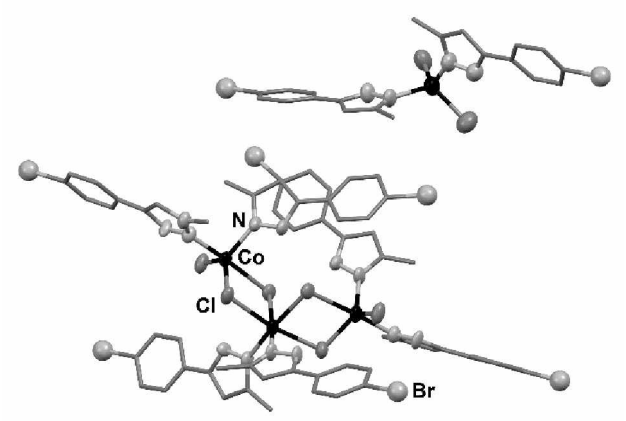

Figure 56. Asymmetric unit consist of one trinuclear and one mononuclear complex.

As can be seen in the Figure 57, in trinuclear complex, the central atom of Co is coordinated with pyridine-like N atoms of two ligands, and with two Cl atoms, in tetrahedral geometry. Central Co is coordinated through four Cl atoms and two ligands through their pyridine-like nitrogens, in octahedral environment. The trinuclear coordination is made possible by four bridging Cl atoms.

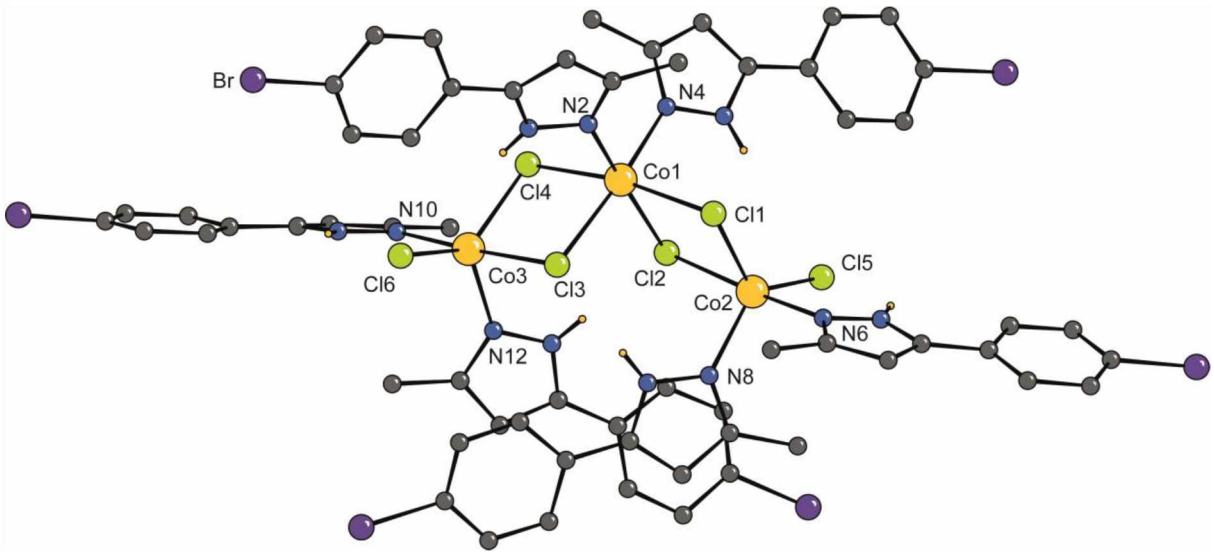

Figure 57 Molecular diagram and atom labeling scheme of trinuclear unit of a complex. Hydrogen atoms bonded to carbon are omitted for clarity

Bond lengths of the chemically equivalent ligands are not significantly different (Table 7). There are no significant differences in the bond lengths of pyrazolyl ligands in comparison to free 5-(4-Bromophenyl)-3-methyl-1H-pyrazole. The selected bond angles of the complex *[$Co_4L_8Cl_8$]* are presented in the Table 8.

Table 7. Selected bond lengths (Å) of [$Co_4L_8Cl_8$]

Bond	Distances (Å)	Bond	Distances (Å)
Co1–Cl2	2.432(3)	Co3–N12	2.112(10)
Co1–Cl3	2.473(3)	Co3–N10	2.048(9)
Co1–Cl4	2.551(3)	Co3–Cl6	2.303(3)
Co1–Cl1	2.575(3)	Co3–Cl3	2.650(3)
Co1–N4	2.110(8)	Br4–C28	1.932(3)
Co2–Cl5	2.303(3)		

Table 8. Selected bond angles (°) of [$Co_4L_8Cl_8$]

Bond	Angles (°)	Bond	Angles (°)
Cl2–Co1–Cl3	87.37(10)	N2–Co1–Cl2	170.4(3)
Cl3–Co1–Cl4	93.38(11)	N2–Co1–Cl3	89.8(2)
Cl1–Co1–Cl2	81.06(10)	Cl1–Co1–Cl3	81.47(10)
N4–Co1–Cl1	88.9(3)	N4–Co1–Cl4	90.4(2)
N4–Co1–Cl3	172.6(3)	N2–Co1–Cl1	88.9(3)
N12–Co3–Cl6	92.0(3)	N12–Co3–Cl3	89.3(3)

The interesting occurrence in the matter of this coordination is the prototrophic annular tautomerism, which took place and is characteristic for pyrazole derivatives. Aggregation of complex molecules in the crystal is achieved through the Br...Br and stacking interactions. Part of the unit cell and significant interactions are depicted in Figures 58 and 59.

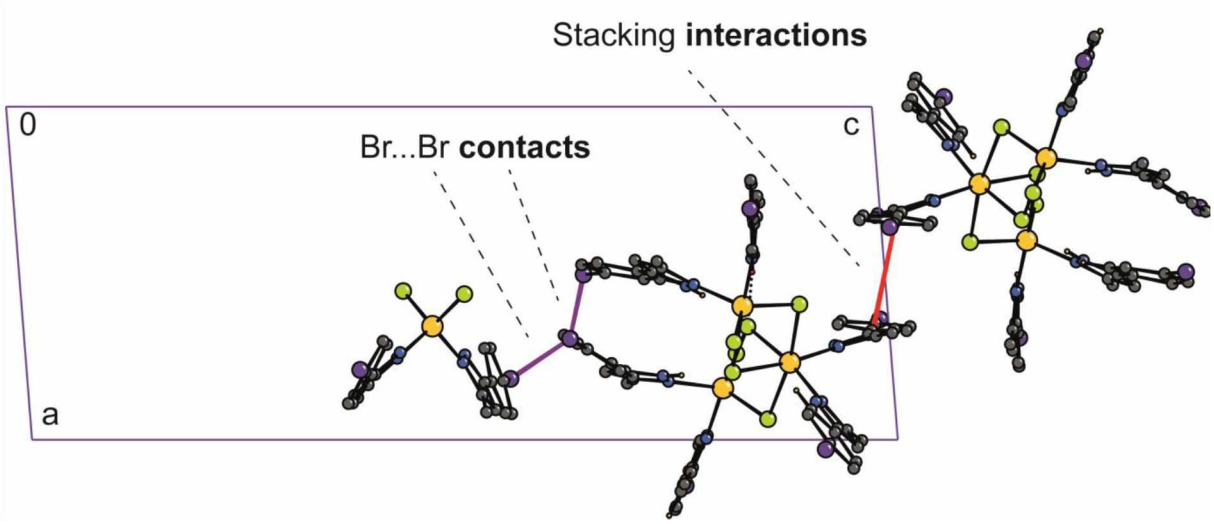

Figure 58 Part of the units cell depicting the connection between the mono- and tri-nuclear complexes through the Br...Br and stacking interactions

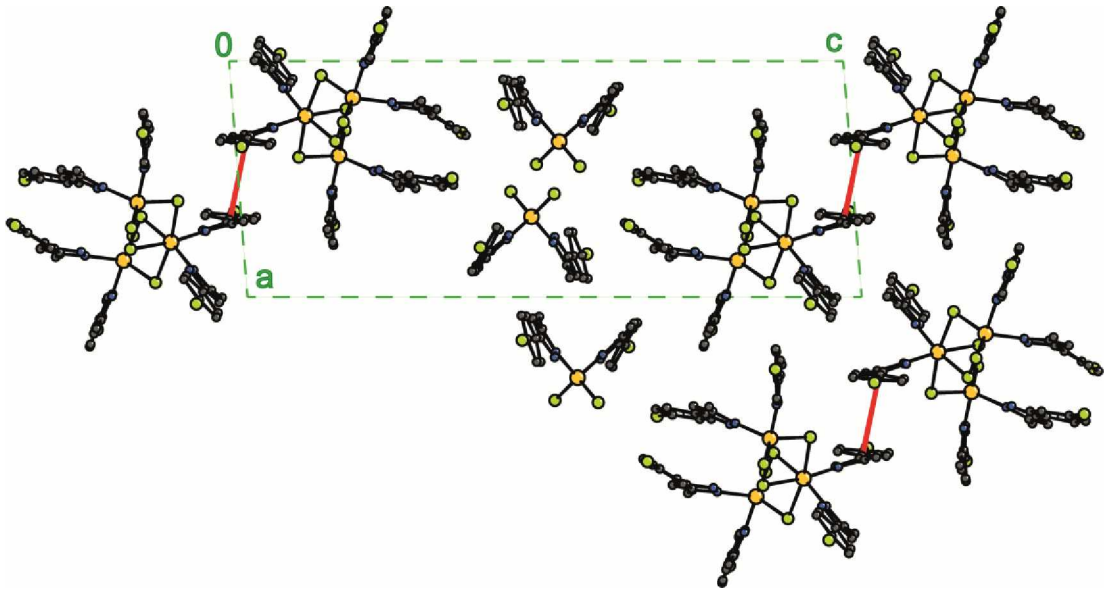

Figure 59 Packing of molecules in the crystal structure. Red lines depict stacking interactions

Mononuclear complex contains Co in tetrahedral environment. Two Cl atoms and two pyrazolyl ligands bonds to Co (Figure 55). Trinuclear complex consists of three Co atoms connected through the dichloro bridges (Fig). Angles in the two Co_2Cl_2 bridging fragments are in the range of 81-101˚. Both terminal Co atoms are five-coordinate in a trigonal-bipyramidal fashion. Apical positions contains bridging Cl and pyridine-like nitrogen from pyrazole ligand. Central Co is in octahedral environment. The equatorial

plane consists of four bridging Cl. Two pyrazolyl ligands coordinates in the axial positions through the pyridine-like nitrogen. Hydrogen bond donors and acceptors as well as five and six membered rings are present in the crystal. In spite of this property there are no significant intermolecular contacts.

4.1.4. Synthesis and characterization of [$CoL_3Cl \cdot H_2O$]

Synthesis of a complex [$CoL_3Cl \cdot H_2O$]: The warm ethanolic solution (3 cm^3) [$CoCl_2 \cdot 6H_2O$] (0.033 g, 0.25 mmol) was mixed with warm ethanolic solution (3 cm^3) of the ligand L1 (0.118 g, 0.5 mmol) with mild heating. The dark blue reaction mixture was left to crystallize. After 3 days, 4 different crystalline products were obtained: azure blue plate crystals (complex [$Co_4L_8Cl_8$]), clear light pink crystals (complex [$CoL_3Cl \cdot H_2O$]), net-like fibrous greyish crystals (ligand) and white monocrystals (ligand). Single crystals of both products were carefully isolated, filtered, washed with ethanol and dried in air. Total yield: 0.092 g (60.9 %). Both complexes originate from the same solution, with two more crystalline products (both identified as ligand). The [$Co_4L_8Cl_8$] complex is obtained as blue prism crystals, while the [$CoL_3Cl] \cdot H_2O$ complex crystallizes in clear light pink crystals. The compounds are characterized by SC-XRD.

From the reaction mixtures, new complex compound of formulae: [$CoL_3Cl \cdot H_2O$] was crystallized (Figure 60). The crystal and molecular structure of the synthesized complex was determined by single-crystal X-ray structure analysis. The complex was prepared by reacting cobalt chloride with 5-(4-Bromophenyl)-3-methyl-1H-pyrazole in hot ethanolic solutions.

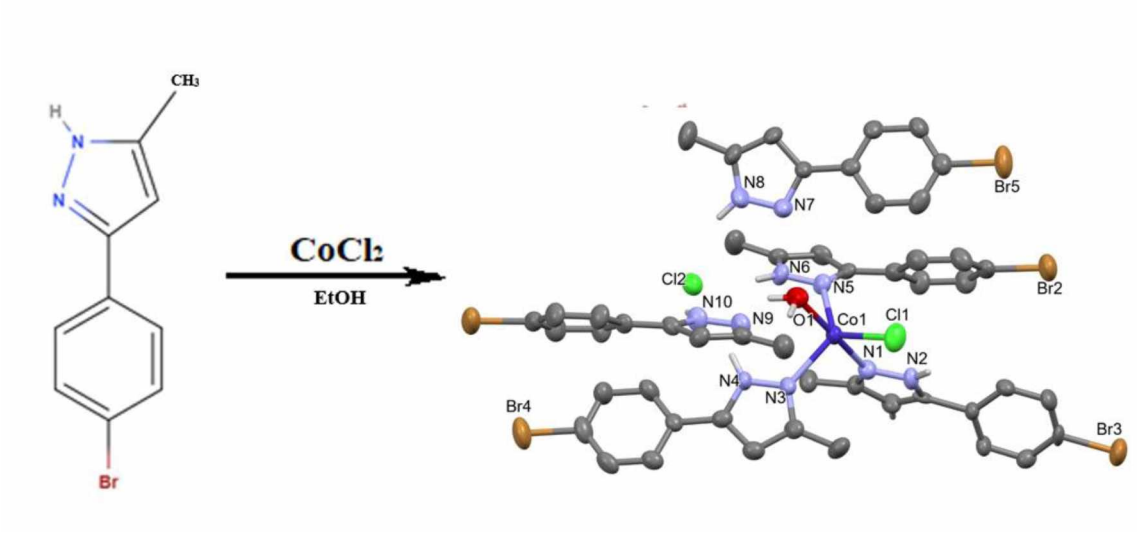

Figure 60. Synthesis of the [$CoL_3Cl{\cdot}H_2O$] complex of 5-(4-Bromophenyl)-3-methyl-1H-pyrazole

4.1.4.1. Crystal and molecular structure of [$CoL_3Cl{\cdot}H_2O$]

The crystal and molecular structure of the obtained complex was solved via SC-XRD analysis. Table 9 contains crystallographic data of the complex $CoL_3Cl{\cdot}H_2O$.

Table 9. Data collection and handling of SC-XRD data of $CoL_3Cl{\cdot}H_2O$

	$CoL_3Cl{\cdot}H_2O$
Empirical formula	$C_{50}H_{47}Br_5Cl_2CoN_{10}O$
Formula weight	1333.35
Temperature	293 K
Wavelength(Å)	0.71073
Crystal size (mm)	0.05 0.05 0.05
Crystal habitus	Prism
Crystal color	Clear light pink
Crystal system	Triclinic
Space group	P -1
Unit cell dimensions(Å)	a= 10.0202(4); b= 11.9578(4); c= 13.1092(5)
Unit cell angles (°)	α= 110.701(3) ; β= 108.951(4); γ= 94.782(3)
Volume	1354.38(10)
Z	1
Density (calc.) (g cm^{-3})	1.635
Absorption coefficient (mm^{-1})	4.149

*R*int	0.067
F (000)	661
Data/Parameters	9511 /628
Goodness-of-fit on F^2	1.023
R/w*R* [I > 2σ (I)]	0.0515 / 0.1211

Isolated complexes are solid substances that are stable in ambiental conditions. The molecular structure of $[CoL_3Cl \cdot H_2O]$ is shown in the Figure 61.

Complex molecule crystallized with two molecules of the free ligand and Cl^- anion. Mononuclear complex contains Co in trigonal bipyramidal environment. Cl and H_2O and three pyrazolyl ligands bond to Co. Cl^- and a molecule of H_2O are in axial positions. There is an occurrence of prototrophic annular tautomerism in ligand units as was presented in the trinuclear Co(II) complex as well. Three pyrazolil ligands coordinate through pyridine-like nitrogen. Hydrogen bond donors and acceptors as well as five and six membered rings from the ligands structure are present in the crystal. Molecular diagram and atom labeling scheme for non-C atoms is shown in Figure 61.

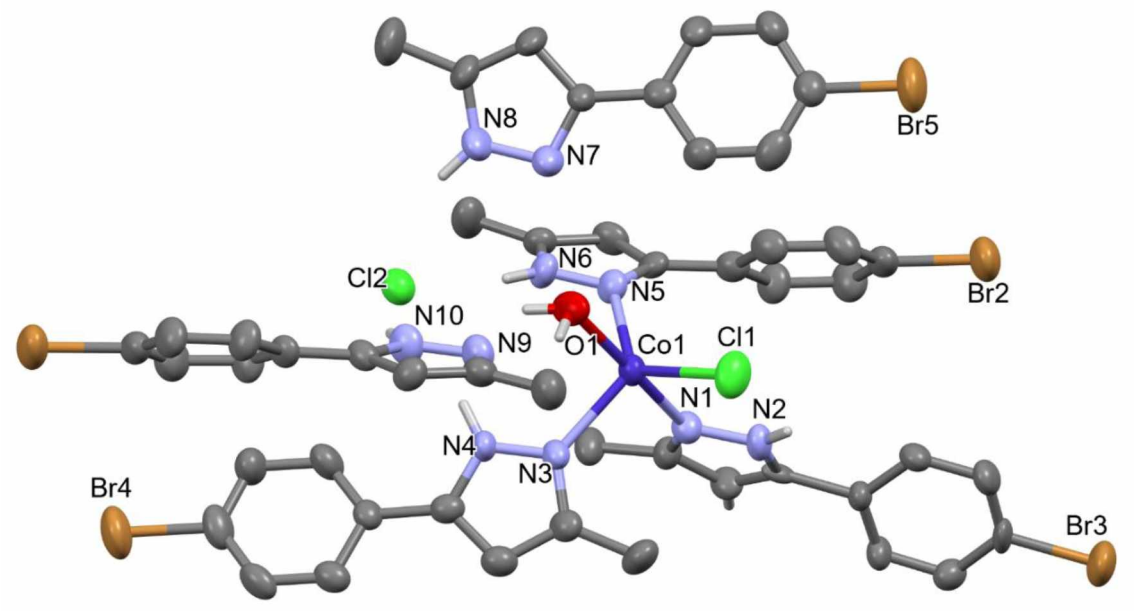

Figure 61. Structure of $CoL_3Cl \cdot H_2O$

Co (II) is coordinated in a trigonal-bipyramidal fashion. Oxygen from water and nitrogen N1 from pyrazole ligand are coordinated in axial positions. Two nitrogens from pyrazole ligands and Cl^- anion are coordinated in equatorial plane. The coordination geometry

around Co (II) can be described as trigonal bipyramidal. The Addison distortion index τ is 0.81 (τ = 0 for a square pyramid and τ = 1 for a trigonal bipyramid). Selected geometrical parameters are shown in Table 10 and Table 11.

Table 10. Selected geometrical parameters for complex $CoL_3Cl{\cdot}H_2O$ - lenght of the bonds in Å

Co1-O1	2.068(8)	*Co1-Cl1*	2.302(3)	*Co1-N5*	2.135(9)	*Co1-N1*	2.149(9)
Co1-N3	2.120(9)	*N1-C3*	1.308(13)	*N1-N2*	1.368(11)	*N2-C1*	1.232(12)
N3-C13	1.339(14)	*N3-N4*	1.342(12)	*N4-C11*	1.346(14)	*N5-C23*	1.335(14)
N5-N6	1.344(11)	*N6-C21*	1.338(14)	*N9-C43*	1.320(15)	*N9-N10*	1.368(13)
N10-C41	1.355(14)	*N7-C31*	1.336(14)	*N7-N8*	1.354(13)	*N8-C33*	1.335(16)

Table 11. Selected geometrical parameters for complex $CoL_3Cl{\cdot}H_2O$ - angles of the bonds

Cl1-Co1-O1	95.3(2)	*Cl1-Co1-N1*	91.5(2)	*N1-Co1-N3*	91.7(3)	*N1-Co1-N5*	87.2(3)
Cl1-Co1-N3	116.5(2)	*Cl1-Co1-N5*	**123.9(3)**	*O1-Co1-N5*	86.0(3)	*N3-Co1-N5*	119.6(3)
O1-Co1-N1	**172.3(3)**	*O1-Co1-N3*	88.5(3)	*O1-Co1-N5*	86.0(3)	*N3-Co1-N5*	119.6(3)

Packing of molecules is determined by the interactions involving free Cl^- anion. Part of the crystal structure viewed down the *c* axis is shown in Figure 62. Hydrogen atoms bonded to carbon are excluded for clarity. Hydrogen bonds are depicted in black, dotted lines (Figure 62).

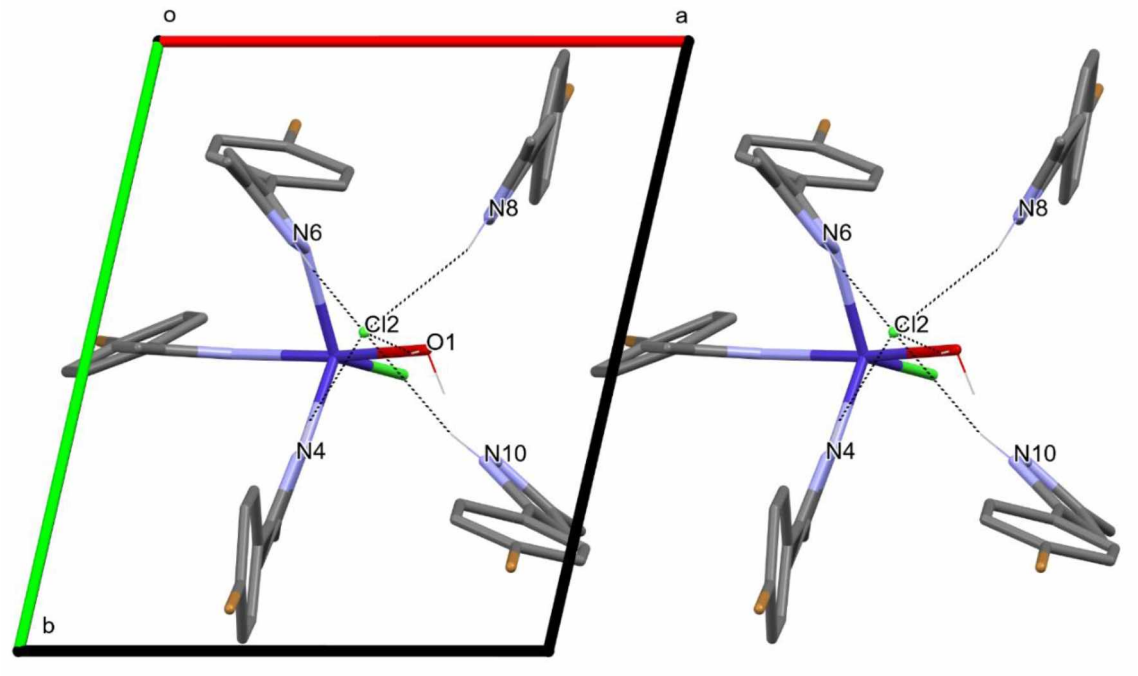

Figure 62. Packing of molecules involving free Cl^- anion

Complex molecule is hydrogen bonded to Cl^- through the interactions of N-H from two coordinated ligands and OH from coordinated water. Third coordinated ligand is not involved in significant nonbonding interactions. Further stabilization of the crystal structure is achieved by interaction of Cl^- with two uncoordinated ligands. Geometry of hydrogen bonds is given in the Table 12.

Table 12. Geometry of hydrogen bonds for complex $CoL_3Cl{\cdot}H_2O$

D-H ..A	H ..A	D-H ..A
N4-H10 .. Cl2	2.5000	170.00
N6-H19 .. Cl2	2.3700	173.00
O1-H47 .. Cl2	2.6500	168.00
N10-H48 .. Cl2	2.3900	156.00
N8-H49 .. Cl2	2.4200	150.00

4.2. Synthesis and characterization of Cu(II), Co(II), Ni (II), Zn(II), Pt(II) and Pd(II) complexes with **4-methylpyrazole (L2)**

During this research the complexes formed with 4-methylpyrazole (L2) were with Cu(II), Co(II), Ni(II), Zn(II), Pt(II) and Pd(II) of formulae $[CuL_2(NO_3)_2]$, $[CoL_4Cl_2]$, $[Ni(OAc)_2L_4]$, $[Zn(OAc)_2L_2]$, $[PtL_3Cl_2]$ and $[Pd(L\text{-}H)_3]$ (Table 13).

Table 13. Formulae and color of complexes of Cu(II), Co(II), Ni(II), Zn(II), Pt(II) and Pd(II) with 4-methylpyrazole

Complex	Color
$CuL_4(NO_3)_2$	Blue
CoL_4Cl_2	Pink
$Ni(OAc)_2L_4$	Azure blue
$Zn(OAc)_2L_2$	Clear light colorless
PtL_3Cl_2	Orange
$Pd(L\text{-}H)_3$	Yellow

4.2.1. Synthesis and characterization of $[CuL_4(NO_3)_2]$

Synthesis of a complex $[CuL_4(NO_3)_2]$: The warm ethanolic solution (3 cm^3) $[Cu(NO_3)_2 \cdot H_2O]$ (0.051 g, 0.25 mmol) was mixed with warm ethanolic solution (3 cm^3) of the ligand L2 (0.041 g, 0.5 mmol) with mild heating. The blue reaction mixture was left to crystallize. After 48 hours, blue single crystals were filtered, washed with ethanol and dried in air. Yield: 0.063 g (81.0 %).

From the reaction mixture, an already structurally characterized and described complex of formulae $[CuL_4(NO_3)_2]$ [130]. As the complex $[CuL_4(NO_3)_2]$ described in literature, was obtained through reaction of water solutions of $Cu(NO_3)_2$ and fomepizole, yielding blue-purple monocrystals [130], and the solvent used for the purpose of the synthesis

presented in this thesis was ethanol, it can be deducted that the solvent did not make the difference in the path of the synthesis. Thus, the results of the single-crystal X-ray structure analysis for this complex $[CuL_4(NO_3)_2]$ will not be presented, yet the results of the XRPD and FTIR analyses as well as deducted bactericidal and cytotoxic activity will be presented as part of the thesis.

As stated the complex was prepared by reacting copper nitrate with 4-methylpyrazole in hot ethanolic solutions (Figure 63).

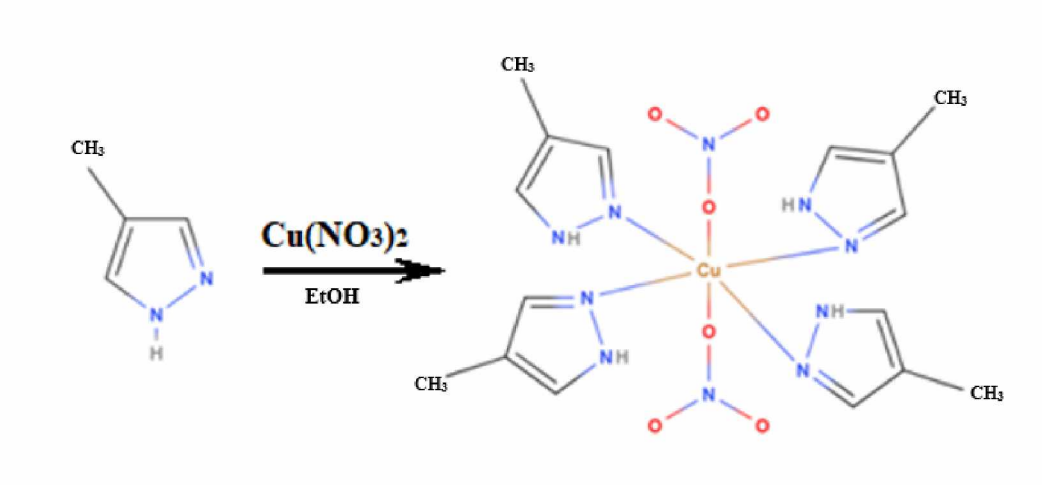

Figure 63. Synthesis of the Cu(II) complex of 4-methylpyrazole

The coordination environment of Cu(II) in its complex is hexahedral. The compound has been characterized by SC-XRD, as well as XRPD spectra and IR spectra. The tests of the antimicrobial and cytotoxic activity of the new copper complex have been conducted and are a part of this thesis.

4.2.1.1. X-ray powder diffraction data of $[CuL_4(NO_3)_2]$

The diffractogram obtained from the XRPD analysis conducted for the obtained complex $[CuL_4(NO_3)_2]$, clearly shows the formation of a crystalline compound with a high dominant peak at the position 9.5791°2θ. For the purposes of identification of the complex in question, most dominant 8 peaks of the diffractogram are listed in the Table 14, with their d spacings and relative intensities.

Table 14. Eight most dominant diffraction lines in powder diffractogram of $CuL_4(NO_3)_2$

Pos. [°2θ]	d-spacing [Å]	Rel. Int. [%]
9.5791	9.22556	100.00
11.4756	7.70483	2.78
12.8579	6.87944	2.21
21.4197	4.14505	2.36
22.8457	3.88946	0.67
23.2640	3.82045	1.90
30.1483	2.96190	1.06
31.1659	2.86748	0.69

As the ligand is used in liquid form (solution), no diffractogram was obtained for it. The conclusion was made by comparing the diffractograms of $Cu(NO_3)_2$ and the product $CuL_4(NO_3)_2$. Similar quantities of both samples were used during the analyses and both samples were analyzed in the same measuring conditions. Diffractograms are part of the Addendum A.

The crystal and molecular structure of the complex was solved by SC-XRD analysis. As previously described and by the obtained SC-XRD results, the complex proved to be an already structurally characterized and described complex [130].

4.2.1.2. FTIR data of $[CuL_4(NO_3)_2]$

IR spectra of the complex $CuL_2(NO_3)_2$ contains the following dominant vibrations: 3188.1 cm^{-1}, 3127.0 cm^{-1}, 1388.2 cm^{-1}, 1314.1 cm^{-1}, 1293.3 cm^{-1}, 1128.2 cm^{-1}, 1075.4 cm^{-1},

1002.6 cm^{-1}, 867.09 cm^{-1}, 826.2 cm^{-1}, 759.3 cm^{-1}, 608.3 cm^{-1}. The IR spectra of the complex is in accordance with the proposed structure.

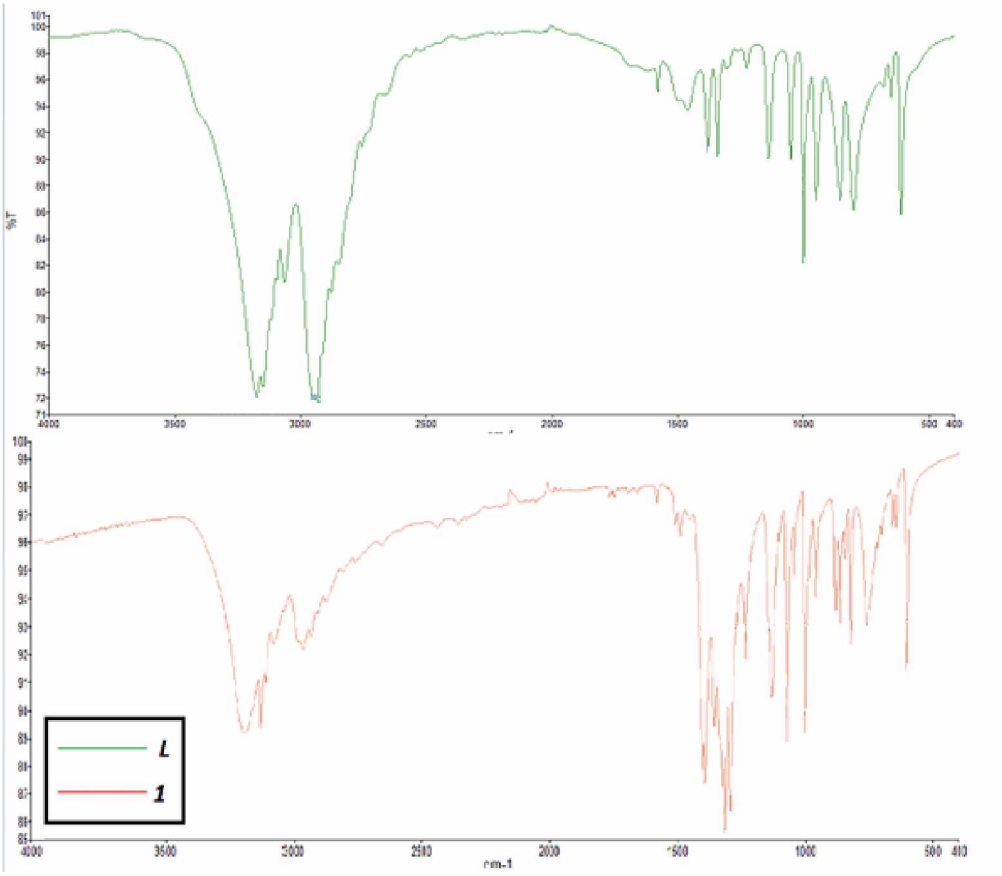

Figure 64. The IR spectra of 4-methylpyrazole – L2 (green) and its complex with copper (red)

4.2.1.3. Bactericidal activity of complex [$CuL_4(NO_3)_2$]

As part of this thesis, complex $CuL_4(NO_3)_2$ was tested for its bactericidal activity. The preparation of test bacteria was carried out by the injection method, a pair of clean colonies were introduced into test tubes with nutrient broth, incubated at 37°C for 24 h with the aim of obtaining a concentration of microbial cells of $1x10_8$ CFU/ml.

The inoculation of the prepared M.H. of the substrate was carried out by the method of sterile swabs, for each bacterial culture in 4 repetitions, by drawing zig zag lines on the substrate. After incubation at 37°C, confluent bacterial growth is expected for 24 h.

The procedure known as the Kirby-Bauer test is a version of the procedure described forty years ago by Bauer, Kirby, Sherris and Turck. The advantages of this method are the simplicity of execution, the possibility of simultaneous testing of a large number of samples, economic profitability and relatively simple reading of the results. The results are qualitative and allow the classification of test microorganisms as sensitive, moderately sensitive or resistant in relation to the antimicrobial agent used [111].

Sterile paper discs with a diameter of 6 mm are placed on the inoculated nutrient medium (M.H. agar) with sterile tweezers, in precisely defined places. 15 μm of the tested preparation of the desired concentration is applied to the disks laid in this way, and then subjected to incubation at 37°C for 24 h. The antimicrobial agent (preparation) diffuses into the agar and inhibits the growth of the test microorganism by creating "empty" zones whose diameter is measured with a millimeter caliper. The diameters of the inhibition zones are compared with standard values for the same bacteria and the antibiotic gentamicin. The results were interpreted according to EUCAST (The European Committee on Antimicrobial Susceptibility Testing) and CLSI (Clinical and Laboratory Standards Institute) standards. According to the mentioned standard, the effect of the essential oil on the microorganism test was evaluated through three categories:

- S (susceptible) - the probability of success of the therapy is high after the use of usual doses of antibiotics, given in the usual way
- I (intermediately (moderately) sensitive) - possible success of the therapy if the antibiotic is given in max. concentrations and through penetration
- R (resistant) - never used in therapy, regardless of the dose, therapy is very likely to be unsuccessful

The results were interpreted according to EUCAST (The European Committee on Antimicrobial Susceptibility Testing) and CLSI (Clinical and Laboratory Standards Institute) standards. According to the mentioned standard, the influence of the preparation on the microorganism test was evaluated through three categories:

- S- sensitive
- I-intermediately (moderately) sensitive
- R-resistant

Based on the measured zones of inhibition of tested samples of preparations and bacteria, a comparative analysis of the obtained results with the standard values of the antibiotic Gentamicin for the bacteria Escherichia coli and Salmonella spp. was performed. The obtained results are shown in a Table 16. The standard values of the antibiotic Gentamicin for the bacteria Escherichia coli and Enterococcus faecalis are shown in the table 15.

Table 15. Inhibition zones for E. coli and Salmonella spp. CISI M100-S21 Performance Standards for Antimicrobial Susceptibility Testing. EUCAST.

Diameter of inhibition zone			
Escherichia coli	S	I	R
Gentamicin	≥15	13-14	≤12
Salmonellla spp.	S	I	R
Gentamicin	≥17	13-16	≤14

Based on the results presented in Table 16 and the presentation in Figure 65, it can be claimed that all three used concentrations of $CuL_4(NO_3)_2$ showed a slightly inhibitory effect both on the growth of *E coli* bacteria and on the growth of bacteria from the genus *Salmonella spp.* The largest zone of inhibition on both investigated bacteria showed a concentration of 10^{-2} with an average inhibition zone of 8.00 mm for *E.coli*, or 8.75 mm for bacteria from the genus *Salmonella spp*. The concentration of 10^{-5} (6.50 mm) had the least inhibitory effect on bacterial species of the genus Salmonella. Comparing the obtained results with the standard values of the antibiotic Gentamicin, it can be claimed that both tested bacteria are resistant to $CuL_4(NO_3)_2$.

Table 16. Results of measurement of zones of inhibition of $CuL_4(NO_3)_2$ for all three concentrations

$CuL_4(NO_3)_2$	Avergae value of inhibition zone (mm)	
	Esherichia coli	*Salmonella spp.*
Concentration 10^{-2}	8,00 mm	8,75 mm
Concentration 10^{-4}	7,00 mm	6,75 mm
Concentration 10^{-5}	7,25 mm	6,50mm

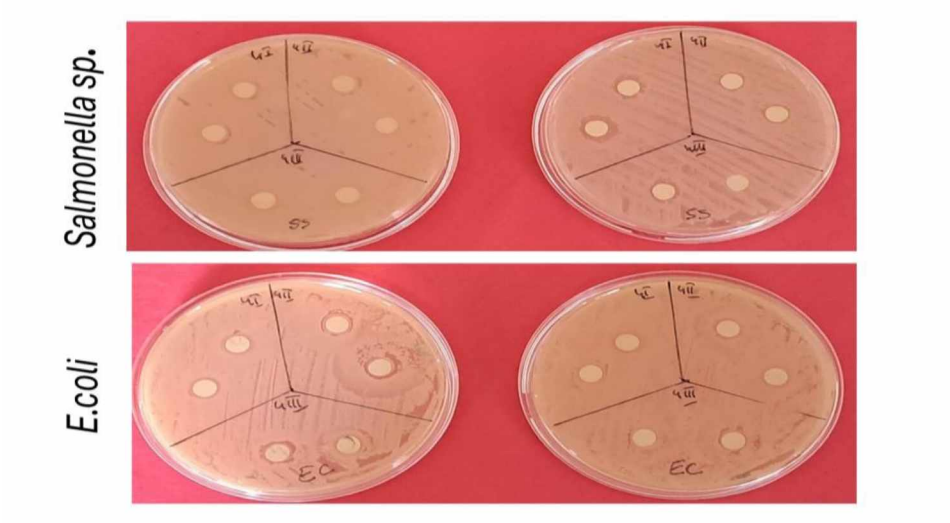

Figure 65. Presentation of the inhibitory effect of $CuL_4(NO_3)_2$ on E. Coli and Salmonella. spp.

4.2.2. Synthesis and characterization of $[CoL_4Cl_2]$

Synthesis of a complex $[CoL_4Cl_2]$: The warm ethanolic solution (3 cm^3) $[CoCl_2 \cdot 6H_2O]$ (0.033 g, 0.25 mmol) was mixed with warm ethanolic solution (3 cm^3) of the ligand L2 (0.041 g, 0.5 mmol) with mild heating. The dark blue reaction mixture was left to crystallize. After 3 days, purple single crystals were filtered, washed with ethanol and dried in air. Yield: 0.024 g (32.7 %).

From the reaction mixtures, new complex compound of formulae $[CoL_4Cl_2]$ was crystallized. The crystal and molecular structure of the synthesized complex $[CoL_4Cl_2]$ was determined by single-crystal X-ray structure analysis. As stated the complexes were prepared by reacting copper nitrate and cobalt chloride with 4-methylpyrazole in hot ethanolic solutions (Figure 66).

The complex was analyzed via XRPD and SC-XRD analyses. The complex was prepared by reacting cobalt chloride with 4-methylpyrazole in hot ethanolic solution.

On the basis of SC-XRD analysis and IR spectra, a structure of the complex was determined (Figure 66).

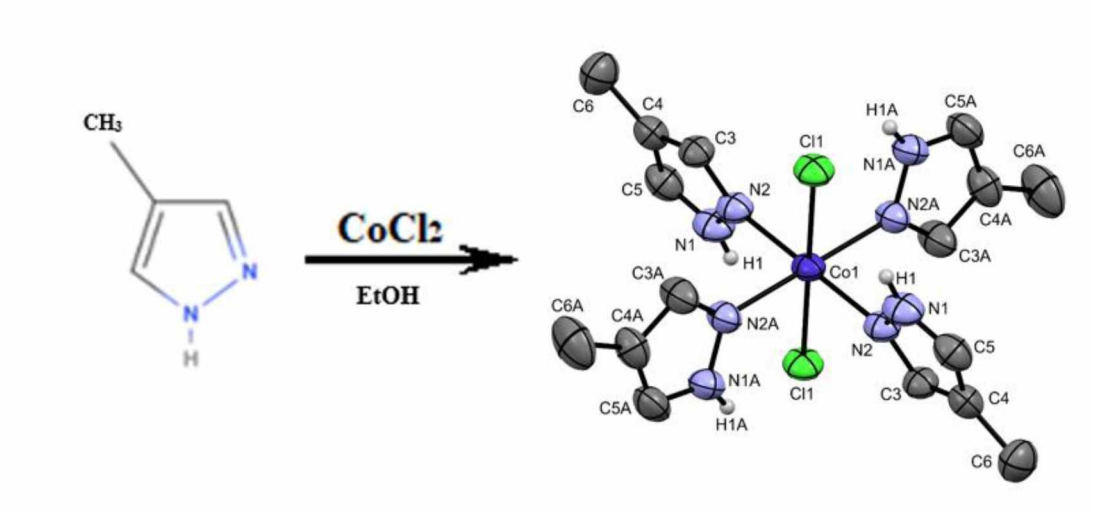

Figure 66. Synthesis of the Co(II) complex of 4-methylpyrazole

4.2.2.1. X-ray powder diffraction data of [CoL_4Cl_2]

The diffractogram obtained from the XRPD analysis conducted for the obtained complex [CoL_4Cl_2], shows the formation of a crystalline compound with a dominant peak at the position 15.7872°2θ. For the purposes of identification of the complex in question, most dominant 8 peaks of the diffractogram are listed in the Table 17, with their d spacings and relative intensities.

Table 17. Eight most dominant diffraction lines in powder diffractogram of CoL_4Cl_2

Pos. [°2θ]	d-spacing [Å]	Rel. Int. [%]
8.1007	10.90568	13.91
10.2154	8.65234	59.14
11.6819	7.56924	45.73
13.3706	6.61680	56.92
15.7872	5.60894	100.00
18.4389	4.80788	14.00

21.2054	**4.18647**	**32.46**
31.8239	**2.80967**	**27.92**

As the ligand is used in liquid form (solution), no diffractogram was obtained for it. The conclusion was made by comparing the diffractograms of $CoCl_2$ and the product CoL_4Cl_2. Similar quantities of both samples were used during the analyses and both samples were analyzed in the same measuring conditions. Diffractograms are part of the Addendum A.

4.2.2.2. Crystal and molecular structure of $[CoL_4Cl_2]$

The obtained single crystals have been analyzed through SC-XRD in order to obtaine its molecular and crystal structure, shown in the Figure 67. Table 18 contains crystallographic data.

Table 18. Data collection and handling of SC-XRD data of CoL_4Cl_2

	$[CoL_4Cl_2]$
Empirical formula	$C_{16}H_{24}Cl_2CoN_8$
Formula weight	458.26
Temperature	293 K
Wavelength(Å)	0.71073
Crystal size (mm)	0.24 0.16 0.03
Crystal habitus	Plate
Crystal color	Pink
Crystal system	Monoclinic
Space group	C -15
Unit cell dimensions(Å)	a= 9.2854(7); b= 13.2723(12); c= 17.417(4)
Unit cell angles (°)	α= 90 ; β= 93.357(6); γ= 90
Volume	2142.7(6)
Z	4
Density (calc.) (g cm^{-3})	1.421
Absorption coefficient (mm^{-1})	1.068
*R*int	0.018
F (000)	948
Data/Parameters	2563 /126
Goodness-of-fit on F^2	1.041
R/w*R* [I > 2σ (I)]	0.0428/ 0.0904
Largest diff. peak and hole (e$Å^{-3}$)	0.219 / -0.184

Presented in the Figures 67 and 68, the complex has a Co central atom in coordination with two Cl atoms in trans disposition, and four ligands coordinated through their pyridine-like nitrogens in octahedral coordination.

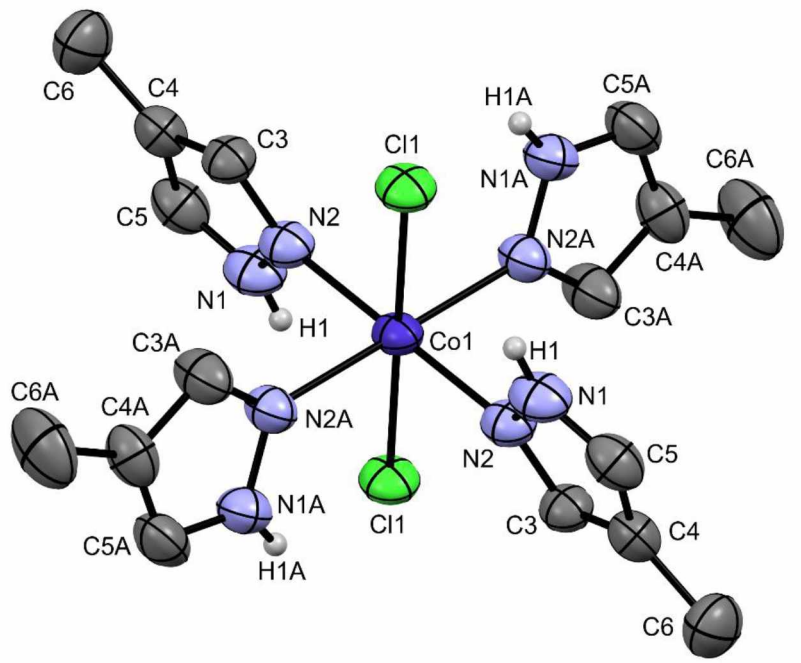

Figure 67. ORTEP diagram and atom labeling scheme of (tetrakis(4-methyl-1H-pyrazole))-dichloro-cobalt(II). Hydrogen atoms bonded to carbon are omitted for clarity

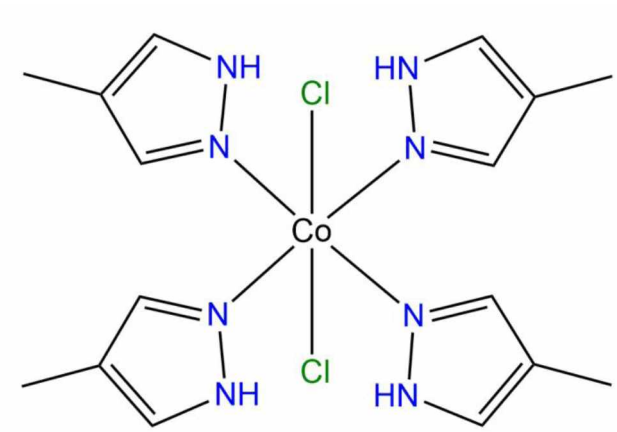

Figure 68. Structure of CoL_4Cl_2

Bond lengths of the chemically equivalent ligands are not significantly different (Table 19). There are no significant differences in the bond lengths of pyrazolyl ligands in comparison to free 4-methyl-pyrazole. Selected bond angles of the complex are presented in the Table 20.

Table 19. Selected bond lengths (Å) of [CoL_4Cl_2]

Bond	Distances (Å)	Bond	Distances (Å)	Bond	Distances (Å)
Co1-N2A	2.1167(2)	N2A-C3A	1.321(3)	N1A-H1A	0.9299
Co1-N2	2.1254(2)	N2A-N1A	1.337(2)	C4-C5	1.366(3)
Co1-Cl1	2.5402(5)	N1-C5	1.329(3)	C4-C3	1.389(3)
N2-C3	1.327(2)	N1-H1	0.9345	C4-C6	1.498(3)
N2- N1	1.351(2)	N1A-C5A	1.338(3)	C3-H3	0.9300
				C5-H2	0.9300

Table 20. Selected bond angles (°) of [CoL_4Cl_2]

Bond	Angles (°)	Bond	Angles (°)
N2A-Co1- N2A	180.00(8)	C3-N2-N1	104.14(17)
N2A - Co1- N2	89.77(6)	C3-N2-Co1	131.92(13)
N2 - Co1-N2	180.00(8)	N1-N2-Co1	123.82(12)
N2A - Co1-Cl1	91.61(5)	C3A-N2A-N1A	104.76(17)
N2 - Co1- Cl1	88.39(5)	C3A-N2A-Co1	132.71(14)
Cl1 - Co1- Cl1	180.00 (8)	N1A-N2A-Co1	132.71(14)

CoL_4Cl_2 complex contains Co in octahedral environment. Two Cl atoms and four 4-methylpyrazole bonds to Co. The methyl group of the ligand (4-methylpyrazole) has C…C contacts with other methyl group of the neigbouring mononuclear complex as presented in Figure 69, which makes the aggregation of the complex molecules in the crystal possible. Atom labelling depicts color codes of atoms.

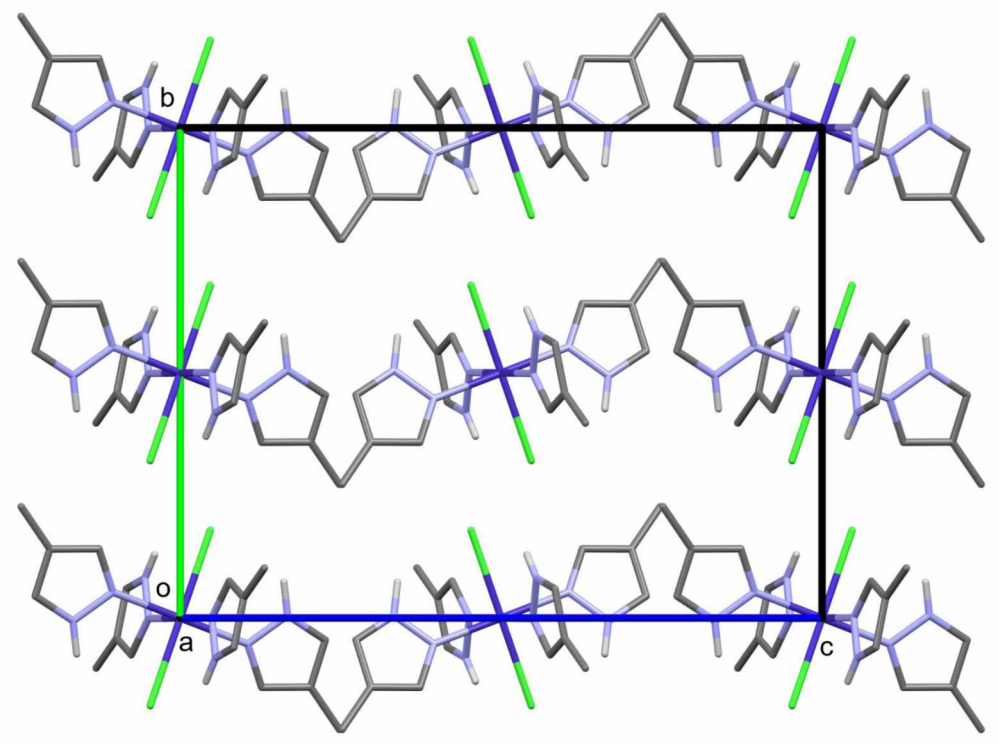

Figure 69. Packing of molecules in the crystal structure

Intramolecural hydrogen bonds are formed between pyrole-like nitrogen and its hydrogen with its neighboring chlorine atom, with slight difference in length of the bond as presented in the Table 21. There are no significant intermolecular contacts.

Table 21. Intramolecular hydrogen bonds:

D-H...A	H...A(Å)	D...A(Å)	D-H...A(°)
N1-H1..Cl1	2.49	3.195(2)	133
N1A-H1A..Cl1	2.43	3.149(2)	134

4.2.3. Synthesis and characterization of $[Ni(OAc)_2L_4]$

Synthesis of a complex $[Ni(OAc)_2L_4]$: The warm ethanolic solution (3 cm^3) $[Ni(OAc)_2 \cdot 4H_2O]$ (0.062 g, 0.25 mmol) was mixed with warm ethanolic solution (3 cm^3) of the ligand L2 (0.041 g, 0.5 mmol) with mild heating. The blue reaction mixture was

left to crystallize. After 2 days, azure blue single crystals were filtered, washed with ethanol and dried in air. Yield: 0.030 g (29.4 %).

From the reaction mixture, new complex compound of formulae: $[Ni(OAc)_2L_4]$ was crystallized. The crystal and molecular structure of the synthesized complex was determined by single-crystal X-ray structure analysis. The complex was prepared by reacting nickel acetates with 4-methylpyrazole in hot ethanolic solutions. The nickel complex crystallizes in light blue prisms. The coordination environment of Ni(II) in its complex is octahedral. Results of CHN analysis are presented in the Table 22.

Table 22. Results of the CHN analysis for the complex $[Ni(OAc)_2L_4]$

	Theoretical $[Ni(OAc)_2L_4]$	Found
C%	*47.7 %*	*47.55 %*
H%	*5.6 %*	*5.99 %*
N%	*21.9 %*	*22.18 %*

On the basis of CHN analysis, FTIR results and single-crystal X-ray structure analysis, a structure of the complex was determined (Figure 70).

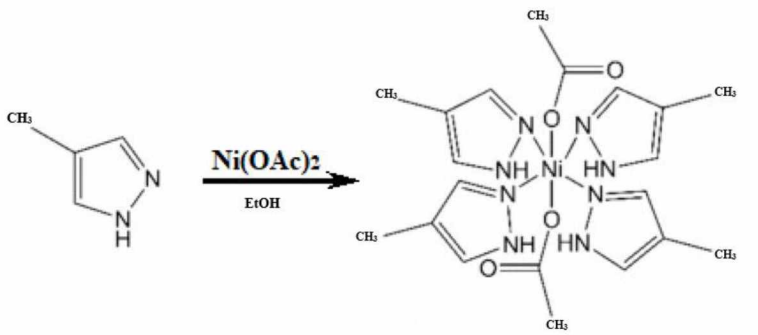

Figure 70. Synthesis of the Ni(II) complex of 4-methylpyrazole

4.2.3.1. X-ray powder diffraction data of $[Ni(OAc)_2L_4]$

The diffractogram obtained from the XRPD analysis conducted for the obtained complex $[Ni(OAc)_2L_4]$, shows the formation of a crystalline compound with a dominant peak at the position 10.7966°2θ. For the purposes of identification of the complex in question, most dominant 8 peaks of the diffractogram are listed in the Table 23, with their d spacings and relative intensities.

Table 23. Eight most dominant diffraction lines in powder diffractogram of $Ni(OAc)_2L_4$

Pos. [°2θ]	d-spacing [Å]	Rel. Int. [%]
10.6179	**8.32518**	**45.16**
10.7966	**8.18780**	**100.00**
11.8767	**7.44550**	**15.67**
11.9792	**7.38203**	**34.21**
12.3475	**7.16265**	**21.62**
20.9663	**4.23365**	**15.80**
23.5038	**3.78202**	**21.22**
28.7929	**3.09818**	**14.34**

As the ligand is used in liquid form (solution), no diffractogram was obtained for it. The conclusion was made by comparing the diffractograms of $Ni(OAc)_2$ and the product $Ni(OAc)_2L_4$. Similar quantities of both samples were used during the analyses and both samples were analyzed in the same measuring conditions. Diffractograms are part of the Addendum A.

4.2.3.2. FTIR data of $[Ni(OAc)_2L_4]$

The IR spectrum of the complex $[Ni(OAc)_2L_4]$ contains the following dominant bands (Figure 71): 2924.6 cm^{-1}, 1550.4 cm^{-1}, 1415.3 cm^{-1}, 1145.5 cm^{-1}, 1003.3 cm^{-1}, 959.5 cm^{-1}, 850.3 cm^{-1}, 653.0 cm^{-1}, 620.2 cm^{-1}. The IR spectra of the complex is in accordance with the proposed structure.

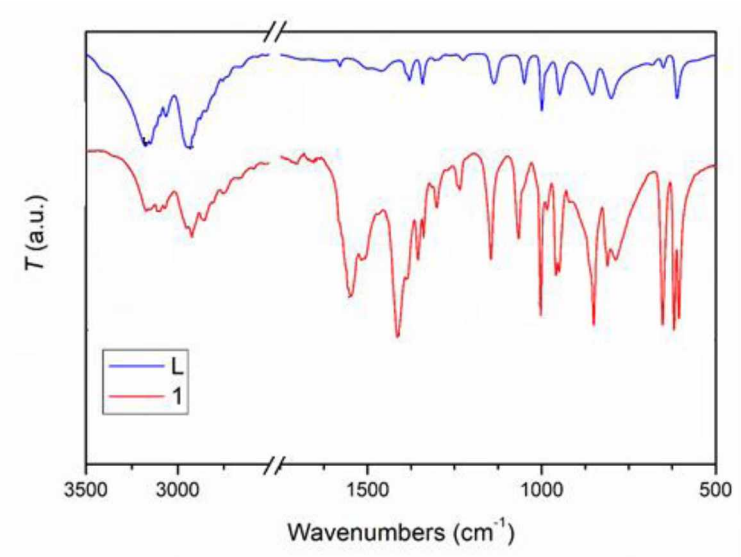

Figure 71. The IR spectra of 4-methylpyrazole – L2 (blue) and its complex - $Ni(OAc)_2L_4$ (red)

4.2.3.3. Crystal and molecular structure of $[Ni(OAc)_2L_4]$

The obtained single crystals have been analyzed through SC-XRD in order to obtain its molecular and crystal structure, shown in the Figure 72. Table 24. contains crystallographic data.

Table 24. Crystallographic and refinement data for the complexes

	$[Ni(OAc)_2L_4]$
Empirical formula	$C_{20}H_{30}N_8O_4Ni$
Formula weight	505.21
Temperature	200 K
Wavelength(Å)	0.71073
Crystal size (mm)	0.4 0.2 0.03
Crystal habitus	Prism
Crystal color	Azure blue
Crystal system	Triclinic

Space group	P -1
Unit cell dimensions(Å)	a= 9.5219(8); b= 9.9441(8); c= 12.8953(11)
Unit cell angles (°)	α= 96.613(3); β= 97.824(3); γ= 93.904(3)
Volume	1197.24(2)
Z	2
Density (calc.) (g cm^{-3})	1.401
Absorption coefficient (mm^{-1})	0.853
*R*int	0.047
F (000)	532
Data/Parameters	9162/307
Goodness-of-fit on F^2	1.018
R/w*R* [I > 2σ (I)]	0.0590/ 0.0903
Largest diff. peak and hole (e$Å^{-3}$)	0.391/-0.433

The asymmetric unit contains two halves of the title molecule (Figure 73) with nickel(II) ions sitting on inversion centers. Four 4-methyl-pyrazole and two acetato ligands are coordinated to Ni(II) in a distorted octahedral geometry. In the following text, two symmetry-unique complexes of the title compound will be referred as **1A** and **1B**. The molecular diagram and atom labeling scheme of molecule **A** is shown in Figure 72. Equivalent atom labels, with the suffix **B**, are used for the second symmetry-unique molecule.

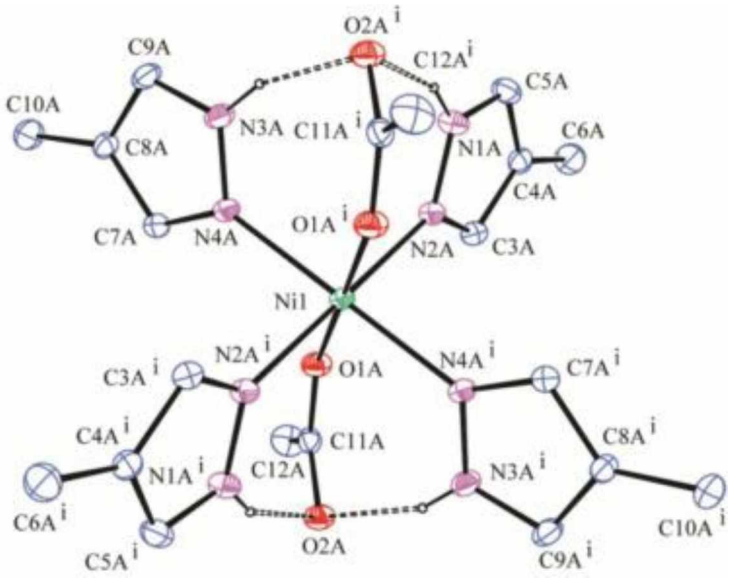

Figure 72. Complex labeled as 1A with Ni1 at the inversion center and atom labeling scheme. C¯H single bond hydrogens are omitted for clarity. A dotted line depicts intramolecular hydrogen bonds

The Ni(II) ion is coordinated with two O atoms from the acetato groups and four pyrazole-N atoms from 4-methyl-pyrazole ligands. The Ni-N distances (Table 25) are close to the range previously observed in a similar coordination environment of Ni. Angles around Ni1/Ni2 are shown in Table 26.

*Table 25 Symmetry-unique bond distances (Å) around Ni1 and Ni2 in compound **1**.*

Bond	Distances (Å)	Bond	Distances (Å)
Ni1-O1A	2.075(1)	Ni2-O1B	2.086(1)
Ni1-N2A	2.093(1)	Ni2-N2B	2.099(1)
Ni1-N4A	2.112(1)	Ni2-N4B	2.094(1)

In both **1A** and **1B** the uncoordinated oxygen atom of each acetato group forms intramolecular hydrogen bonds with two N–H hydrogen atoms attached to the pyrazole rings. The position of intramolecular hydrogen bonds in complex **1A** is depicted in Figure 73. Coordination angles involving only pyrazole-N are close to octahedral. Deviations from ideal octahedral geometry are associated with acetato ligands involved in intramolecular hydrogen bonds.

Table 26 Angles involving Ni1 and Ni2 with coordinated atoms.

Bond	Angles (°)	Bond	Angles (°)
N2A-Ni1-N4A	90.30(5)	N2B-Ni2-N4B	91.32(5)
N2A-Ni1-N4A^{i}	89.71(5)	N2B-Ni2-N4B^{ii}	88.68(5)
O1A^{i}-Ni1-N4A	93.88(4)	O1B^{ii}-Ni2-N4B	94.11(4)
O1A^{i}-Ni1-N2A	93.96(5)	O1B^{ii}-Ni2-N2B	94.28(5)
O1A-Ni1-N2A	86.05(5)	O1B-Ni2-N2B	85.73(5)
O1A-Ni1-N4A	86.12(4)	O1B-Ni2-N4B	85.90(4)

Symmetry codes: i=1-x,1-y,1-z; ii= −x,-y,-z.

Both symmetry-unique complex molecules (**1A**, **1B**) exhibit similar geometrical features. The overlay of molecules **1A** and **1B** shown in Figure 73 illustrates the structural similarity of two crystallographically nonequivalent complexes.

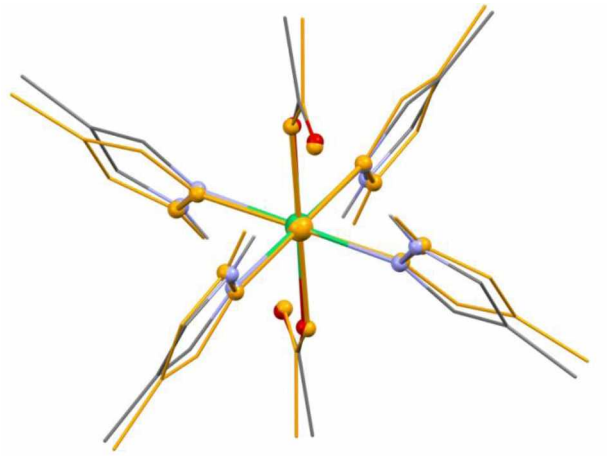

Figure 73. Structure overlay of complexes 1A and 1B illustrates structural similarity. 1A is colored according to elemental composition, and 1B is shown in orange. A. H atoms bonded to C have been omitted.

Comparison of the molecular structure of the free ligand 4-methylpyrazole [131] and its corresponding Ni(II) complexes (**1A**, **1B**) indicates a similar pattern of bonding in the pyrazole ring in both free and coordinated ligands. N-N bond distances in the title compound range from 1.341 to 1.347Å. In the free ligand, this bond range is 1.343-1.349Å. The N-C bonds in the uncoordinated ligand are in the range 1.333-1.349Å, while in the title complexes, these distances are 1.330-1.349Å. The geometrical properties of the intramolecular hydrogen bonds in **1A** and **1B** are similar (Table 27).

Table 27. Geometrical properties of intramolecular hydrogen bonds in molecules 1A and 1B.

D-H..A	H..A (Å)	D-H..A (°)
N3B-H1..O2B^{i}	1.96	156
N1B-H3..O2B^{i}	1.95	156
N3A-H4..O2A^{ii}	1.92	161
N1A-H5..O2A^{ii}	1.98	158

symmetry codes: i= -x,-y,-z; ii= 1-x,1-y,1-z

The closest intermolecular contacts in the title structure are listed in Table 28. There are no significant intermolecular contacts.

Table 28. Geometrical properties of the closest intermolecular contacts in the title structure.

D-H..A	H..A (Å)	D-H..A (°)
C9B-H2..O2A^{iii}	2.49	155

C9A-H13..O2B^{iv}	2.32	169
C12A-H20C..O2A^{v}	2.59	169

symmetry codes: iii= 1-x,-y,1-z; iv= 2-x,1-y,1-z; v= -x,1-y,-z

CSD survey identified two relevant structurally related compounds, bis(acetato-κO)tetrakis(1H-pyrazole-κN1)nickel(II) ([Ni(OAc)$_2$(L')$_4$]) [132] (Figure 74) and its hydrated form ([Ni(OAc)$_2$(L')$_4$]·4H$_2$O) [133] (Figure 74); where L' denotes the pyrazole ligand. Structurally related molecules of [Ni(OAc)$_2$(L')$_4$] and [Ni(OAc)$_2$(L')$_4$]·4H$_2$O differ from molecules **1A** and **1B** in the absence of methyl substituent at C4. Additionally, in the crystal structure of ([Ni(OAc)$_2$(L')$_4$]·4H$_2$O, the solvent water is present. The coordination environment and geometry in complexes **1A**, **1B**, and ([Ni(OAc)$_2$(L')$_4$] are similar. The patterns of intermolecular interactions in the title compound **1** and ([Ni(OAc)$_2$(L')$_4$] are also similar. In complex ([Ni(OAc)$_2$(L')$_4$]·4H$_2$O however, the solvent water with the capacity for both donating and accepting hydrogen bonds influences the coordination environment and the packing of molecules in the crystal. The main structural difference between [Ni(OAc)$_2$(L')$_4$]·4H$_2$O and the other more similar complexes (**1A/1B** and [Ni(OAc)$_2$(L')$_4$]) is the difference in the orientations of the two pyrazole rings. In **1A/1B** and [Ni(OAc)$_2$(L')$_4$], two pyrazole rings are oriented towards the closest noncoordinated acetato oxygen which is associated with the formation of an intramolecular hydrogen bond. In **1** and [Ni(OAc)$_2$(L')$_4$] the crystal structure is characterized by the absence of strong intermolecular contacts. The packing of molecules in [Ni(OAc)$_2$(L')$_4$] and **1** are shown in Figures 75 and 76.

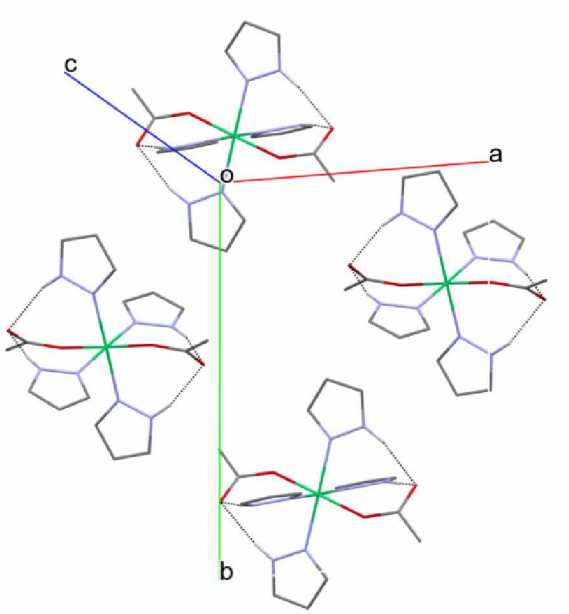

Figure 74. Aggregation of molecules of [Ni(OAc)$_2$(L')$_4$] in the unit cell. Intramolecular hydrogen bonds are depicted as dotted black lines. C-H atoms are omitted for clarity. Significant intermolecular interactions are absent.

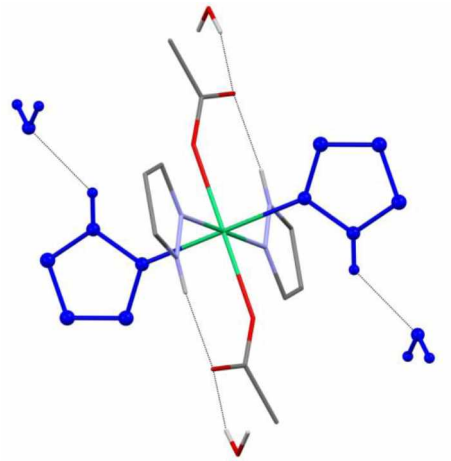

Figure 75. Part of the crystal structure of [Ni(OAc)$_2$(L')$_4$]·4H$_2$O, showing a difference in the orientation of two pyrazole rings in comparison to 1 and [Ni(OAc)$_2$(L')$_4$]. Relevant pyrazole rings and intermolecular interactions with water are depicted in blue, in a 'ball and stick' representation. This feature is important for different modes of molecular aggregation in [Ni(OAc)$_2$(L')$_4$]·4H$_2$O, compared to 1 and [Ni(OAc)$_2$(L')$_4$].

In [Ni(OAc)$_2$(L')$_4$]·4H$_2$O, two pyrazole rings retain a similar position relative to the closest acetato oxygen, but the other two rings point away from the acetato oxygen and orients to form an intermolecular hydrogen bond with solvent water. Figure 75 illustrates the most significant difference in the overall molecular shape of [Ni(OAc)$_2$(L')$_4$]·4H$_2$O

relative to **1** and $[Ni(OAc)_2(L')_4]$. Pyrazole rings point away from acetato oxygen and associated intermolecular interactions are depicted in a 'ball and stick' representation, while the rest of the molecule is shown in a 'capped sticks' representation. C-H atoms are omitted for clarity. Intramolecular hydrogen bonding is depicted in dotted black lines.

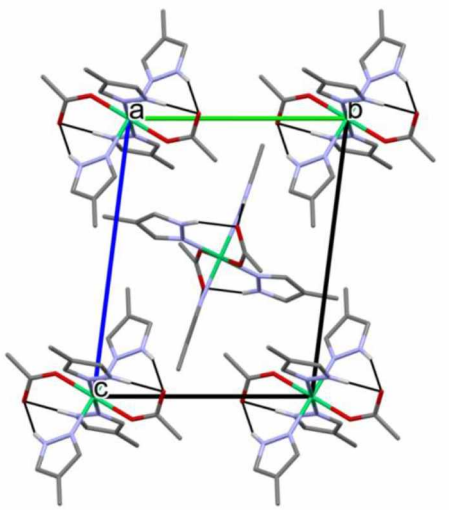

Figure 76. Part of the crystal structure of 1 illustrates the absence of significant intermolecular interaction. Intramolecular N-H…O interactions are depicted as black lines.

These differences lead to markedly different modes of molecular aggregation in $[Ni(OAc)_2(L')_4]\cdot 4H_2O$ compared to **1** and $[Ni(OAc)_2(L')_4]$. In $[Ni(OAc)_2(L')_4]\cdot 4H_2O$, due to the presence of solvent water and the capability of complex molecule to change the overall conformation, strong intermolecular hydrogen bonds are formed, and as a consequence, extended network of metallo-organic units is formed (Figure 77).

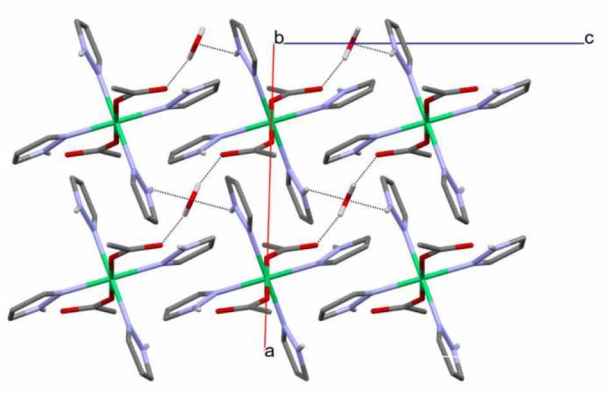

Figure 77. Part of the crystal structure of $[Ni(OAc)_2(L')_4]\cdot 4H_2O$ viewed down the b axis, illustrating the interconnection of molecules. Only intermolecular bonds are depicted (dotted black lines).

4.2.3.4. Thermal properites of $[Ni(OAc)_2L_4]$

Since the thermal stability of the newly prepared compounds is crucial for their future application, the stability of Ni(II) complex was determined and its thermal decomposition was analyzed in an inert atmosphere. The thermogravimetric (TG) and derivative thermogravimetric (DTG) curves of the decomposition of $[Ni(OAc)_2L_4]$ are presented in Figure 78. The complex is stable up to 118 °C, onset. Above this temperature, it loses 56.4 % of its mass, which may correspond to the evaporation of two acetates and two 4-methylpyrazole ligands (55.87 %). However, the nature of gaseous decomposition products needs to be additionally proved. The intermediate starts to decompose above 300 °C and up to 600 °C loses 31.9 % of the mass, which is in good agreement with the mass percent of two 4-methylpyrazole ligands (32.50 %). The final solid decomposition product is 11.6 % of the sample mass and suggests the formation of elemental nickel. The starting complex $[Ni(OAc)_2L_4]$ contains 11.62 % Ni.

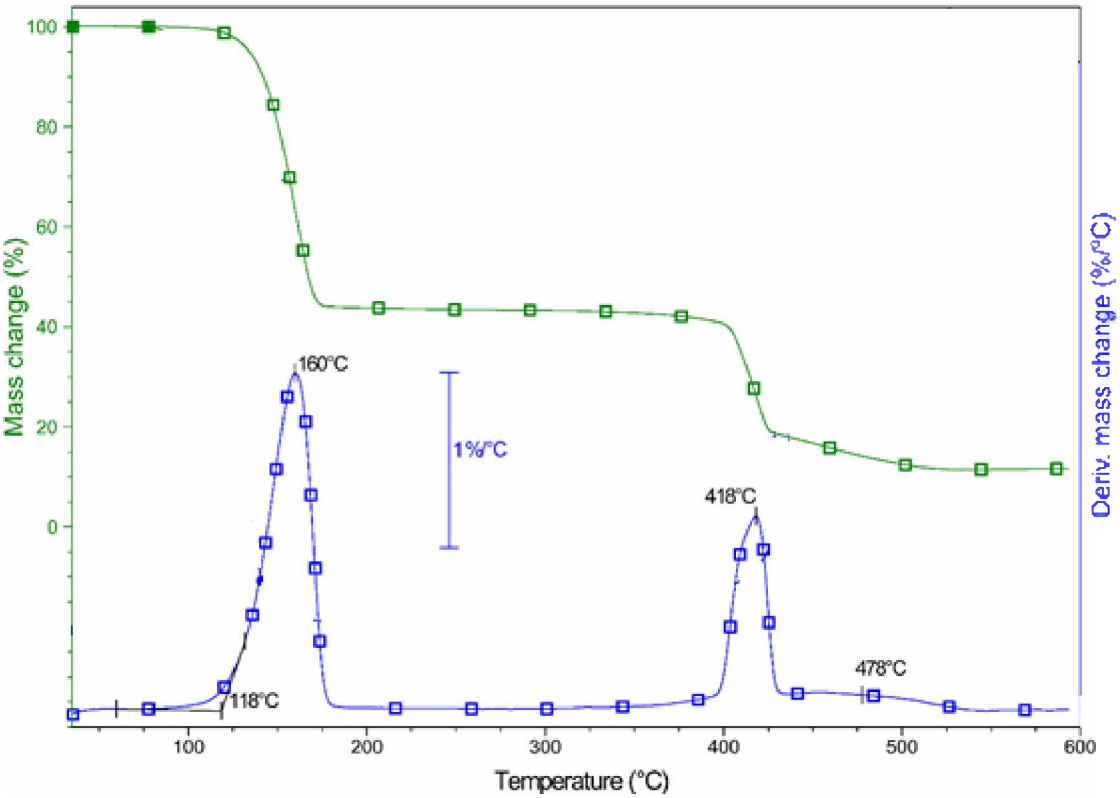

Figure 78. TG and DTG curves of the complexe [Ni(OAc)$_2$L$_4$] in Argon.

To get a better insight into the decomposition mechanism of the complex, it was also analyzed by coupled TG-MS measurements. During the first decomposition step of [Ni(OAc)$_2$L$_4$] fragments of both acetates were detected (CO_2^+, CO^+, H_2O^+) and L (CHN^+, $C_2H_3^+$, HN_2^+, CH_3N^+, $C_2H_5^+$, and $C_3H_3^+$). Besides, the peaks 44 and 30 *m/z* of almost the same intensity together with 17, 18, and 28, (Figure 79) suggest the formation of different oxidized products such as CO_2, N_2O, NO, CO, and H_2O. These nitrogen oxides and the evolved water confirm not only the decomposition of two acetates and two L but their interactions with each other, too. Since pyrazole does not contain oxygen, its oxidation and formation of nitrogen oxides is possible only in the presence of oxygen from other sources, in this case from acetate. In the second step, the rest of the complex is decomposed. Based on the detected fragments, the oxygen from the acetates is enough to oxidize the rest of the pyrazole ligands, but the final decomposition product is mainly metallic nickel, reduced during the intramolecular redox processes, and not its oxide.

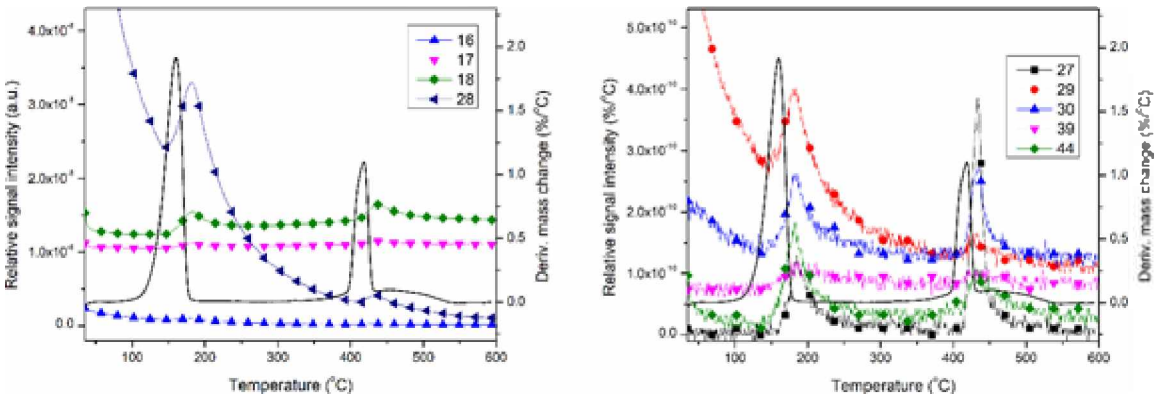

Figure 79. MS curves of the characteristic fragments of [Ni(OAc)$_2$L$_4$] in argon.

4.2.3.5. Antioxidative potential of [Ni(OAc)$_2$L$_4$]

The synthesized sample was tested for the scavenging effect on the DPPH radical (DPPH). The DPPH radical is a relatively stable whose solution in methanol is purple with an absorption maximum at λ_{max} = 515 nm. The presence of potential electron donors or H atoms leads to the neutralization of DPPH radicals and the transition to a neutral form, which is followed by a change in absorbance and the disappearance of the purple color of the solution.

The tested sample was dissolved in ethanol, and two concentrations were prepared for both complexes, 10 and 20 mg/mL. Fifty microliters of the sample's solution were added to the 160 Âµl of DPPH solution (previously prepared as a 0.4 mmol/l solution in 96 % ethanol, which was then diluted four times in methanol to give an absorbance at 515 nm of 0.9) and 90 Âµl of methanol were added to reach the final volume of 300 µl. Blank (the tested sample is substituted with the used solvent) and matrix blank (solvent and samples without DPPH solution) probes have also been added. The series of Trolox solutions (ranging from 1 to 100 mg/ml) were used as calibration standards. The DPPH solution and methanol were added to the Trolox samples in the exact amounts as the tested samples. Absorbance at 515 nm was measured after 60 min. The results are presented in the Figure 80.

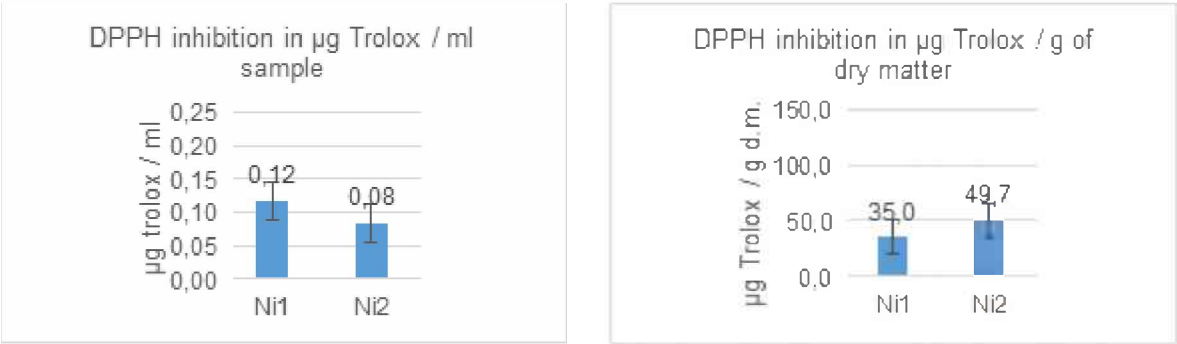

Figure 80. The radical scavenger capacity (RSC) of the [NiL$_4$(OAc)$_2$] complex was determined in solutions of different concentrations: Ni1 20 mg/mL and Ni2 10 mg/mL. RSC is expressed as µg of Trolox equivalent per mL of sample solution (left) and as µg of Trolox equivalent per g of dry sample (right).

Comparing the results with some recalculated results of the antioxidative potential of some pyrazole-containing compounds found in the literature [134-137] indicates that analyzed compound possesses comparable DPPH• scavenging activity, which presents potential for further biological assays. However, results found in scientific papers are expressed differently, and it must be considered that pyrazole structures in various complexes have different chemical surroundings and that antioxidative potential results from overall structure properties, arrangement, dynamics, and interactions of chemical species within the complex.

4.2.4. Synthesis and characterization of [Zn(OAc)$_2$L$_2$]

Synthesis of a complex [Zn(OAc)$_2$L$_2$]: The warm ethanolic solution (3 cm^3) [Zn(OAc)$_2$·2H$_2$O] (0.055 g, 0.25 mmol) was mixed with warm ethanolic solution (3 cm^3) of the ligand L2 (0.041 g, 0.5 mmol) with mild heating. The colorless reaction mixture was left to crystallize. After 2 days, white transparent single crystals were filtered, washed with ethanol and dried in air. Yield: 0.034 g (34.3 %).

From the reaction mixture, new complex compounds of formulae: [Zn(OAc)$_2$L$_2$] was crystallized. The crystal and molecular structure of the synthesized complex was determined by single-crystal X-ray structure analysis. The complex was prepared by reacting zinc acetate with 4-methylpyrazole in hot ethanolic solutions. The zinc complex

is obtained as a white crystalline compound. The coordination environment Zn(II) is tetrahedral. Results of CHN analysis are presented in the Table 29.

Table 29. Results of the CHN analysis for the complex [$ZnL_2(OAc)_2$]

	Theoretical $[Zn(OAc)_2L_2]$	Found
C%	*41.9 %*	*41.45 %*
H%	*5.5 %*	*5.22 %*
N%	*15.9 %*	*16.11 %*

On the basis of CHN analysis, FTIR results and single-crystal X-ray structure analysis, a structure of the complex was determined (Figure 81).

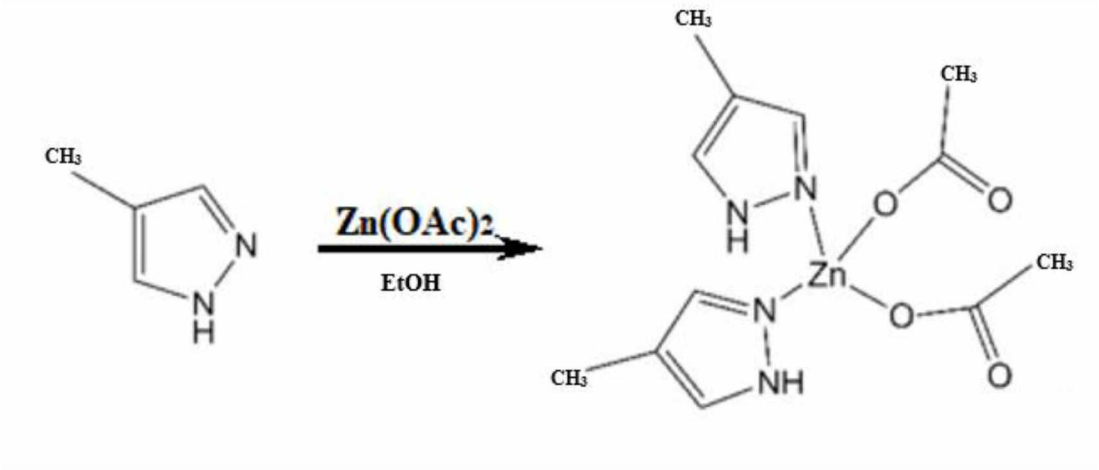

Figure 81. Synthesis of the Zn(II) complex of 4-methylpyrazole

4.2.4.1. X-ray powder diffraction data of $[Zn(OAc)_2L_2]$

The diffractogram obtained from the XRPD analysis conducted for the obtained complex [*$Zn(OAc)_2L_2$*], shows the formation of a crystalline compound with a dominant peak at the position 8.4706°*2θ*. For the purposes of identification of the complex in question, most dominant 8 peaks of the diffractogram are listed in the Table 30, with their d spacings and relative intensities.

Table 30. Eight most dominant diffraction lines in powder diffractogram of $Zn(OAc)_2L_2$

Pos. [°2θ]	d-spacing [Å]	Rel. Int. [%]
8.4706	10.43020	100.00
12.2029	7.24722	16.70
14.8842	5.94714	12.85
15.0680	5.87501	9.13
17.8674	4.96035	9.48
21.1447	4.19834	8.68
21.8002	4.07357	6.58
25.0119	3.55729	8.64

As the ligand is used in liquid form (solution), no diffractogram was obtained for it. The conclusion was made by comparing the diffractograms of $Zn(OAc)_2$ and the product $Zn(OAc)_2L_2$. Similar quantities of both samples were used during the analyses and both samples were analyzed in the same measuring conditions. Diffractograms are part of the Addendum A.

4.2.4.2. FTIR data of $[Zn(OAc)_2L_2]$

The IR spectrum of the complex $[Zn(OAc)_2L_2]$ contains the following dominant bands (Figure 82): 3098.0 cm^{-1}, 2920.0 cm^{-1}, 1633.7 cm^{-1}, 1371.2 cm^{-1}, 1322.2 cm^{-1}, 1072.9 cm^{-1}, 851.1 cm^{-1}, 618.0 cm^{-1}. The IR spectra of the complex is in accordance with the proposed structure.

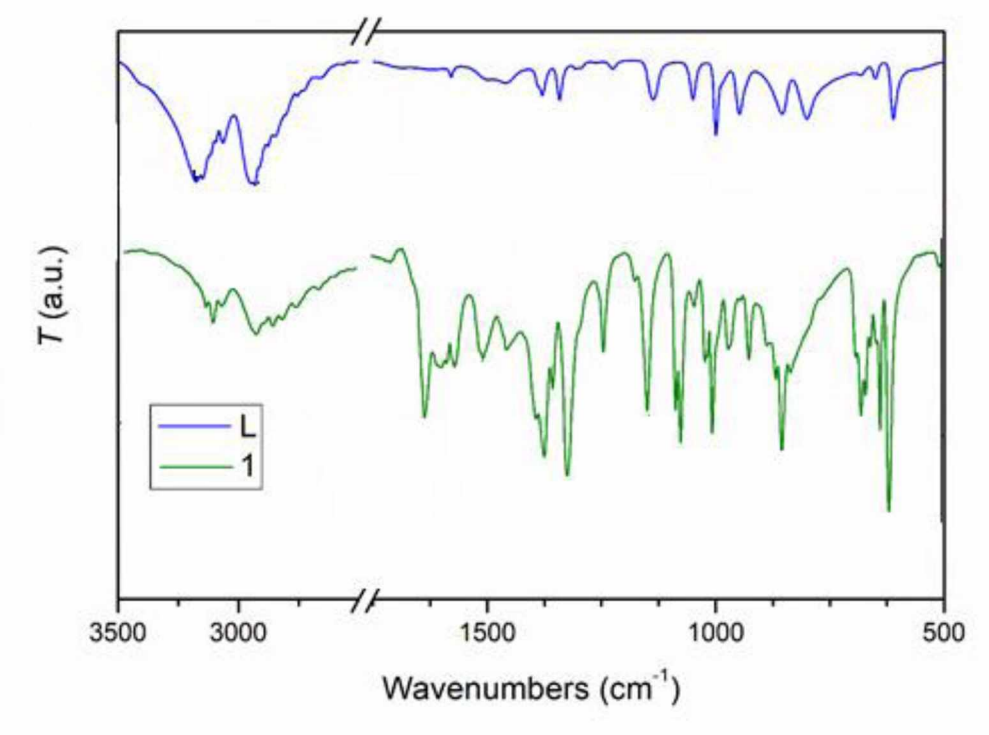

Figure 82. The IR spectra of 4-methylpyrazole – L2 (blue) and its complex - $Zn(OAc)_2L_2$ (green)

4.2.4.3. Crystal and molecular structure of $[Zn(OAc)_2L_2]$

The obtained single crystals have been analyzed through SC-XRD in order to obtain its molecular and crystal structure, shown in the Figure 83. Table 31 contains crystallographic data.

Table 31. Crystallographic and refinement data for the complexes

	$[Zn(OAc)_2L_2]$
Empirical formula	$C_{12}H_{18}N_4O_4Zn$
Formula weight	347.67
Temperature	293(2) K
Wavelength(Å)	0.71073
Crystal size (mm)	0.3 0.2 0.05
Crystal habitus	Plate
Crystal color	Clear light colorless
Crystal system	Triclinic
Space group	P -1
Unit cell dimensions(Å)	a=8.0748(7); b=9.4981(7); c=10.7206(7)
Unit cell angles (°)	α=83.013(6); β=86.077(6); γ=82.590(6)

Volume	808.1(1)
Z	2
Density (calc.) (g cm^{-3})	1.429
Absorption coefficient (mm^{-1})	1.539
*R*int	0.027
F (000)	360
Data/Parameters	3772/203
Goodness-of-fit on F^2	1.039
R/w*R* [I > 2σ (I)]	0.0523/0.0792
Largest diff. peak and hole ($eÅ^{-3}$)	0.342/-0.309

Zn(II) is coordinated by two nitrogen from 4-methyl-pyrazole and two oxygen atoms from acetate ligands, in a distorted tetrahedral environment (Figure 83).

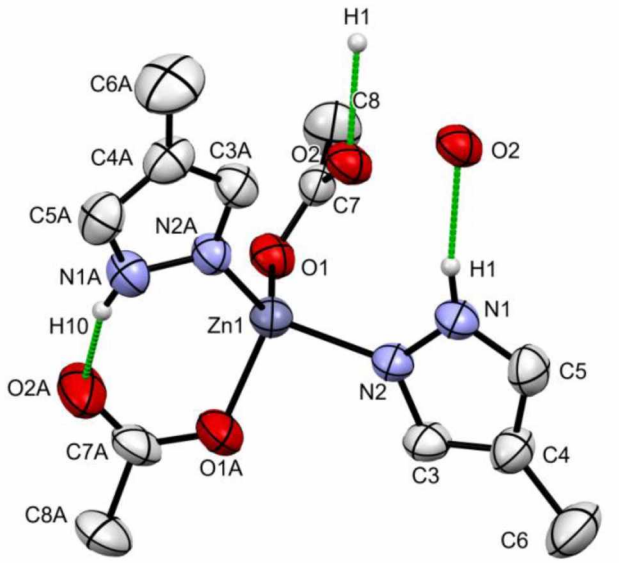

*Figure 83. Molecular diagram and atom labeling scheme of [Zn(OAc)$_2$L$_2$] (**2**). Green lines depict intra and intermolecular hydrogen bonds. C-bonded H atoms are not shown for clarity.*

Bond lengths of the chemically equivalent ligands are not significantly different (Table 32). There are no significant differences in the bond lengths of pyrazolyl ligands in comparison to free 4-methyl-pyrazole. The largest deviation from the regular tetrahedral geometry is observed for the O1A-Zn1-N2 angle whose value is 97.05(8)° (Table 33).

Table 32. Bond lengths (Å) of $[Zn(OAc)_2L_2]$ (2)

Bond	Distances (Å)	Bond	Distances (Å)	Bond	Distances (Å)
Zn1-O1	1.965(2)	Zn1-O1A	1.953(2)	N1-N2	1.337(3)
Zn1-N2	2.011(2)	Zn1-N2A	1.997(2)	N1-C5	1.331(4)
O1-C7	1.267(3)	O1A-C7A	1.264(3)	N2-C3	1.327(3)
O2-C7	1.241(3)	O2A-C7A	1.224(4)	C4-C5	1.365(4)
C7-C8	1.491(4)	C7A-C8A	1.509(4)	C4-C6	1.510(4)
				C3-C4	1.374(3)

Table 33. Bond angles (°) of $[Zn(OAc)_2L_2]$ (2)

Bond	Angles (°)	Bond	Angles (°)
N1A-N2A	1.340(3)	O1-Zn1-O1A	101.55(8)
N1A-C5A	1.321(4)	O1-Zn1-N2	112.08(7)
N2A-C3A	1.320(3)	O1-Zn1-N2A	116.90(7)
C4A-C5A	1.361(4)	O1A-Zn1-N2	97.05(8)
C4A-C6A	1.499(4)	O1A-Zn1-N2A	115.16(8)
C3A-C4A	1.387(3)	N2-Zn1-N2A	112.00(7)

Additional stabilization of the tetrahedral coordination is achieved through the intramolecular hydrogen bond between the NH and uncoordinated acetato-O, (N1A-H10...O2A=1.93(3) Å / 158(3) °), (Figure 83). The same type of intramolecular hydrogen bond between the pyrazolyl and acetato ligands in a tetrahedral environment around Zn was found previously in a tetrahedrally coordinated Zn. In the crystal structure of the title compound neighboring molecules connect through interactions between the acetato and pyrazolyl ligands not involved in intramolecular hydrogen bond (N1-H1...O2^{i}=1.93(3)Å/170(3)°; i=1-x,1-y,1-z). These interactions lead to the formation of centrosymmetric dimer units (Figure 84).

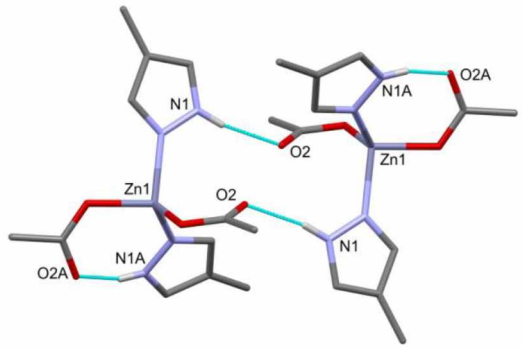

Figure 84. Formation of centrosymmetric dimers in the crystal of $[Zn(OAc)_2L_2]$ (2) due to a pair of hydrogen bonds between uncoordinated acetate oxygen atom and pyrazolyl NH group.

Different patterns of non-bonding interactions involving chemically equivalent ligands influence the overall shape of the complex molecule. This is reflected in different mutual positions of the pyrazolyl and acetate ligands, associated with different types of hydrogen bonds. The angle between the mean planes of the pyrazole ring and COO (acetate) atoms connected through the intramolecular hydrogen bond is 25.1°. The equivalent angle involving a pair of ligands participating in intermolecular interactions is 72.9°. It is interesting to note that the smallest angle around Zn (O1A-Zn1-N2) is associated with pyrazolyl and acetate ligands not involved in mutual interaction through hydrogen bonds. There are no significant intermolecular contacts between centrosymmetric dimeric units. The packing of molecules in the crystal is shown in Figure 85.

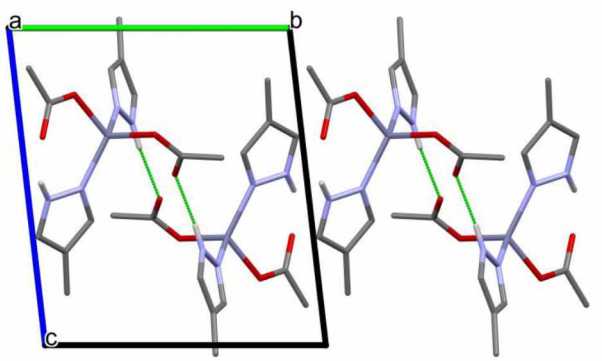

Figure 85. View of the crystal packing of 2 along a crystallographic axis (CH hydrogens are omitted). Green dotted lines depict hydrogen bonds leading to the formation of dimeric units.

It is interesting to compare the complex $[Zn(OAc)_2L_2]$ (**2**) with the structurally related bis(acetato)-bis(pyrazole)-zinc(II) ($[Zn(OAc)_2(L')_2]$) [138]; where L' denotes the pyrazole ligand. Two molecules differ in the substituent at C4 (CH_3 in **2**, *vs.* H in its analog $[Zn(OAc)_2(L')_2]$). Additionally, in the crystal structure of $[Zn(OAc)_2(L')_2]$ a free acetic acid is also present. Besides the free acetic acid, there are no significant differences in the structural properties of complexes **2** and $[Zn(OAc)_2(L')_2]$.

In $[Zn(OAc)_2(L')_2]$ the chemically equivalent atoms participate in the same type of intra and intermolecular hydrogen bonds (Figure 86). As in **2**, these interactions lead to the formation of hydrogen-bonded dimer (Figure 86).

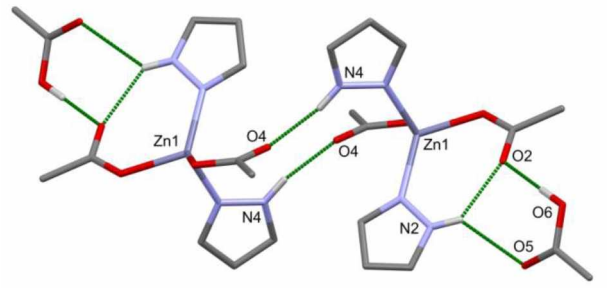

Figure 86. Depiction of the molecular structure of [Zn(OAc)$_2$(L')$_2$], intra- and intermolecular interactions (green dotted lines), and formation of dimeric units.

In [Zn(OAc)$_2$(L')$_2$], the crystal structure is stabilized by additional hydrogen bonds involving free acetates (Figure 86). In both **2** and [Zn(OAc)$_2$(L')$_2$], the presence of pyrazolyl and acetato ligands creates possibilities for forming the extended hydrogen-bonded structures. However, both compounds crystallize in the form of dimers without significant interaction between the dimeric units.

4.2.4.4. Thermal properites of [Zn(OAc)$_2$L$_2$]

Since the thermal stability of the newly prepared compounds is crucial for their future application, the stability of Zn(II) complex was determined and its thermal decomposition was analyzed in an inert atmosphere. The thermogravimetric (TG) and derivative thermogravimetric (DTG) curves of the decomposition of [Zn(OAc)$_2$L$_2$] are presented in Figure 87. The tetrahedral complex is less stable and starts to decompose at 80 °C. Up to ~150 °C, two partially overlapped steps are observed with DTG maximum at 103 and 131 °C. The mass losses in these steps are 14.9 and 17.7 %, which may be correlated to acetate (16.98 % per acetate ligand) loss. Above 150 °C, the thermal decomposition continues at a steady rate up to about 280 °C, at which temperature it becomes more intensive with a DTG maximum at 432 °C. The complex in this step loses 43.4 % of its mass, which may be assigned to the decomposition of the two pyrazole fragments (47.22 %). Although the mass losses and the calculated values are in good agreement, the nature of evaporated decomposition products cannot be proved without coupled techniques.

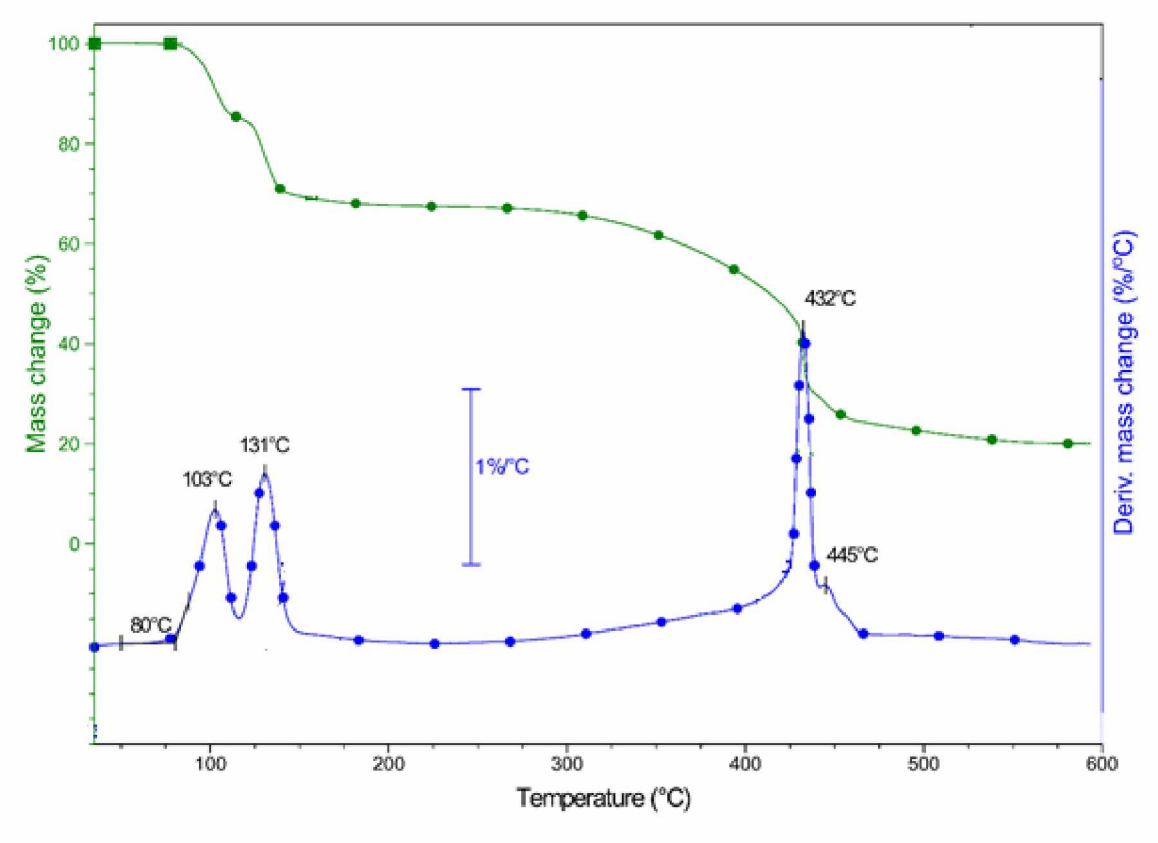

Figure 87. TG and DTG curves of the complex [Zn(OAc)$_2$L$_2$] in Argon.

To get a better insight into the decomposition mechanism of the complex, it was also analyzed by coupled TG-MS measurements. During the decomposition of [ZnL$_2$(OAc)$_2$] the products of the interactions of L and acetate, as well as their decomposition products, are also detected like 17, 18 (H_2O^+), 27 (CHN^+, $C_2H_3^+$), 28 (N_2^+, CO^+), 29 (HN_2^+, CH_3N^+, $C_2H_5^+$), 30 (NO^+), 44(CO_2^+ or N_2O^+), and 54 *m/z* ($C_2H_2N_2^+$ and/or $C_3H_4N^+$) (Figure 88). However, the acetate fragments are more intensive during the first mass loss step, while the fragments of pyrazole ligands are in the second one. It partially proves the decomposition mechanism, supposed on the TG curve, that in the first step is expressed the decomposition of the acetate ligands, and in the second step, the decomposition of the pyrazole ligands. On the other hand, these results also suggest that both kinds of ligands are reactive and partly interact with each other during the decomposition process.

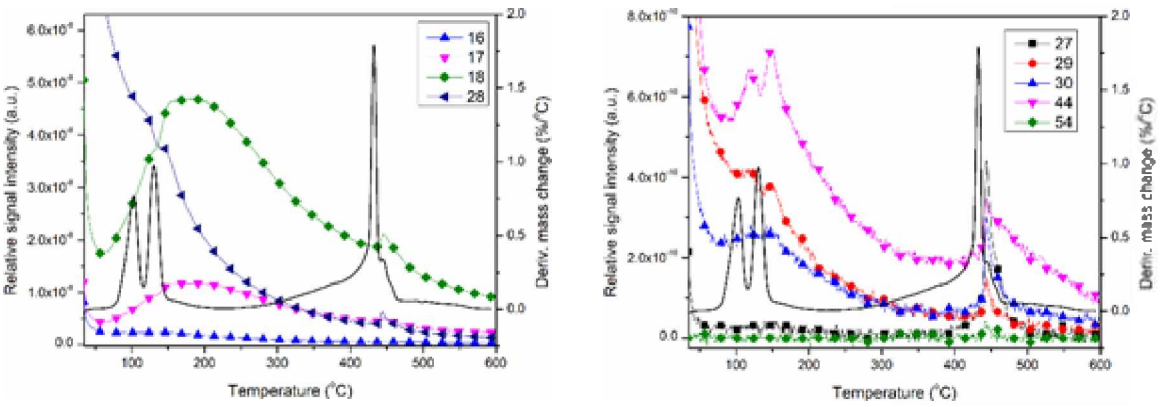

Figure 88. MS curves of the characteristic fragments of [ZnL$_2$(OAc)$_2$] in argon.

As can be seen from the thermoanalytical curves of Zn(II) and Ni(II) their thermal properties are different in accordance with their different molecular structure. Due to different molecular structures, the arrangement of their molecules in crystal lattice is also different and affects not only the IR spectra but also the thermal properties and stability.

4.2.4.5. Antioxidative potential of [Zn(OAc)$_2$L$_2$]

The synthesized sample was tested for the scavenging effect on the DPPH radical (DPPH). The methodology is described in the heading 4.2.3.5.

Since 4-methylpyrazole (also known as fomepizole) is a pharmacologically active compound, it was reasonable to make a screening test on its complexes with Zn(II) and Ni(II). Earlier pyrazole complexes [139,140] show interesting antioxidant activity due to their accessible hydrogens and stable radical form after the neutralization of 2,2-diphenyl-1-picrylhydrazyl (DPPH) radical. Thus, the fomepizole complexes were also tested by DPPH radical neutralization capacity. The complex was tested as ethanolic solution in two concentrations. The results show that the radical scavenger capacity (RSC) of the [ZnL$_2$(OAc)$_2$] complex is higher than that of [NiL$_4$(OAc)$_2$] (Figure 89). Considering the molecular structures, the pyrrolic H atom is most possibly a radical scavenging part of our complexes. Most probably, the different geometry around the different central atoms of the compounds causes different availability and reactivity of the pyrrole hydrogen of the pyrazole ring in these complexes. These H atoms are more hindered by hydrogen

bonds in the Ni(II) complex. Thus, it shows less activity. The results expressed as micrograms of Trolox equivalents per mL of the sample showed higher activity of the more concentrated solutions. However, after determination of the antioxidant activity, expressed as micrograms of Trolox equivalents per gram of dry sample weight (µg TE/g dew), it became clear that less concentrated solutions are more active. The stronger antioxidant capacity of the solutions with lower concentrations compared to those with higher concentrations can be explained by the different dynamics of antioxidant activity in the more diluted solutions due to the better availability of active centers with antioxidant activity within the complexes.

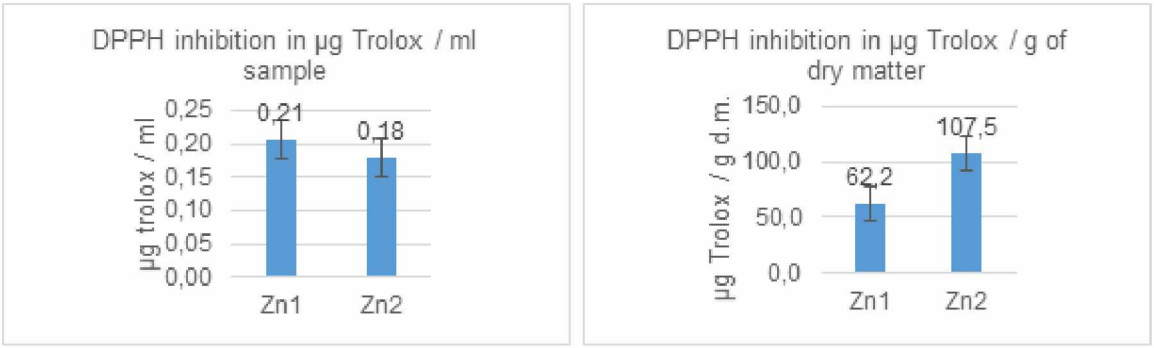

Figure 89. The radical scavenger capacity (RSC) of the [ZnL$_2$(OAc)$_2$] complex was determined in solutions of different concentrations: Zn1 20 mg/mL and Zn2 10 mg/mL. RSC is expressed as µg of Trolox equivalent per mL of sample solution (left) and as µg of Trolox equivalent per g of dry sample (right).

Comparing the results with some recalculated results of the antioxidative potential of some pyrazole-containing compounds found in the literature [134-137] indicates that analyzed compounds possess comparable DPPH• scavenging activity, which is promising for further biological assays. In this case, the DPPH• scavenging activity of Ni(II) and Zn(II) is in correlation with their thermal stability too. The thermally more stable Ni(II) complex shows less RSC, but the RSC of the less stable Zn(II) complex is higher. It is possible that the Zn(II) complex, dimer in crystalline form, is less stable in solution too, dissociates during solution, and becomes easily available for radical scavenging. Differently, the thermally more stable Ni(II) complex may be more stable in solution and, therefore less available for reaction with DPPH•.

4.2.5. Synthesis and characterization of $[PtL_3Cl_2]$

Synthesis of a complex $[PtL_3Cl_2]$: The warm ethanolic solution (3 cm^3) $[K_2PtCl_4]$ (0.104 g, 0.25 mmol) was mixed with warm ethanolic solution (3 cm^3) of the ligand L2 (0.041 g, 0.5 mmol) with mild heating. The dark orange reaction mixture was left to crystallize. After 3 days, orange microcrystalline precipitate was filtered, washed with ethanol and dried in air. Yield: 0.081 g (56.3 %).

From the reaction mixture, new complex compound of formulae: $[PtL_3Cl_2]$ was crystallized. The platinum complex is obtained as an orange crystalline compound. The complex was prepared by reacting potassium tetrachloroplatinate with 4-methylpyrazole in hot mixtures of water and ethanol. Results of CHN analysis are presented in the Table 34.

Table 34. Results of the CHN analysis for the complex $[PtL_3Cl_2]$

	Theoretical $[PtL_3Cl_2]$	Found
C%	*28.05 %*	*28.11 %*
H%	*3.28 %*	*3.51 %*
N%	*16.21 %*	*16.40 %*

On the basis of CHN and FTIR analyses, structures of the complex was determined (Figure 90).

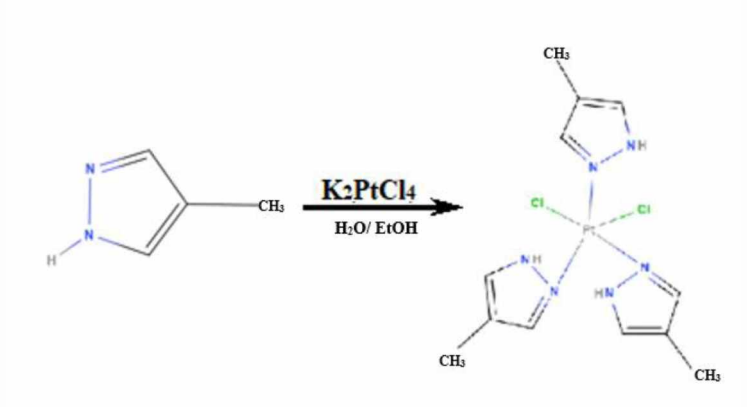

Figure 90. Synthesis of the Pt(II) complex of 4-methylpyrazole

With its recognized potential, the cytotoxicity and antimicrobial activity tests have been carried out for the complex.

4.2.5.1. X-ray powder diffraction data of [PtL_3Cl_2]

The powder diffractogram of PtL_3Cl_2 is presented in Figure 91. Most dominant 8 peaks of the diffractogram are listed in the Table 35, with their d spacings and relative intensities.

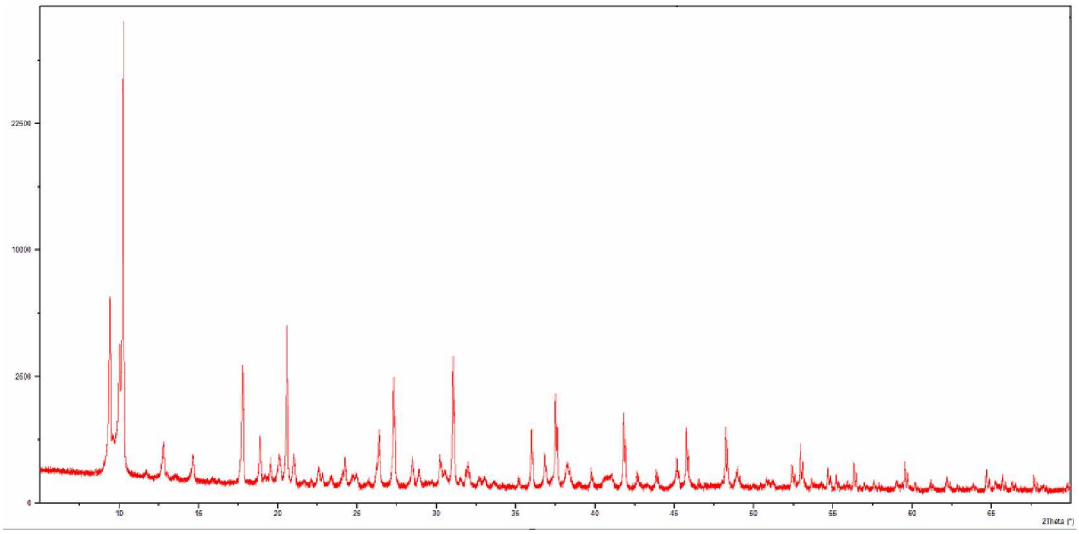

Figure 91. The powder diffractogram of PtL_3Cl_2

Table 35. Eight most dominant diffraction lines in powder diffractogram of PtL_3Cl_2

Pos. [°2θ]	d-spacing [Å]	Rel. Int. [%]
9.4082	9.39276	15.50
10.0064	8.83253	9.66
10.2493	8.62377	100.00
17.7776	4.98520	7.55

20.5551	**4.31741**	**14.70**
27.2967	**3.26450**	**7.17**
31.0368	**2.87911**	**11.40**
37.5077	**2.39593**	**6.09**

Presented in the Figure 92 are the diffractograms of K_2PtCl_4 and the product PtL_3Cl_2. Similar quantities of both samples were used during the analyses and both samples were analyzed with the same measuring conditions.

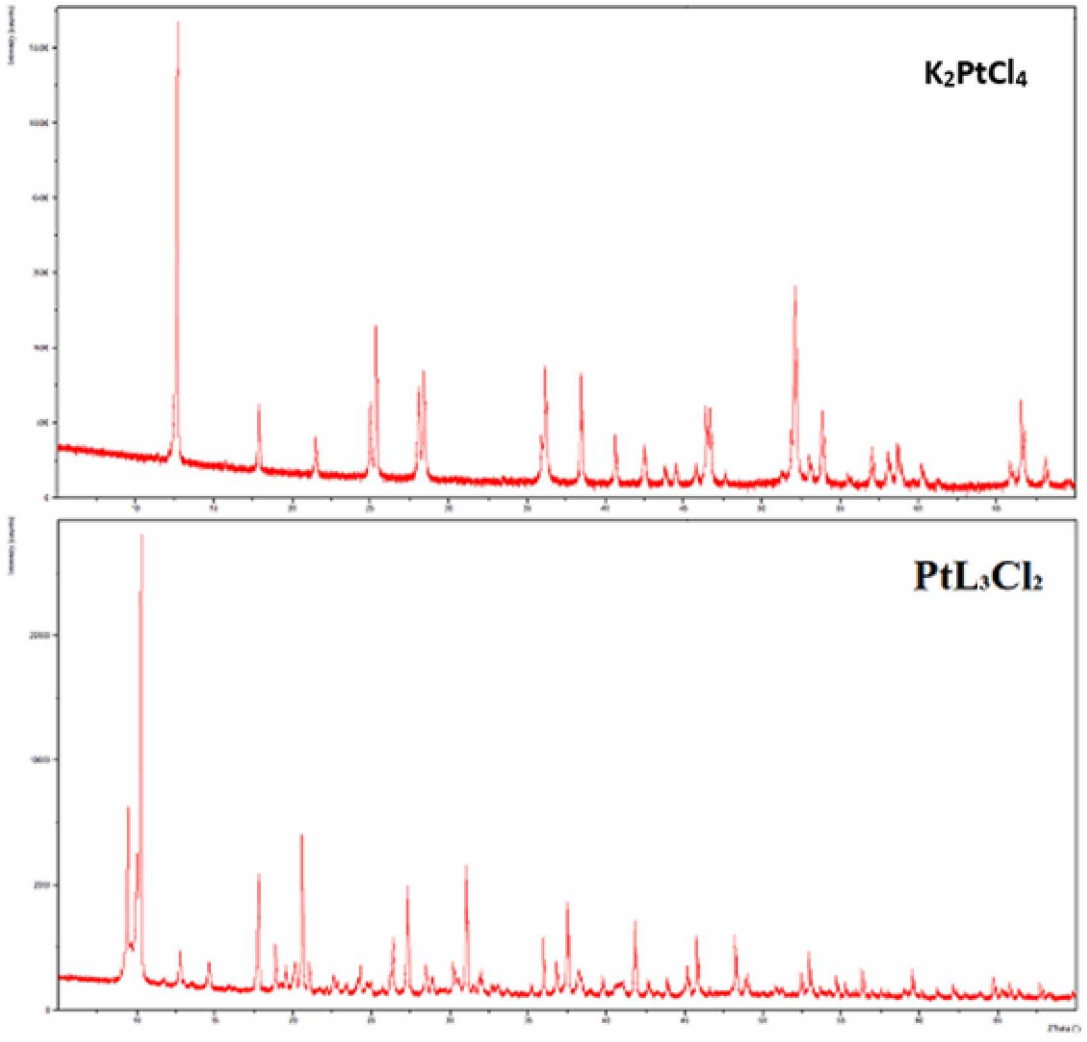

Figure 92. The powder diffractograms of K_2PtCl_4 and the product PtL_3Cl_2

4.2.5.2. *FTIR data of [PtL_3Cl_2]*

The IR spectrum of the PtL_3Cl_2 complex exhibits several dominant vibrational bands at 3205.3 cm^{-1}, 3098.2 cm^{-1}, 2984.8 cm^{-1}, 1399.7 cm^{-1}, 1392.3 cm^{-1}, 1146.5 cm^{-1}, 1087.5 cm^{-1}, 1006.1 cm^{-1}, 871.08 cm^{-1}, 818.0 cm^{-1}, 679.9 cm^{-1}, and 595.1 cm^{-1}. The IR spectra of the complex is in accordance with the proposed structure.

4.2.5.3. *Bactericidal activity of [PtL_3Cl_2]*

As part of this thesis, complex PtL_3Cl_2 was tested for its bactericidal activity. As previously described, the antimicrobial activity of the samples was assessed using the Kirby-Bauer disc diffusion method, following EUCAST and CLSI standards. The results were interpreted by measuring the inhibition zones and categorizing bacterial susceptibility as sensitive (S), intermediate (I), or resistant (R). Gentamicin was used as a reference standard, and the obtained inhibition zones for *Escherichia coli* and *Salmonella spp.* were compared to established threshold values to evaluate the effectiveness of the tested preparations.

Based on the results presented in Table 36 and the visible representations in Figure 93, it can be claimed that all three used concentrations of PtL_3Cl_2 showed a slightly inhibitory effect both on the growth of E coli bacteria and on the growth of bacteria from the genus Salmonella spp., with an average inhibition zones from 6.75 mm to 7.5 mm. Comparing the obtained results with the standard values of the antibiotic Gentamicin, it can be claimed that both tested bacteria are resistant to PtL_3Cl_2.

Table 36. Results of measurement of inhibition zones of PtL_3Cl_2 for all three concentrations

PtL_3Cl_2	Avergae value of inhibition zone (mm)	
	Esherichia coli	*Salmonella spp.*
Concentration 10^{-2}	7,25 mm	7,50 mm
Concentration 10^{-4}	7,00 mm	6,75 mm
Concentration 10^{-5}	7,00 mm	6,75mm

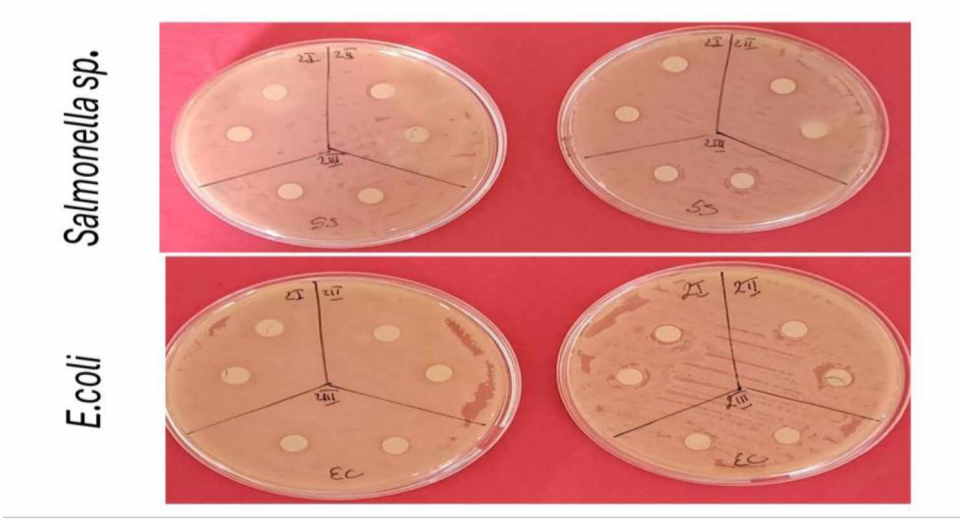

Figure 93. Presentation of the inhibitory effect of PtL_3Cl_2 on E. Coli and Salmonella. spp.

4.2.5.4. Cytotoxic activity of $[PtL_3Cl_2]$

Target cells HeLa (2000 cells per well), LS174 (7000 cells per well), A549 (5000 cells per well) and MRC-5 (5000 cells per well) were seeded into wells of a 96-well flat-bottomed micro titre plate. Stock solutions (10mM) of test samples, made in dimethylsulfoxide (DMSO) ,were diluted with complete nutrient medium to the required working concentrations. Twenty-four hours later, after the cell adherence, five different concentrations of investigated extracts were added to the wells, except for the control cells to which only nutrient medium was added. Final concentrations reached in treated

wells were 200, 100, 50, 25, and 12.5 μM, except in the control wells. All investigated concentrations were set up in triplicate. Nutrient medium with corresponding concentrations of investigated compounds, but without cells, was used as a blank, also in triplicate. The cultures were incubated for 72 h.

Briefly, 20 mL of MTT solution (5 mg/mL phosphate-buffered saline) was added to each well. Samples were incubated for a further 4 h at 37°C in a humidified atmosphere of 95% air/5% CO2 (v/v). Then 100 μL of 100 g/L sodium dodecyl sulfate was added to dissolve the insoluble product formazan resulting from conversion of the MTT dye by viable cells. The absorbance (A) at 570 nm was measured 24 h later. The number of viable cells in each well was proportional to the intensity of the absorbance of light, which was read in an enzyme-linked immunosorbent assay (ELISA) plate reader. To determine cell survival (%), the A of a sample with cells grown in the presence of various concentrations of the investigated extracts was divided by the control optical density (the A of control cells grown only in nutrient medium) and multiplied by 100. In each experiment, the A of the blank was always subtracted from the A of the corresponding sample with target cells. IC50 is defined as the concentration of an agent inhibiting cell survival by 50% compared with a vehicle-treated control. All experiments were done in triplicate.

The cytotoxic activity against human malignant cell lines and human normal lung fibroblasts of the complex PtL_3Cl_2 can be seen in Table 37.

Table 37. Cytotoxic activity (IC50 values) of extract against human cancer cell lines.

Compound	HeLa	LS174T	A549	MRC-5
IC50 (μM)				
PtL_3Cl_2	6.89 ± 0.28	25.41 ± 12.46	19.71 ± 2.09	13.10 ± 0.53

IC50 values (μM) were expressed as the mean ± SD determined from the results of MTT assay in three independent experiments.

The obtained data show a significant cytotoxic activity of tested compound PtL_3Cl_2 against the tested cell lines. IC 50s for compound PtL_3Cl_2 ranging from 6.89 ± 0.28μM on Hela cells to 19.71 ± 2.09 μM on A549 were obtained. As to compare, the activity of

cisplatin for HeLa cell line was 4.00 ± 0.47, for A549 line was 12.74 ± 1.26, and for MRC-5 line 5.91 ± 0.32 [141]. Additionally, cisplatin had shown activity towards LS174T cell line with the IC50 value of 20.38 ± 0.44 [142]. Data on activiy of cisplatin on different cell lines varies from paper to paper, and depends on the conditions of the experiment, and so simillar works presented cisplatin had IC50 value of 9.3±3.0 for A549 cell line [143], and cisplatin IC50 values of 3.46 ± 0.25 for HeLa cell line, 17.93 ± 0.88 for A549 cell line, and 10.52 ± 0.22 for MRC-5 cell line [142].

From the obtained results of cytotoxicity presented in this work, great activity for HeLa cell line was shown by the compound PtL_3Cl_2 with similar activity as cisplatin, yet MRC-5 activity is much better compared and cisplatin, which proves better selectivity towards normal cells.

4.2.6. Synthesis and characterization of $[Pd(L\text{-}H)_4]$

Synthesis of a complex $[Pd(L\text{-}H)_4]$: The warm ethanolic solution (3 cm^3) $[Pd(OAc)_2]$ (0.056 g, 0.25 mmol) was mixed with warm ethanolic solution (3 cm^3) of the ligand L2 (0.041 g, 0.5 mmol) with mild heating. The brown reaction mixture was left to crystallize. After 4 days, yellow-milky microcrystalline precipitate was filtered, washed with ethanol and dried in air. Yield: 0.028 g (29.2 %).

From the reaction mixtures, new complex compounds of formulae: $[PtL_3Cl_2]$ and $[Pd(L\text{-}H)_3]$ were crystallized. The platinum complex is obtained as an orange crystalline compound, while the palladium complex is obtained as a yellow crystalline compound. The complexes were prepared by reacting potassium tetrachloroplatinate and palladium acetate with 4-methylpyrazole in hot mixtures of water and ethanol. Results of CHN analysis are presented in the Table 38.

Table 38. Results of the CHN analysis for the complexes $[PtL_3Cl_2]$ and $[Pd(L\text{-}H)_3]$

	Theoretical $[Pd(L\text{-}H)_3]$	Found
C%	*41.25 %*	*41.18 %*
H%	*4.15 %*	*4.29 %*
N%	*23.79 %*	*24.02 %*

On the basis of CHN and FTIR analyses, structures of the complexes were determined (Figure 94).

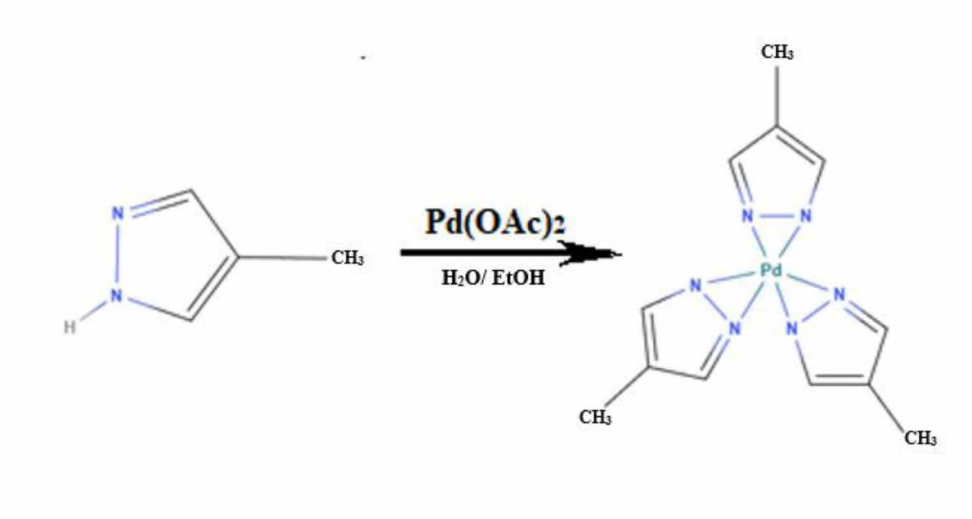

Figure 94. Synthesis of the Pd(II) complex of 4-methylpyrazole

4.2.6.1. X-ray powder diffraction data of $[Pd(L\text{-}H)_4]$

The powder diffractogram of *$Pd(L\text{-}H)_3$* is presented in Figure 95. Most dominant 8 peaks of the diffractogram are listed in the Table 39, with their d spacings and relative intensities.

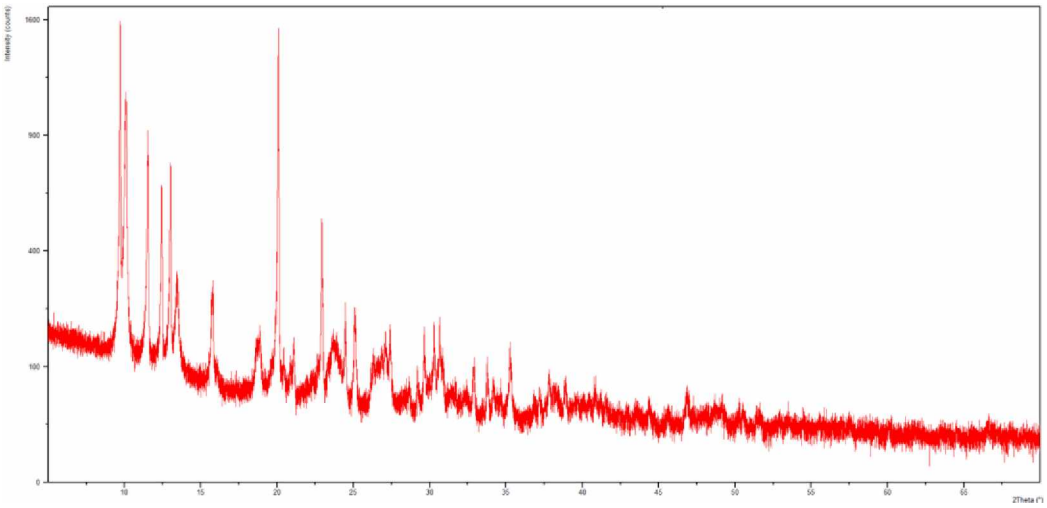

Figure 95. The powder diffractogram of $Pd(L\text{-}H)_3$

Table 39. Eight most dominant diffraction lines in powder diffractogram of $Pd(L\text{-}H)_3$

Pos. [°2θ]	d-spacing [Å]	Rel. Int. [%]
9.7206	9.09163	80.50
10.1048	8.74673	67.97
11.5358	7.66476	50.46
12.4420	7.10848	33.98
13.0171	6.79569	41.06
15.7719	5.61437	12.86
20.0824	4.41797	100.00
22.9445	3.87293	33.10

Presented in the Figure 96 are the diffractograms of $Pd(OAc)_2$ and the product $Pd(L\text{-}H)_3$. Similar quantities of both samples were used during the analyses and both samples were analyzed with the same measuring conditions.

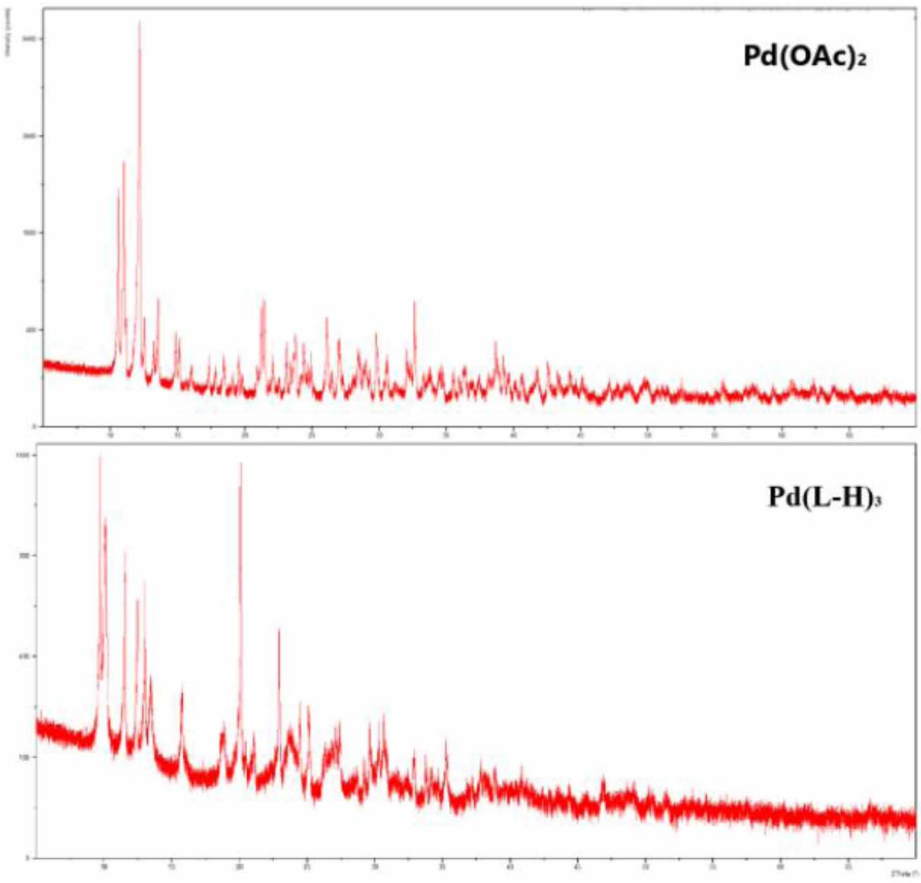

Figure 96. The powder diffractograms of $Pd(OAc)_2$ and the product $Pd(L\text{-}H)_3$

4.2.6.2. FTIR data of $[Pd(L\text{-}H)_4]$

The IR spectrum of the $Pd(L–H)_3$ complex contains the following dominant vibrations: 2926 cm^{-1}, 1380 cm^{-1}, 1320 cm^{-1}, 1086 cm^{-1}, 1015 cm^{-1}, 982 cm^{-1}, 825 cm^{-1}, 615 cm^{-1}, and 438 cm^{-1}. The IR spectra of the complex is in accordance with the proposed structure.

4.2.6.3. Bactericidal activity of $[Pd(L\text{-}H)_4]$

As part of this thesis, complex $Pd(L\text{-}H)_3$ was tested for its bactericidal activity. As previously described, the antimicrobial activity of the samples was assessed using the Kirby-Bauer disc diffusion method, following EUCAST and CLSI standards. The results were interpreted by measuring the inhibition zones and categorizing bacterial

susceptibility as sensitive (S), intermediate (I), or resistant (R). Gentamicin was used as a reference standard, and the obtained inhibition zones for *Escherichia coli* and *Salmonella spp.* were compared to established threshold values to evaluate the effectiveness of the tested preparations.

The results shown in Table 40 and presented in Figure 97 indicate that $Pd(L\text{-}H)_3$ (preparation) had an almost identical slightly superior effect, that is, it had an inhibitory effect on both tested bacteria in the range from 8.75 mm to 7.00 mm. The obtained inhibition diameters confirm that *E.coli* and *Salmonella sp.* resistant to the concentrations used $Pd(L\text{-}H)_3$.

Table 40. Results of measurement of zones of inhibition of $Pd(L\text{-}H)_3$ for all three concentrations

$Pd(L\text{-}H)_3$	Avergae value of inhibition zone (mm)	
	Esherichia coli	*Salmonella spp.*
Concentration 10^{-2}	8,75 mm	8,00 mm
Concentration 10^{-4}	7,50 mm	7,75 mm
Concentration 10^{-5}	7,00 mm	7,00mm

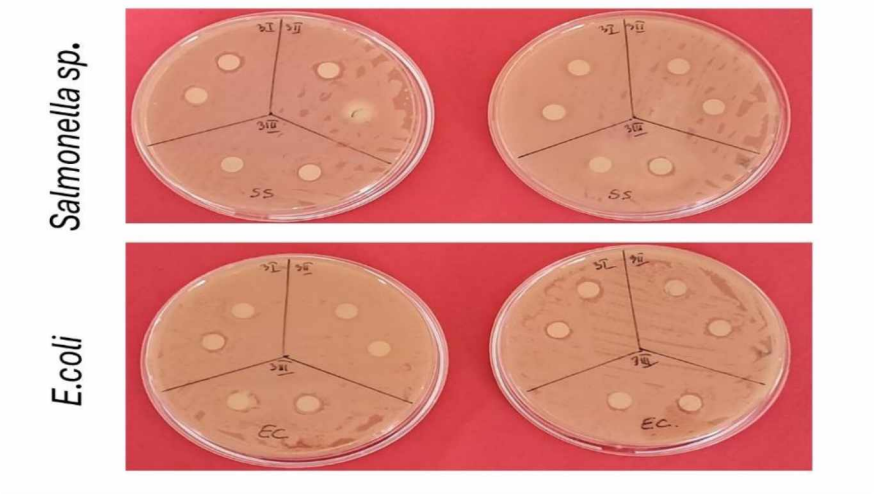

Figure 97. Presentation of the inhibitory effect of $Pd(L\text{-}H)_3$ on E. Coli and Salmonella. spp.

4.2.6.4. *Cytotoxic activity of [Pd(L-H)$_4$]*

As previously described, the cytotoxic activity of the tested extracts was evaluated using the MTT assay on HeLa, LS174, A549, and MRC-5 cell lines. Cells were treated with five different concentrations of the extracts (12.5–200 µM) and incubated for 72 hours. Cell viability was assessed based on the reduction of MTT dye, and absorbance was measured at 570 nm. Results were calculated as a percentage of viable cells relative to untreated controls, and IC_{50} values were determined as the concentration required to reduce cell viability by 50%. All experiments were performed in triplicate.

The cytotoxic activity against human malignant cell lines and human normal lung fibroblasts of the complex Pd(L-H)$_3$ can be seen in Table 41.

Table 41. Cytotoxic activity (IC50 values) of extract against human cancer cell lines.

Compound	HeLa	LS174T	A549	MRC-5
		IC50 (µM)		
Pd(L-H)$_3$	7.73 ± 0.61	8.96 ± 0.58	10.06 ± 1.00	6.56 ± 0.29

IC50 values (µM) were expressed as the mean ± SD determined from the results of MTT assay in three independent experiments.

The obtained data show a significant cytotoxic activity of tested compound Pd(L-H)$_3$ against the tested cell lines. Compound Pd(L-H)$_3$ showed excellent cytotoxic activity, IC50 ranging from 7.73 ± 0.61µM for Hela cells to 10.06 ± 1.00 µM on the tested A549 cells. From the obtained results of cytotoxicity presented in this work, best overall activity is shown by compound Pd(L-H)$_3$, with LS174T and A549 cell line IC50 values that show better activity than cisplatin, and similar activity on MRC-5 to that of cisplatin.

4.3. Synthesis and characterization of Pd(II) and Pt(II) complexes with **3-Amino-4,5-dihydro-1-phenyl-1H-pyrazole (L3)**

During this research the complexes formed with 3-Amino-4,5-dihydro-1-phenyl-1H-pyrazole (L3) were with Pt(II) and Pd(II) of formulae $[PtL_2Cl_2]$ and $[PdL_2(OAc)_2]$ (Table 42).

Table 42. Forulae and color of complexes of Pt(II) and Pd(II) with 3-Amino-4,5-dihydro-1-phenyl-1H-pyrazole

Complex	Color
PtL_2Cl_2	Dark grey
$PdL_2(OAc)_2$	Orange

4.3.1. Synthesis and characterization of $[PtL_2Cl_2]$

Synthesis of a complex $[PtL_2Cl_2]$: The warm water (ASTM Type II) solution (3 cm^3) $[K_2PtCl_4]$ (0.104 g, 0.25 mmol) was mixed with warm ethanolic solution (3 cm^3) of the ligand L3 (0.080 g, 0.5 mmol) with mild heating. The colorless reaction mixture was left to crystallize. After 2 days, white amorphous precipitate was filtered, washed with ethanol and dried in air. Yield: 0.034 g (34.3 %).

From the reaction mixture, new complex compound of formulae: $[PtL_2Cl_2]$ was crystallized. The molecular structure of the synthesized complex was determined by CHN, XRPD and IR analyses. The complex was prepared by reacting potassium tetrachloroplatinate with 3-Amino-4,5-dihydro-1-phenyl-1H-pyrazole in hot ethanolic and water solutions. The result of CHN elemental analysis indicates on the structure with calculated (Found) composition for $PtC_{18}H_{22}N_6Cl_2$ (PtL_2Cl_2) being: C 37.34 (37.50%); H 3.83 (3.80%); N 14.52 (14.60%);

Results of CHN analysis are presented in the Table 43.

Table 43. Results of the CHN analysis for the complexes [PtL_2Cl_2]

	Theoretical [PtL_2Cl_2]	Found
C%	*37.34 %*	*37.50 %*
H%	*3.83 %*	*3.80 %*
N%	*14.52 %*	*14.60 %*

On the basis of CHN and FTIR analyses, structure of the complex was determined (Figure 98).

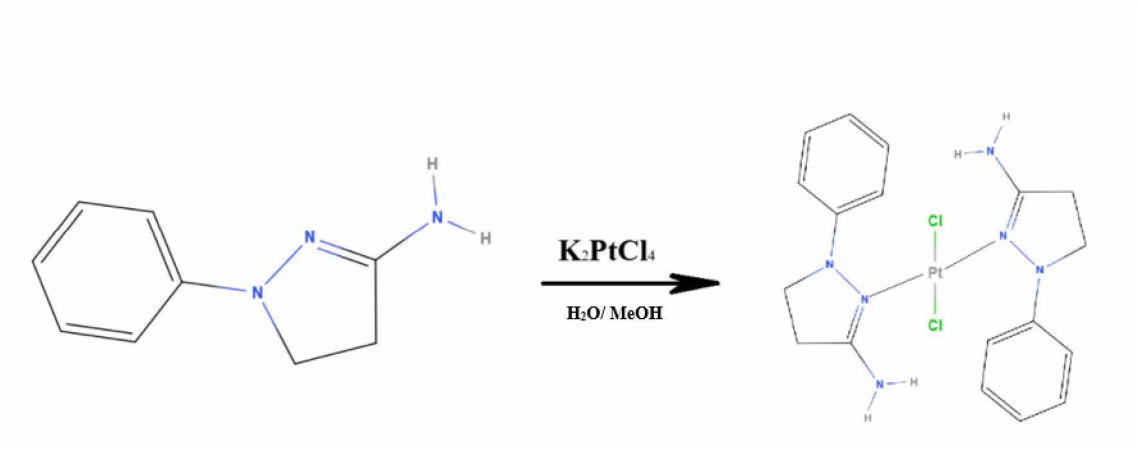

Figure 98. Synthesis of the Pt(II) complex of 3-Amino-4,5-dihydro-1-phenyl-1H-pyrazole

4.3.1.1. X-ray powder diffraction data of [PtL_2Cl_2]

The powder diffractogram of *PtL_2Cl_2* is presented in Figure 99.

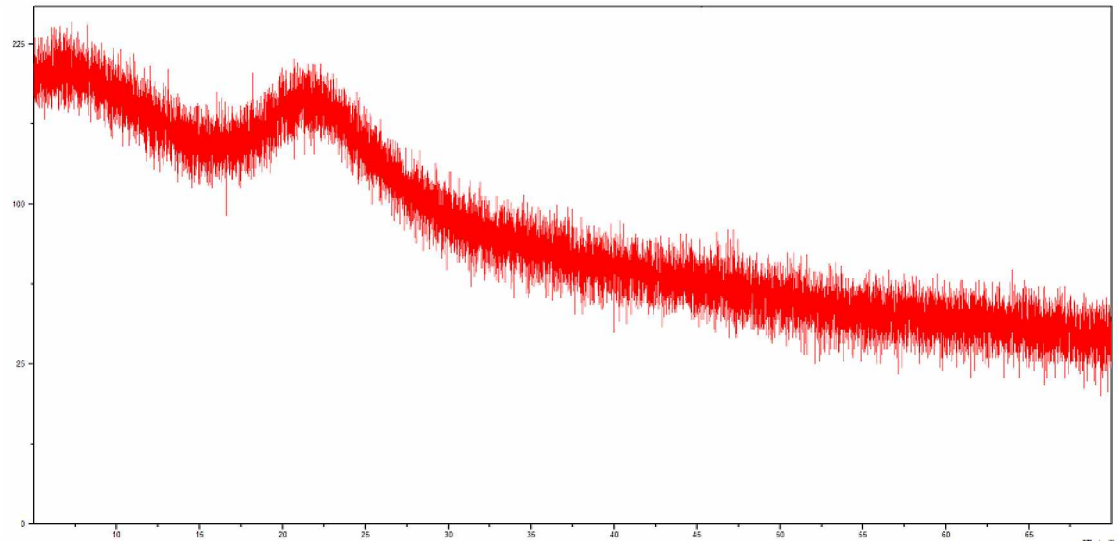

Figure 99. The powder diffractogram of PtL_2Cl_2

Presented in the Figure 100 are the diffractograms of *L3*, K_2PtCl_4 and the product PtL_2Cl_2. Similar quantities of all samples were used during the analyses and all samples were analyzed with the same measuring conditions. From the diffractogram of the product, it is clear that the product has amorphous polymorphic state.

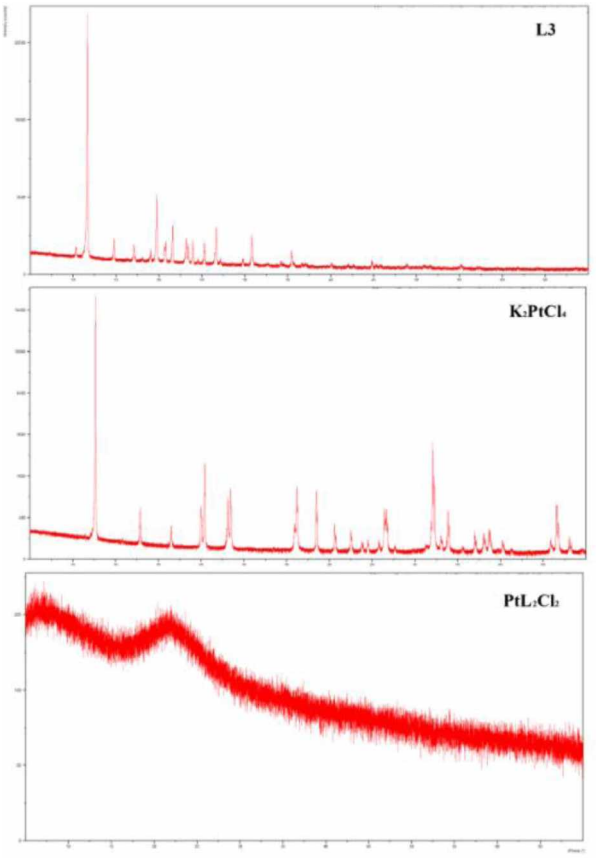

Figure 100. The powder diffractograms of L3, K_2PtCl_4 and PtL_2Cl_2

4.3.1.2. FTIR data of [PtL_2Cl_2]

IR spectra of the complex PtL_2Cl_2 contains the following dominant vibrations: 1648.2 cm^{-1}, 1597.5 cm^{-1}, 1490.1 cm^{-1}, 759.4 cm^{-1}, 696.77 cm^{-1}. The IR spectra of the complex is in accordance with the proposed structure.

4.3.2. Synthesis and characterization of [$PdL_2(OAc)_2$]

Synthesis of a complex [$PdL_2(OAc)_2$]: 0.25 mmol (0.044 mg) of [$PdCl_2$] with 0.5 mmol (0.080 g) L3 of respective ligand and metal salt powders were put in the mechanical ball mill with a zirconium ball, and mechanosynthesis process was conducted on 25 Hz for 10 minutes. The dark brown powder was collected.

Synthesis of a complex $PdL_2(OAc)_2$ was conducted as follows: Powder equal to 0.25 mmol; 56 mg of $Pd(OAc)_2$ was weighted and mixed with 0.5 mmol (80 mg) of 3-Amino-4,5-dihydro-1-phenyl-1H-pyrazole (L3) in powder form, put into a zirconium grinder and pulverized for 10 min at 25 Hz. Afterwards, the obtained orange powder was collected. From the reaction mixture, new complex compound of formulae: [$PdL_2(OAc)_2$] was crystallized. The molecular structure of the synthesized complex was determined by CHN, XRPD and IR analyses. The complex was prepared by reacting palladium(II)acetate with 3-Amino-4,5-dihydro-1-phenyl-1H-pyrazole mechanochemically.

Results of CHN analysis are presented in the Table 44.

Table 44. Results of the CHN analysis for the complex [$PdL_2(OAc)_2$]

	Theoretical [$PdL_2(OAc)_2$]	Found
C%	*48.28 %*	*48.10 %*
H%	*5.16 %*	*4.96 %*
N%	*15.36 %*	*15.12 %*

On the basis of CHN and FTIR analyses, structure of the complex was determined (Figure 101).

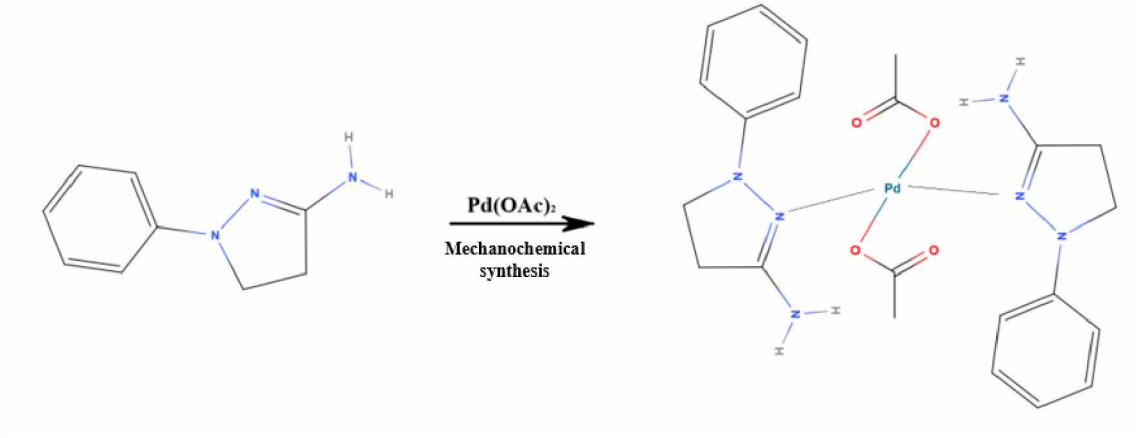

Figure 101. Synthesis of the Pd(II) complex of 3-Amino-4,5-dihydro-1-phenyl-1H-pyrazole

4.3.2.1. X-ray powder diffraction data of [$PdL_2(OAc)_2$]

The powder diffractogram of $PdL_2(OAc)_2$ is presented in Figure 102. Most dominant 8 peaks of the diffractogram are listed in the Table 45, with their d spacings and relative intensities.

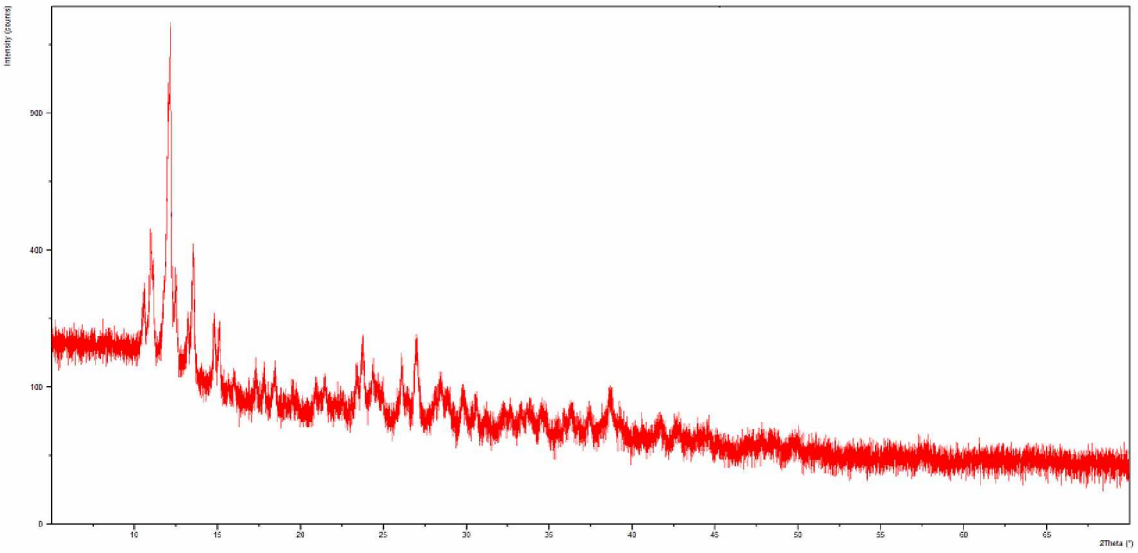

Figure 102. The powder diffractogram of $PdL_2(OAc)_2$

Table 45. Eight most dominant diffraction lines in powder diffractogram of $PdL_2(OAc)_2$

Pos. [°2θ]	d-spacing [Å]	Rel. Int. [%]
10.9646	8.06271	23.37
11.1053	7.96093	11.91
12.0074	7.36475	62.83
12.1334	7.28854	100.00
12.4681	7.09362	11.09
13.5025	6.55246	22.19
14.8007	5.98051	10.77
26.9652	3.30388	9.79

Presented in the Figure 103 are the diffractograms of L3, *$Pd(OAc)_2$* and the product [$PdL_2(OAc)_2$]. Similar quantities of all samples were used during the analyses and all samples were analyzed with the same measuring conditions. From diffractograms, it is

visible that the crystallinity of the product is lesser than that of both metal salt and the ligand, which is most likely a result of mechanochemical synthesis process.

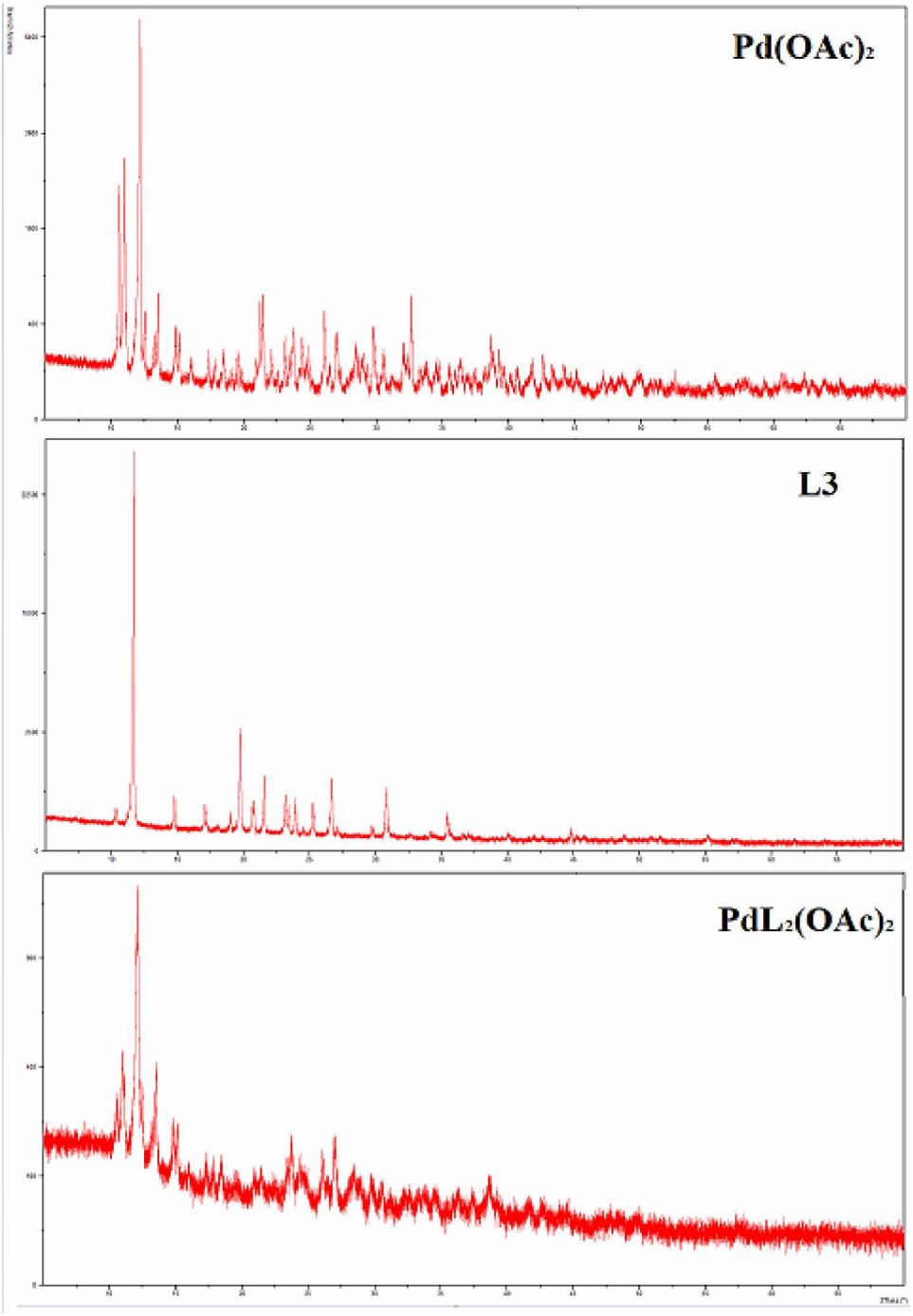

Figure 103. The powder diffractograms of $Pd(OAc)_2$, L3 and $PdL_2(OAc)_2$

4.3.2.2. FTIR data of $[PdL_2(OAc)_2]$

IR spectra of the complex $PdL_2(OAc)_2$ contains the following dominant vibrations: 3433.8 cm^{-1}, 1660.7 cm^{-1}, 1597.6 cm^{-1}, 1501.4 cm^{-1}, 1426.9 cm^{-1}, 751.6 cm^{-1}, 693.9 cm^{-1}. The IR spectra of the complex is in accordance with the proposed structure.

4.3.3. Bactericidal and cytotoxic activity of 3-Amino-4,5-dihydro-1-phenyl-1H-pyrazole (L3)

Prior to investigating the biological activity of metal complexes, the evaluation of the properties of the free ligand was conducted to determine the potential of the complexes. 3-Amino-4,5-dihydro-1-phenyl-1H-pyrazole (L3) was selected for preliminary screening due to its structurally promising framework. The aim was to assess the cytotoxic and bactericidal potential of L3 as a free ligand in order to establish a baseline for comparison with its metal complexes. By examining its activity against selected tumor cell lines and bacterial cultures, this screening provided insight to the potential of the complexes to show significant biological effects even with enhanced properties through metal coordination.

4.3.3.1. Bactericidal activity of 3-Amino-4,5-dihydro-1-phenyl-1H-pyrazole (L3)

As part of this thesis, and to estimate the potential of L3, bactericidal activity was also conducted for L3.

From the obtained results, it can be claimed that all three used concentrations L3 did not show an inhibitory effect on the growth of *E coli* bacteria, the average zone of inhibition was 6mm. In contrast, L3 showed a slight inhibitory effect on the growth of *Salmonella spp*. with an average inhibition zone of 10 -2, 7.5 mm, 10-4, 6.75 mm and 10-5, 6.5 mm. Comparing the obtained results with the standard values of the antibiotic Gentamicin, it can be claimed that both tested bacteria are resistant to L3, which can be seen from the results presented in Table 46, i.e. Figure 104.

Table 46. Results of measurement of inhibition zones of L3 for all three concentrations

L3	Cut-off value of inhibition zone (mm)	
	Escherichia coli	*Salmonella spp.*
Concentration 10 $^{-2}$	6mm	7,5 mm
Concentration 10 $^{-4}$	6mm	6,75 mm
Concentration 10 $^{-5}$	6mm	6,50mm

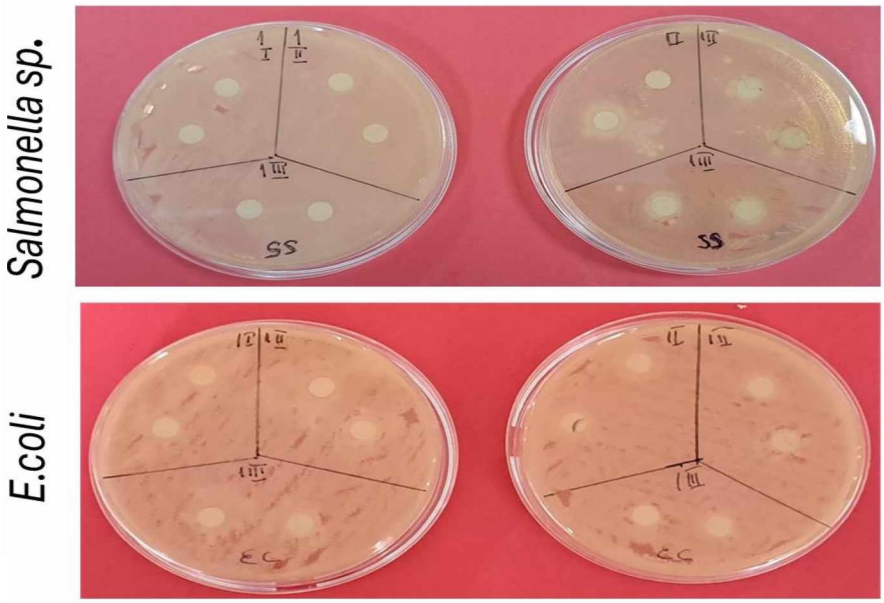

Figure 104. Presentation of the inhibitory effect of sample 1 on E. Coli and Salmonella. spp.

4.3.3.2. Cytotoxic activity of 3-Amino-4,5-dihydro-1-phenyl-1H-pyrazole (L3)

The cytotoxic activity against human malignant cell lines and human normal lung fibroblasts of the L3 (3-Amino-4,5-dihydro-1-phenyl-1H-pyrazole) can be seen in Table 47.

Table 47. Cytotoxic activity (IC50 values) of extract against human cancer cell lines.

compounds	HeLa	LS174T	A549	MRC-5
		IC50 (μM)		
L3	129.82 ± 19.24	124.18 ± 0	119.44 ± 0	129.80 ± 34.42

IC50 values (μM) were expressed as the mean ± SD determined from the results of MTT assay in three independent experiments.

The obtained data for L3 shows a cytotoxic activity inferior to previously described complexes tested for cytotoxicity (heading 4.2.1) as well as cisplatin. L3 has moderate cytotoxic activity against all tested malignant cells. As to compare and as previously described, the activity of cisplatin for HeLa cell line was 4.00 ± 0.47, for A549 line was 12.74 ± 1.26, and for MRC-5 line 5.91 ± 0.32 [141], and for LS174T cell line cisplatin had shown activity with the IC50 value of 20.38 ± 0.44 [142].

4.4. Synthesis and characterization of complex and products of Zn(II), Cu(II), Pd(II) and Co(II) with **Amoxicillin trihydrate (L5)**

From the attempts of synthetic reactions of Amoxicillin (L5) with metal salts: $Cu(NO_3)_2{\cdot}H_2O$ (in ethanol), $Zn(OAC)_2{\cdot}2H_2O$ (in DMSO), K_2PtCl_4 (in water), $Pd(OAC)_2$ (in water), RuI_3 (in water), $RuCl_3$ (in water), $Cu(OAC)_2$ (mechanochemical synthesis, methanol/water), $Co(OAC)_2$ (mechanochemical synthesis, methanol/water), $Pd(OAC)_2$ (mechanochemical synthesis, methanol/water), $Cu(NO_3)_2{\cdot}H_2O$ (in methanol/water), $CoCl_2$ (in methanol/water) a new complex of formulae $[ZnL(H_2O)_2]$, a degradation product *Methyl 5-(4-hydroxyphenyl)-6-oxo-1,6-dihydropyrazine-2-carboxylate*, as well as three more products have been obtained.

Syntheses with L5 as ligand produced a complex $[ZnL(H_2O)_2]$ and 4 more products: single crystals of a structurally previously described in literature yet obtained through different synthesis process - a degradation product: *Methyl 5-(4-hydroxyphenyl)-6-oxo-1,6-dihydropyrazine-2-carboxylate*, and 3 amorphous products with $Pd(OAc)_2$,

$Co(OAc)_2$, and $CoCl_2$; however, due to their insufficient purity and/or instability, these amorphous products could not be subjected to further characterization.

4.4.1. Synthesis and characterization of $[ZnL(H_2O)_2]$

Synthesis of a complex $[ZnL(H_2O)_2]$: The warm DMF solution (1 cm^3) $[Zn(OA)_2]$ (0.053 g, 0.25 mmol) was mixed with warm DMF solution (2 cm^3) of the ligand L5 (0.209 g, 0.5 mmol) with mild heating. The colorless reaction mixture was left to crystallize. After 2 months, yellow-orange amorphous precipitate was filtered and dried in air. Yield: 0.042 g (16.0 %).

From the reaction mixture, new complex compound of formulae: $[ZnL(H_2O)_2]$ was obtained. The molecular structure of the synthesized complex was determined by CHN, XRPD and IR analyses. The complex was prepared by reacting zinc acetate with amoxicillin trihydrate in hot DMF solution.

Results of CHN analysis are presented in the Table 48. The slight difference between the theoretical and obtained results are attributed to presence of impurities.

Table 48. Results of the CHN analysis for the complex $[ZnL(H_2O)_2]$

	Theoretical $[ZnL(H_2O)_2]$	Found
C%	*41,17 %*	*40,21 %*
H%	*4,96 %*	*4,46 %*
N%	*9,00 %*	*8,61 %*

On the basis of CHN analysis and FTIR results, a structure of the complex was determined (Figure 105).

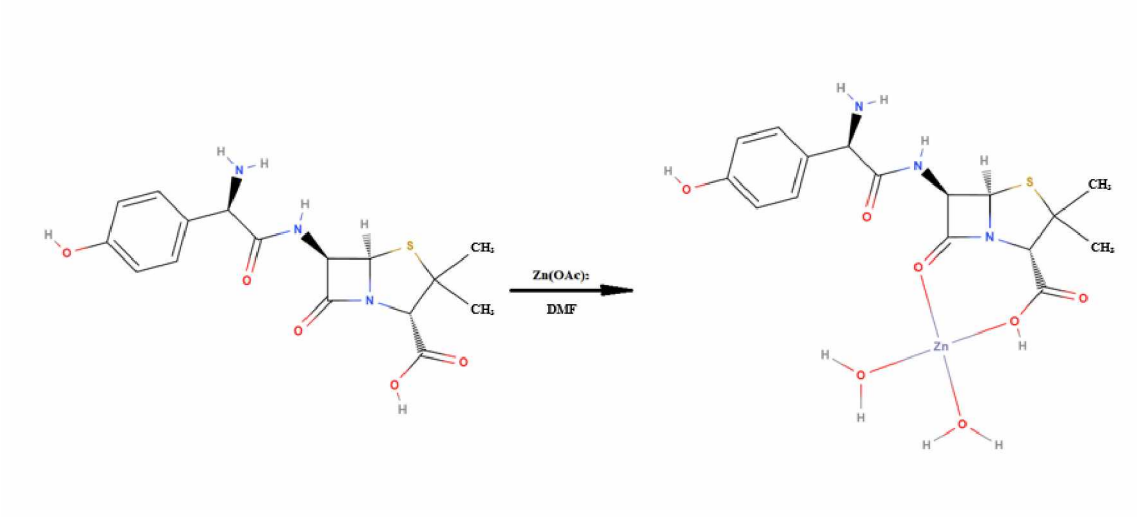

Figure 105. Synthesis of the Zn(II) complex of Amoxicillin trihydrate (L5)

4.4.1.1. X-ray powder diffraction data of [ZnL(H2O)2]

The powder diffractogram of *ZnL(H2O)2* is presented in Figure 106.

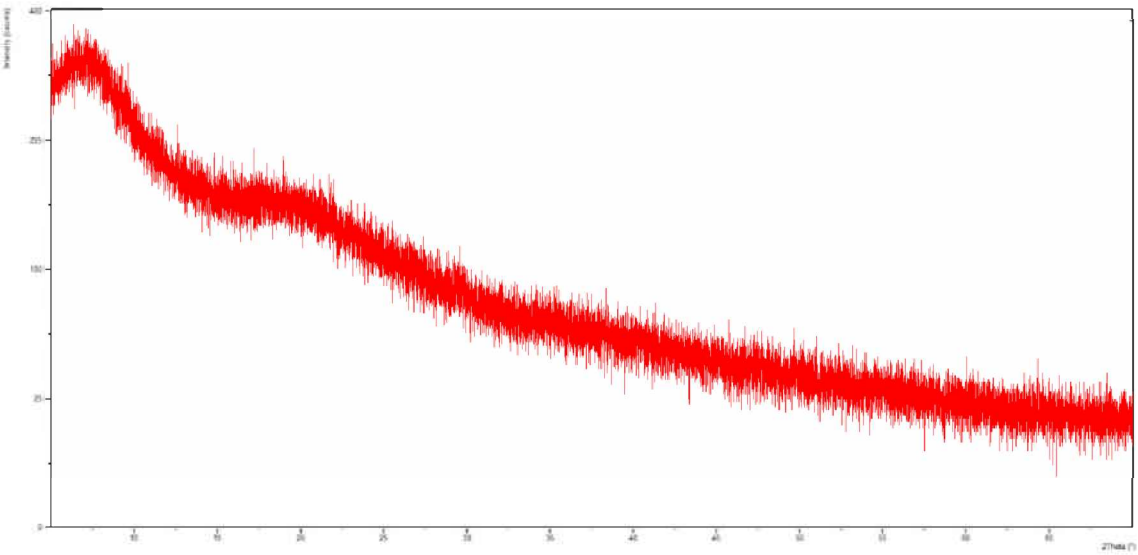

Figure 106. The powder diffractogram of ZnL(H2O)2

Presented in the Figure 107 are the diffractograms of *Amoxicillin trihydrate*, *Zn(OAc)2* and the product *ZnL(H2O)2)*. Similar volumes of all 3 samples were used during the analyses and all of the samples were analyzed with the same measuring conditions. From

the Figure 107, it is visible that the synthesis resulted in a new amorphous product, and not a mixture of metal salt and ligand.

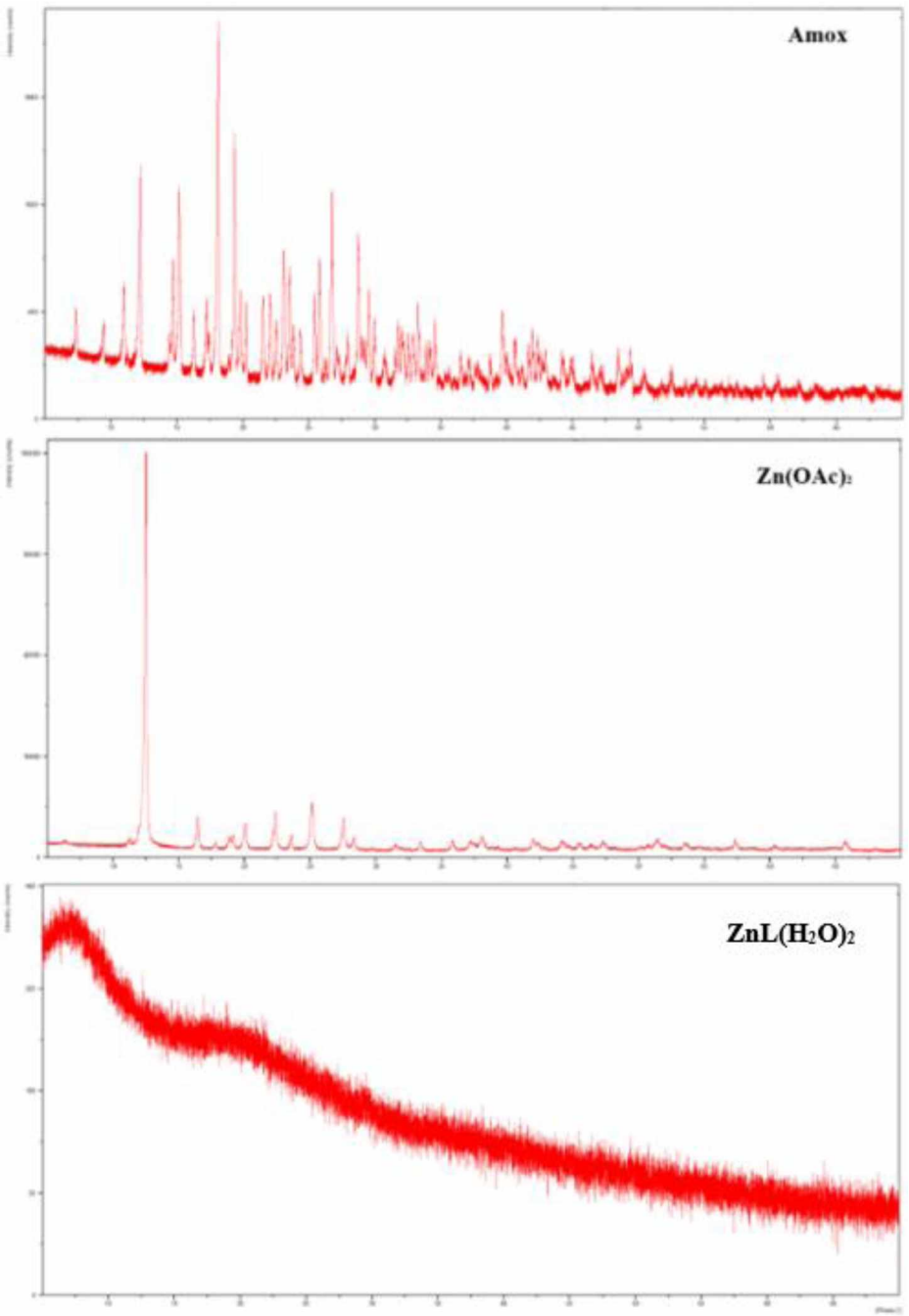

Figure 107. The powder diffractograms of L5, $Zn(OAc)_2$ and $ZnL(H_2O)_2$

4.4.1.2. *FTIR data of $[ZnL(H_2O)_2]$*

IR spectra of the complex $ZnL(H_2O)_2$ contains the following dominant vibrations: 3224.5 cm^{-1}, 2360.2 cm^{-1}, 1574.2 cm^{-1}, 1513.0 cm^{-1}, 1386.5 cm^{-1}, 1239.6 cm^{-1}, 1169.0 cm^{-1}, 841.8 cm^{-1}, 667.0 cm^{-1}, 613.0 cm^{-1}. The IR spectra of the complex is in accordance with the proposed structure.

4.4.2. Synthesis and characterization of Methyl 5-(4-hydroxyphenyl)-6-oxo-1,6-dihydropyrazine-2-carboxylate

Synthesis of *Methyl 5-(4-hydroxyphenyl)-6-oxo-1,6-dihydropyrazine-2-carboxylate*: Through reactions of warm water solution (1 cm^3) of $Cu(NO_3)_2 \cdot H_2O$ (0.052 g, 0.5 mmol) with warm methanol/water solutions (15 cm^3) of L5 (0.210 g, 0.5 mmol), after 5 days, green single crystals were filtered, washed with ethanol and dried in air, with the yield of 0.011 g (4.2 %). The obtained single crystals were analyzed through XRPD, IR and SC-XRD.

The product was analyzed via XRPD, IR and the crystal and molecular structure was determined by SC-XRD (Figure 108).

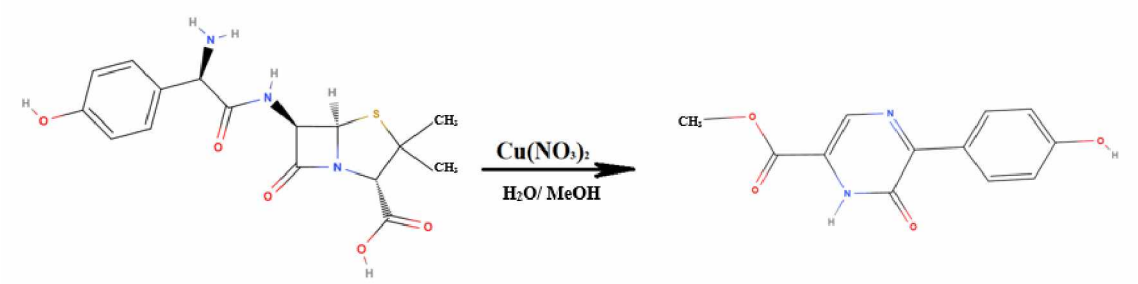

Figure 108. Formation of degradation product during the process of synthesis with L5 and $Cu(NO_3)_2$

Upon realization of SC-XRD analysis, it was deducted that the data of this degradation product have been previously reported in literature [144]. The differences in these syntheses reflect in the use of $CuSO_4$ instead of $Cu(NO_3)_2$, and the resulting crystal color that presented dark green in our product, compared to the colorless single crystals

described in literature [144] Apart from these distinctions, the crystallographic parameters were essentially identical, with only negligible variations observed.

4.4.2.1. X-ray powder diffraction data of Methyl 5-(4-hydroxyphenyl)-6-oxo-1,6-dihydropyrazine-2-carboxylate

The powder diffractogram of *Methyl 5-(4-hydroxyphenyl)-6-oxo-1,6-dihydropyrazine-2-carboxylate* is presented in Figure 109.

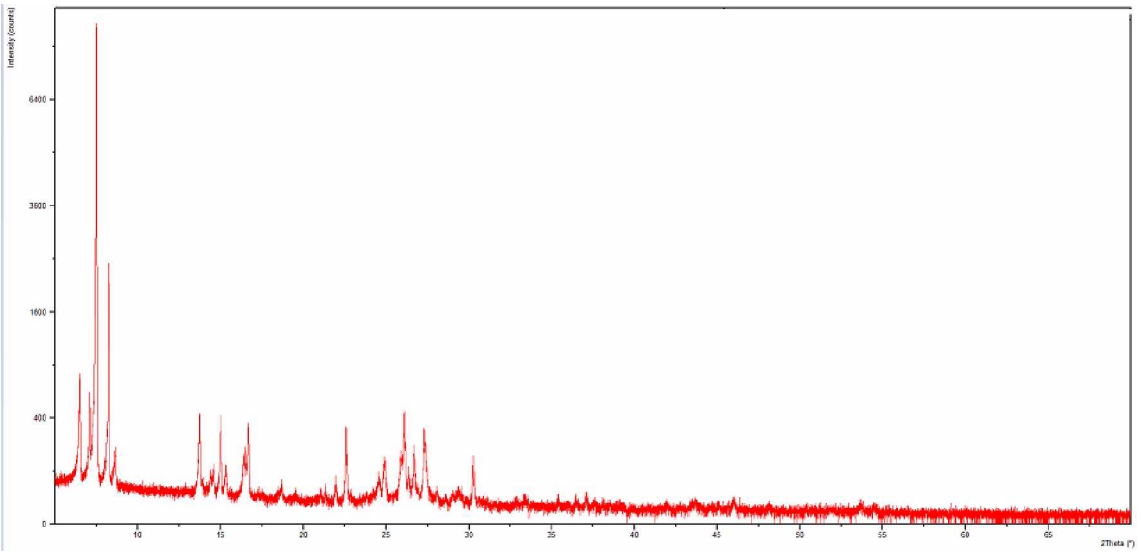

Figure 109. The powder diffractogram of Methyl 5-(4-hydroxyphenyl)-6-oxo-1,6-dihydropyrazine-2-carboxylate

Most dominant 8 peaks of the diffractogram are listed in the Table 49, with their d spacings and relative intensities.

Table 49. Eight most dominant diffraction lines in powder diffractogram of Methyl 5-(4-hydroxyphenyl)-6-oxo-1,6-dihydropyrazine-2-carboxylate

Pos. [°2θ]	d-spacing [Å]	Rel. Int. [%]
6.4880	**13.61236**	**8.25**
7.0808	**12.48426**	**8.92**

7.4829	**11.80458**	**100.00**
8.2276	**10.73778**	**26.54**
13.7175	**6.45023**	**4.84**
14.9919	**5.90466**	**5.51**
22.5759	**3.93533**	**4.89**
26.0847	**3.41337**	**6.08**

Presented in the Figure 110 are the diffractograms of *L5*, *$Cu(NO_3)_2$* and the product *Methyl 5-(4-hydroxyphenyl)-6-oxo-1,6-dihydropyrazine-2-carboxylate*. Similar quantities of all samples were used during the analyses and all samples were analyzed with the same measuring conditions. From the diffractogram of the product, it is clear that the new crystalline product was formed.

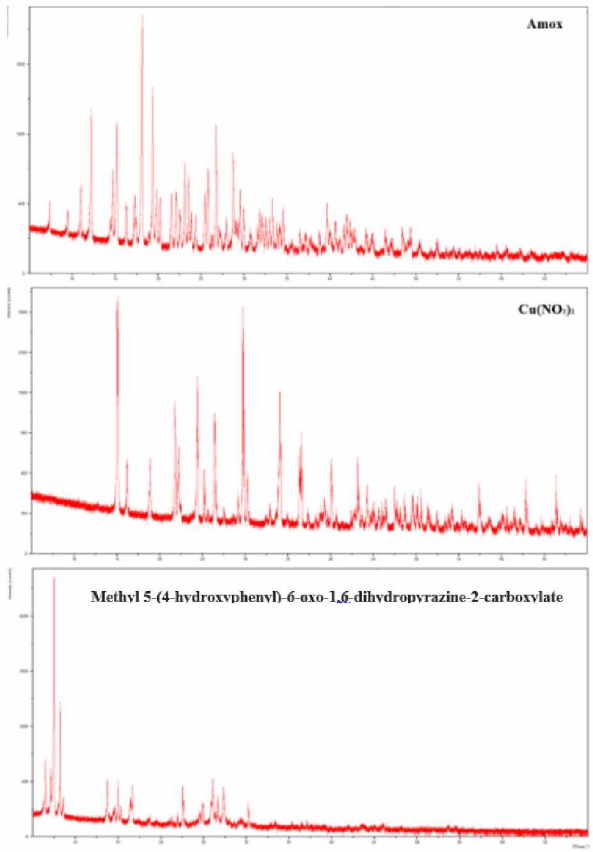

Figure 110. The powder diffractograms of L5, $Cu(NO_3)_2$ and Methyl 5-(4-hydroxyphenyl)-6-oxo-1,6-dihydropyrazine-2-carboxylate

4.4.2.2. *FTIR data of Methyl 5-(4-hydroxyphenyl)-6-oxo-1,6-dihydropyrazine-2-carboxylate*

IR spectra of the degradation product *Methyl 5-(4-hydroxyphenyl)-6-oxo-1,6-dihydropyrazine-2-carboxylate* contains (Figure 111) the following dominant vibrations: 3541.3 cm^{-1}, 3419.7 cm^{-1}, 3162.6 cm^{-1}, 3044.6 cm^{-1}, 2956.2 cm^{-1}, 1708.7 cm^{-1}, 1645.1 cm^{-1}, 1599.3 cm^{-1}, 1509.6 cm^{-1}, 1429.9 cm^{-1}, 1286.6 cm^{-1}, 1160.5 cm^{-1}, 844.2 cm^{-1}, 761.5 cm^{-1}, 567.2 cm^{-1}, 439.3 cm^{-1}. The IR spectra of the product is in accordance with the proposed structure.

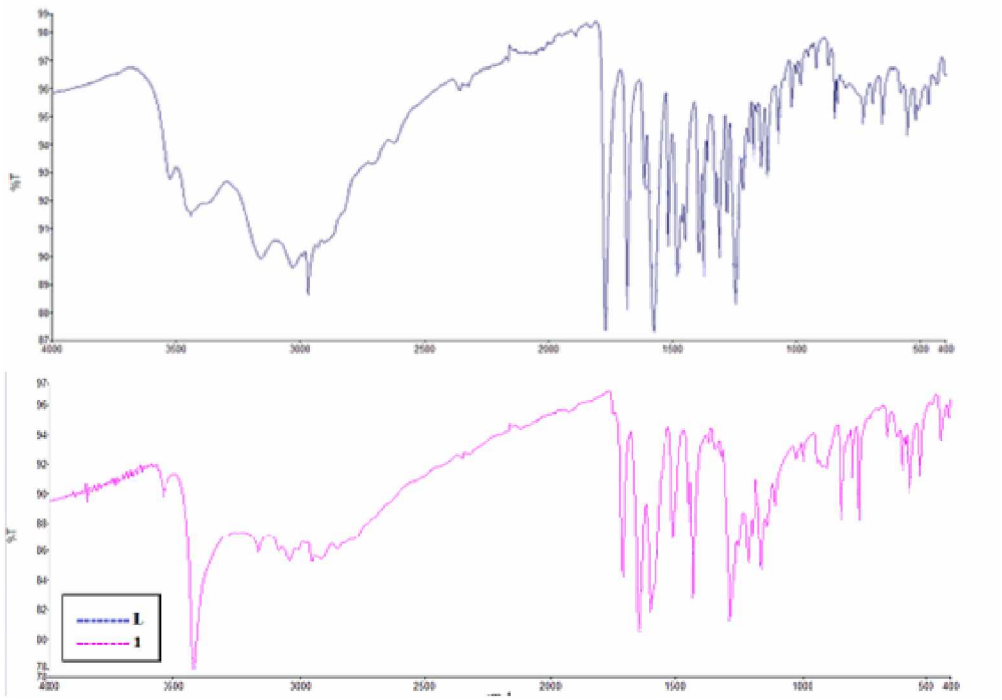

Figure 111. The IR spectra of L5 (blue) and Methyl 5-(4-hydroxyphenyl)-6-oxo-1,6-dihydropyrazine-2-carboxylate (pink)

4.4.2.3. *Crystal and molecular structure of Methyl 5-(4-hydroxyphenyl)-6-oxo-1,6-dihydropyrazine-2-carboxylate*

Finally, the crystal and molecular structure of the product was determined by SC-XRD analysis. The determined structure of the product is presented in the Figure 112.

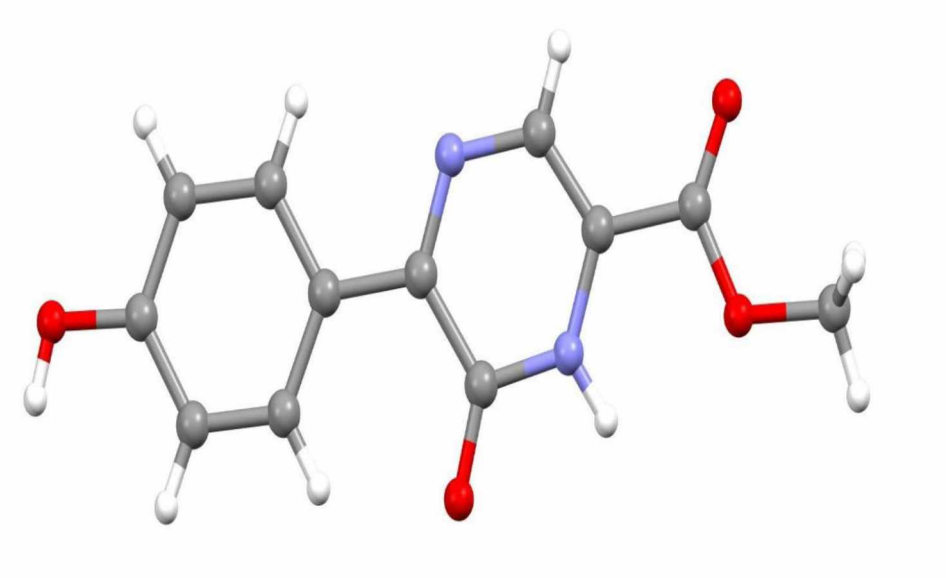

Figure 112. Structure of Methyl 5-(4-hydroxyphenyl)-6-oxo-1,6-dihydropyrazine-2-carboxylate

With the conclusion of the structure for this product, it was deducted that the SC-XRD data on this degradation product was already described by *Eltayeb N. E.* [144]. The difference between the process of synthesis, that showed the same outcome, was the use of $CuSO_4$ as a metal salt, instead of $Cu(NO_3)_2$. Additional difference was the colour of the obtained single crystals. Etlayeb described the crystals as colourless plate single crystals, yet the product obtained through synthesis with $Cu(NO_3)_2$ presented in this thesis was plate green single crystals. Other than the previously stated, differences between crystal data of the product, such are geometric parameters, were neglectably small.

4.4.3. Synthesis and characterization of products obtaied through syntheses with $Co(OAC)_2$, $Pd(OAC)_2$ and $CoCl_2$

Synthesis of a product obtained with *L5* and $CoCl_2$: Through reaction of warm water solution (1 cm^3) of $CoCl_2$ (0.033 g, 0.5 mmol) with warm methanol/water solutions (15 cm^3) of L5 (0.210 g, 0.5 mmol) the pink solution was left to crystallize. After 5 days,

green amorphous precipitate was filtered and dried in air, with the yield of 0.153 g (62.1 %). The obtained product was analyzed through XRPD. As the XRPD analysis showed the insufficient purity of the product, with present phase of metal salt $CoCl_2$, multiple tries of separation proved ineffective due to degradation (possible hydrolysis) of the product (detected by change of colour of the solutions). Further characterizations were not possible.

Synthesis of products obtained with *L5* and metal salts *Co(OAC)₂* and *Pd(OAC)₂*: through mechanosynthesis process of 0.25 mmol (0.050 mg) of *Co(OAC)₂* with 0.5 mmol (0.210 g) L5 of respective ligand and metal salt powders, and 0.25 mmol (0.056 mg) of *Pd(OAC)₂* with 0.5 mmol (0.210 g) L5 of respective ligand and metal salt powders was put in the mechanical ball mill with a zirconium ball, and mechanosynthesis process was conducted on 25 Hz for 15 minutes. Once the process was finalized, 1 cm^3 of ice (water) was added and the process was repeated for 30 seconds. The milky yellow solution (synthesis with *Pd(OAC)₂*) and milky pink solution (synthesis with *Co(OAC)₂*) were transferred to glass beakers and left to crystallize. The milky yellow and milky pink precipitates were collected, analyzed through XRPD and afterwards seperatelly dissolved in 6 cm^3 of methanol/water mixture respectively. After 3 days, amorphous dark yellow (synthesis with *Pd(OAC)₂*) and brown (synthesis with *Co(OAC)₂*) precipitates were collected and analyzed on XRPD. The products did not show crystal impurities from the results of XRPD analysis, yet have shown properties of instability, and with that made further characterizations impossible.

4.4.3.1. X-ray powder diffraction data of products obtained through syntheses with Co(OAC)₂, Pd(OAC)₂ and $CoCl_2$

In the Figure 113 powder diffractograms of the products are presented.

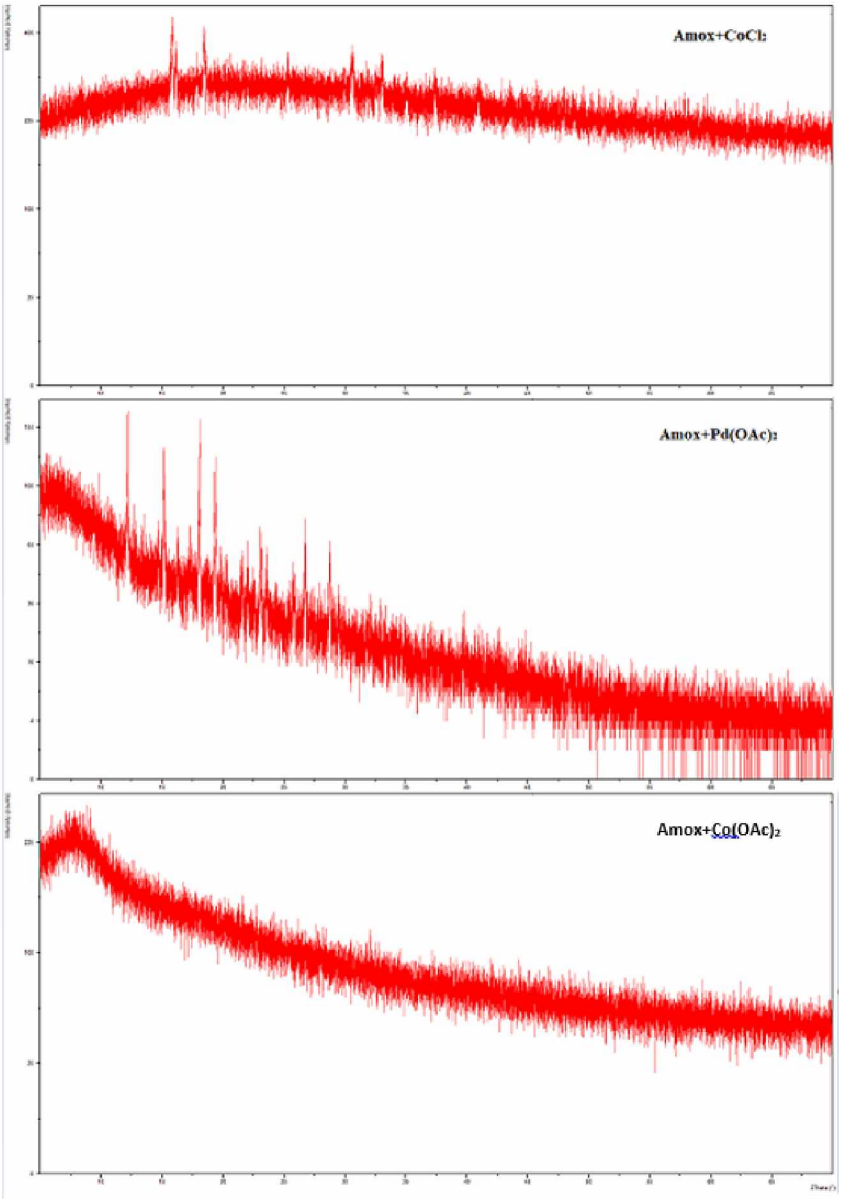

Figure 113. The powder diffractograms of products obtained through syntheses with $CoCl_2$, $Co(OAC)_2$ and $Pd(OAC)_2$.

Presented in the Figure 114 are the diffractograms of *L5*, $Co(OAc)_2$ and the product. Similar quantities of all samples were used during the analyses and all samples were analyzed with the same measuring conditions. From the diffractogram of the product, it is clear that the product has amorphous polymorphic state.

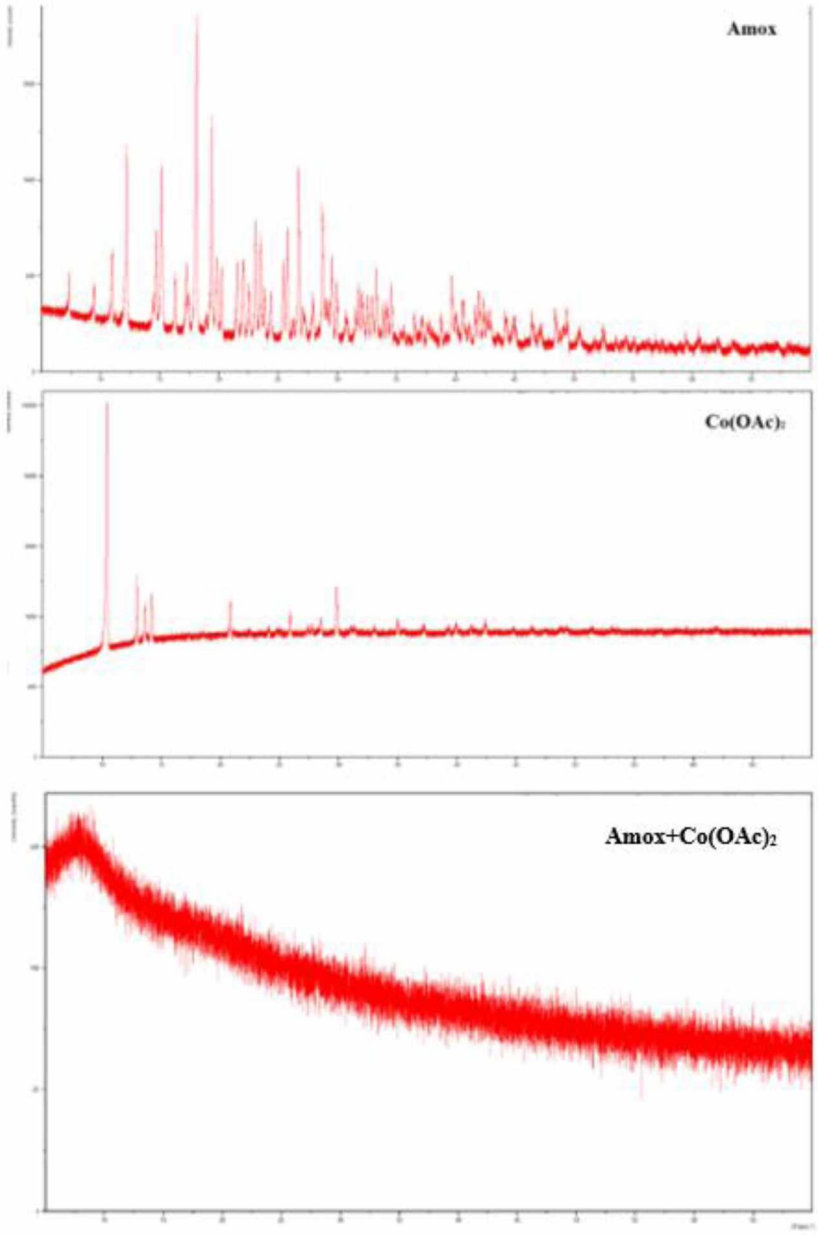

Figure 114. The powder diffractograms of L5, $Co(OAc)_2$ and the product

Presented in the Figure 115 are the diffractograms of *L5*, *$Co(OAC)_2$*, *$Pd(OAC)_2$* and the products of the syntheses. Similar quantities of all samples were used during the analyses and all samples were analyzed with the same measuring conditions. From the diffractogram of the product, it can be seen that the product has amorphous polymorphic state with crystal phase impurities from metal salt in case of synthesis with $CoCl_2$, and crystal phase impurities from metal salt and the ligand (L5) in case of synthesis with $Pd(OAc)_2$.

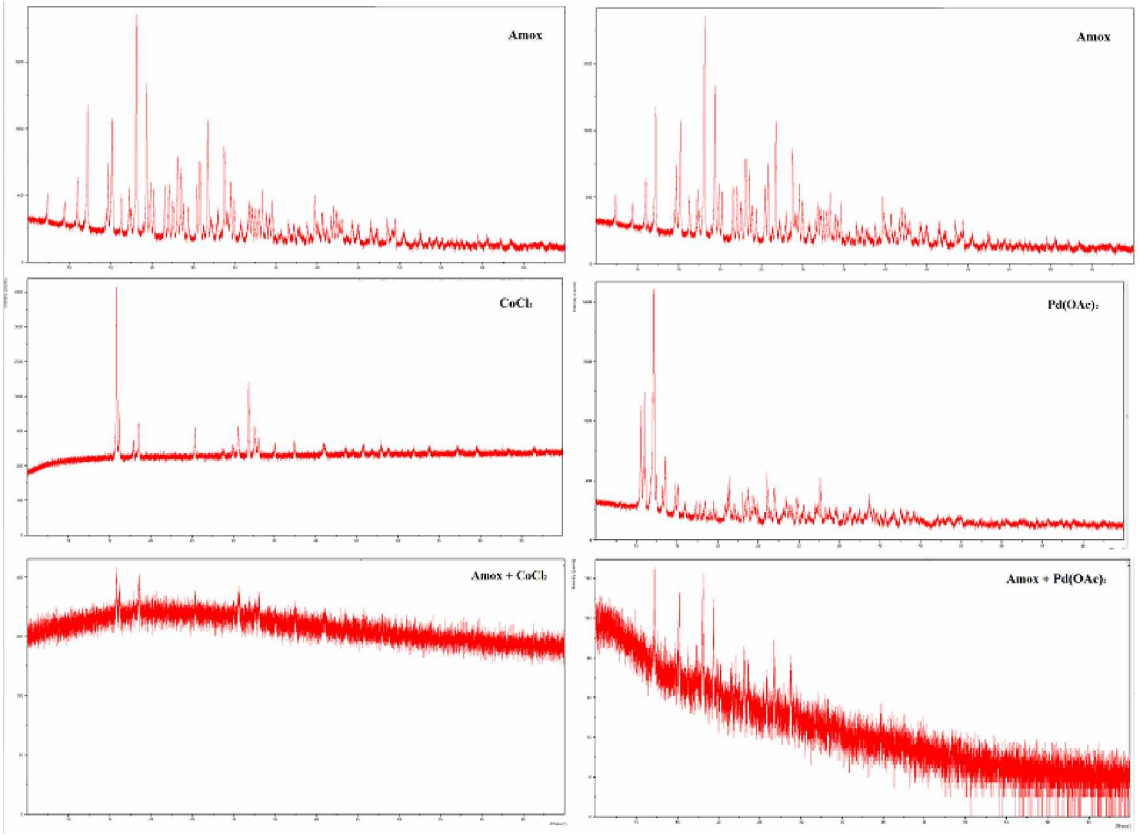

Figure 115. The powder diffractograms of L5, $CoCl_2$, $Pd(OAc)_2$ and the products of sytheses

4.4.3.2. FTIR data of the obtained product of L5 and $[Co(OAc)_2]$

Due to the impurities of products obtained through syntheses with $CoCl_2$ and $Pd(OAc)_2$ the FTIR analysis was only conducted for the product obtained with $Co(OAc)_2$. IR spectra of the product contains the following dominant vibrations: 3217.9 cm^{-1}, 2966.0 cm^{-1}, 1732.2 cm^{-1}, 1592.6 cm^{-1}, 1515.2 cm^{-1}, 1435.4 cm^{-1}, 1370.8 cm^{-1}, 1235.1 cm^{-1}, 1167.7 cm^{-1}, 1012.0 cm^{-1}, 838.3 cm^{-1}.

5. Conclusion

In this PhD thesis, a set of new coordination complexes based on pyrazole derivatives and amoxicillin trihydrate has been synthesized, characterized, with evaluated potential biological activity for a selected part. The syntheses explored five ligands with a series of transition metal salts. The ligands that have been used were pyrazole derivatives: *5-(4-bromophenyl)-3-methyl-1H-pyrazole* (L1), *4-methylpyrazole* (L2), *3-amino-4,5-dihydro-1-phenyl-1H-pyrazole* (L3), and *2-(3-aminophenyl)-5-methyl-2,4-dihydro-pyrazol-3-one hydrochloride* (L4), as well as a well known active pharmaceutical ingredient: *amoxicillin trihydrate* (L5). In total, this thesis reports the syntheses and characterizations of eleven novel complexes, presents the SC-XRD structure of the previously uncharacterized ligand, provides new data on two previously obtained compounds (one complex and one degradation product), and includes a discussion on three products/complexes for which complete characterization could not be achieved.

The ligand *5-(4-bromophenyl)-3-methyl-1H-pyrazole* (L1) enabled the successful formation of three complexes and an obtained single crystal of the ligand that has not been previously characterized through SC-XRD analysis. From the attempts of syntheses with following metal salts: $Cu(NO_3)_2{\cdot}H_2O$, $Zn(OAC)_2{\cdot}2H_2O$, $Ni(OAC)_2{\cdot}2H_2O$, $PdCl_2$, K_2PtCl_4, $CoCl_2$, $Co(OAC)_2$, $Pd(OAC)_2$, RuI_3, in different conditions, syntheses of L1 with $Zn(OAC)_2{\cdot}2H_2O$ in ethanol, and L1 with $CoCl_2$ in ethanol, yielded three complexes: $[ZnL_2(OAc)_2]$, $[Co_4L_8Cl_8]$ and $[CoL_3Cl{\cdot}H_2O]$. Two obtained monocrystal complexes $[Co_4L_8Cl_8]$ and $[CoL_3Cl{\cdot}H_2O]$ have been obtained simultaneously from the reaction with $CoCl_2$ in ethanol, and have been characterized with SC-XRD technique. The crystalline complex $[ZnL_2(OAc)_2]$ obtained from the reaction of L1 and $Zn(OAC)_2{\cdot}2H_2O$ in ethanol, has been characterized by XRPD, CHN and IR analyses. The obtained monocrystal of the ligand has been characterized with SC-XRD technique. The interesting synthesis with L1 and $CoCl_2$ in ethanol, presented four different types of single crystals, from which two new complexes have been obtained: $[Co_4L_8Cl_8]$ and $[CoL_3Cl{\cdot}H_2O]$. The azure blue single crystal-clusters, representing the trinuclear complex $[Co_4L_8Cl_8]$ exhibit a particularly intriguing structural arrangement.

With the *fomepizole* (L2), which has shown to be the most synthetically productive ligand, six metal complexes have been obtained. From the attempts of synthetic reactions with metal salts: $Cu(NO_3)_2 \cdot H_2O$, $Zn(OAC)_2 \cdot 2H_2O$, $Ni(OAC)_2 \cdot 2H_2O$, $PdCl_2$, K_2PtCl_4, $CoCl_2$, $Co(OAC)_2$, $Pd(OAC)_2$, $RuCl_3$, in different conditions, syntheses of L2 with $Cu(NO_3)_2 \cdot H_2O$ in ethanol, L2 with $CoCl_2 \cdot 6H_2O$ in ethanol, L2 with $Ni(OAc)_2 \cdot 4H_2O$ in ethanol, L2 with $Zn(OAc)_2 \cdot 2H_2O$ in ethanol, L2 with $PtL2_3Cl_2$ in ethanol/water, L2 with $Pd(OAc)_2$ in ethanol/water, yielded six complexes: $[CuL_2(NO_3)_2]$, $[CoL_4Cl_2]$, $[Ni(OAc)_2L_4]$, $[Zn(OAc)_2L_2]$, $[PtL_3Cl_2]$ *and* $[Pd(L\text{-}H)_3]$. Due to L2 being an already widely used as an API, several of the complexes were subject of different additional assays. For the complex obtained from synthesis of ligand with $Cu(NO_3)_2 \cdot H_2O$ the characterization has been done via XRPD, SC-XRD and IR analyses, additionally the tests of bactericidal properties have been conducted for this complex. Complex obtained with $CoCl_2$ the characterization was conducted through XRPD and SC-XRD analyses. Complexes of L2 and $Zn(OAC)_2 \cdot 2H_2O$ and $Ni(OAC)_2 \cdot 2H_2O$ were characterized through SC-XRD, CHN and IR analyses. Crystalline complexes with K_2PtCl_4 and $Pd(OAC)_2$ have been characterized by CHN, IR and XRPD techniques. The selection of complexes: $[Ni(OAc)_2L_4]$ and $[Zn(OAc)_2L_2]$ was made for the determination of their thermic characteristics through TG and DTG analyses, as well as their antioxidative potential. the DPPH• scavenging activity of Ni(II) and Zn(II) is in correlation with their thermal stability too. The thermally more stable Ni(II) complex shows less RSC, but the RSC of the less stable Zn(II) complex is higher. It is possible that the Zn(II) complex, dimer in crystalline form, is less stable in solution too, dissociates during solution, and becomes easily available for radical scavenging. Differently, the thermally more stable Ni(II) complex may be more stable in solution and, therefore less available for reaction with DPPH•. From the structural standpoint $[Ni(OAc)_2L_4]$ has shown very interesting properties. However, perhaps the most notable results of this thesis have been achieved with $[PtL_3Cl_2]$ and $[Pd(L\text{-}H)_3]$. These complexes have demonstrated remarkable cytotoxic activity, showing higher activity against LS174T and A549 cancer cell lines compared to cisplatin, while maintaining similar or improved selectivity toward normal cells (MRC-5), showing promising results and potential to be used as chemotherapeutic agents.

Through syntheses with ligand *3-Amino-4,5-dihydro-1-phenyl-1H-pyrazole* (L3), two metal complexes have been synthesized. From the attempts of syntheses with following

metal salts: $Cu(NO_3)_2 \cdot H_2O$, $Zn(OAC)_2 \cdot 2H_2O$, $Ni(OAC)_2 \cdot 2H_2O$, $PdCl_2$, K_2PtCl_4, $CoCl_2$, $Co(OAC)_2$, $Pd(OAC)_2$, RuI_3, $Mn(OAC)_2 \cdot 4H_2O$, in different conditions, syntheses of L3 with K_2PtCl_4 in ethanol/water, and L3 with $PdCl_2$ through mechanosynthesis, yielded two complexes: *[PtL_2Cl_2]* and *[$PdL_2(OAc)_2$]*. The obtained amorphous complexes were characterized by XRPD, CHN and IR analyses. Other than their characterization, the ligand was evaluated for its biological properties through the estimation of its bactericidal and cytotoxic activities, as to indicate the biopotential of its complexes. Indicating somewhat moderate bioactivity, no further assays with the complexes of this ligand have been conducted.

Ligand *2-(3-Aminophenyl)-5-methyl-2,4-dihydro-pyrazol-3-one hydrochloride* (L4) did not form any complexes, despite variations in approaches of numerous syntheses. The attempted syntheses that have been conducted were with metal salts: $Cu(NO_3)_2 \cdot H_2O$ (in ethanol), $Zn(OAC)_2 \cdot 2H_2O$ (in DMSO), $Ni(OAC)_2 \cdot 2H_2O$ (in DMSO), K_2PtCl_4 (in water), $CoCl_2$ (in water), $Pd(OAC)_2$ (in water), RuI_3 (in water). With that said, the ligand L4 has shown limited coordination behavior and low stability of potential products.

Finally, syntheses with *Amoxicillin trihydrate* (L5) resulted in a complex *[$ZnL(H_2O)_2$]*, a degradation product *Methyl 5-(4-hydroxyphenyl)-6-oxo-1,6-dihydropyrazine-2-carboxylate* and three products, while using different solution-based and mechanochemical approaches. From the attempts of syntheses with following metal salts: $Cu(NO_3)_2 \cdot H_2O$ (in ethanol), $Zn(OAC)_2 \cdot 2H_2O$ (in DMSO), K_2PtCl_4 (in water), $Pd(OAC)_2$ (in water), RuI_3 (in water), $RuCl_3$ (in water), $Cu(OAC)_2$ (mechanochemical synthesis, methanol/water), $Co(OAC)_2$ (mechanochemical synthesis, methanol/water), $Pd(OAC)_2$ (mechanochemical synthesis, methanol/water), $Cu(NO_3)_2 \cdot H_2O$ (in methanol/water), $CoCl_2$ (in methanol/water), one complex, one degradation product and three products of insufficient purity and observed instability have been obtained. Out of the stated, from the reaction of L5 with $Zn(OAC)_2 \cdot 2H_2O$ (in DMSO) one novel amorphous complex has been characterized of formulae *[$ZnL(H_2O)_2$]* through XRPD, CHN and IR analyses. Through synthesis with $Cu(NO_3)_2 \cdot H_2O$ (in methanol/water) single crystals of a, in literature previously described, degradation product *Methyl 5-(4-hydroxyphenyl)-6-oxo-1,6-dihydropyrazine-2-carboxylate,* has been obtained, via a synthetic reaction different from the one described in literature, and additional analytical data was provided in the

form of XRPD data and IR spectra. Finally, additional three amorphous products of insufficient purity and observed instability have been achieved, yet were not characterized, due to the stated drawbacks. Even though amoxicillin seems structurally quite favorable to be used as a ligand in coordinations with transition metals, from a theoretical perspective, the empirical observations have shown the opposite. Most of the published data on achieved metal complexes with amoxicillin have shown amorphous products, with insufficient characterization techniques utilized to provide concrete data on the structure of the complexes. And as the behavior of the amoxicillin changes in different pH values of the environment, amoxicillin has proven to be a challenge for the syntheses of stable complexes with transition metals.

The results presented as part of this thesis have allowed to expand the knowledge in coordination behaviour of pyrazole- and amoxicillin-based metal complexes with detailed structural, thermal, and in-vitro biological evaluations. The identification of platinum and palladium complexes with 4-methylpyrazole have shown remarkable cytotoxic activity compared with established therapies such is cisplatin. Introduced novel complexes can serve as a potential for next-generation metal-based therapeutics. These findings provide a basis for future in vivo studies focused on the development of more potent metallopharmaceuticals.

References

[1] T. Sharma, R. Kumar, S. Chandra Sahoo, J. Sindhu, J. Singh, B. Singh, S. Kumar Mehta, A. Umar, T. Singh Saini, V. Kumar, R. Kataria, Synthesis, structural and pharmacological exploration of 2-(3, 5-dimethyl-1H-pyrazol-1-yl)-acetophenone oximes and their silver complexes, Polyhedron 195 (2021) 114972. https://doi.org/10.1016/j.poly.2020.114972.

[2] Soliman Saied M., Sobhy E. Elsilk, Ayman El-Faham, Synthesis, structure and biological activity of zinc (II) pincer complexes with 2, 4-bis (3, 5-dimethyl-1H-pyrazol-1-yl)-6-methoxy-1, 3, 5-triazine, Inorganica Chimica Acta 508 (2020) 119627. https://doi.org/10.1016/j.ica.2020.119627.

[3] A. Burmudžija, J. Muskinja, Z. Ratkovic, M. Kosanic, B. Rankovic, S. B. Novakovic, A. G. Bogdanovic, Pyrazoline derivatives of acryloyl substituted ferrocenyl ketones: Synthesis, antimicrobial activity and structural properties, Inorganica Chimica Acta 471 (2018): 570-576. https://doi.org/10.1016/j.ica.2017.11.061.

[4] Y. Bseiso, A. Alqudah, E. Qnais, M. Wedyan, K. Abu-Safieh, O. Gammoh, 2′,3,3,5′-Tetramethyl-4′-nitro-2′H-1,3′-bipyrazole exerts antinociceptive effect using various nociception models, Pharmacia 70 (2023) 509–517. https://doi.org/10.3897/pharmacia.70.e104828.

[5] X. Zhang, L. Hu, X. Wang, Y. Zhao,X. Chen, Cu (II) and Zn (II) crystal complexes based on pyrazolone: synthesis and application as antibacterial agents. Inorganica Chimica Acta 556 (2023): 121618. https://doi.org/10.1016/j.ica.2023.121618

[6] P.A. Moraes, E.S. Brum, I. Brusco, M.A. Marangoni, M.M. Lobo, A.F. Camargo, P.A. Nogara, H.G. Bonacorso, M.A.P. Martins, J.B.T. Da Rocha, S.M. Oliveira, N. Zanatta, Pyrazole-Enaminones as Promising Prototypes for the Development of Analgesic Drugs, ChemistrySelect 5 (2020) 14620–14625. https://doi.org/10.1002/slct.202004049.

[7] A.A. Bekhit, S.N. Nasralla, E.J. El-Agroudy, N. Hamouda, A.A. El-Fattah, S.A. Bekhit, K. Amagase, T.M. Ibrahim, Investigation of the anti-inflammatory and analgesic activities of promising pyrazole derivative, European Journal of Pharmaceutical Sciences 168 (2022). https://doi.org/10.1016/j.ejps.2021.106080.

[8] L.K. da S. Moreira, R.R. Silva, D.M. da Silva, M.A.S. Mendes, A.F. de Brito, F.S. de Carvalho, G. Sanz, M.F. Rodrigues, A.C.G. da Silva, D.V. Thomaz, V. de Oliveira, B.G. Vaz, L.M. Lião, M.C. Valadares, E. de S. Gil, E.A. Costa, F. Noël, R. Menegatti, Anxiolytic- and antidepressant-like effects of new phenylpiperazine derivative LQFM005 and its hydroxylated metabolite in mice, Behavioural Brain Research 417 (2022). https://doi.org/10.1016/j.bbr.2021.113582.

[9] da Silva Dayane Moreira, S. German, B. G. Vaz, et al, Tert-butyl 4-((1-phenyl-1H-pyrazol-4-yl) methyl) piperazine-1-carboxylate (LQFM104)–new piperazine derivative with antianxiety and antidepressant-like effects: putative role of serotonergic system, Biomedicine & pharmacotherapy 103 (2018): 546-552. https://doi.org/10.1016/j.biopha.2018.04.077.

[10] K. Avasthi, N. Garg, T. Chandra, D.S. Bhakuni, P.P. Gupta, R.C. Srimal, Synthesis of 4-amino/hydroxy-6-methylthio-l/2-(2',2'-diethoxyethyl)-lH/2H-pyrazolo[3,4-dpyrimidines and their antiallergic activity·, Eur J Med Chem 28 (1993) 585–591. https://doi.org/10.1016/0223-5234(93)90089-W.

[11] D. Woschko, S. Millan, M.A. Ceyran, R. Oestreich, C. Janiak, Synthesis of a Chiral 3,6T22-Zn-MOF with a T-Shaped Bifunctional Pyrazole-Isophthalate Ligand Following the Principles of the Supramolecular Building Layer Approach, Molecules 27 (2022). https://doi.org/10.3390/molecules27175374.

[12] R. R. Liang, Z. Han, P. Cai, Y. Yang, J. Rushlow, Z. Liu, K. Y. Wang, H. C. Zhou, A Robust Pyrazolate Metal–Organic Framework for Efficient Catalysis of Dehydrogenative C–O Cross Coupling Reaction, Journal of the American Chemical Society (2024). https://doi.org/10.1021/jacs.4c03038.

[13] V. V. Serushkin, V.P. Sinditskii, T.H. Hoang, S.A. Filatov, A.S. Shipulina, I.L. Dalinger, A.K. Shakhnes, A.B. Sheremetev, Thermal and combustion behavior of novel oxygen-rich energetic pyrazoles, J Therm Anal Calorim 132 (2018) 127–142. https://doi.org/10.1007/s10973-017-6911-2.

[14] U. Mithra, S. Sarveswari, A review on pyrazole moieties as organic chemosensors in the detection of cations and anions, Inorganica Chimica Acta (2024): 122118. https://doi.org/10.1016/j.ica.2024.122118

[15] M.M. Hammouda, H.M. Metwally, A. Fekri, J. Van der Eycken, Synthesis and Molecular Modeling Studies on Novel C2 Alkylated Benzoazonine Scaffold and Corresponding 2-Pyrazoline Derivatives as Acetylcholinestrase Enzyme Inhibitors, Polycycl Aromat Compd 41 (2021) 1223–1240. https://doi.org/10.1080/10406638.2019.1666888.

[16] M. Pellei, L. Bagnarelli, S. Gabrielli, G. Lupidi, C. Cimarelli, F. Stella, A. Dolmella, C. Santini, Copper (II) complexes based on isopropyl ester derivatives of bis (pyrazol-1-yl) acetate ligands with catalytic potency in organic macro (molecules) synthesis, Inorganica Chimica Acta 544 (2023): 121234. https://doi.org/10.1016/j.ica.2022.121234.

[17] M. L. Soriano, F. A. Jalon, B. R. Manzano, M. Maestro, Synthesis and characterization of Ru (arene) complexes of bispyrazolylazines: Catalytic hydrogen transfer of ketones, Inorganica Chimica Acta 362.12 (2009): 4486-4492. doi:10.1016/j.ica.2009.04.011.

[18] M.B. Bushuev, V.P. Krivopalov, E. V. Lider, N. V. Semikolenova, N. V. Pervukhina, D.Y. Naumov, L.G. Lavrenova, V.A. Zakharov, S. V. Larionov, Copper(II) complexes with 4-(3,5-dimethyl-1H-pyrazol-1-yl)-2-methyl-6- phenylpyrimidine: Syntheses, crystal structures and catalytic activity in ethylene polymerization, Polyhedron 31 (2012) 235–240. https://doi.org/10.1016/j.poly.2011.09.024.

[19] B. Barta Holló, M.M. Radanović, M. V. Rodić, S. Krstić, Ž.K. Jaćimović, L.S. Vojinović Ješić, Synthesis, Physicochemical, Thermal and Antioxidative Properties of Zn(II) Coordination Compounds with Pyrazole-Type Ligand, Inorganics (Basel) 10 (2022) 1–21. https://doi.org/10.3390/inorganics10020020.

[20] B. Barta Holló, L.S. Vojinović Ješić, M.M. Radanović, M. V. Rodić, Ž.K. Jaćimović, K. Mészáros Szécsényi, Synthesis, physicochemical, and thermal characterization of coordination compounds of Cu(II) with a pyrazole-type ligand, J Therm Anal Calorim 142 (2020) 451–460. https://doi.org/10.1007/s10973-020-09260-3.

[21] Ž. Jaćimović, M. Kosović, V. Kastratović, B.B. Holló, K.M. Szécsényi, I.M. Szilágyi, N. Latinović, L. Vojinović-Ješić, M. Rodić, Synthesis and characterization of copper, nickel, cobalt, zinc complexes with 4-nitro-3-pyrazolecarboxylic acid ligand, J Therm Anal Calorim 133 (2018) 813–821. https://doi.org/10.1007/s10973-018-7229-4.

[22] N.D. Radnović, N. Štetin, M.M. Radanović, I. n. Borišev, M. V. Rodić, Ž.K. Jaćimović, B. Barta Holló, Two Isomers of a Novel Ag(I) Complex with Pyrazole-Type Ligand—Synthesis, Structural, Thermal, and Antioxidative Characterization, Inorganics (Basel) 12 (2024). https://doi.org/10.3390/inorganics12010004.

[23] K. Karrouchi, S. Radi, Y. Ramli, J. Taoufik, Y. N. Mabkhot, F. A. Al-Aizari, & M. H. Ansar, Synthesis and pharmacological activities of pyrazole derivatives: A review, Molecules, *23*, 134 (2018). https://doi.org/10.3390/molecules23010134

[24] A. Secrieru, P. M. O'Neill & M. L. S. Cristiano, Revisiting the Structure and Chemistry of 3(5)-Substituted Pyrazoles, Molecules, 25 (1) :42 (2020). https://doi.org/10.3390/molecules25010042

[25] J. P. Castaneda, G. S. Denisov, S. Y. Kucherov, V. M. Schreiber & A. V. Shurukhina, Infrared and ab initio studies of hydrogen bonding and proton transfer in the complexes formed by pyrazoles, Journal of molecular structure, 660, 25–40 (2003). https://doi.org/10.1016/j.molstruc.2003.07.010

[26] Ş. G. Küçükgüzel & S. Şenkardeş, Recent advances in bioactive pyrazoles, European Journal of Medicinal Chemistry, 97, 786-815 (2015). https://doi.org/10.1016/j.ejmech.2014.11.059

[27] Goddard, R., Claramunt, R. M., & Escolástico, C. (1999). Structures of NH-pyrazoles bearing only C-methyl substituents: 4-methylpyrazole is a hydrogen-bonded trimer in the solid (100 K). *New Journal of Chemistry*, *23*(2), 237-240.

[28] Khan, M. F., Alam, M. M., Verma, G., Akhtar, W., Akhter, M., & Shaquiquzzaman, M. (2016). The therapeutic voyage of pyrazole and its analogs: a review. European journal of medicinal chemistry, *120*, 170-201.

[29] Yi, X. J., El-Idreesy, T. T., Eldebss, T. M., Farag, A. M., Abdulla, M. M., Hassan, S. A., & Mabkhot, Y. N. (2016). Synthesis, biological evaluation, and molecular docking studies of new pyrazol-3-one derivatives with aromatase inhibition activities. Chemical Biology & Drug Design, 88(6), 832-843.

[30] Penning, T. D., Talley, J. J., Bertenshaw, S. R., Carter, J. S., Collins, P. W., Docter, S., ... & Isakson, P. C. (1997). Synthesis and biological evaluation of the 1, 5-diarylpyrazole class of cyclooxygenase-2 inhibitors: identification of 4-[5-(4-methylphenyl)-3-

(trifluoromethyl)-1 H-pyrazol-1-yl] benzenesulfonamide (SC-58635, celecoxib). Journal of medicinal chemistry, 40(9), 1347-1365.

[31] Boever, S. D., Neirinckx, E., Meyer, E., Baere, S. D., Beyaert, R., Backer, P. D., ... & Croubels, S. (2010). Pharmacodynamics of tepoxalin, sodium-salicylate and ketoprofen in an intravenous lipopolysaccharide inflammation model in broiler chickens. Journal of Veterinary Pharmacology and Therapeutics, 33(6), 564-572. https://doi.org/10.1111/j.1365-2885.2010.01184.x

[32] Boo, P. A., Casas, J. S., Castellano, E. E., Couce, M. D., Freijanes, E., Furlani, A., ... & Varela, M. (2001). Synthesis, characterization and cytotoxic activity of complexes of diorganotin(iv) dihalides with mepirizole. Applied Organometallic Chemistry, 15(1), 75-81. https://doi.org/10.1002/1099-0739(200101)15:13.0.co;2-4

[33] Escrivà, E., García-Lozano, J., Martínez-Lillo, J., Nuñez, H., Server-Carrió, J., Soto, L., ... & Cano, J. (2003). Synthesis, Crystal Structure, Magnetic Properties, and Theoretical Studies of [{Cu (mepirizole) Br} 2 (μ-OH)(μ-pz)](Mepirizole= 4-Methoxy-2-(5-methoxy-3-methyl-1 H-pyrazol-1-yl)-6-methylpyrimidine; pz= Pyrazolate), a Novel μ-Pyrazolato− μ-Hydroxo-Dibridged Copper (II) Complex. Inorganic chemistry, 42(25), 8328-8336.

[34] Lusardi, M., Spallarossa, A., & Brullo, C. (2023). Amino-pyrazoles in medicinal chemistry: A review. International journal of molecular sciences, *24*(9), 7834.

[35] Delpe-Acharige, A., Zhang, M., Eschliman, K., Dalecki, A., Covarrubias-Zambrano, O., Minjarez-Almeida, A., ... & Bossmann, S. H. (2021). Pyrazolyl Thioureas and Carbothioamides with an NNSN Motif against MSSA and MRSA. ACS omega, 6(9), 6088-6099.

[36] Hu, Y.; Shi, H.; Zhou, M.; Ren, Q.; Zhu, W.; Zhang, W.; Zhang, Z.; Zhou, C.; Liu, Y.; Ding, X.; et al. Discovery of Pyrido[2,3-b]indole Derivatives with Gram-Negative Activity Targeting Both DNA Gyrase and Topoisomerase IV. J. Med. Chem. 2020, 63, 9623–9649.

[37] Guillemont, J.; Benjahad, A.; Oumouch, S.; Decrane, L.; Palandjian, P.; Vernier, D.; Queguiner, L.; Andries, K.; De Béthune, M.P.; Hertogs, K.; et al. Synthesis and biological evaluation of C-5 methyl substituted 4-arylthio and 4-aryloxy-3-Iodopyridin-2(1H)-one type anti-HIV agents. J. Med. Chem. 2009, 52, 7473–7487.

[38] Ravelli, R.B.G.; Gigant, B.; Curmi, P.A.; Jourdain, I.; Lachkar, S.; Sobel, A.; Knossow, M. Insight into tubulin regulation from a complex with colchicine and a stathmin-like domain. N Liu, T.; Cui, R.; Chen, J.; Zhang, J.; He, Q.; Yang, B.; Hu, Y. 4,5-Diaryl-3-aminopyrazole derivatives as analogs of Combretastatin A-4: Synthesis and biological evaluation. Arch. Pharm. 2011, 344, 279–286. ature 2004, 428, 198–202.

[39] Liu, T., Cui, R., Chen, J., Zhang, J., He, Q., Yang, B., & Hu, Y. (2011). 4, 5-Diaryl-3-aminopyrazole Derivatives as Analogs of Combretastatin A-4: Synthesis and Biological Evaluation. Archiv der Pharmazie, 344(5), 279-286.

[40] Chalkha, M., Bakhouch, M., Akhazzane, M., Bourass, M., Nicolas, Y., Al Houari, G., & El Yazidi, M. (2020). Design, synthesis and characterization of functionalized pyrazole derivatives bearing amide and sulfonamide moieties from aza-aurones. Journal of Chemical Sciences, 132, 1-8.

[41] Kumar, H., Bansal, K. K., & Goyal, A. (2022). An Insight into Pyrazole-containing Compounds: Synthesis and Pharmacological Activities. Anti-Infective Agents, 20(5), 1-26.

[42] S. Bieller, A. Haghiri M. Bolte, J. W. Bats, M. Wagner, & H. W. Lerner, Transition metal complexes with pyrazole derivatives as ligands. Inorganica chimica acta, 359(5), 1559-1572. (2006). https://doi.org/10.1016/j.ica.2005.10.034

[43] Perez, J., & Riera, L. (2009). Pyrazole complexes and supramolecular chemistry. European Journal of Inorganic Chemistry, 2009(33), 4913-4925.

[44] Guzei, I. A., & Winter, C. H. (1997). Structural diversity in the reaction of mono-and disubstituted pyrazoles with titanium tetrachloride. Importance of hydrogen bonding and trends in cis/trans geometry of binary adducts with unidentate ligands. *Inorganic chemistry*, *36*(20), 4415-4420.

[45] Pitarch-Jarque, J., Belda, R., Blasco, S., Navarro, P., Tejero, R., Junquera-Hernández, J. M., ... & García-España, E. (2016). A water molecule in the interior of a 1 H-pyrazole Cu 2+ metallocage. New Journal of Chemistry, 40(7), 5670-5674.

[46] Guzei, I. A., Baboul, A. G., Yap, G. P., Rheingold, A. L., Schlegel, H. B., & Winter, C. H. (1997). Surprising Titanium complexes bearing η2-pyrazolato ligands: synthesis, structure, and molecular orbital studies. Journal of the American Chemical Society, 119(14), 3387-3388.

[47] Trofimenko, S. (1986). The coordination chemistry of pyrazole-derived ligands. Progress in inorganic chemistry, 115-210.

[48] Comba, P., Morgen, M., & Wadepohl, H. (2013). First row transition metal complexes of a hexadentate pyrazole-based bispidine ligand. *Polyhedron*, *52*, 1239-1245.

[49] Trofimenko, S. (2005). Polypyrazolylborates: scorpionates. *Journal of chemical education*, *82*(11), 1715.

[50] Pettinari, C., Tăbăcaru, A., & Galli, S. (2016). Coordination polymers and metal–organic frameworks based on poly (pyrazole)-containing ligands. Coordination Chemistry Reviews, 307, 1-31.

[51] Dunitz, J. D., & Gavezzotti, A. (2012). Supramolecular synthons: Validation and ranking of intermolecular interaction energies. Crystal growth & design, 12(12), 5873-5877.

[52] Basu, T., Sparkes, H. A., & Mondal, R. (2009). Construction of extended molecular networks with heterosynthons in cocrystals of pyrazole and acids. Crystal growth & design, 9(12), 5164-5175.

[53] Keter, F. K., & Darkwa, J. (2012). Perspective: the potential of pyrazole-based compounds in medicine. Biometals, 25, 9-21.

[54] Sakai K, Tomista Y, Ue T, Goshima K, Ohminato M, Tsubomura T, Matsumoto K, Ohmura K, Kawakami K (2000) Syntheses, antitumor activity, and molecular mechanics studies of cis-PtCl2(pzH)2 (pzH=pyrazole) and related complexes. Crystal structure of a novel Magnus-type double-salt $[Pt(pzH)_4][PtCl_4][cis\text{-}PtCl_2(pzH)_2]_2$ involving two perpendicularly aligned 1D chains. Inorg Chim Acta 297:64–71

[55] Komeda S, Lutz M, Spek AL, Chikuma M, Reedijk J (2000) New antitumor-active azole-bridged dinuclear platinum(II) complexes: synthesis, characterization, crystal structures, and cytotoxic studies. Inorg Chem 39:4230–4236

[56] Al-Allaf TAK, Rashan LJ (2001) Cis- and trans-platinum and palladium complexes: a comparative study review as antitumor agents. Boll Chim Farm 140:205–210

[57] Wheate NJ, Collins JG (2003) Multi-nuclear platinum complexes as anti-cancer drugs. Coord Chem Rev 241:133–145

[58] Pettinari C, Caruso F, Zaffaroni N, Villa R, Marchetti F, Pettinari R, Phillips C, Tanski J, Rossi M (2006) Synthesis, spectroscopy (IR, multinuclear NMR, ESI-MS), diffraction, density functional study and in vitro antiproliferative activity of pyrazole-beta-diketone dihalotin(IV) compounds on 5 melanoma cell lines. J Inorg Biochem 100: 58–69

[59] Keter FK, Nell MJ, Omondi B, Guzei IA, Darkwa J (2009a) Anticancer activities of bis(pyrazol-1-ylthiocarbonyl)disulfides against HeLa cells. J Chem Res 5:322–325

[60] Casas JS, Castellano EE, Ellena J, Garcı´a-Tasende MS, Pe´rezParalle´ ML, Sa´nchez A, Sa´nchez-Gonza´lez A, Sordo J, Touceda A (2008) New Pd(II) and Pt(II) complexes with N,S-chelated pyrazolonate ligands: molecular and supramolecular structure and preliminary study of their in vitro antitumoral activity. J Inorg Biochem 102:33–45

[61] Segapelo TV, Guzei IA, Spencer LC, Van Zyl WE, Darkwa J (2009) Pyrazolylmethyl)pyridine platinum(II) and gold (III) complexes: synthesis, structures and evaluation as anticancer agents. Inorg Chim Acta 362:3314–3324

[62] Zhang Y, Zhang L, Liu L, Guo J, Wu D, Xu G, Wang X, Jia D (2010) Anticancer activity, structure, and theoretical calculation of N-(1-phenyl-3-methyl-4-propyl-pyrazolone-5)-salicylidene hydrazone and its copper(II) complex. Inorg Chim Acta 363:289–293

[63] Ghorbanpour, M., Shayanfar, A., & Soltani, B. (2024). Copper pyrazole complexes as potential anticancer agents: evaluation of cytotoxic response against cancer cells and their mechanistic action at the molecular level. Coordination Chemistry Reviews, 498, 215459.

[64] Al-Allaf TAK, Al-Bayati RH, Khalaf SH (1993) Synthesis and spectroscopic studies on organotin(IV) complexes of some pyrazoles and pyrazol-5-ones and their antibacterial activity. Appl Organomet Chem 7:635–640

[65] Nomiya K, Noguchi R, Ohsawa K, Tsuda K, Oda M (2000) Synthesis, crystal structure and antimicrobial activities of two isomeric gold(I) complexes with nitrogen-containing

heterocycle and triphenylphosphine ligands, [Au(L) (PPh3)] (HL = pyrazole and imidazole). J Inorg Biochem 78:363–370

[66] Mahmud K, Khan MA, Iqbal MZ (2001) Antibacterial property of some transition metal complexes of pyrazole derivatives. Pak J Biol Sci 4:1000–1001

[67] Fang J, Jin Z, Li Z, Liu W (2003) Synthesis, structure and antibacterial activities of novel ferrocenyl-containing 1-phenyl-3-ferrocenyl-4-triazolyl-5-aryl-dihydropyrazole derivatives. J Organomet Chem 674:1–9

[68] Tharmaraj P, Kodimunthiri D, Sheela CD, Priya CS (2009) Synthesis, spectral studies and antibacterial activity of Cu(II), Co(II) and Ni(II) complexes of 1-(2-hydroxyphenyl)-3-phenyl-2-propan-1-one, N2-[(3,5-diemthyl-1Hpyrazol-1-yl)methyl]hydrazone. J Serb Chem Soc 74: 927–938

[69] Sharma KV, Sharma V, Tripathi UN (2009) Synthesis, spectroscopic, antibacterial and antifungal studies of nickel(II)5 (20 -hydroxyphenyl)-3-(4-X-phenyl)pyrazolinates and their addition complexes with N and P donor ligands. J Coord Chem 62:676–690

[70] Negm NA, Said MM, Morsy SMI (2010) Pyrazole derived cationic surfactants and their tin and copper complexes: synthesis, surface activity, antibacterial and antifungal efficacy. J Surfactants Deterg 13:521–528

[71] Kulkarni NV, Revankar VK (2011) Synthesis, antimicrobial screening, and DNA-binding/cleavage of new pyrazolebased binuclear CoII, NiII, CuII, and ZnII complexes. J Coord Chem 64:725–741

[72] Kratz F, Nuber B, Weiss J, Keppler BK (1992) Synthesis and characterization of potential antitumour and antiviral gallium(III) complexes of N-heterocycles. Polyhedron 11:487–498

[73] Fonteh P, Keter FK, Meyer D, Guzei IA, Darkwa J (2009) Tetrachloro-bis(3, 5-dimethylpyrazolylmethane)gold(III) chloride: an HIV-1 reverse transcriptase and protease inhibitor. J Inorg Biochem 103:190–194

[74] Keter, F. K., Kanyanda, S., Lyantagaye, S. S., Darkwa, J., Rees, D. J. G., & Meyer, M. (2008). In vitro evaluation of dichloro-bis (pyrazole) palladium (II) and dichloro-bis (pyrazole) platinum (II) complexes as anticancer agents. Cancer chemotherapy and pharmacology, 63, 127-138.

[75] Budzisz, E., Krajewska, U., Rozalski, M., Szulawska, A., Czyz, M., & Nawrot, B. (2004). Biological evaluation of novel Pt (II) and Pd (II) complexes with pyrazole-containing ligands. European journal of pharmacology, 502(1-2), 59-65.

[76] Gama, S., Mendes, F., Marques, F., Santos, I. C., Carvalho, M. F., Correia, I., ... & Paulo, A. (2011). Copper (II) complexes with tridentate pyrazole-based ligands: synthesis, characterization, DNA cleavage activity and cytotoxicity. Journal of Inorganic Biochemistry, 105(5), 637-644.

[77] Sobiesiak, M., Lorenz, I. P., Mayer, P., Woźniczka, M., Kufelnicki, A., Krajewska, U., ... & Budzisz, E. (2011). Synthesis, X-ray structure and cytotoxic effect of nickel (II) complexes with pyrazole ligands. European journal of medicinal chemistry, 46(12), 5917-5926.

[78] Ribeiro, N., Di Paolo, R. E., Galvao, A. M., Marques, F., Pessoa, J. C., & Correia, I. (2018). Photophysical properties and biological evaluation of a Zinc (II)-5-methyl-1H-pyrazole Schiff base complex. Spectrochimica Acta Part A: Molecular and Biomolecular Spectroscopy, 204, 317-327.

[79] Adach, A., Daszkiewicz, M., & Tyszka-Czochara, M. (2016). A family of complexes with N-scorpionate-type and other N-donor ligands obtained in situ from pyrazole derivative and zerovalent cobalt. Physicochemical and cytotoxicity studies. RSC advances, 6(50), 44070-44079.

[80] Sivaram, H., Tan, J., & Huynh, H. V. (2012). Syntheses, characterizations, and a preliminary comparative cytotoxicity study of gold (I) and gold (III) complexes bearing benzimidazole-and pyrazole-derived N-heterocyclic carbenes. Organometallics, 31(16), 5875-5883.

[81] Adhikari, S., Nath, P., Das, A., Datta, A., Baildya, N., Duttaroy, A. K., & Pathak, S. (2024). A review on metal complexes and its anti-cancer activities: Recent updates from in vivo studies. Biomedicine & Pharmacotherapy, 171, 116211.

[82] Huttner, A., Bielicki, J., Clements, M. N., Frimodt-Møller, N., Muller, A. E., Paccaud, J. P., & Mouton, J. W. (2020). Oral amoxicillin and amoxicillin–clavulanic acid: properties, indications and usage. Clinical Microbiology and Infection, 26(7), 871-879.

[83] Bird, A. E. (1994). Amoxicillin. In Analytical profiles of drug substances and excipients (Vol. 23, pp. 1-52). Academic Press.

[84] Deng, S., Ma, X., Su, E., & Wei, D. (2016). Efficient cascade synthesis of ampicillin from penicillin G potassium salt using wild and mutant penicillin G acylase from Alcaligenes faecalis. Journal of Biotechnology, 219, 142-148.

[85] Orabi, A. S., Abdelhameed, M., Abbas, A. M., & Mostafa, G. M. (2022). Modern view for binary and ternary complexes of metal ions with amoxicillin and some amino acids. Advances in Environmental and Life Sciences, 1(1), 22-39.

[86] Hrioua, A., Loudiki, A., Farahi, A., Laghrib, F., Bakasse, M., Lahrich, S., ... & El Mhammedi, M. A. (2021). Complexation of amoxicillin by transition metals: Physico-chemical and antibacterial activity evaluation. Bioelectrochemistry, 142, 107936.

[87] Zayed, M. A., & Abdallah, S. M. (2005). Synthesis and structure investigation of the antibiotic amoxicillin complexes of d-block elements. Spectrochimica Acta Part A: Molecular and Biomolecular Spectroscopy, 61(9), 2231-2238.

[88] Jibril, S., Sani, S., Kurawa, M. A., & Shehu, S. M. (2019). Mechanochemical synthesis, characterization and antimicrobial screening of Metal (II) complexes derived from amoxicillin. Bayero Journal of Pure and Applied Sciences, 12(1), 106-111.

[89] Anacona, J. R., Mago, K., & Camus, J. (2018). Antibacterial activity of transition metal complexes with a tridentate NNO amoxicillin derived Schiff base. Synthesis and characterization. Applied Organometallic Chemistry, 32(7), e4374.

[90] Boros, E., & Packard, A. B. (2018). Radioactive transition metals for imaging and therapy. Chemical reviews, 119(2), 870-901.

[91] Sekhon, B. S. (2011). Inorganics/bioinorganics: Biological, medicinal and pharmaceutical uses. Journal of Pharmaceutical Education and Research, 2(1), 1.

[92] Sorenson, J. R. (2012). Biology of copper complexes (Vol. 16). Springer Science & Business Media.

[93] Watson, S. A., & McStay, G. P. (2020). Functions of cytochrome c oxidase assembly factors. International Journal of Molecular Sciences, 21(19), 7254.

[94] Islam, M. N., Rauf, A., Fahad, F. I., Emran, T. B., Mitra, S., Olatunde, A., ... & Mubarak, M. S. (2022). Superoxide dismutase: an updated review on its health benefits and industrial applications. Critical Reviews in Food Science and Nutrition, 62(26), 7282-7300.

[95] Mermer, A., & Demirci, S. (2023). Recent advances in triazoles as tyrosinase inhibitors. European Journal of Medicinal Chemistry, 115655.

[96] Mclntire, W. S., & Hartmann, C. (2020). Copper-containing amine oxidases. In Principles and applications of quinoproteins (pp. 97-172). CRC Press.

[97] Trothen, S. (2023). Novel Roles of PACS-1 Within the Nucleus and the Regulated Secretory Pathway.

[98] Iakovidis, I., Delimaris, I., & Piperakis, S. M. (2011). Copper and its complexes in medicine: a biochemical approach. Molecular biology international, 2011(1), 594529.

[99] Bonham, J. M. O'Connor, B. M. Hannigan, and J. J. Strain, "The immune system as a physiological indicator of marginal copper status?" British Journal of Nutrition, vol. 87, no. 5, pp. 393–403, 2002.

[100] Zdrojewicz, Z., Popowicz, E., & Winiarski, J. (2016). Nickel-role in human organism and toxic effects. Polski Merkuriusz Lekarski: Organ Polskiego Towarzystwa Lekarskiego, 41(242), 115-118.

[101] Chang, E. L., Simmers, C., & Knight, D. A. (2010). Cobalt complexes as antiviral and antibacterial agents. Pharmaceuticals, 3(6), 1711-1728.

[102] Heffern, M. C., Yamamoto, N., Holbrook, R. J., Eckermann, A. L., & Meade, T. J. (2013). Cobalt derivatives as promising therapeutic agents. Current opinion in chemical biology, 17(2), 189-196.

[103] Bajema, E. A., Roberts, K. F., & Meade, T. J. (2019). Cobalt-Schiff base complexes: preclinical research and potential therapeutic uses. Met Ions Life Sci, 19, 269-274.

[104] Prakash A, Bharti K, Majeed AB: Zinc: indications in brain disorders. Fundam Clin Pharmacol. 2015 Apr;29(2):131-49. doi: 10.1111/fcp.12110. Epub 2015 Mar 12. (PubMed ID 25659970)

[105] Nowak, G. (2015). Zinc, future mono/adjunctive therapy for depression: mechanisms of antidepressant action. Pharmacological reports, 67(3), 659-662.

[106] Fukunaka, A., & Fujitani, Y. (2018). Role of zinc homeostasis in the pathogenesis of diabetes and obesity. International journal of molecular sciences, 19(2), 476.

[107] Alam, M. N., & Huq, F. (2016). Comprehensive review on tumour active palladium compounds and structure–activity relationships. Coordination Chemistry Reviews, 316, 36-67.

[108] Alam, M. N., & Huq, F. (2016). Comprehensive review on tumour active palladium compounds and structure–activity relationships. Coordination Chemistry Reviews, 316, 36-67.

[109] Tookad. European Medicines Agency. Available at: https://www.ema.europa.eu/en/medicines/human/EPAR/tookad

[110] Soler-Rivas, C., Espín, J. C., & Wichers, H. J. (2000). An easy and fast test to compare total free radical scavenger capacity of foodstuffs. Phytochemical Analysis: An International Journal of Plant Chemical and Biochemical Techniques, 11(5), 330-338.

[111] Bubonja, M., Mesarić, M., Miše, A., Jakovac, M., & Abram, M. (2008). Factors affecting the antimicrobial susceptibility testing of bacteria by disc diffusion method. Medicina Fluminensis: Medicina Fluminensis, 44(3-4), 280-284.

[112] Balouiri, M., Sadiki, M., & Ibnsouda, S. K. (2016). Methods for in vitro evaluating antimicrobial activity: A review. Journal of pharmaceutical analysis, 6(2), 71-79.

[113] Mosmann T (1983) Rapid colorimetric assay for cellular growth and survival: Application to proliferation and cytotoxicity assays. J. Immunol. Methods 65 (1-2):55-63.

[114] Ohno M. Abe T. (1991)Rapid colorimetric assay for the quantification of leukemia inhibitory factor (LIF) and interleukin-6 (IL-6). Journal of Immunological Methods. 145 (1-2):199-203.

[115] Sheldrick, G. M. (2015). Crystal structure refinement with SHELXL. Crystal Structure Communications, 71(1), 3-8.

[116] Gajda, R., Tchon, D. M., & Makal, A. (2022). Hierarchy of intermolecular interactions in highly luminescent pyrenyl-pyrazole-aldehyde. Crystal Growth & Design, 23(2), 862-872.

[117] Aakeröy, C. B., Spartz, C. L., Dembowski, S., Dwyre, S., & Desper, J. (2015). A systematic structural study of halogen bonding versus hydrogen bonding within competitive supramolecular systems. *IUCrJ*, 2(5), 498-510.

[118] Jaćimović, Ž. K., Radović, A., Leovac, V. M., Tomić, Z. D., & Evans, I. R. (2007). Crystal structure of bis (μ2-thiocyanato) tetrakis (3, 5-dimethyl-1-(thiocarbamoyl) pyrazole) dinickel (II) dichloride ethanol disolvate, $[Ni(NCS)_2(C_6H_6N_3S)_4][Cl]_2 \cdot 2C_2H_5OH$. Zeitschrift für Kristallographie-New Crystal Structures, 222(4), 430-432.

[119] Bai, Y. L., Bao, X., Zhu, S., Fang, J., & Tao, J. (2013). Ligand field effect tuned magnetic behaviors of two chain compounds based on Mn^{III} units: from slow magnetic relaxation to metamagnetism. Dalton Transactions, 42(4), 1033-1038.

[120] Viciano-Chumillas, M., Tanase, S., Mutikainen, I., Turpeinen, U., de Jongh, L. J., & Reedijk, J. (2009). Manganese (III) compounds with phenol–pyrazole based-ligands: impact of the co-ligand and the carboxylate ligand on the trinuclear core $[Mn_3(\mu_3\text{-}O)(phpzR)_3(O_2CR')_n]^{1-n}$. Dalton Transactions, (36), 7445-7453.

[121] Liu, C. M., Zhang, D. Q., & Zhu, D. B. (2008). Solvatomagnetic effect and spin-glass behavior in a 1D coordination polymer constructed from EE-azido bridged Mn^{III}_3O units.

[122] Liu, C. M., Zhang, D. Q., & Zhu, D. B. (2009). 1D Coordination Polymers Constructed from anti− anti Carboxylato-Bridged MnIII3O (Brppz) 3 Units: From Long-Range Magnetic Ordering to Single-Chain Magnet Behaviors. *Inorganic chemistry*, *48*(11), 4980-4987.

[123] Tao, J., Zhang, Y. Z., Bai, Y. L., & Sato, O. (2006). One-dimensional ferromagnetic complexes built with Mn^{III}_3O units. *Inorganic chemistry*, *45*(13), 4877-4879.

[124] Mede, R., Gläser, S., Suchland, B., Schowtka, B., Mandel, M., Görls, H., ... & Westerhausen, M. (2017). Manganese (I)-based CORMs with 5-substituted 3-(2-pyridyl) pyrazole ligands. *Inorganics*, *5*(1), 8.

[125] Puello, J. Q., Obando, B. I., Foces-Foces, C., Infantes, L., Claramunt, R. M., Cabildo, P., ... & Elguero, J. (1997). Structure and tautomerism of 3 (5)-amino-5 (3)-arylpyrazoles in the solid state and in solution: An X-ray and NMR study. *Tetrahedron*, *53*(31), 10783-10802.

[126] Sun, J., Lv, P. C., Yin, Y., Yuan, R. J., Ma, J., & Zhu, H. L. (2013). Synthesis, structure and antibacterial activity of potent DNA gyrase inhibitors: N′-benzoyl-3-(4-bromophenyl)-1 H-pyrazole-5-carbohydrazide derivatives. *PloS one*, *8*(7), e69751.

[127] Desiraju, G. R., & Parthasarathy, R. (1989). The nature of halogen. cntdot.. cntdot.. cntdot. halogen interactions: are short halogen contacts due to specific attractive forces or due to close packing of nonspherical atoms?. *Journal of the American Chemical Society*, *111*(23), 8725-8726.

[128] Nakamoto, K. (2009). Infrared and Raman spectra of inorganic and coordination compounds, part B: applications in coordination, organometallic, and bioinorganic chemistry. John Wiley & Sons.

[130] Giles, I. D., DePriest, J. C., & Deschamps, J. R. (2015). Effect of substitution and the counterion on the structural and spectroscopic properties of CuII complexes of methylated pyrazoles. Journal of Coordination Chemistry, 68(20), 3611-3635.

[131] Goddard, R., Claramunt, R. M., & Escolástico, C. (1999). Structures of NH-pyrazoles bearing only C-methyl substituents: 4-methylpyrazole is a hydrogen-bonded trimer in the solid (100 K). New Journal of Chemistry, 23(2), 237-240.

[132] Papánková, B., Svoboda, I., & Fuess, H. (2005). Bis (acetato-κO) tetrakis (1H-pyrazole-κN1) nickel (II). Structure Reports, 61(10), m2036-m2038.

[133] Döring, M., Ludwig, W., & Görls, H. (1994). Thermal latent coordination compounds: The thermal degradation of imidazole and pyrazole adducts of metal acetates. Journal of Thermal Analysis and Calorimetry, 42(2-3), 443-459.

[134] Aroua, L. M., Alkhaibari, I. S., Alminderej, F. M., Messaoudi, S., Chigurupati, S., Al-mahmoud, S. A., ... & Mohammed, H. A. (2025). Synthesis, bioactivity, and molecular docking of pyrazole bearing Schiff-bases as prospective dual alpha-amylase and alpha-glucosidase inhibitors with antioxidant activity. Journal of Molecular Structure, 1320, 139291.

[135] Todorov, L., Saso, L., & Kostova, I. (2023). Antioxidant activity of coumarins and their metal complexes. Pharmaceuticals, 16(5), 651.

[136] Ali, S. A., Awad, S. M., Said, A. M., Mahgoub, S., Taha, H., & Ahmed, N. M. (2020). Design, synthesis, molecular modelling and biological evaluation of novel 3-(2-naphthyl)-1-phenyl-1H-pyrazole derivatives as potent antioxidants and 15-Lipoxygenase inhibitors. Journal of enzyme inhibition and medicinal chemistry, 35(1), 847-863.

[137] Silva, V. L., Elguero, J., & Silva, A. M. (2018). Current progress on antioxidants incorporating the pyrazole core. European journal of medicinal chemistry, 156, 394-429.

[138] Cingolani, A., Galli, S., Masciocchi, N., Pandolfo, L., Pettinari, C., & Sironi, A. (2006). The competition between acetate and pyrazolate in the formation of polynuclear Zn (II) coordination complexes. Dalton Transactions, (20), 2479-2486.

[139] Barta Holló, B., Radanović, M. M., Rodić, M. V., Krstić, S., Jaćimović, Ž. K., & Vojinović Ješić, L. S. (2022). Synthesis, physicochemical, thermal and antioxidative properties of Zn (II) coordination compounds with pyrazole-type ligand. Inorganics, 10(2), 20.

[140] Radnović, N. D., Štetin, N., Radanović, M. M., Borišev, I. Đ., Rodić, M. V., Jaćimović, Ž. K., & Barta Holló, B. (2023). Two isomers of a novel Ag (I) complex with Pyrazole-type Ligand—Synthesis, Structural, Thermal, and antioxidative Characterization. Inorganics, 12(1), 4.

[141] Güney, S., Ergün, S., Matıc, I., Petrovic, N., & Stanojkovic, T. (2020). The Investigation of Anti-Proliferative Effects of [Ag2 (sac) 2 (dap) 2] Complex on Different Types of Cancer. Middle Black Sea Journal of Health Science, 6(1), 54-58.

[142] Stanojkovic, T. P., Filimonova, M., Grozdanic, N., Petovic, S., Shitova, A., Soldatova, O., ... & Nikitovic, M. (2022). Evaluation of in vitro cytotoxic potential of avarol towards human cancer cell lines and in vivo antitumor activity in solid tumor models. Molecules, 27(24), 9048.

[143] Quirante, J., Ruiz, D., Gonzalez, A., López, C., Cascante, M., Cortés, R., ... & Biot, C. (2011). Platinum (II) and palladium (II) complexes with (N, N′) and (C, N, N′)− ligands derived from pyrazole as anticancer and antimalarial agents: Synthesis, characterization and in vitro activities. Journal of Inorganic Biochemistry, 105(12), 1720-1728.

[144] Eltayeb, N. E. (2016). Methyl 5-(4-hydroxyphenyl)-6-oxo-1, 6-dihydropyrazine-2-carboxylate. IUCrData, 1(11), x161689.

Addendum A – XRPD diffractograms

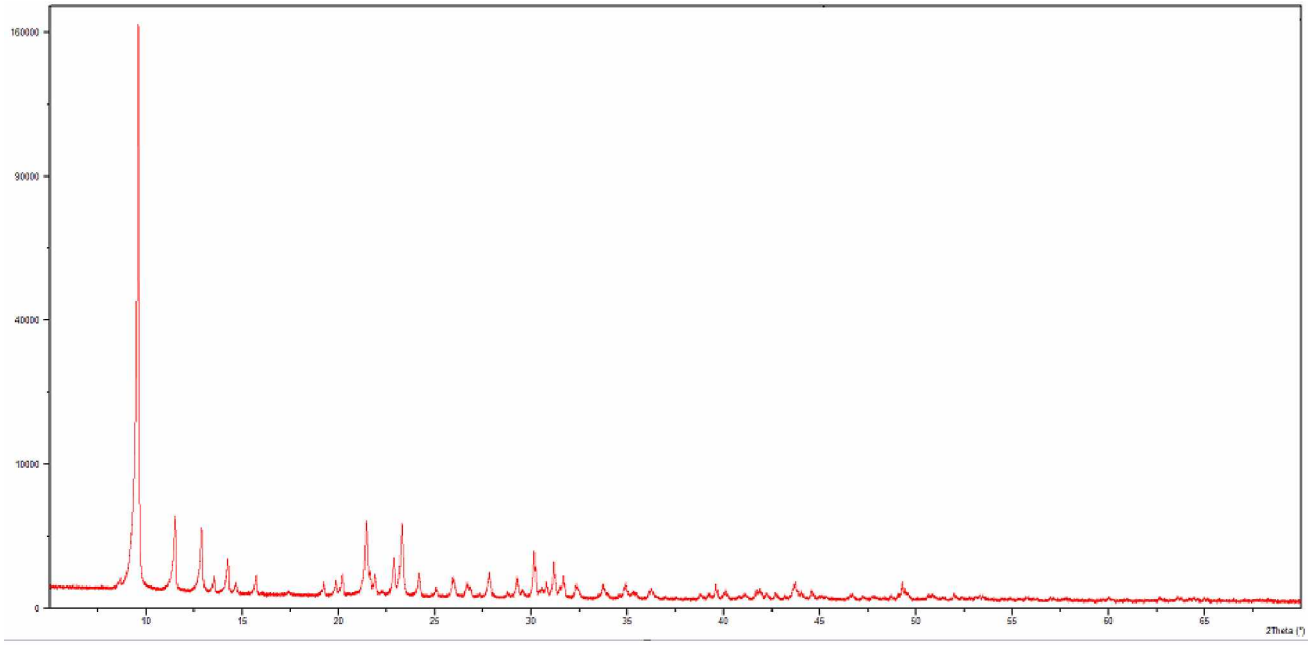

Figure 1. The powder diffractogram of $CuL_4(NO_3)_2$

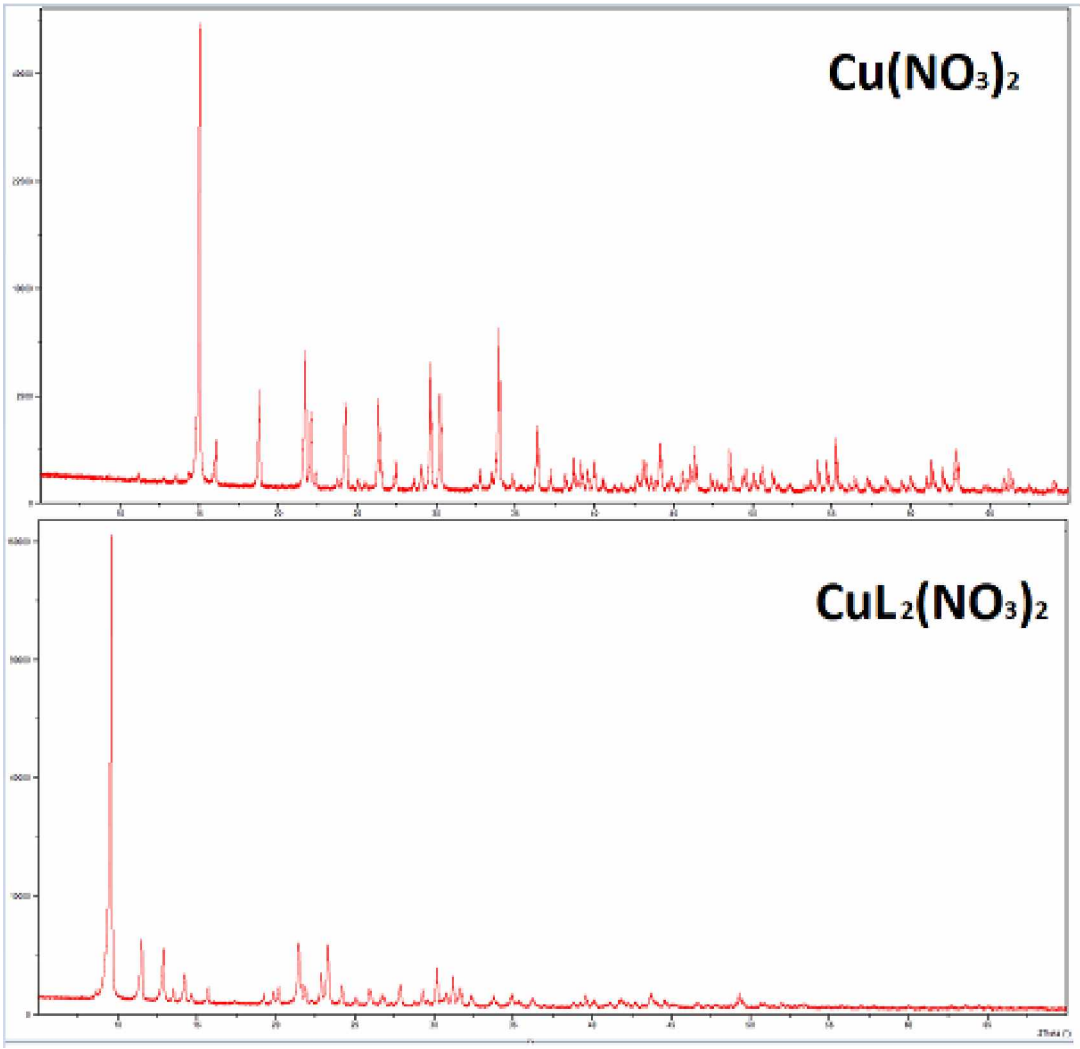

Figure 2. The powder diffractograms of $Cu(NO_3)_2$ and $CuL_2(NO_3)_2$

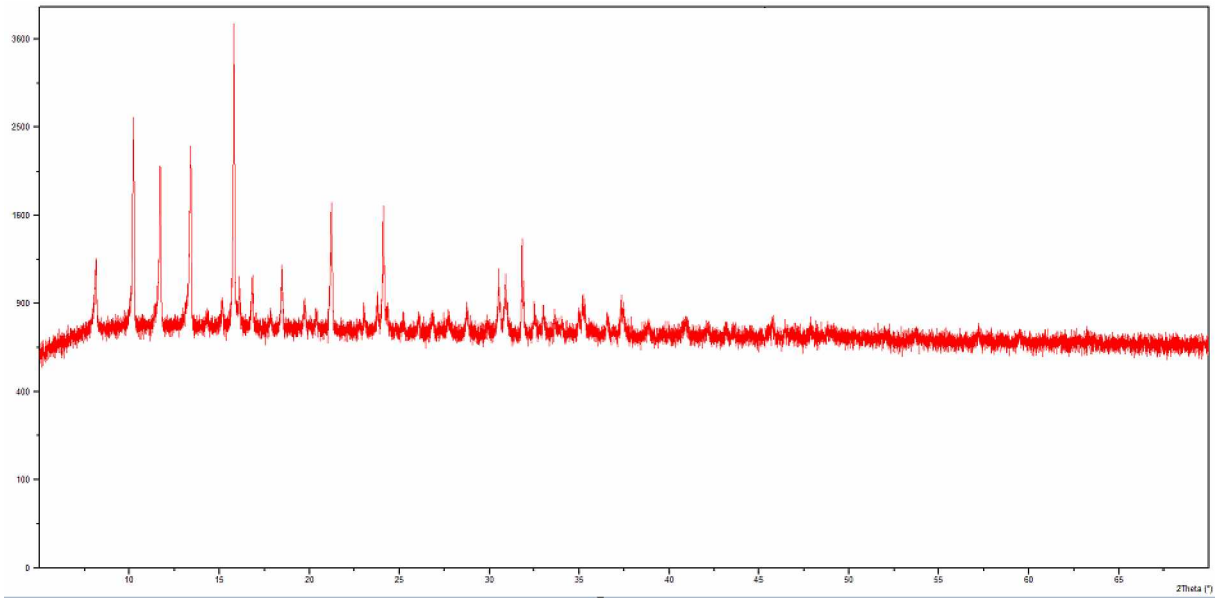

Figure 3. The powder diffractogram of CoL_4Cl_2

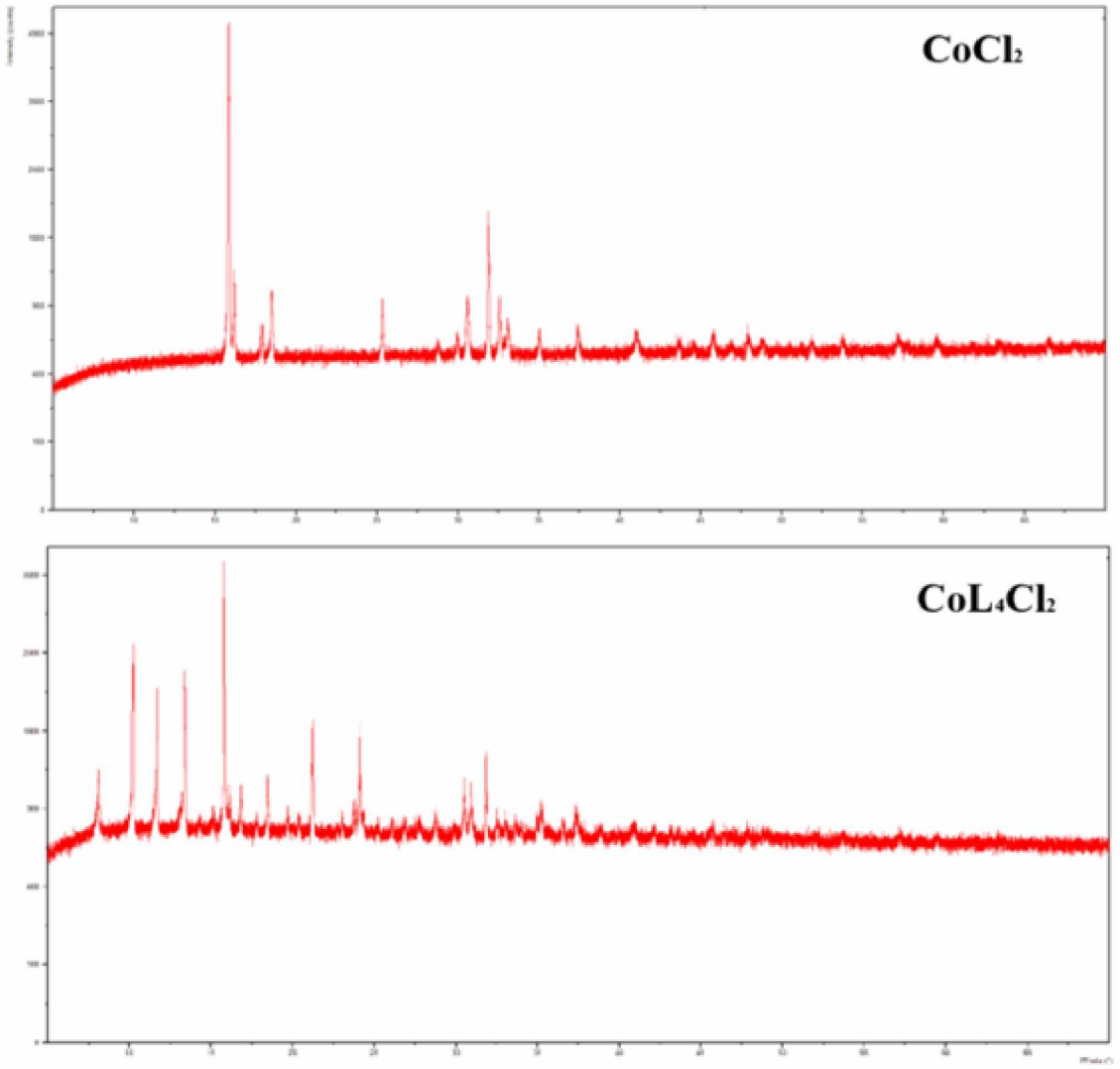

Figure 4. The powder diffractograms of $CoCl_2$ and CoL_4Cl_2

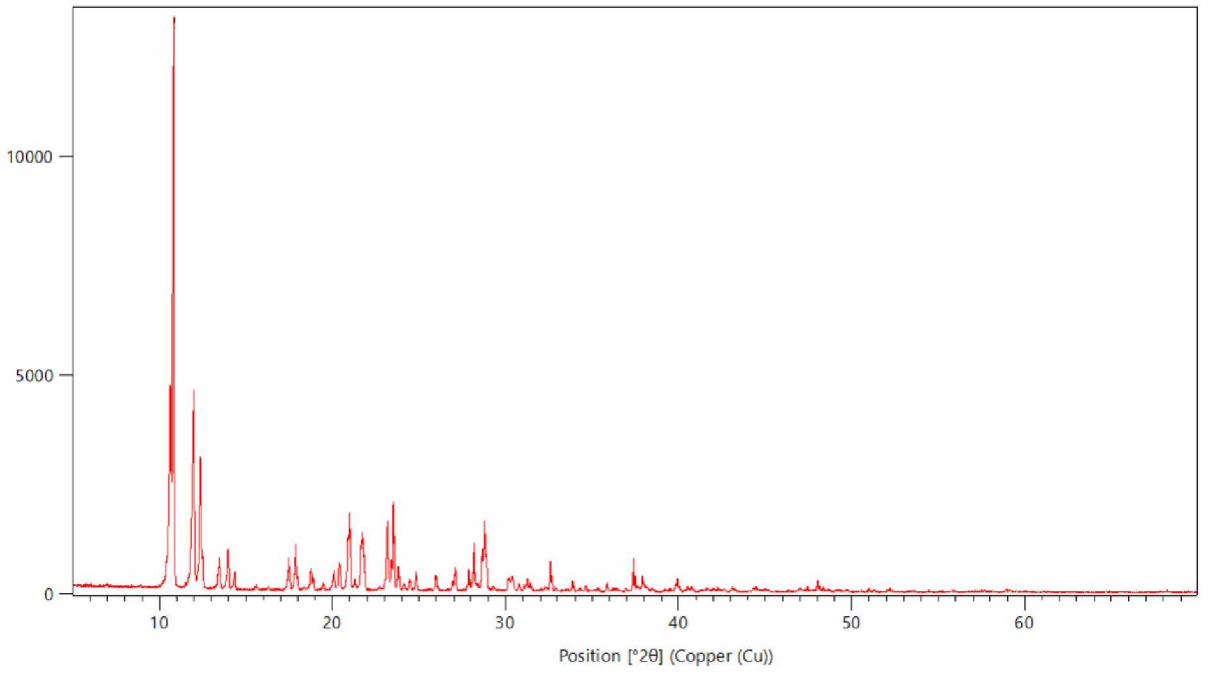

Figure 5. The powder diffractogram of $Ni(OAc)_2L_4$

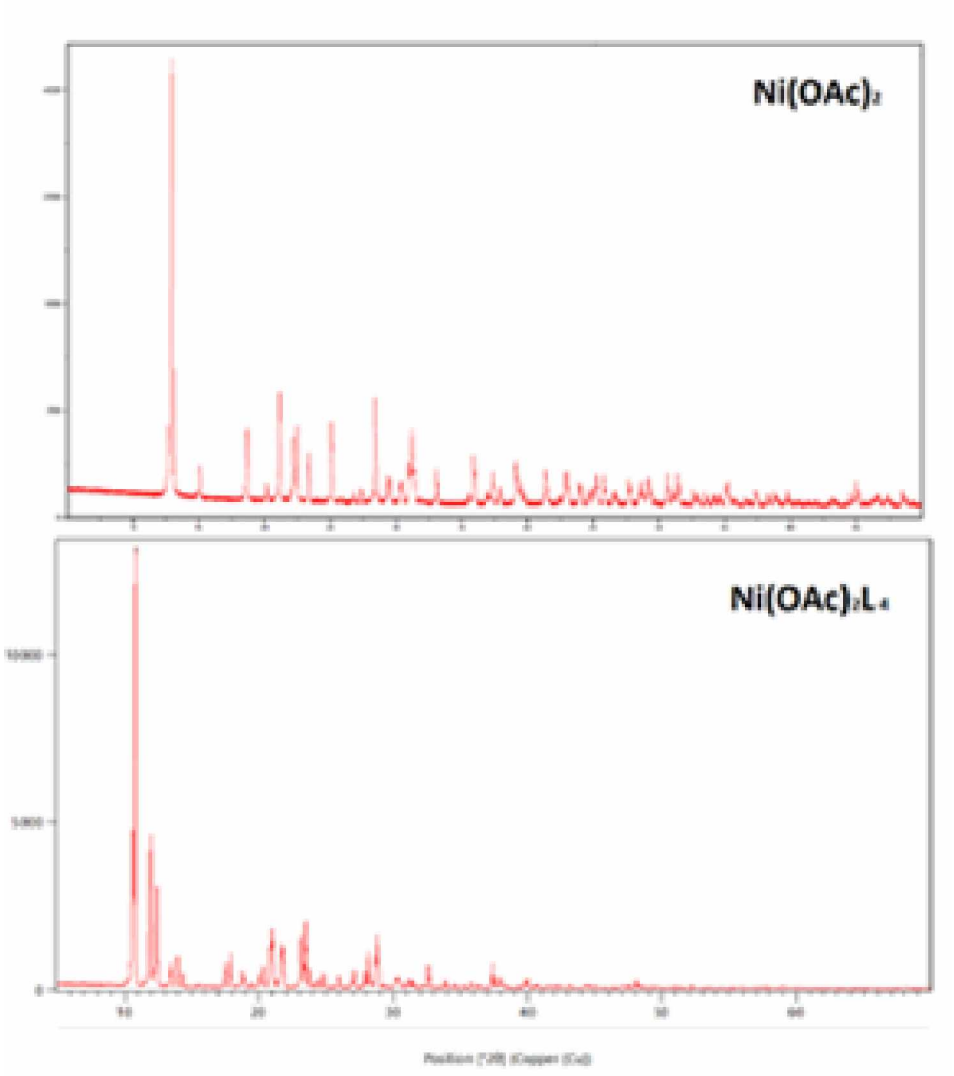

Figure 6. The powder diffractograms of $Ni(OAc)_2$ and $Ni(OAc)_2L_4$

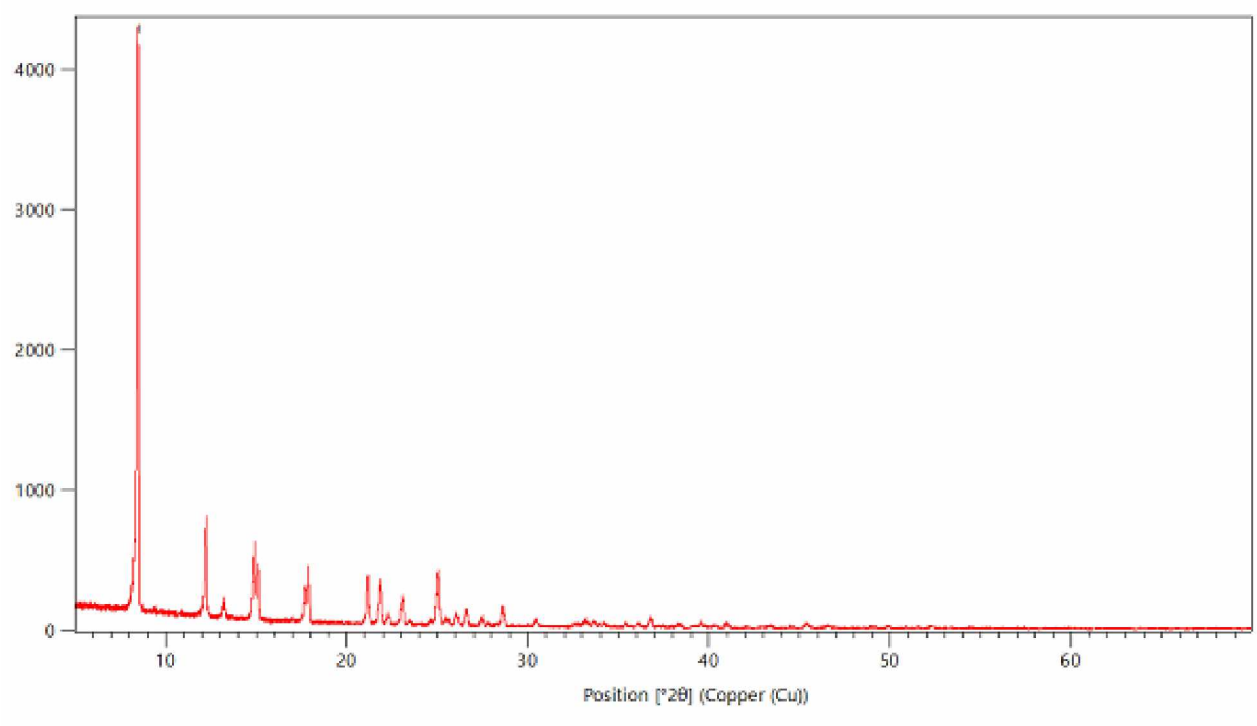

Figure 7 The powder diffractogram of $Zn(OAc)_2L_2$

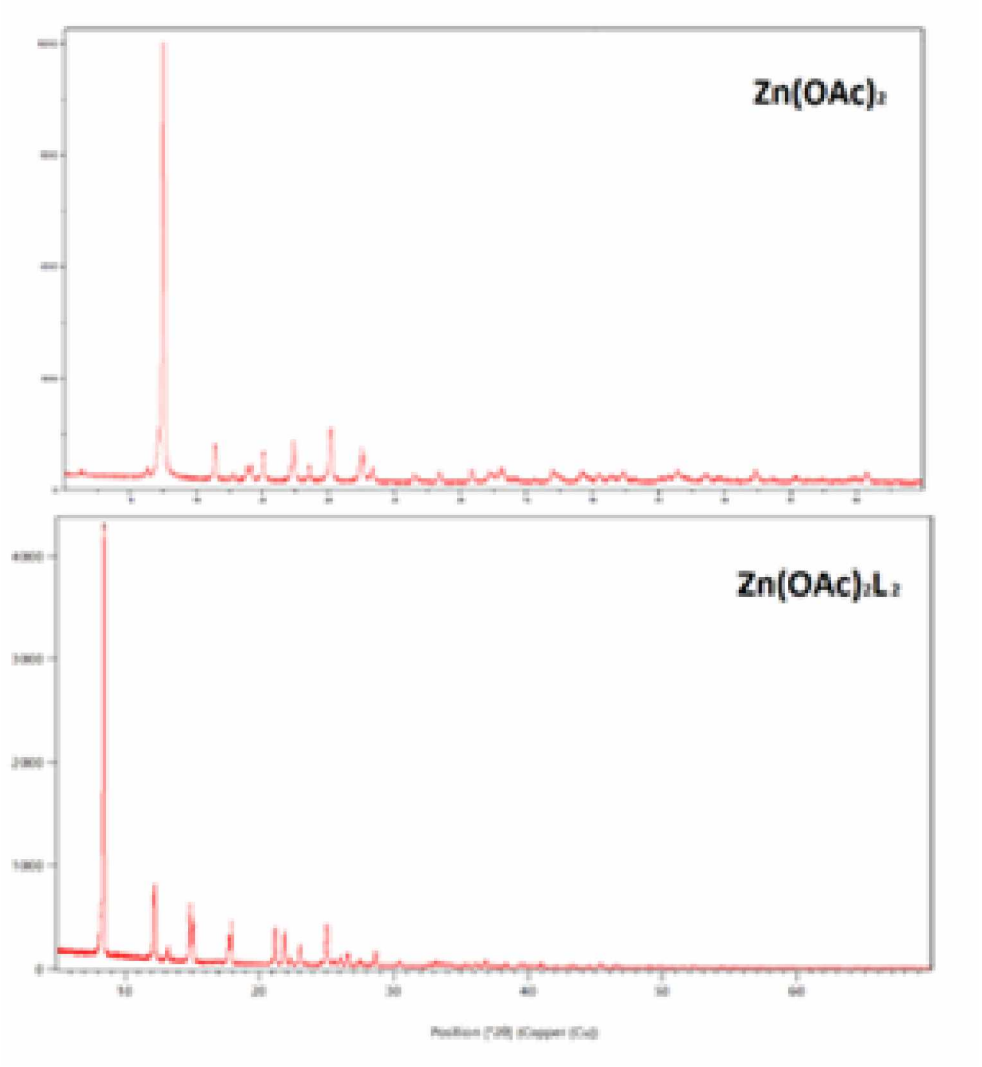

Figure 8. The powder diffractograms of $Zn(OAc)_2$ and $Zn(OAc)_2L_2$

Addendum B – Publications

Inorganica Chimica Acta
Volume 574, 1 January 2025, 122363

Research paper

Synthesis, characterization and antioxidative capacity of nickel(II) and zinc(II) complexes with 4-methylpyrazole

David Kočović [a], Berta Barta Holló [b], Ivana Borišev [b], Vukadin Leovac [b], Ljiljana Vojinović Ješić [b], Gerald Giester [c], Sergiu Shova [d], Zoran D. Tomić [e], Željko Jaćimović [f]

Show more

+ Add to Mendeley Share Cite

https://doi.org/10.1016/j.ica.2024.122363

Get rights and content

Full text access

David Kočović, Snežana Mugoša, Sergiu Shova, Zoran D. Tomić and Željko K. Jaćimović*

Crystal structure of 3-(4-bromophenyl)-5-methyl-1*H*-pyrazole, $C_{10}H_9BrN_2$

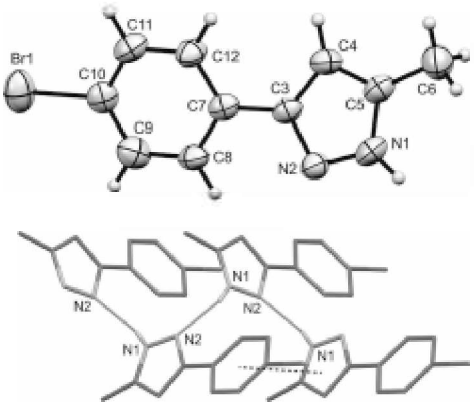

https://doi.org/10.1515/ncrs-2023-0242
Received May 18, 2023; accepted June 14, 2023; published online July 5, 2023

Abstract

$C_{10}H_9BrN_2$, orthorhombic, $P2_12_12_1$ (no. 19), a = 5.9070(3) Å, b = 9.2731(7) Å, c = 17.5641(14) Å, V = 962.09(12) Å^3, Z = 4, $R_{gt}(F)$ = 0.0504, $wR_{ref}(F^2)$ = 0.0947, T = 293(2) K.

CCDC no.: 2269982

The molecular structure is shown in the figure. Table 1 contains crystallographic data and Table 2 contains the list of the atoms including atomic coordinates and displacement parameters.

*Corresponding author: **Željko K. Jaćimović**, Faculty of Metallurgy and Technology, Džordža Vašingtona bb University of Montenegro, Podgorica, Montenegro, E-mail: zeljko@ac.me, https://orcid.org/0000-0001-6803-3835

David Kočović and Snežana Mugoša, Institute for Medicines and Medical Devices of Montenegro, 81000 Podgorica, Montenegro

Sergiu Shova, Inorganic Polymer Department 'Petru Poni', Institute of Macromolecular Chemistry, Aleea Gr. Ghica Voda 41A, 700487 Iasi, Romania

Zoran D. Tomić, Department of Theoretical Physics and Condensed Matter Physics 'VINČA', Institute of Nuclear Sciences, National Institute of the Republic of Serbia, University of Belgrade, PO Box 522 11001 Belgrade, Serbia, https://orcid.org/0000-0002-4436-1724

Table 1: Data collection and handling.

Crystal:	Pink prism
Size:	0.30 × 0.20 × 0.15 mm
Wavelength:	Mo $K\alpha$ radiation (0.71073 Å)
μ:	4.22 mm^{-1}
Diffractometer, scan mode:	Xcalibur, ω
θ_{max}, completeness:	29.2°, >99 %
$N(hkl)_{measured}$, $N(hkl)_{unique}$, R_{int}:	4442, 2196, 0.039
Criterion for I_{obs}, $N(hkl)_{gt}$:	$I_{obs} > 2\ \sigma(I_{obs})$, 1346
$N(param)_{refined}$:	119
Programs:	CrysAlis^{Pro} [1], Shelx [2], Mercury [3], Platon [4], WinGX/Ortep [5, 6]

1 Source of materials

3-(4-bromophenyl)-5-methyl-1*H*-pyrazole (L) was purchased from Sigma–Aldrich. 0.05 g L was dissolved in 5 ml of ethanol, slowly heated and left to crystallize. After 24 h clear light pink single crystals of the title compound were filtered and washed with ethanol.

2 Experimental details

The H atoms bonded to pyrazole and phenyl ring were placed at calculated positions and refined as riding atoms with U_{iso}(H) set to 1.2U_{eq} of the parent atom. The H atoms of the methyl group were positioned geometrically and allowed to rotate around the C–C bond to best fit the experimental electron density (HFIX 137 in the Shelx program suite [2]), with U_{iso}(H) set to 1.5U_{eq}(C).

3 Comment

Pyrazole and its derivatives have important pharmacological properties [7]. They bonds to metal atoms as monodentate or bridging bidentate ligands [8]. Strong affinity towards metals may lead to the formation of metal-organic frameworks [9]. N–H···N hydrogen bonding is prevalent interaction in the assembly of pyrazolyl molecules [10]. Their hydrogen bonding capacity may lead to the formation of extended molecular networks [11]. Substituents at the pyrazole ring give more possibilities for supramolecular arrangements. Between phenyl-pyrazole molecules

Biografija autora

David Kočović je rođen 17.06.1996. godine u Baru. Osnovnu i srednju školu je završio u Podgorici. Osnovne studije završio je 2018. godine na Fakultetu za prehrambenu tehnologiju, bezbjednost hrane i ekologiju Univerziteta Donja Gorica, sa prosjekom 9.73. Specijalističke i master studije nastavio je na istom fakultetu, sa usmjerenjem: "Tehnologija proizvoda biljnog porijekla", 2020. godine je magistrirao sa prosjekom 9.63 na specijalističkim i 9.50 na master studijama. Doktorske studije, program Održivi razvoj upisao je 2021. godine.

Na poziciji rukovodioca Laboratorije u Institutu za ljekove i medicinska sredstva nalazi se od marta 2022. godine, a u Institutu radi od 2020. godine na poslovima stručnog saradnika za instrumentalne metode i kvalifikaciju opreme, radeći na X-ray tehnikama (XRPD i XRF). Prethodno radno iskustvo stekao je u laboratorijama Centra za ekotoksikološka ispitivanja i Instituta za javno zdravlje, radeći na tehnikama gasne (GC-FID, GC-ECD, GC-MS) i tečne hromatografije (LC-MS, LC-MS/MS).

Od oktobra 2020. godine, obavlja funkciju nacionalnog fokal pointa u „Globalnoj mreži fokal pointa za substandardne i falsifikovane medicinske proizvode" Svjetske zdravstvene organizacije. Takođe u organizaciji SZO David je predsjedavajući član radne grupe „Detekcione tehnologije za substandardne i falsifikovane medicinske proizvode" koju čini 20 predstavnika iz 12 zemalja. Takođe, član je savjetodavne grupe za razvoj profila ručnog uređaja za skrining i detekciju falsifikovanih ljekova, osnovane u saradnji SZO i Univerziteta u Oksfordu. U sklopu Evropskog direktorata za kvalitet ljekova i brigu o zdravlju (EDQM) član je „Komiteta eksperata za minimizaciju rizika po javno zdravlje od falsifkovanih ljekova i povezanih krivičnih djela (CD-P-PH/CMED)".

Tokom studija učestvovao je i osvojio 3. mjesto na međunarodnom Zero Hackathon takmičenju održanom u Rimu u oktobru 2016. godine.

Dobitnik je Verner Baltes stipendije, a ovom prilikom je proveo tri mjeseca u Njemačkom saveznom institutu za procjenu rizika (BfR) tokom 2022. godine, učestvujući u naučno-istraživačkim projektima.

Bio je član Organizacionog odbora 23. Evropskog skupa o hemiji životne sredine.

Od 2018. do 2020. godine učestvovao je u projektu BUGI (Western Balkans Urban Agriculture Initiative), projekta sa fokusom se na implementaciju i akreditaciju master programa Urbana poljoprivreda na UDG-u. Učestvovao je i u Medi-Theft projektu od aprila 2022. do novembra 2023. godine, baveći se kritičnim pitanjima u vezi sa bezbjednošću farmaceutskog tržišta. U sklopu COST akcije CA221707 "Bringing Experiment and Simulation Together in Crystal Structure Prediction", David je član radnih grupa *Crystallographic data* i *Crystallisation techniques*.

David je sertifikovani interni provjerivač za ISO standarde 9001:2015, 27001:2013 i 17025:2017. Pored toga, poseduje brojne sertifikate iz oblasti instrumentalnih analiza.

Izjava o autorstvu

Potpisani: David Kočović
Broj indeksa: 10/2021

Izjavljujem

da je doktorska disertacija pod naslovom
Synthesis, physicochemical characterization and potential biological activity of new pyrazole and amoxicillin complex compounds

- rezultat sopstvenog istraživačkog rada,
- da predložena disertacija ni u cjelini ni u djelovima nije bila predložena za dobijanje bilo koje diplome prema studijskim programima drugih ustanova visokog obrazovanja,
- da su rezultati korektno navedeni, i
- da nijesam povrijedio autorska i druga prava intelektualne svojine koja pripadaju trećim licima.

Potpis doktoranda

U Podgorici, 01.09.2025.

Authorship Statement

Signed: David Kočović
Index number: 10/2021

I declare

that the doctoral dissertation entitled
Synthesis, physicochemical characterization and potential biological activity of new pyrazole and amoxicillin complex compounds

- is the result of my own research work,
- that the proposed dissertation, neither in whole nor in part, has been submitted for the award of any degree under the study programs of other higher education institutions,
- that the results are correctly stated, and
- that I have not infringed the copyright or other intellectual property rights belonging to third parties.

Signature of the doctoral candidate

Podgorica, 01.09.2025.

Izjava o istovjetnosti štampane i elektronske verzije doktorskog rada

Ime i prezime autora: David Kočović
Broj indeksa/upisa: 10/2021
Studijski program: Održivi razvoj
Naslov rada: Sinteza, fizičko-hemijska karakterizacija i procjena potencijalne biološke aktivnosti novosintetizovanih kompleksnih jedinjenja na bazi pirazola i amoksicilina
Mentor: Prof. dr Željko Jaćimović

Potpisani: David Kočović

Izjavljujem da je štampana verzija mog doktorskog rada istovjetna elektronskoj verziji koju sam predao za objavljivanje u Digitalni arhiv Univerziteta Crne Gore.

Istovremeno izjavljujem da dozvoljavam objavljivanje mojih ličnih podataka u vezi sa dobijanjem akademskog naziva doktora nauka, odnosno zvanja doktora umjetnosti, kao što su ime i prezime, godina i mjesto rođenja, naziv disertacije i datum odbrane rada.

U Podgorici, 01.09.2025.

Potpis doktoranda

Statement on the Identity of the Printed and Electronic Versions of the Doctoral Dissertation

Author's Name and Surname: David Kočović
Index/Enrollment Number: 10/2021
Study Program: Sustainable Development
Thesis Title: Synthesis, physicochemical characterization and potential biological activity of new pyrazole and amoxicillin complex compounds
Mentor: Prof. dr Željko Jaćimović Ž. Jaćimović

Signed: David Kočović

I hereby declare that the printed version of my doctoral dissertation is identical to the electronic version submitted for publication in the Digital Archive of the University of Montenegro.

At the same time, I declare that I consent to the publication of my personal data related to the awarding of the academic title of Doctor of Science, or the title of Doctor of Arts, such as my name and surname, year and place of birth, dissertation title, and date of defense.

Signature of the doctoral candidate

D. Kočović

Podgorica, 01.09.2025.

Izjava o korišćenju

Ovlašćujem Univerzitetsku biblioteku da u Digitalni arhiv Univerziteta Crne Gore pohrani moju doktorsku disertaciju pod naslovom:

Sinteza, fizičko-hemijska karakterizacija i procjena potencijalne biološke aktivnosti novosintetizovanih kompleksnih jedinjenja na bazi pirazola i amoksicilina

koja je moje autorsko djelo.

Disertaciju sa svim prilozima predao sam u elektronskom formatu pogodnom za trajno arhiviranje.

Moju doktorsku disertaciju pohranjenu u Digitalni arhiv Univerziteta Crne Gore mogu da koriste svi koji poštuju odredbe sadržane u odabranom tipu licence Kreativne zajednice (Creative Commons) za koju sam se odlučio.

1. Autorstvo
2. Autorstvo – nekomercijalno
3. Autorstvo – nekomercijalno – bez prerade
4. Autorstvo – nekomercijalno – dijeliti pod istim uslovima
5. Autorstvo – bez prerade
6. Autorstvo – dijeliti pod istim uslovima

(Molimo da zaokružite samo jednu od šest ponuđenih licenci, kratak opis licenci dat je na poleđini lista).

Potpis doktoranda

U Podgorici, 01.09.2025.

Statement of Use

hereby authorize the University Library to deposit my doctoral dissertation in the Digital Archive of the University of Montenegro under the title:

Synthesis, physicochemical characterization and potential biological activity of new pyrazole and amoxicillin complex compounds

which is my original work.

I have submitted the dissertation with all appendices in an electronic format suitable for permanent archiving.

My doctoral dissertation deposited in the Digital Archive of the University of Montenegro may be used by all those who comply with the provisions contained in the selected type of Creative Commons license I have chosen:

1. Attribution
2. Attribution – NonCommercial
3. Attribution – NonCommercial – NoDerivatives
4. Attribution – NonCommercial – ShareAlike
5. Attribution – NoDerivatives
6. Attribution – ShareAlike

Signature of the doctoral candidate

Podgorica, 01.09.2025.